Fabrication of new organic probes for chromo-fluorogenic detection of environmentally hazardous ions and molecules

Thesis submitted for the degree of

DOCTOR OF PHILOSOPHY (SCIENCE)

February-2024

by

Mr. Atanu Maji

Department of Chemistry

Jadavpur University, Kolkata - 700 032

India

Dr. T.K. Mondal, Ph. D.
Professor
Department of Chemistry
Inorganic Chemistry Section

JADAVPUR UNIVERSITY
Kolkata – 700 032, India
Telephone: 91-033-2457-2970
tapank.mondal@jadavpuruniversity.in

CERTIFICATE FROM THE SUPERVISOR(S)

This is to certify that the thesis entitled "**Fabrication of new organic probes for chromo-fluorogenic detection of environmentally hazardous ions and molecules**" submitted by **Mr. Atanu Maji**, M.Sc., who got his name registered on **16.03.2021** for the award of Ph.D. (Science) degree of Jadavpur University, is absolutely based upon his own work under the supervision of Dr. Tapan Kumar Mondal and that neither this thesis nor any part of it has been submitted for either any degree / diploma or any other academic award anywhere before.

.....16/02/2024.....

(Signature of the Supervisor(s) date with official seal

Dr. TAPAN KUMAR MONDAL
Professor
Department of Chemistry
Jadavpur University
Kolkata-700032

"Research means that you don't know, but are willing to find out"

~ Charles Kettering

Dedicated to

My parents and teachers…

ACKNOWLEDGEMENTS

My research journey which commenced on 8th July, 2019, is at last coming to an end through making me a better and more mature researcher as well as a human being. Many persons I have come across during this time will certainly hold a special place in my heart. Foremost name to be mentioned will be my supervisor Dr. Tapan Kumar Mondal, Professor, Department of Chemistry, Jadavpur University, Kolkata - 700032 for allowing me to do research freely in his research group. My obeisance will always be there for him in a sense of reverence and deepest gratitude. He almost curved the path suitable and convenient for me to summit my desired peak overcoming the sky touching mountains of problem and rough and hard cliffs of difficulty, I had to undergo throughout the course of my research work.

It is also a pleasure to me to express my gratitude to the faculty members of Department of Chemistry, Jadavpur University, Prof. Kajal Krishna Rajak, Head, Department of Chemistry, Prof. Ashis Kumar Sarkar, Dean of Science, JU, Prof. Partha Roy, Section-In-Charge, Inorganic Chemistry Section and all other faculty members of Department of Chemistry, Jadavpur University. I am whole-heartedly indebted to all the teaching as well as non-teaching staff members of chemistry department and university for their help and support in various aspects.

I must say, I am really feeling proud to express my affection and endless gratitude to all my past and present labmates namely, Dr. Ajoy Kr. Pramanik, Dr. Sujan Biswas, Mr. Subhankar Kundu, Dr. Deblina Sarkar, Dr. Puspendu Roy, Dr. Apurba Sau Mondal, Dr. Saswati Gharami, Dr. Lakhsman Patra, Dr. Chandan Kumar Manna, Dr. Rahul Naskar, Dr. Samik Acharyya, Mr. Biswajit Bera, Mr. Akash Das, Mr. Amitav Biswas, Mr. Sandipan Mandal, Mr. Subrata Mandal, Mr. Arpan Halder, Ms. Moumita Ghosh, Mr. Chandrasekhar Mandi, Mr. Wasim Akram and last but not the least, Dr. Krishnendu Aich for their constant cooperation and making the lab-atmosphere perfectly compatible to feed the journey of my research. So much fun and golden moments happened with them throughout this course, that I will always cherish all those memories in my solitude.

I express my deepest gratitude to my M.Sc. project supervisor, Dr. Braja Gopal Bag, Professor, Vidyasagar University for initializing the spirit of research through me during my masters which ultimately led me to begin this research journey. I am forever grateful to Mr. Ranendu Samanta and his family for their constant support. I am grateful to all of M. Sc. project students in my lab, who helped me to extend the barrier of my knowledge by asking queries about their woks and also to entertain me in their own way. I also express my thankfulness to Mr. Santanu Giri, Ms. Ayantika Samanta, Ms. Priyanka Manna, Mr. Ayan Hazra, Mr. Lakhmikanta Manna and some other helpful friends and relatives of mine to support me continuously during my research journey.

Moreover, I know it is needless to say, that my education, my research, my works, all of me, in one word the very existence of mine would have not been there in this universe without two persons; my father Sri Hari Pada Maji and my mother Smt. Chhaya Rani Maji. It might seem awkward to show them my gratitude, as they are beyond all these. My emotion for them cannot be bound by words. What I can do for them is to try, forever, though unsuccessfully, to love them as fiercely as they love me. Their constant encouragement, support and unflinching belief in me and my abilities have made me what I am today.

Atanu Maji 16.02.2024

(Atanu Maji)
Department of Chemistry
Jadavpur University

CONTENTS

PREFACE

In present time, design and fabrication of chromogenic as well as fluorogenic chemosensors are immensely interdisciplinary field of research due to their importance and extensive application in diverse fields, such as chemistry, medicine, biology and environmental studies etc. A molecule that is capable of detecting a particular analyte through the alteration realized by one or more characteristics of the structure like absorption, emission, can be defined as chemosensors as well as chemodosimeters. The advancement of this research area is now successfully applied for onsite detection of various environmentally hazardous analytes and also in live cell bioimaging purpose in case of biological studies.

My thesis work entitled, **"Fabrication of organic probes for chromo-fluorogenic detection of environmentally hazardous ions and molecules"** contains newly design as well as the development of several organic probes with extensive and thorough sensing studies for specific and precise recognition of toxic analytes and metal ions. The synthesis of newly designed chemosensors is simple, low cost and fascile. The chemical structure of the probes is confirmed by various spectroscopy studies such as ^{1}HNMR, ^{13}CNMR, mass spectrometry, IR spectra as well as single X-ray diffraction study. The binding of the host-guest and the formation of the complexes or adducts have been thoroughly investigated by UV-Vis, fluorescence, Job's plot analysis and ^{1}H as well as ^{13}C NMR and HRMS methods. Biological applications of the some chemosensors have also been executed by using them as cellular bioimaging agent in live-cells. This thesis consists of seven chapters based on the fabrication, characterization and extensive study of sensing properties of the newly constructed organic probes. Density Functional Theory (DFT) and Time Dependent Density Functional Theory (TDDFT) were also performed to further support the sensing mechanisms. Some of the synthesized probes have been successfully employed for real samples analysis and also proved to have applications as logic function gate.

Chapter 1 describes the brief introduction on the basic definition of a chemosensor, its classification and working principle along with the basic concept of various non-covalent forces. The essential criteria for the design of host and guest are also included in this chapter. A concise

literature survey of various published chemosensors based on different sensing mechanisms have been described elaborately.

Chapter 2 deals the thorough instrumentation procedures like ^{1}H, ^{13}C NMR, HRMS, IR, UV-Vis, fluorescence detection, crystallography, lifetime decay measurement etc. which are essential in order to study more about the organic probes. In this chapter, some other methods such as detection limit determination, quantum yield calculation along with association constant derivation were also discussed which are needed in further study of a chemosensor.

Chapter 3 represents the fabrication of a new coumarin based fluorescent "turn-on" probe (PCEH) for distinct and sequential recognition of Al^{3+} and F^{-} in methanol-water mixture (4:1, v/v) at physiological pH. The chemical structure and the sensing properties of the chemosensor towards Al^{3+} have been thoroughly investigated by spectroscopic methods. Finally, to establish its practical advantage in biological fields, cellular bioimaging experiments with PCEH are carried out to recognize Al^{3+} in human breast cancer cell lines (MDA-MB-231 cell).

Chapter 4 introduces the modulation in the binding sites for adaptable DNA interactive probe efficient at chromo-fluorogenic meticulous recognition of Al^{3+} in methanol at pH 7.2, using HEPES buffer. DNA binding study is also executed to elucidate possible bioactivity and compared potentiality among analogues. Reversible nature is also proven in presence of EDTA. The biological applications of the probe (HMCP) through behaving as a biomarker tool in breast cancer cell lines (MDA-MB-231 cell) and application in molecular logic gate function were also executed here.

Chapter 5 reports a novel AIE active carbazole-benzothiazole based chemodosimeter (CBTA) for chromogenic and fluorogenic recognition of CN^{-} in 60 % mixed aqueous DMSO solution. The sensor is thoroughly characterized by spectroscopic techniques and also described via theoretical calculations. The practical application of the chemodosimeter is executed through the 'dip-stick method' as well as waste water treatment.

Chapter 6 describes the efficient solid and solution state emissive reusable solvatochromic fluorophore (CPI) for colorimetric and fluorometric detection of CN^{-} in DMSO. The chemical structure of CPI has been confirmed by single crystal X-ray diffraction, ^{1}HNMR, ^{13}CNMR, IR and mass spectroscopy. Significantly, the sensor can detect low-level water in organic solvents. More importantly, the practicability of the sensor is investigated through the real sample analysis (foods and water) and dip-stick methods.

Lastly, Chapter 7 deals with the rapid and swift recognition of lethal nerve agent simulant, diethyl chlorophosphate (DCP) through a new chemodosimetric approach. The synthesized probe (BIPQ) displays a ratiometric detection of DCP distinctly in chloroform solvent over other coexisting toxic analytes. All the needful photophysical studies are executed thoroughly and the limit of detection value is determined to be in the order of 10^{-8} M which signifies its efficiency to detect DCP in a very minute level in solution phase. This newly constructed ratiometric switch has also a potential application as a portable tool for detecting DCP vapour with high sensitivity.

In brief, this thesis reports the fabrication of several newly designed organic probes which have the efficiency to detect specific environmentally hazardous analytes and metal ions along with their practical application. I am happy to note that some of these works have been published in several reputed international journals.

In keeping with the general practice of reporting scientific observation, due acknowledgement has been made whenever the work described as based on the findings of other investigators. I further promulgates that I am responsible for any undesirable errors or lacunae in my thesis and any such error is extremely regretted. I hope it will not fail to intrigue its readers.

Atanu Maji 16.02.2024

(Atanu Maji)

Department of Chemistry

Jadavpur University

1 | Chapter 1

A compendious and fundamental overview of fluorescent sensing probes along with various sensing mechanisms and its wide application

1.1. Introduction

Metal ions are fundamental and essential elements for the maintenance of a series of biological functions in humans, animals and plants.[1] Some metal ions are the vital constituents of the various enzymes which plays significant roles in several biochemical processes. Besides, their presence in excess, scarcity or absence may lead to several diseases. Essential metal ions include magnesium(Mg), sodium(Na), potassium(K), calcium(Ca) that belong to main group of elements, and chromium (Cr), copper (Cu), Zinc (Zn), vanadium (V), manganese (Mn), iron (Fe), cobalt (Co), nickel (Ni), cadmium (Cd) and molybdenum (Mo) that belong to transition metal group of elements in the periodic table. The scarcity of Co and Fe leads to anemia, whereas the insufficient presence of Zn leads to skin changes and growth retardation, that of Cu leads to heart and brain diseases and absence of Cr leads to the reduction of the glucose tolerance and that of Ca leads to bone deterioration. Due to no recognized cellular function, some metal elements such as lead (Pb), arsenic (As), germanium (Ge), bismuth (Bi), tin (Sn), nickel (Ni), strontium (Sr), uranium (Ur), barium (Ba), aluminum (Al), cadmium (Cd), lithium (Li), gold (Au), platinum (Pt), tellurium (Te), antimony (Sb), Titanium (Ti), beryllium (Be), gallium (Ga), mercury (Hg), indium (In), thallium (Tl), silver (Ag), and vanadium (V) are nonessential for biochemical reaction.[2-4] On the other hand, heavy metal elements are known to have very harmful impact on biological system. They can damage the cell membrane and affect the mitochondrial lysosome, endoplasmic reticulum, and the nuclei.[5] Some enzymes can lose their activities due to heavy metal toxicity. The presence of heavy metals can affect the conformations of DNA and nuclear proteins thereby causing the cell cycle modulation and carcinogenesis. Presently, toxicity of mercury (Hg), arsenic (As), lead (Pb), cadmium (Cd), and chromium (Cr) are of great concern for public health.[6] Basically, the toxicity of these metal elements comes through the formation of reactive oxygen species as well as oxidative stress.[7] As every metal elements possess different physicochemical properties, they show different mechanistic aspects of toxicology, some of which are still unknown. Therefore, due to the negative impact in biosphere, proper identification and monitoring of each of these elements is very necessary for medication of the various difficult diseases caused by these metals. Apart from metal toxicity, our human race is also facing new threat caused by organic compounds. In present time, chemical warfare (CW) is probably one of the most brutal one among the weapons of mass destruction created by mankind.[8-12] CW agents are extremely dangerous synthetic chemicals and used in the form of gas, liquid or aerosol or powder. In 1915, the first time in World,

german army attacked Belgium with chlorine gas (CWA).[13] Almost 1,00,000 deaths and 12,00,000 casualties were caused by such kinds of CWA attack in World War I.[14] Since then, so many CWA attacks on the mankind have been instigated, killing millions of innocent civilians. During World War II, millions of innocent people were killed by the Nazis with Zyklon B gas (hydrogen cyanide gas). In 1980, the largest single CW occurred during the Iran-Iraq War where around 5000 people were died. Among all the chemical warfare agents, organophosphorus nerve agents are extremely lethal and need a special concern. In 1995, when Tokyo Subway Attack occurred, Sarin gas was released in Tokyo metro, 12 people were died and 6200 people were injured in this incident. In 2013, in case of Ghouta Chemical Attack, Sarin gas was deployed on Ghouta during Syrian civil war. In 2017, Syria has faced a fatal chemical weapons attack of Sarin in one of its city, Khan Shaykhun.[15] Organophosphorus compounds are conceived as one of the most exceptional hazardous nerve agent and extremely harmful towards the nervous system of every living beings if inhaled through breathing or any kind of contamination to food or drinks.[16-19] Some of the known nerve agents including tabun (GA), soman (GD) and sarin (GB) are extremely dangerous organophosphates, which bear excellent leaving groups owing to which they are known as essential phosphonylating and phosphorylating agents.[20-24] These poisonous chemicals along with the advantages of them being cheap, their simplicity in manufacturing and their demolishing effects on civilians encourage terrorism. The phosphate group present in these chemicals binds irreversibly with the hydroxyl group present in the acetylcholinesterase (AChE), thereby blocking the hydrolysis of acetylcholine neurotransmitters and detaining the decomposition of acetylcholine.[25-28] This excessive storage of acetylcholine causes the neuromuscular paralysis, neurological imbalance in the cholinergic synapse, resistance of muscle relaxation, organ failure, finally leading to sudden death.[29-35] So it becomes a massive threat to all man-kind. As most of these compounds are odorless, colorless and tasteless, making them very difficult to detect,[36] it is very urgent to develop a very sensitive, reliable and rapid method for easy and quick detection of these substances in both the solution and vapour phase. Highly volatile sarin (GB) is one of the forbidden CWAs used by terrorists. But due to its too much toxic nature and hard availability, an associated substance, diethyl chlorophosphate (DCP) has used as a nerve gas-mimic agent for experiments which has similar chemical structure, comparable reactivity and very low toxicity. Not only organophosphorus nerve agents, cyanide is also used as a chemical weapon in World War I, in the form of HCN. Cyanides are also very hazardous due to their highly toxic nature and

also considered as one of the fatal warfare agents. Cyanide is currently extensively used in many industrial processes such as electroplating, petrochemicals, photography, steel production, gold mining, metallurgy and the synthesis of resin and fibre due to its critical role in multi-functional reaction.[37] World health organization (WHO) stipulates the permissible acceptable concentration of cyanide in drinking water is 1.9×10^{-6} mol/L.[38] By the way, cyanide is present in some insects, fruits, seeds, roots where it is released through the hydrolysis process of cyanogenic glycosides.[39-43] Cyanide binds to the iron ion in cytochrome c oxidase and blocks the electron transport in metabolism and inhibits the production of ATP in cells, resulting in the inefficiency of the biological system to provide sufficient energy to heart, central nervous system and other vital organs ultimately.[44,45] Considering the above fact, development of simple, efficient and rapid detection tools with high selectivity and sensitivity towards cyanide is an ongoing hot topic to prevent harmful effects in human body from contaminated food and environment.

A chemosensor is an organic or inorganic complex that is used for detecting specific analytes through a detectable change or signal. All chemosensors are comprised of a signaling moiety and a recognition unit, that is joined either directly to each other or through some kind of spacer or connector. The utilization of chemosensors is referred to as chemosensing. In other words, an indicator acts as a transducer for the chemical species that cannot be determined directly by optical means. There is a region where selective chemical reaction takes place and transducer where the chemical reaction generates a signal such as the emission of a fluorescent light or color change which results into a change in the electrical potential at the surface. Afterwards, the transducer acts in response to this signal and translates the magnitude of the signal into measure of the amount of the analytes.[46] According to the transducers, the chemosensor can be classified into optical, mass-sensitive, electrochemical and heat sensitive sensors. Among them, optical sensors are highly impressive and widely employed in various fields including clinical, biomedical, and environmental monitoring and process controlling.[47-52] They can be used to detect origins of contamination in an industrial process, follow the formation and movement of environmental hazardous pollutants and can raise the alarm when a toxic species surpasses an expected level of exposure. Therefore, these optical sensors are proved to be an attractive and workable analytical tool. However, there are many indicators, which cannot be served as optical chemosensors due to low stability, analytical interferences, unfavorable analytical wavelengths, low molar absorptivity or the need for additional reagents. In this case, fluorescent based indicators are superior tool in

the sense of sensitivity and selectivity as it is very unlikely that the interfering analytes possess the same absorption and emission property as the targeted one.[53-55] Besides the fluorescent "turn-on" chemosensor, there is also a group of probe based on the fluorescent "turn off" or quenching behavior upon interaction with the guest analyte. Quenching phenomenon of the emission can be attributed to static and dynamic or collision quenching process. In the static quenching process, quencher interacts with the fluorophores in the ground state; in case of the dynamic quenching, analyte interacts with the fluorophores in the excited state and reduce both the emission intensity and the decay time remarkably. Synthesized chemosensors are susceptible to specific sensing of the targeted guest analyte via the enhancement or quenching or ratiometric shift of the emission maxima followed by distinct and prominent color change under UV lamp which help one to get the rapid detection. The chemistry behind the function of chemosensor is based on the co-ordination chemistry that is not only limited to the transition-metal cations but also extended to all kind of cationic, anionic as well as neutral species of inorganic, organic and biological systems. The implementation of molecular detection stands for such a quantitative evaluation of complementarities between the associating partners or of its inverse. Measurement of similarity rests on the definition and construction of molecular shape and potential maps. Thus the pre-origination to the generation of the molecular receptor is the prime factor.[56] The complexation ability of a probe with guest analytes mainly governs by the number of degrees of freedom occurred during a binding process.[57] To synthesize an ideal probe, the following points are to be considered.

(1) Steric (size and shape) complementarity between receptor and the guest analytes, i.e. presence of convex and concave domains in the suitable position on probe and on analytes;

(2) Interactional complementarity, i.e. presence of complementary binding sites (electrostatic such as positive/negative, charge/dipole, dipole/dipole, hydrogen bond donor/acceptor etc.) in the correct disposition on the probe and on analytes so as to achieve complementary electronic and nuclear distribution (electrostatic, H-bonding and Van der Waals) maps;

(3) Strong Vanderwaals force i.e., large areas of contact between probe and analyte;

(4) Multiple binding sites as non-covalent interactions are weak in nature compared to covalent bonds.

(5) Strong overall binding with high stability and high selectivity is required.

(6) Polarity of medium also plays significant role as it interacts both with probes as well as with the guest analytes.

Thus the two partners should present geometrically matched solvophilic/solvophilic or solvophobic/solvophobic domain. A variety of receptor has been introduced in recent history of research in sensors areas that can recognize any specific analyte. In spite of the increasing surge in fabricating probes for sensing analytes, the research and development in the field of sensor has always expanded exponentially in terms of lower limit of detection, cost-effective for synthesis, the number of published papers, kinetic and thermodynamic aspect of the binding interaction between the receptor and the guest analyte and the number of active researchers worldwide. Compared to instrumental based analysis, chemical sensors are portable, simple to use as well as easily synthesized, *in-situ* and miniature in size. These characteristics are perfect for real-time and on field monitoring of various environmentally hazardous analytes and if any errors were made by the sample storage and transportation, then that can be largely diminished. The aim of my thesis is to design and fabrication of the new organic probes in terms of facile, low-cost, biocompatible, portable chromo-fluorogenic detection of environmentally hazardous compounds and ions in the semi aqueous solution, solid state as well as in vapour phase.

1.2. Molecular recognition

Molecular recognition is a well-known phenomenon which is fundamentally a crucial part in chemistry, material science, biology as well as in environmental area[58]. The term molecular recognition signifies about the specific interaction between two or more molecules via different non-covalent bonding such as metal coordination, hydrogen bonding, hydrophobic forces, π-π interactions, vanderwaals forces, halogen bonding, electrostatic interactions and or electromagnetic forces, resonant interaction effects etc. In addition, solvents can play a vital role in driving molecular recognition in solution phase. It is also defined by the energy involved in the binding and assortment of a substrate by a specified receptor molecule. In this phenomenon, a host molecule is designed and fabricated purposely for the identification of target substrates or biologically important guests which is referred to as Host-guest interaction. Molecular recognition basically depends upon the size, shape, nature of binding sites, chemical functionalities of host-guest molecules. The design and fabrication of model probes usually termed as hosts to recognize substrates, usually called guests of biological implication is a vital ground in molecular recognition research.[59] Basically, host-guest interaction depends upon the size, shape, chemical functionalites

as well as nature of binding sites of host-guest molecules.[60]The development of chemistry of crown-ether by C. J. Pedersen first introduced the concept of molecular recognitions.[61] Afterwards, J. M. Lehn, prolong the research on macrocycles to macro-bicyclic or the stranded crown ethers for recognition of ions and other neutral species.[62,63] Later on, in 1987, Donald J. Cram, Jean-marie Lehn and Charles J. Pedersen were awarded Novel Prize for their massive contribution for developing of specific host-guest complexes and providing the concept such as mechanically interlocked molecular architectures emerging. The "Host-Guest" chemistry was first reported with crown ethers stand-in as a molecular host to the guest (cation).[64-66] The concept of molecular recognition is extensively used in the fundamental biology of the enzyme reaction (substrate-enzyme interactions), immunological reactions, gene expression (retrieval and storage of genetic information), selective complexation and transportation of metal cations via cell membrane, and in the host guest complexation as well as catalytic reactions in bio-mimetic chemistry.[67]

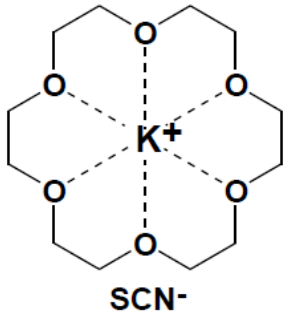

Macrocyclic ether:
Pedersen's Model

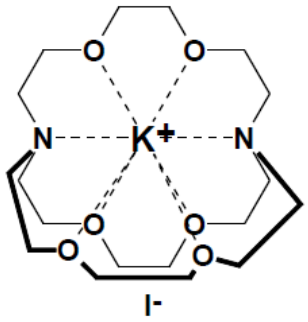

Macrobicyclic ether:
Lehn's Model

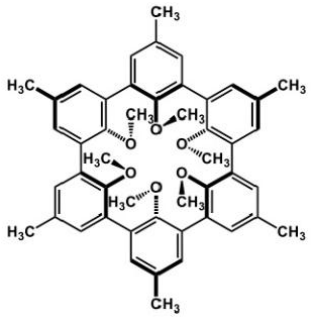

Cram's Model

1.3. Chemosensing

A chemosensor is an organic or inorganic complex that is used for detecting specific analytes (chemical or biochemical compounds) through a detectable change or signal of absorptions and fluorescence activity and offers an interesting field of research nowadays. Chemosensors bind with target analytes through various non-covalent interactions to yield measurable optical signals with a real time response. Such interactions are usually reversible in nature. Therefore, they have a significant advantage in terms of reusability and recyclability. All chemosensors are comprised of a signaling moiety and a recognition unit, that is joined either directly to each other or through

some kind of spacer or connector (Fig. 1.1). The utilization of chemosensors is referred to as chemosensing.

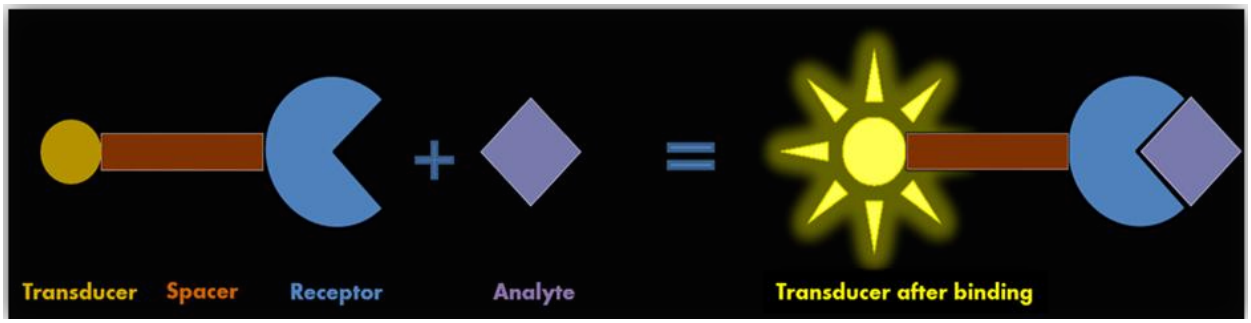

Figure 1.1: Schematic representation of Host-Guest Interaction

1.3.1. Different kind of interactions in chemosensing

In general, the action of chemosensor is governed by noncovalent interaction. The term Noncovalent" signifies vast assortment of attractive and repulsive forces. These interactions involve no formation or breaking of chemical bond. Hence non-covalent interactions are reversible in nature and often refered to non-bonded interactions. The most significant and vital non-covalent interactions and effects relating both to the host and guest as well as their surroundings (e.g. solvation, crystal lattice, gas phase etc.)[68] along with their approximate energies, are discussed below.

(a) Electrostatic interactions [ion-ion interaction (100-350 KJ/mole), ion-dipole interaction (50-200 KJ/mole and dipole-dipole interaction (5-50 KJ/mole)

(b) Hydrogen bonding (4-120 kJ/mole)] interactions

(c) π-π stacking (0-50 kJ/mole), cation-π (5-50 KJ) interactions

(d) Van der Waals forces i.e, dispersion and induction forces (< 5 kJ/mole)

(e) Close packing in the solid phase

(f) Solvophobic/hydrophobic effect

1.3.1.1. Coulombic interaction

Coulombic interaction generally implies electrostatic attraction forces between two opposite electric charges. There are three types of electrostatic interaction (i) Ion-ion interactions (Figure 1.2) are basically non-directional forces that hold together ionic compounds, but in case of ion-dipole interactions the dipole of polar molecule must be properly aligned for optimal binding

efficiency with ion. Dipole-dipole interaction results when the partially negative portion of one of the polar molecules interacts with the partially positive portion of a second polar molecule. Based on this electrostatic interaction, many receptors for cations (crown ethers, cryptands and spherands) and anions (protonated or alkylated polyammonium macrobicycles) have been employed to bind the guest in place.

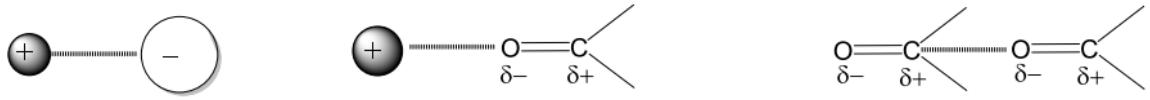

Ion-Ion interaction Ion-dipole interaction Dipole-dipole interaction

Figure 1.2: Different electrostatic interactions: (a) ion-ion (b) ion-dipole and (c) dipole-dipole

1.3.1.2. Hydrogen bonding interaction

Hydrogen bonding interaction is primarily an electrostatic force of attraction between a hydrogen atom covalently bonded to a more electronegative atom (hydrogen bond donor) with another more electronegative atom bearing lone pairs of electron (hydrogen bond acceptor). This type of interaction is generally denoted as Dn-H…Ac, where solid line indicates a polar covalent bond and the dotted line denotes hydrogen bond. When this type of interaction is observed in a single molecule, it is called intramolecular hydrogen bonding and if it occurs between two different or same molecules then it is referred as intermolecular hydrogen bonding. The chemistry of hydrogen bonding is widely utilized in host-guest complexes in nature and as well as in article molecular recognition.[69-71] Donor-acceptor ability and their different arrangement governs the strength of hydrogen bond. The secondary, tertiary and quaternary structures of biologically important proteins, nucleic acids and double helical structures of DNA.[72] C. Zhang et al. have developed an intra-molecular $NH^{\cdots}NH_2$ hydrogen bonding based chemosensor**(1)** to recognize cyanide in aqueous medium with excellent selectivity.[73] Kang et al. also have reported a chemosensor**(2)** for CO_2 through intra molecular H-bonding stabilization.[74]

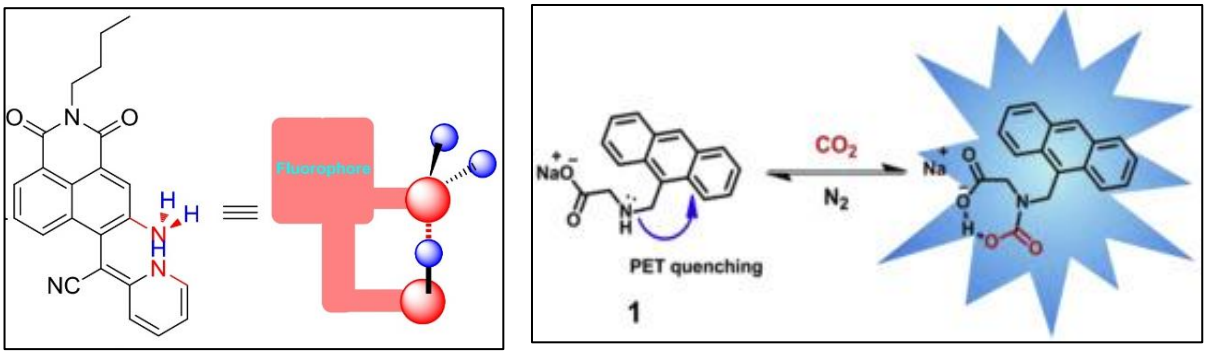

(1) **(2)**

Figure 1.3: Examples of some H-bonding based chemosensors

1.3.1.3. Van der waals forces

Van der Waals force are developed by fluctuating polarizations of nearby atoms, molecules and surface. Hydrophobic guests are coordinated into the hydrophobic cavity of guest through this kind of forces and gained an additional enthalpic stabilization. The energy associated with this force of attraction is much less than hydrogen bond.

1.3.1.4. π-stacking interactions[75]

The first synthetic application of pi stacking interactions was proposed by E. J. Corey in 1972 for the chiral reduction of ketone during the synthesis of prostaglandins.[76] Later on, organic chemists are increasingly using the concept of pi-stacking interaction in host-guest chemistry now-a-days.

1.3.1.4.1. π-π stacking interactions

Pi-conjugated organic compounds can stack through the intermolecular overlapping of p-orbitals present in the pi-conjugated system. The molecules are facing pi-pi interaction in one of the three mode, either a 'face-to-face' or 'edge-to-face' or in 'offset' geometry (Fig. 1.4). Organic compounds containing aromatic units assembled each other via aromatic interaction and make a large molecular based crystal structure in solid state molecular recognition,[77] complexation and porphyrin aggregation etc.[78] The exact nature as well as origin of pi-stacking interaction (either charge transfer or simple van der waals force) is not cleared yet. Various models have been proposed to explain the pi-stacking effect. EDA model proposed that the electronic interaction between an electron donor and electron acceptor units produce strong attraction. In 2004, Lehn and coworkers have reported a crystal structure of trinitrofluorene via aromatic pi-stacking interactions (Fig. 1.5).[79]

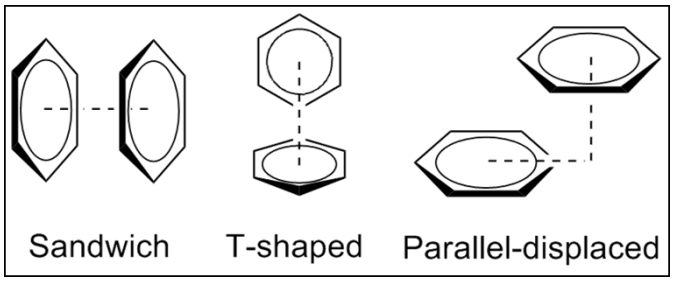

Figure 1.4: Different modes of π-stacking interactions: (a) Sandwich (face to face), (b) T-shaped (edge to face) and (c) Parallel-displaced (offset).

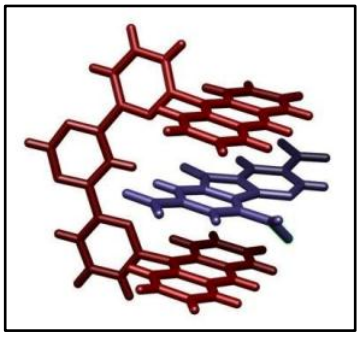

Figure 1.5: Crystal structure of trinitrofluorene bound via aromatic π-stacking interactions.

1.3.1.4.2 Role of CH-π interactions

The CH-pi interaction is one kind of weak hydrogen bonding interaction produces between a soft acid (CH_3 in an alkyl group) and soft base (pi-system) (Fig. 1.6), also plays a crucial role in molecular recognition in terms of selectivity of organic reactions, chromatographic properties and substrate specificity of bio-relevant macromolecules.[80] CH-π interaction associated with very small enthalpic energy, around 1 kcal/mol. Thus it is not easy to distinguish CH-π interaction from van der waals force, a weak nonstereospecific interactions, attractive as well as respulsive. A. Sing et al. published a chemosensor based on CH-π and π-π interaction between pyrene moieties.[81]

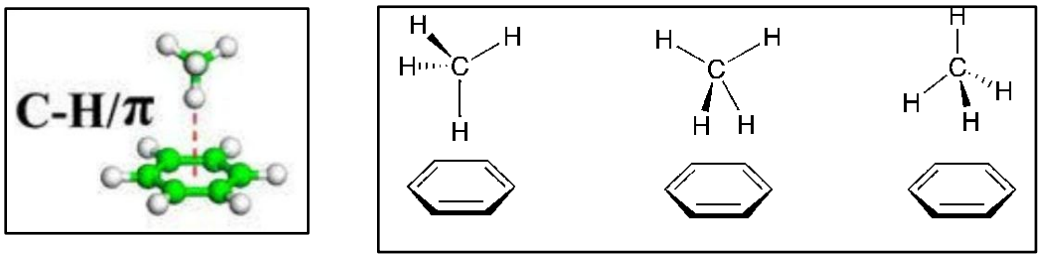

Figure 1.6: Modes of CH-π interactions

1.3.1.5. Dispersion forces

Dispersion forces are often referred as induced dipole-induced interactions, arises among the molecules possessing instantaneous dipole in the electron clouds. This force provides additional stabilization energy to the coordination of organic analytes (hydrophobic guest) into the hydrophobic cavity of receptor. One such system may be a self-assembled "tennis-ball" that can incorporate xenon atom. [82]

1.3.1.6. Solvophobic interaction

Hydrophobic interaction, also known as solvophobic interaction, is a kind of characteristics of nonpolar molecules, which can drive these molecules to assemble to form anhydrous domains in aqueous phase. It provides another possible effect to construct DNA-based nanomaterials for biomedical applications. Essentially, the origin of the solvophobic effect is the entropy effect caused by apolar solutes destroying hydrogen bonds between water molecules. This type of interaction is dynamic and greatly adjustable, which will offer the desired materials to respond more sensitively to environmental stimuli, facilitating the design of smarter biomaterials. Therefore, receptor bearing hydrophobic interior cavities can be designed to incorporate organic guest molecules in aqueous medium.

1.3.1.7. Close packing in solid phase

The theory of close packing is first introduced by Kitaigorodsky. It is a simple phenomenon to maximize the favourable isotropic van der waals interactions in the solid state crystalline structure. Organic compounds show maximum entropy as they acquire conformational flexion and chaotic motion. Opposing this property is the formation of non-covalent bonds, which minimizes the overall free energy of the system. This relationship is ascribed by Gibbs' law,

$$\Delta G = \Delta H - T\Delta S$$

1.4 Designing principle and binding patterns of chemosensors.

1.4.1. Binding with metal cations

The specificity of selected host for a particular metal ion signifies upon the ratio between the host's affinity for a targeted metal and other guest cations. Sensitivity and selectivity is the basis of

molecular recognition. Thus a successful chemosensor exhibits a strong affinity for a specific guest cation and much lower affinity for other coexisting cations. Designing a synthetic chemosensor (host for selectivity towards a cation) is governed by several factors such as size match between the host cavity and approaching cation, solvent polarity, electrostatic charge and degree of pre-organization etc. Therefore, the development of chemosensor that will be extremely specific for a distinct metal cation is a very intricate assignment (Fig.1.7).

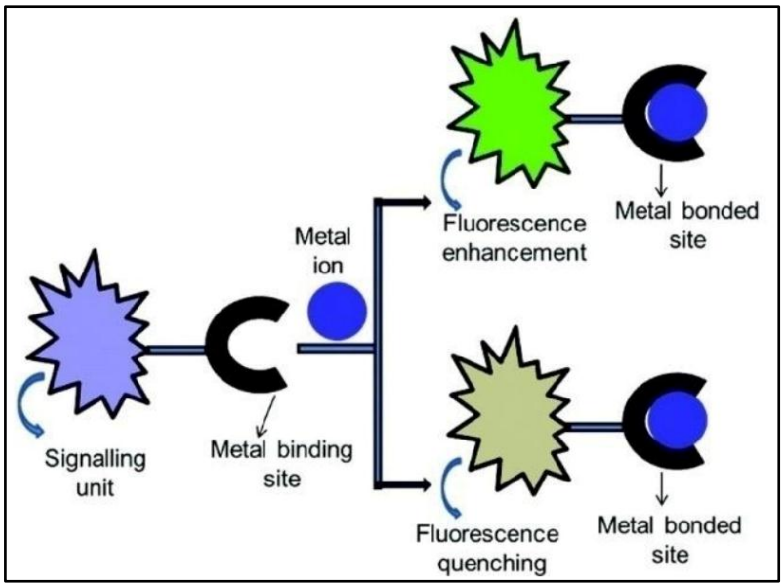

Figure 1.7: Modes of metal ion binding interaction and fluorescence response

1.4.2. Binding with anionic species

A general approach for the fabrication of anionic chemosensors is the coupling of at least two units which are the signaling subunit and the binding site.

1.4.2.1. Binding site and signaling subunit covalent attachment approach

Many chemosensors interact with anionic species through the formation of covalent bond as schematically depicted in fig. the approach of the covalent attachment of signaling subunits and binding sites as schematically shown in Figure 1.8.

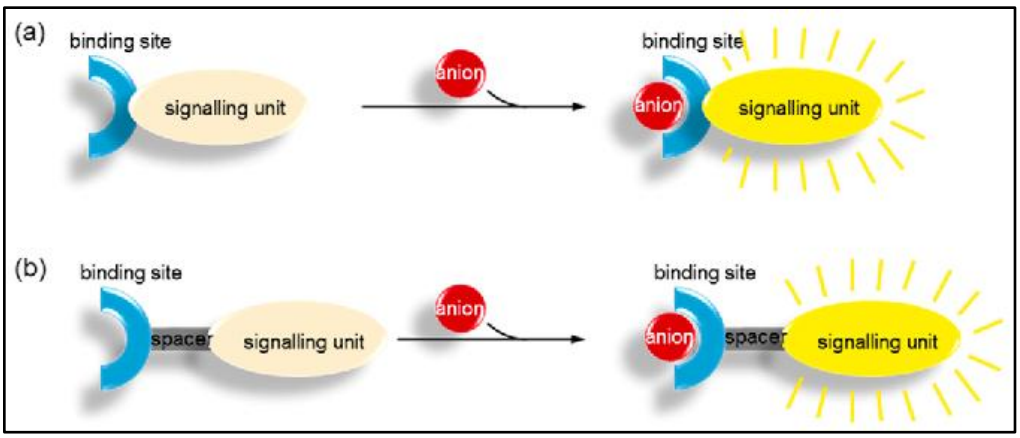

Figure 1.8: Anionic chemosensors based on the binding site-signaling subunit approach: (a) binding site is an integral part of the signaling unit (receptor); (b) binding site and signaling subunit connected covalently by a short spacer.

The coordination site of the sensor binds the approaching anion in such a way that it triggers the signaling subunit to change its photophysical characteristics either in terms of color, giving rise to variations (chromogenic chemosensor) or in its emission property (fluorogenic chemosensor).

1.4.2.2. Displacement approach

In this case, both signaling subunit and binding site are attached coordinatively to form a molecular ensemble. Then, when a guest anion is added to the solution of the chemosensor containing the binding site-signaling unit ensemble, a displacement reaction takes place; the binding site binds the target anion coordinatively whereas the signaling subunit reverts back to the solution retrieving its non-coordinated spectroscopic property (Figure 1.9).

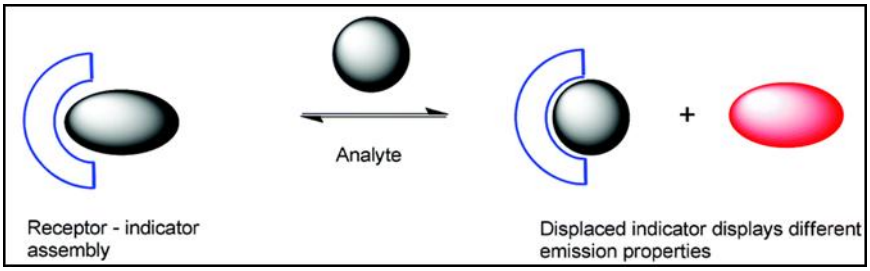

Figure 1.9: Anionic chemosensor based on the displacement approach

If the photo-physical characteristics of the signaling subunit in the free form of molecular ensemble are different to those in its non-coordinated state, the anion binding process is coupled to a signaling event and can be visualized through measuring the change in photo-physical

properties. The specificity can be achieved by opting for an indicator binding site couple with a formation of stability constant larger than that between the signaling unit and the potentially interfering anions.[83]

1.4.2.3. Chemodosimetric approach

Chemodosimeters are used to recognize analytes through the concomitant irreversible transduction of an observable signal. The action of chemodosimeter is associated with the chemical reaction of analytes with molecular probes through irreversibly breaking and making of covalent bonds. This process leads to formation of new product differing from the starting chemodosimeter concomitantly with optically different features.[84,85] The concept of 'chemodosimeter' actually came into the field of molecular recognition as an anion sensing approach. A compound fabricated for a specific sensing of a particular analyte actually takes part in chemical reactions with it, which is usually irreversible, resulting into changes in fluorescence or color.[86,87] That compound is termed as a chemodosimeter. Therefore, the action of chemodosimeter towards an analyte is based on a specific irreversible reaction thereby making the probe highly selective and anti-interferring.

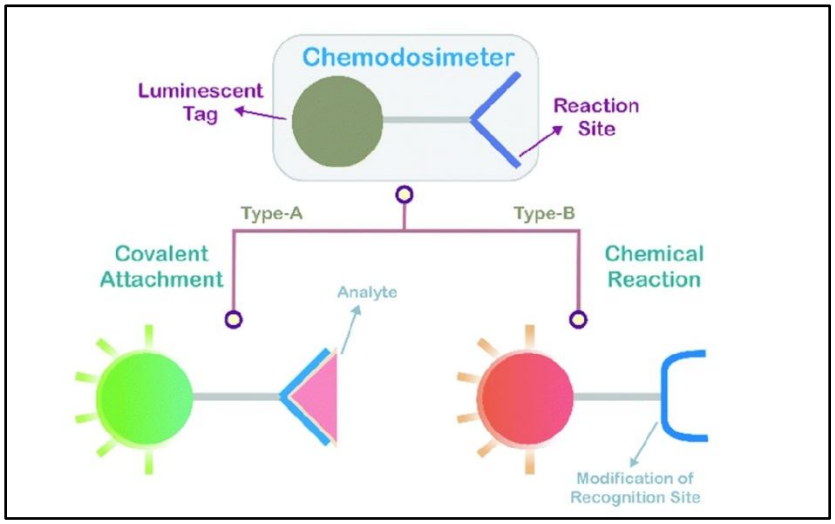

Figure 1.10: Chemoreactands or chemodosimeters: In the first sequence, the anionic analyte interacts with the chemodosimeter and remains covalently attached and in the second sequence, the anion catalyzes a chemical reaction.

Fig. 1.10 schematically represents two examples of chemodosimeter: one in which the anion interacts with the chemodosimeter retaining covalently bonded to the product and the other in which the anionic species catalyzes a chemical process.

1.5. Different fluorogenic principles of sensing

Fluorogenic chemosensors are one kind of molecular machines which changes its luminescent characteristics upon binding with targeted analytes. It also comprises of two sub units: a binding site subunit and a signaling subunit (Fluorophore). Binding site coordinates guest analyte and signaling subunit transduce the emission response. Fluorescence response is one of the superior optical signaling process in chemosensor chemistry. It has enormous applications in diverse fields due to its high sensitivity and is able to detect very low level concentration of analytes present in the medium. It is an exceptionally versatile tool of spectroscopy that can even detect small change in emission in real time. Based on the mode of excitation, the terms chemoluminescence, radioluminescence, electroluminescence, sonoluminescence, etc. are used. In a fluorescent compound, the absorption of light at a certain wavelength results in an immediate fluorescence of light at a longer wavelength.[88]

1.5.1. FRET (Fluorescence resonance energy transfer) mechanism

FRET mechanism based sensing system is very appealing due to its simplicity of building ratiometric fluorescent systems. In this mechanism, energy is non-radiatively transferred from excited donor fluorophore to the acceptor fluorophore ($D^* + A \rightarrow D + A^*$) by means of intermolecular long-range dipole-dipole coupling (Fig. 1.11).[89] The extent of energy transfer is dependent on the magnitude of spectral overlap between the absorption spectrum of one fluorophore (Acceptor) and emission spectra of other fluorophore (Donor). The spectral overlap is defined by the Förster distance and the rate of energy transfer $k_t(r)$ is follows:

$$k_t(r) = (1/\tau_d)(R_0/r)^6$$

where 'r' is the distance between the donor (*D*) and acceptor (*A*) and 'τ_d' is the lifetime of the donor in absence of energy transfer.

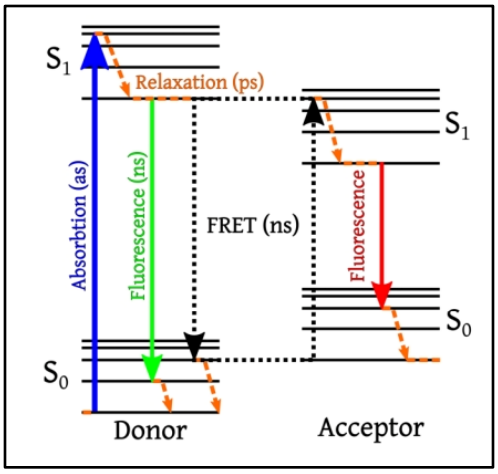

Figure 1.11: General FRET based signaling mechanism.

In most of the cases, FRET process is become active when the probe interacts with a specific guest analyte. In 2018, Zhang et al. fabricated a rhodamin-B containing fluorescent and colorimetric receptor for the sensitive and selective detection of picric acid.[90] Upon addition of picric acid, the probe solution displayed a noteworthy emission change followed by a distinctive color change from colorless to pink which can be attributed by an intramolecular fluorescence resonance energy transfer (FRET) effect. As shown in the diagram in Figure 1.15, the spiro-lactam ring in the receptor was opened in presence of picric acid and hydrogen bond was developed between the probe and picric acid. The formation of the delocalized xanthene pattern results in the notable color changes which was from colorless to pink and the emission enhancement owing to the intramolecular FRET process of the probe solution (Fig. 1.12).

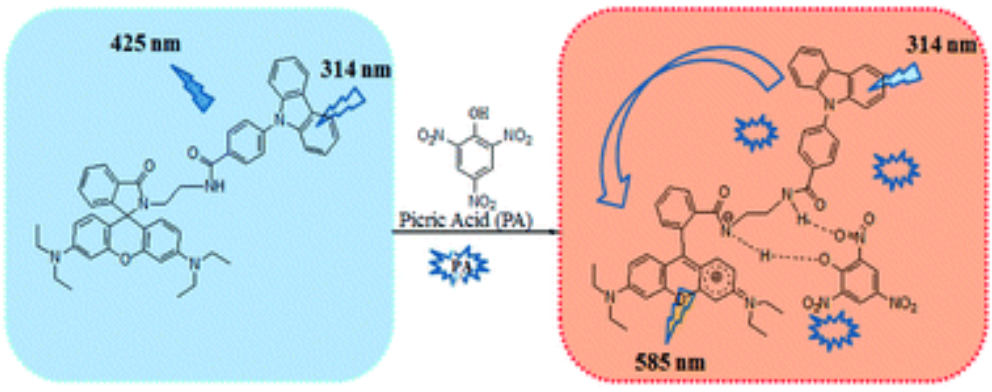

Figure 1.12: Signaling mechanism based on FRET process by Zhang et al.

In 2022, Behera et. al. synthesized a pyrene-rhodamine FRET couple which functions as a detector for picric acid (Fig. 1.13). As in other rhodamine based probes in this case also the

rhodamine part acts as the acceptor and the pyrene moiety acts as the donor in FRET. The Pyrene-rhodamine FRET couple is spaced by a 1,3- diamminopropane linker with high spatial flexibility which allows optimum receptor-analyte interaction. It was also found from the lifetime data and steady state that the FRET occurs through-space by singlet-singlet excitation energy transfer as a mode of dipole– dipole interaction between the excited donor (D*) and acceptor (A) couple. Among the dual fluorescence output channel, i.e., the pyrene (at 428 nm) and the rhodamine (at 578 nm), the peak at 428 nm increases then decreases steadily upon incremental addition of picric acid and a new peak at 578 nm noticed only upon addition of 2.0 equivalent of the analyte.[91]

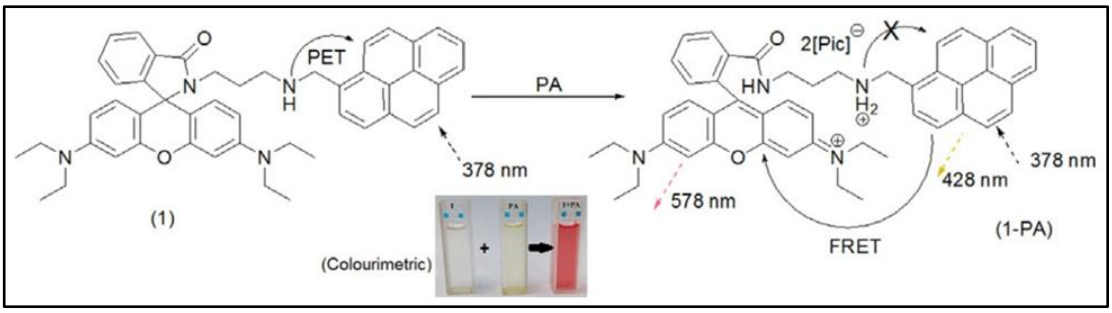

Figure 1.13: Dansyl to Rhodamine FRET 'turn-on' upon spirolactam ring opening (Behera et. al.)

1.5.2. PET (Photo-induced electron transfer) process

PET process has been extensively studied and widely involved for sensing purposes of various probes towards targeted analytes.[92,93] In general, a molecule shows fluorescence when an excited electron from lowest unoccupied molecular orbital (LUMO) goes to highest occupied molecular orbital (HOMO), releasing excess energy. It could be possible that an orbital from another molecule or another part of the same molecule might have energy between that of the HOMO and that of the LUMO of the fluorophore. This 'alien' orbital may be empty or full as a donor group. In both cases, PET process can be happened. If this orbital is full, a PET process from this full orbital to the HOMO of the fluorophore can occur followed by a further electron transfer from the LUMO of the fluorophores to the external orbital retrieves the stable ground state (Fig. 1.14). A similar process can also happen when the vacant alien orbital lies between the HOMO and LUMO of the fluorophore. In this case, a PET process from excited LUMO to the empty alien orbital can happen followed by a sequential electron transfer from this orbital to HOMO of the fluorophore. Thus fluorescence quenching is observed again. If a molecule contains both donor unit and

acceptor moiety, then they must be segregated by a spacer that is small enough for efficient electron transfer, but long enough to decrease the degree of electronic delocalization between them.[94] The strategy of molecular design of a chemosensor is completed in such a way that the approaching analyte bind with it and induce the emergence or the divergence of energy level between the HOMO and the LUMO of the fluorophore causing quenching or enhancement in emission intensity. The thermodynamic basis for PET has been first ascribed for intermolecular systems by the pioneering work of Weller.[94]

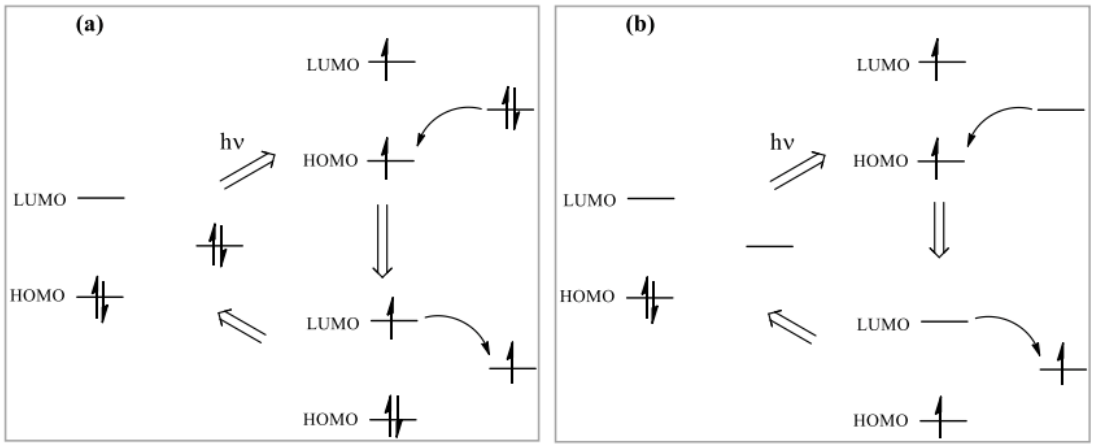

Figure 1.14: (a) PET process with the participation of HOMO and LUMO of the fluorophore and an external molecular orbital. (b) PET process with the participation of the HOMO and LUMO of the fluorophore and an empty external molecular orbital.

In 2020 Pavel A. Panchenko et. al. reported a Zn^{2+} chemosensor based on PET turn-off upon complexation (Fig. 1.15). The receptor comprised of two distinct units among which napthalimide moiety is pretty common in previously reported PET based fluorescence chemoreceptors.[95] In the PET process occurring in the free receptor, the electron donation occurs from the filled HOMO which is localized on the the salicylidine moiety and the electron accepting half-filled HOMO (-1) belongs to the napthalimide chromophore. This non-radiative process is disrupted in the Zn^{2+}-complex due to donation of electron pair on imine nitrogen to Zn^{2+} ion. Subsequently fluorescence gets turned on upon complexation with zinc ion.[96]

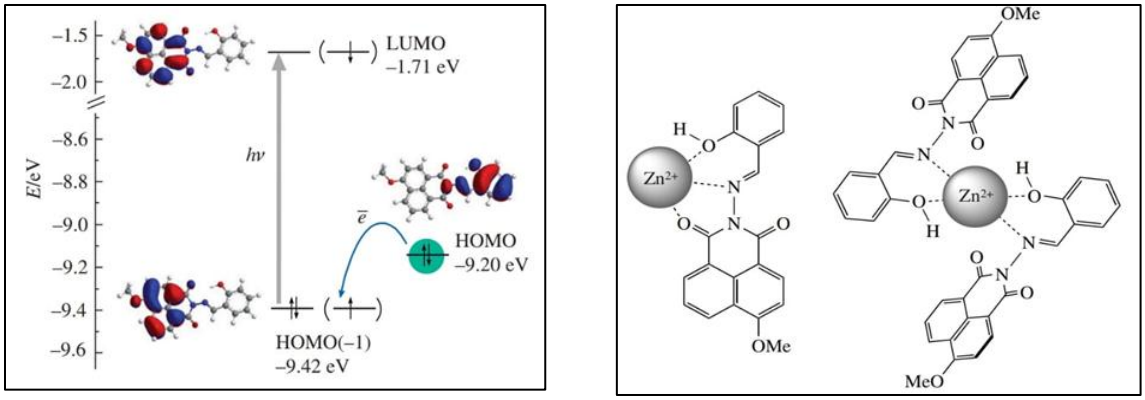

Figure 1.15: a) MO diagram based on energy calculations showing PET process in the free receptor. And b) two proposed modes of complexation of the receptor and Zn^{2+} reported by Pavel A. Panchenko et. al.

Gangopadhyay et al. have published a simple, targeted Betti base, BB for the chemodosimetric fluorescent sensing of harmful phosgene gas based PET process with appreciably low detection limit of 0.40 μM.[97]

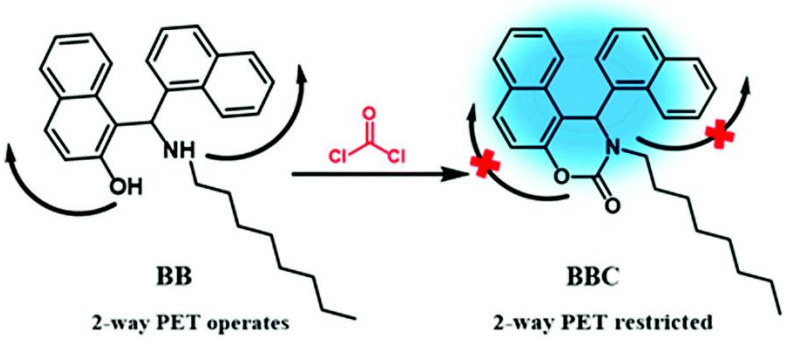

Figure 1.16: PET based phosgene sensor by A. Gangopadhyay et al.

1.5.3. ICT (Intramolecular charge transfer) process

This process is mostly observed in the chemosensors which detect the analytes by 'naked eyes' i.e. colorimetrically. ICT based chemosensor comprised of an electron donating unit and an electron accepting moiety connected directly through a π-linker (Fig. 1.17). A charge transfer process occurred in this chemeosensor from donor unit to acceptor unit. Upon exposure to analyte, the electron transfer process is prohibited, causing in the prohibition of ICT followed by significant shifts in the absorption and fluorescence emission bands. Colorimetric chemosensor will be extremely user friendly in the term that it does not require extensive calibrations and sample preparation and can be operated even by less skilled personnel. Although the use of a colorimetric

detection method is a less advanced approach, it is easy to use in comparison with other spectroscopic methods and it can also provide with a simply visual result for "naked-eye" detection. Therefore, this technique is fascinating as a sensing technique.[98] and widely used in molecular recognition. To date, many ICT based chemosensors have been reported. For example,

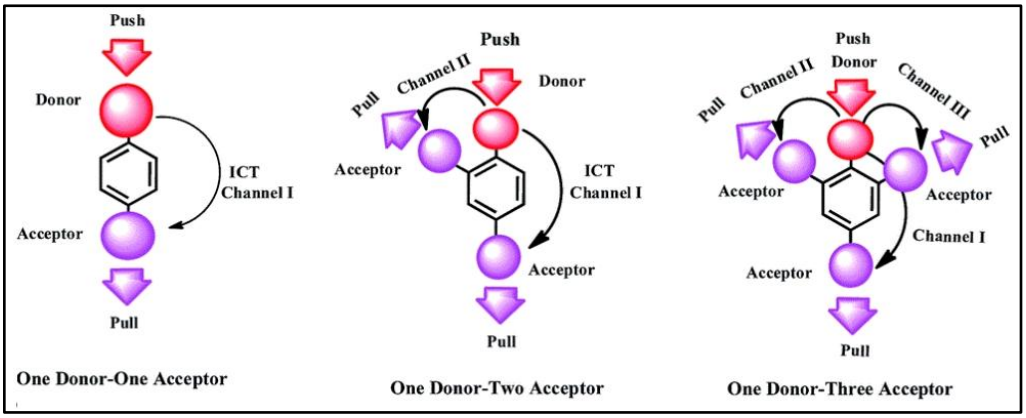

Figure 1.17: ICT process in organic probes having electron withdrawing and electron donating moiety.

Liu et al. reported a colorimetric and ratiometric fluorescent sensor with anthracene carboximide as fluorophore and ethylenediamine group as recognition moiety for phosgene detection in solutions and in the gas phase based on ICT mechanism (Fig. 1.18). The probe, AC-6ED taps phosgene through intramolecular cyclization reaction to afford color and fluorescence color change.[99]

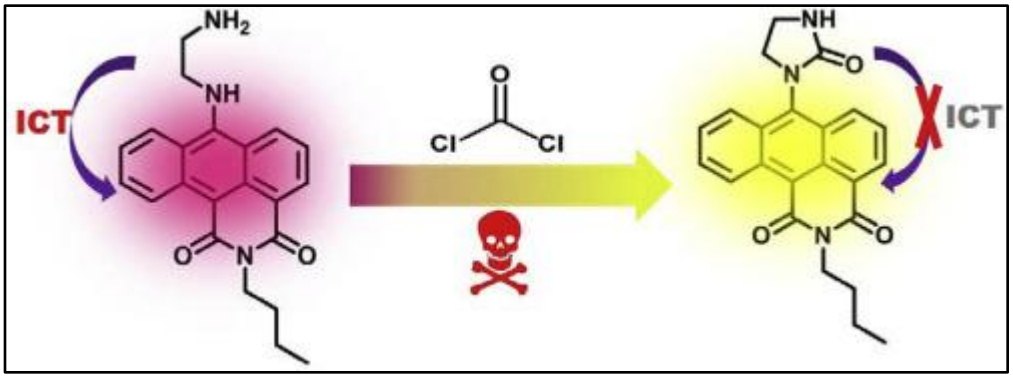

Figure 1.18: ICT mechanism based phosgene detection by Liu et al.

Patra et al. developed a carbazole-benzothiazole based chemodosimeter for chromo-fluorogenic detection of CN^- based on ICT mechanism in DMSO-water (4/1, v/v, pH=7.2) solution (Fig. 1.19). Here, the nucleophilic addition of cyanide cut off the intra-molecular charge transfer (ICT) process responsible for the photophysical changes.[100]

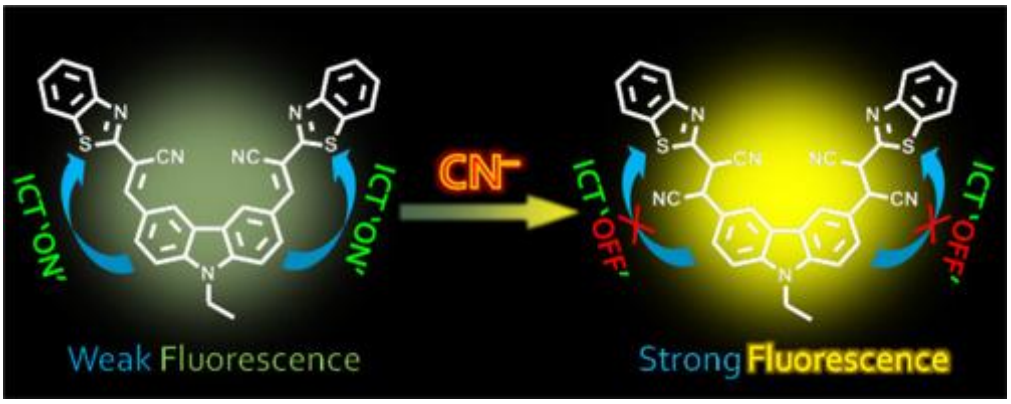

Figure 1.19: An ICT based cyanide detection by Patra et al.

1.5.4. ESIPT (Excited State Intramolecular Proton Transfer) mechanism

The ESIPT mechanism is mainly observed in the chromophores which bears the exclusive characteristic of the keto tautomer.[101] The ground state of the ESIPT based chromophores usually exist in the *cis*-enol form and stabilised through the intramolecular hydrogen bonding (Fig. 1.20). Upon excitation, the 1st singlet excited state of the enol form gets populated according to Frank-Condon principle. After that, due to a fast ESIPT process in the molecule, the excited singlet state of the *cis*-keto form gets populated. The *cis*-keto form of the chromophore is also stabilized via intramolecular hydrogen bonding. The excited State Intramolecular Proton Transfer process is a much faster process compared to the fluorescence radiative decay. Therefore, the ESIPT based chromophores mainly exhibit fluorescence due to the keto tautomer with a few exceptions. The schematic of the mechanism is depicted in Scheme 1.5. Many researchers have paid attention on ESIPT based chemosensor due to its application in several areas such as luminescent materials,[102] molecular probes,[103] logic gates[104] etc.

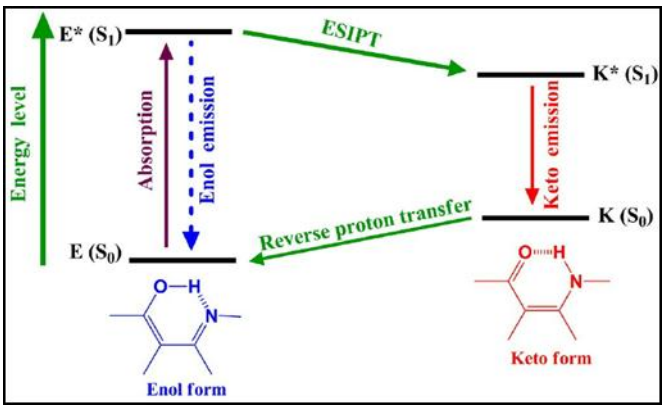

Figure 1.20: Principle photophysics of the ESIPT process

Recently in 2019, Kaur and co-workers developed a new naphthalene based fluorescent chemosensor for sequential recognition of Hg^{2+} and cysteine based on ESIPT sensing mechanism.[105] Due to the presence of the hydroxyl unit as a functional group in the naphthalene based probe, the tautomerization process can be observed in it leading to the ESIPT (excited state intramolecular proton transfer) phenomenon within the sensor as illustrated in Figure 1.21 which is responsible for the fluorescence quenching.

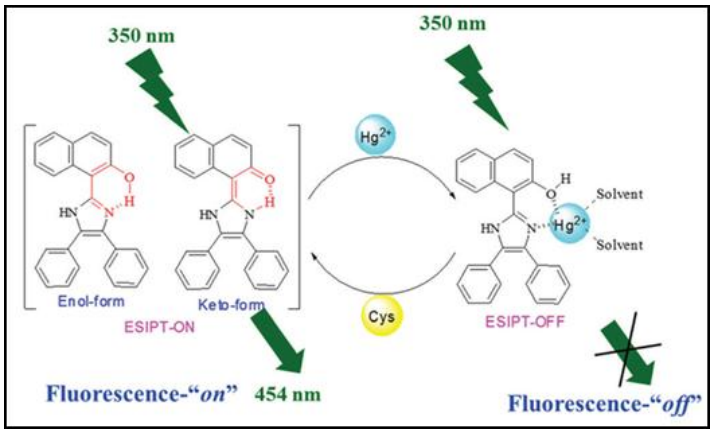

Figure 1.21: Naphthalene based ratiometric chemosensors depending on ESIPT process by Kaur et al.

In 2021, Zeng et al. published a new fluorescent (**APQ)** sensor for ultrasensitive detection of phosgene in solution and the gas phase. The probe exhibits very weak fluorescence in acetonitrile due to the free rotation of the 2-aminophenyl moiety (Fig. 1.22). After binding with phosgene, **APQ** is converted to a new restricted intramolecular motion adduct **APQU1**within very short time period (less than 20 s) and shows low detection limit (0.16 ppm).[106]

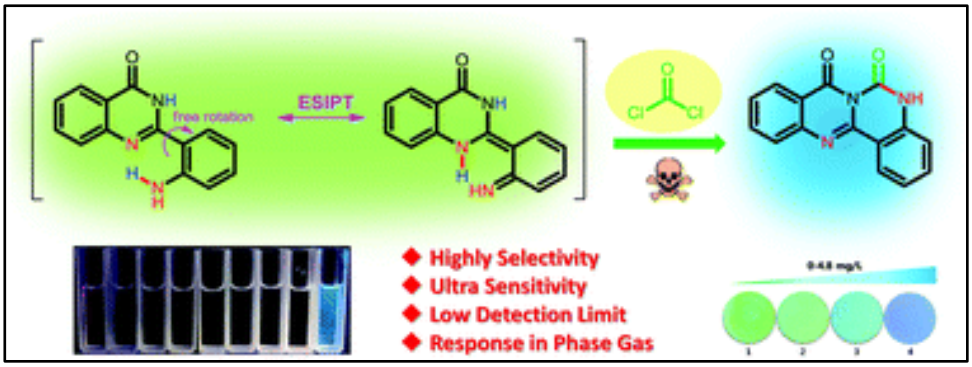

Figure 1.22: Lethal pulmonary agent phosgene detection based on ESIPT process by Zeng et al.

1.5.5. Chelation enhanced fluorescence (CHEF) effect or rigidity effect

Although there are no strong evidences of the real existence of CHEF effect, this process has been employed many times to support the fluorescence enhancement of a chemosensor upon coordination with ions. As a result of the ion complexation, the rigidity gets increased in the formed complex, leading the non-radiative decay from the excited state less probable; consequently, the fluorescence intensity enhances. There are many examples where chelation enhanced fluorescence effect has been used to establish the sensing mechanisms of newly fabricated chemosensors.

In some cases, upon complexation with an appropriate metal cation, a large chelation-enhanced fluorescence (CHEF) effect is noticed because the chelation overrules the PET process and results into a 'turn-on' fluorescence. As for example, in 2018, Gupta et al. reported a "turn-on" fluorescent receptor for selective detection of aluminum in MeOH solution.[107] The sensor exhibits the appearance of a new absorption band at 405 nm and an emission enhancement at 505 nm via the CHEF effect, and restricting the PET phenomenon with a sufficiently low LOD value of 28 nM. The sensing mechanism is depicted in Figure 1.23.

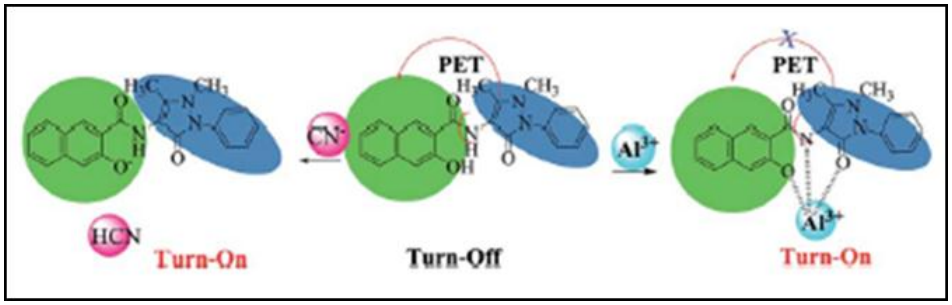

Figure 1.23: Schematic representation of sensing mechanism of an Al^{3+} sensor by Gupta et al.

Another work on an Al^{3+} sensor by a rhodamine and azobenzene based sensor was published by Mabhai et al. in 2018.[108] The sensing of aluminium may be due to the CHEF as well as PET process due to the rigidity of the structure (Figure 1.24).

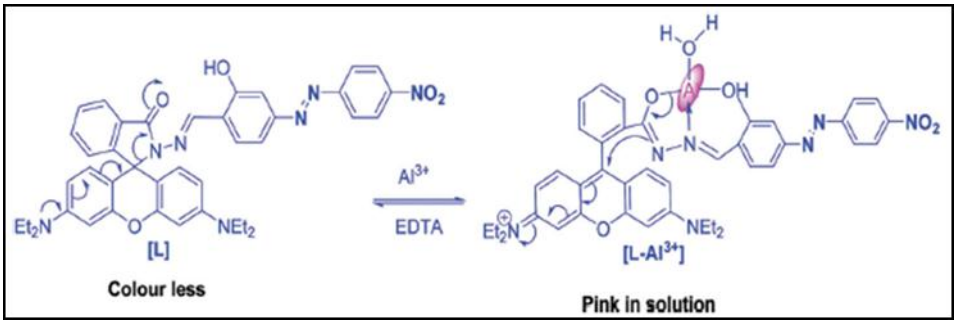

Figure 1.24: Probable sensing pattern of the Al^{3+} sensing probe by Mabhai et al.

1.5.6. Monomer excimer formation

An excimer is a short life span molecule formed through the interaction of two molecules, one of which is in the excited state and another is in the ground state (Fig. 1.25). An important feature of this process is that the emission spectrum is red shifted with respect to that of monomer and in some cases, the dual emission of the monomer and excimer is noticed. Therefore, the excimer formation upon interaction with analyte causes in the sensing by simple monitoring of the emission excimer band. To date, many research groups have developed chemosensors based on the emission excimer property.

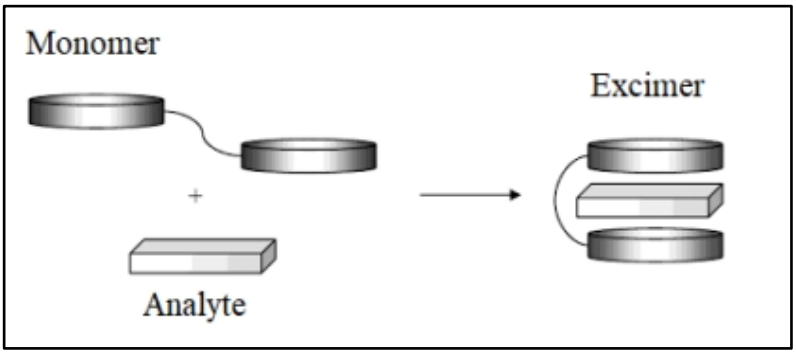

Figure 1.25: Coordination with an anion induced spatial proximity between the two fluorophores and dual emission from the monomer and the excimer.

In 2019, J. B. Li et al. have developed a new chemosensor for mercury based on the excimer emission of the anthracene.[109] J. Rodr'iguez-Lavado et al. have reported another pyrene excimer based probe for the recognition of Ag^{+} and Hg^{2+} (Fig. 1.26).[110]

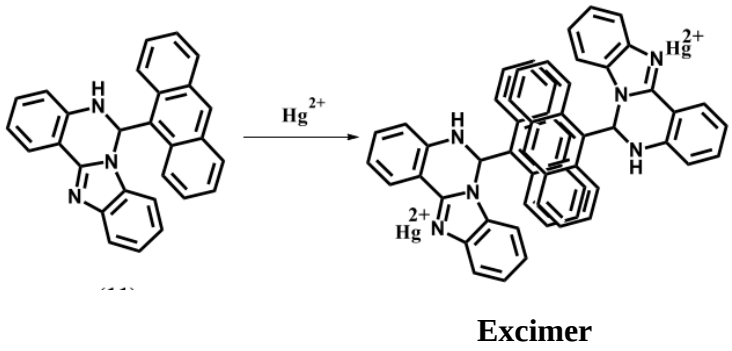

Figure 1.26: Eamples of some monomer-excimer formation based chemosensors

1.5.7. Fluorescence quenching

A number of chemosensors operates through the decrease in fluorescence intensity, which is referred to as quenching. This process occurs when molecule get relaxed from excited state to ground state via non-radiative decay. There are basically two types of quenching processes: (1) collitional or dynamic quenching and (ii) static quenching.

1.5.7.1. Collisional quenching

Collisional quenching happens when the excited-state fluorophore is promoted to ground state through the release of energy upon contact with some other molecule in solution phase, called quencher. Jablonski diagram depicted in Figure 1.27 well represents the quenching of fluorescent intensity due to collision. The decrease in fluorescence intensity due to collisional quenching is ascribed by Stern-Volmer equation:

$$F/F_0 = 1 + K\,[Q] = 1 + kq\tau_0[Q]$$

where K is the Stern-Volmer rate quenching constant, τ_0 is the unquenched lifetime, kq is the bimolecular quenching constant and [Q] is the quencher concentration. The constant K mainly represents the effectiveness of the fluorophore to a quencher. A diversity of molecules like oxygen, amines, halogens etc. can act as fluorescence quenchers. Quenching by heavy elements occurs because of the spin-orbit coupling and inter-system crossing to the triplet state. Collisional quenching also reduces the lifetime of the fluorophore.

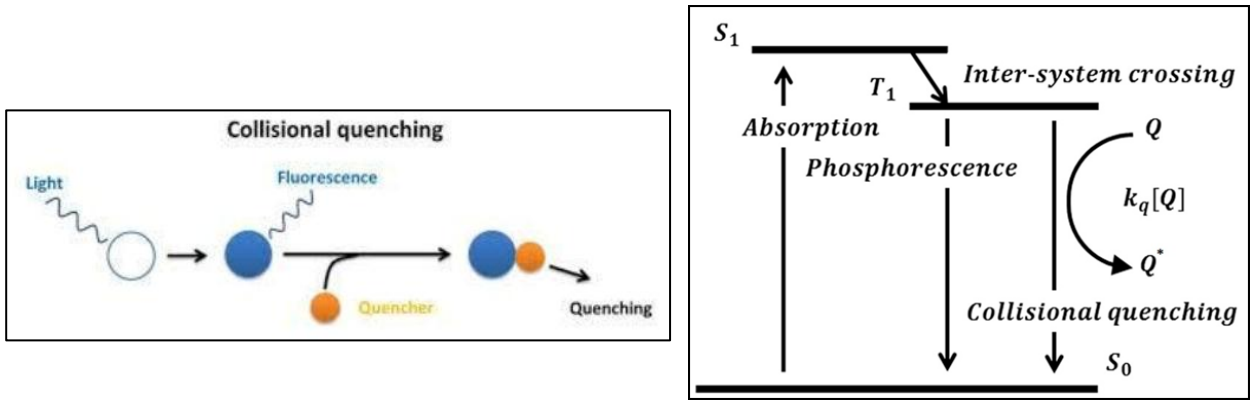

Figure 1.27: Simple mechanism showing collisional quenching (left side) and Jablonski diagram showing collision quenching (right side)

1.5.7.2. Static quenching

In case of static quenching mechanism, the fluorophore molecule can form a stable complex with an additional compound. If this ground-state is non-emissive then the fluorophore is called statically quenched. In such cases, the dependence of the fluorescence as a function of the quencher concentration is related through the following relation:

$F_0/F = 1 + K_a[Q]$, where Ka is the binding constant of the complex.

Unlike the dynamic quenching, static quenching (Figure 1.28) will not decrease the lifetime of the sample as the fluorophore molecules being non-complexed are able to emit after excitation. So they will have normal excited state properties. So the quencher is basically reducing the number of fluorophores which can emit, as a result, the emission from the sample is diminished.

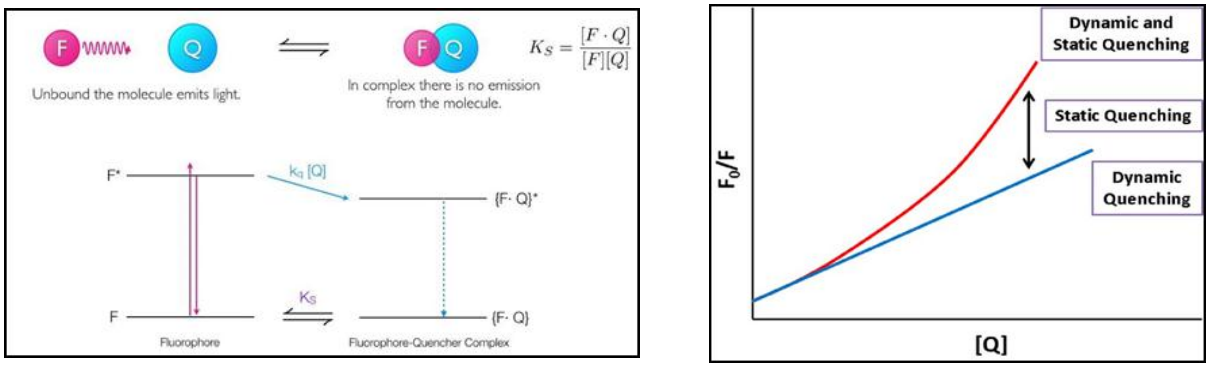

Figure 1.28: A schematic of Stern-Volmer plot was shown displaying different forms of fluorescence quenching; Stern-Volmer plot showing different fluorescence quenching.

1.6. Classification of chemosensors

Based on the working principles of transducer, chemosnsors may be classified into two major groups: (i) "physical" and (ii) "chemical" sensors. They also can be divided into several sub groups as optical, electrical, electrochemical, magnetic, mass sensitive and thermometric devices.[111]

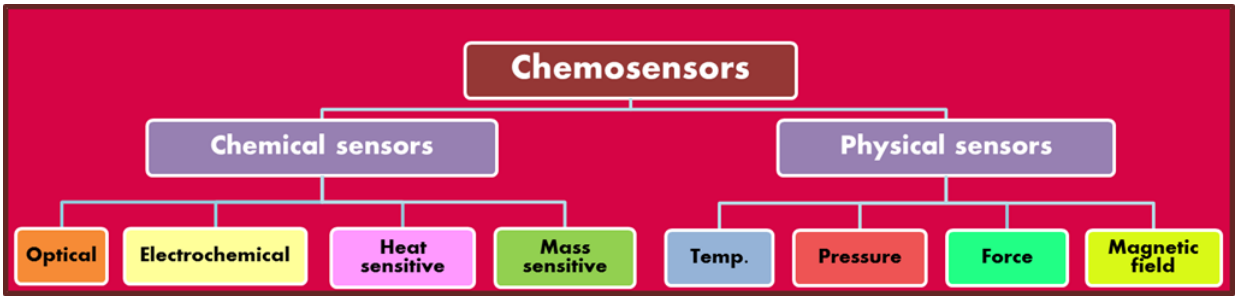

1.7. Features of an ideal chemosensors

Always an efficient chemosensor is highly desired in the field of molecular recognition. The characteristics of an ideal chemosensor are pointed below:

1. The sensor should be very specific in sensing.
2. Upon binding with guest analytes, the change in photophysical properties of guest should be very strong.
3. The sensor should produce an optical signal of high signal-to-noise ratio.
4. The detection limit of the probe should be up to very lower concentration of the analytes.
5. Synthesis of probe should be facile, simple and cost-effective.
6. The receptor should be stable over time for the storage purpose.
7. Sensor should be low toxic and should be synthesized from low toxic components.
8. Sensor should detect guest analytes rapidly.
9. The optical response of sensor upon exposure to guest should be described by a fairly uncomplicated mathematical equation.

1.8 Application of chemosensors and chemodosimeters

1.8.1. Optical biosensor

An optical biosensor mainly consists of an immobilised bio-component coupling with transducers and presents a synergistic combination of biotechnology and microelectronics.[112] The application of optical biosensors for the monitoring of heavy metal ions has been developed based on the

molecular recognition of biological systems. Protein (metal-binding protein, antibody and enzyme) and whole cell (genetically and naturally engineered microorganism) have all been utilized to develop sensors for heavy metal cations.[113-117] This is because generally heavy metal ions can play a role as catalysts or inhibitors by chemical reaction with binding units of protein as well microorganisms in the cells.[118] A number of enzymes including glucose oxidise,[119] cholinesterase,[120,121] urease,[122] protein,[123] and etc. have been utilized for the development of optical biosensors. Jiang and coworkers reported a biosensor for the detection of Hg^2 in aqueous solution based on the inhibiting the reaction of urea to urease upon addition of mercury.[124] Thus the detection of Hg^{2+} information is transduced by pH or ammonia or carbon dioxide measurements. Since mercury binds with the thiol and methyl-thiol group of enzyme thus significantly decrease the activity of enzyme.[125] Therefore, the studies of inhibition by mercury was achieved using an optical fiber biosensor configuration, where the pH change due to the bio-catalytic hydrolysis of urea was recorded at the wavelength of 615 nm spectroscopically.

$$(H_2N)_2CO + H_2O \xrightarrow{\text{Urease}} .2NH_4^+ + HCO_3^- + OH^-$$

1.8.2. Application through live cell bio-imaging

To date, various chemosensors have been proposed and used for *in-vitro* cell imaging studies to investigate whether the developed chemosensors are capable of recognition of various ions and compound in the intracellular region. For example, S. Das et al. and co-workers successfully developed a triphenylamine and rhodamine-B (donor–acceptor) hybrid switch (TPRH) (Fig. 1.29).

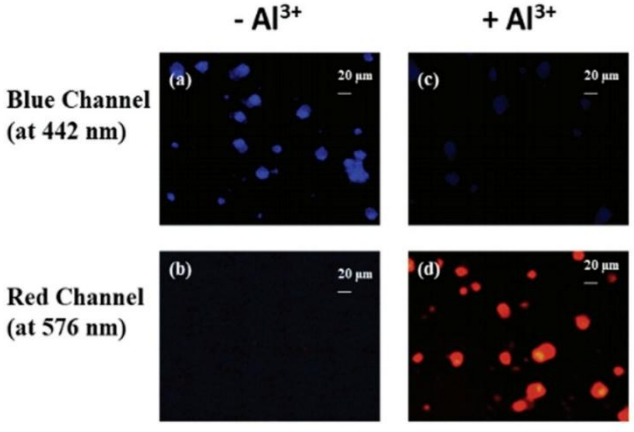

Figure 1.29: Fluorescence images of human PBMCs treated with (c and d) and without (a and b) Al^{3+} (Das et al.)

They reported that the probe in hand (TPRH) is non-toxic and can be successfully engaged to detect the Al^{3+} ion in human peripheral blood mononuclear cells (PBMCs). They evidenced a significant ($p < 0.05$) shift from blue to red fluorescence when aluminum was added to the cell suspension, thus proving the probe, TPRH as a potential candidate to recognize intracellular Al^{3+}.[126] Subsequently in 2022, P. Das et al. developed a piperazine based Schiff base chemosensor for the recognition of Zn(II), Cu(II) and F^-. The cellular imaging studies has been carried out with HeLa cells which have been incubated with the bare chemoreceptor(HL) and subsequently with Zn(II). The addition triggers blue fluorescence in the intra cellular region indicating that the probe can detect Zn(II) in the intracellular environment (Fig. 1.30).[127]

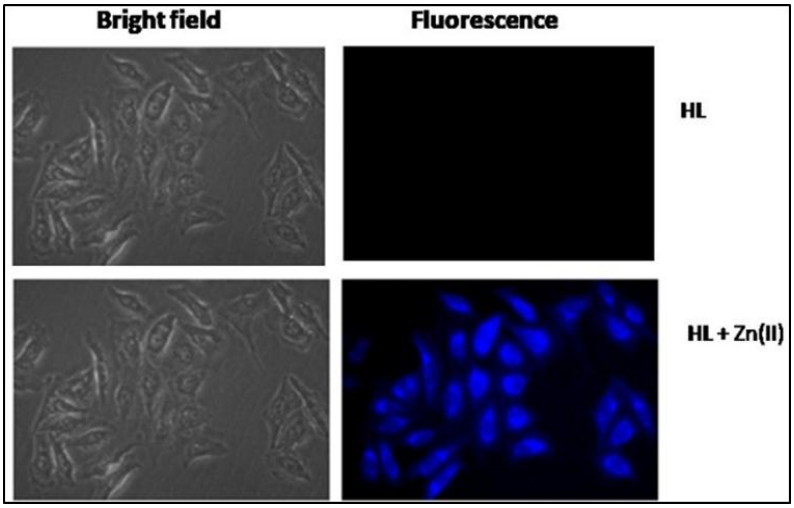

Figure 1.30: Fluorescence microscopy images of HeLa cells incubated with HL and HL- Zn(II) by P. Das et al.

L. Hou et al. reported a novel receptor for the specific detection of cyanide ions in neutral aqueous solution (HEPES buffer, pH 7.4) (Fig. 1.31). This probe exhibits a rapid response via visible colorimetric and fluorogenic changes toward cyanide, allowing for ratiometric sensing of CN^- in aqueous media. The compound **L** is the first mitochondria-targeting probe for CN^- detection and can be utilized for sensing CN^- in living cells with dual channel ratiometric fluorescence imaging.[128]

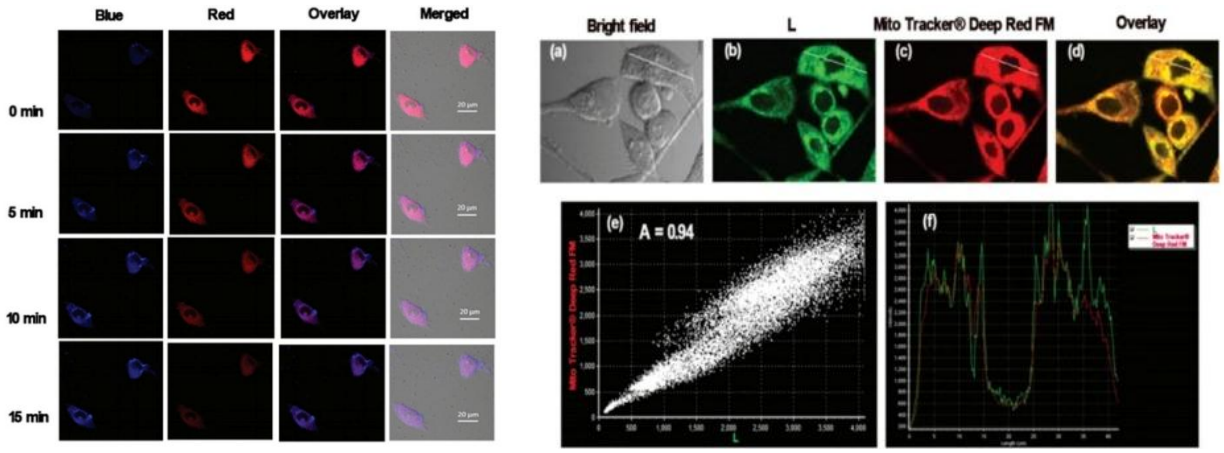

Figure 1.31: Dynamic fluorescence imaging of SMMC-7721 cells incubated with probe at cetain concentration of cyanide (left side) and Pseudo-colour confocal fluorescence image of probe by Hou et al. (right side)

In 2019, Ali et al. published a colorimetric and ratiometric fluorescent probe TPOD for efficient and rapid detection of real nerve agent simulant DCP in aqueous acetonitrile solution (Fig. 1.32). Moreover, the sensor was successfully used in cellular imaging of DCP containing bio-samples.[129]

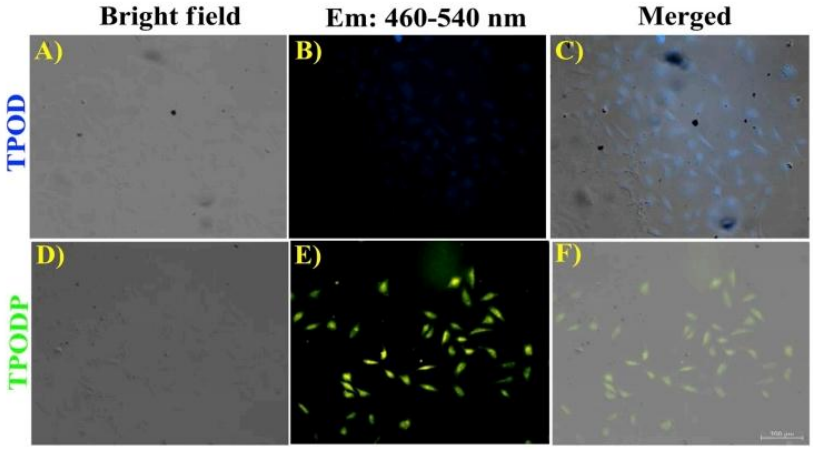

Figure 1.32: Confocal microscopy imaging of probe (TPOD) and probe-DCP adduct (TPODP)

1.8.3. Application through Dip-stick experiment

For visual detection of various compounds and ions, we have performed a proficient portable method called dip-stick in which the probe can act as a portable kit showing its sensing property towards CN^- in solid state too. So to execute this experiment, few thin-layer chromatography

(TLC) plates were prepared using Whatman filter papers or TLC plate and they are immersed into probe solution and then kept for some time so as to evaporate the solvent in air. When the probe coated test kit comes into contact with the guest analyte, the visual color or fluorescence colour change was observed when exposed in ambient light as well as under UV light respectively. Till now, numerous colorimetric, fluorometric chemosensors have been reported and successfully applied for qualitative identification of analytes through this experiment.

Recently, in 2023, Zhao et al. reported a FRET-based ratiometric fluorescent probe for mercury ion detection in aqueous solution. They have established a test strips experiment for qualitative identification of Hg^{2+} ion in different concentration.[130]

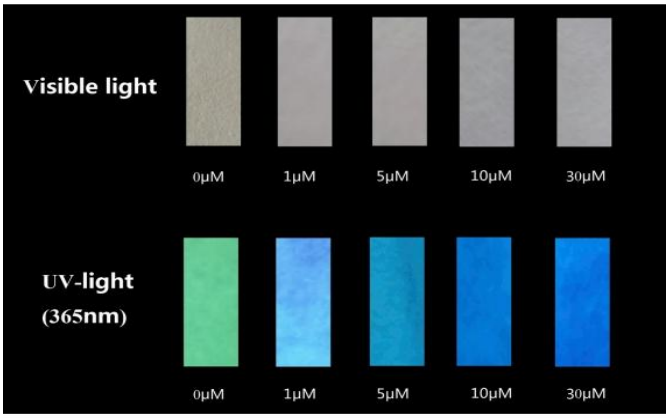

Figure 1.33: The color change of the test strips loaded with APS-NA under visible light and ultraviolet light (Zhao et al.).

Again in 2021, Padghan et al. synthesized an alkoxy-substituted 1,3-indanedione based chemodosimeter for ultrasensitive and selective sensing of CN^- (Fig. 1.34). They were also established simple, easy to prepare low cost paper strips for visual detection of cyanide.[131]

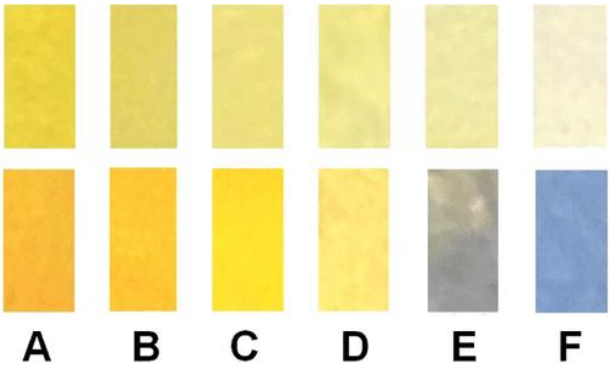

Figure 1.34: Photographs of sensor upon addition of cyanide (mM) on filter paper under natural (top) and UV light (bottom): (A) 0, (B) 0.2, (C) 0.4, (D) 0.6, (E) 0.8, (F) 1.0

H. Xu et al. reported a naphthalimide-based fluorescent sensor for the highly selective and sensitive recognition of nerve agent simulant DCP in both liquid and solid state. They also executed that probe-coated dip-stick can be served as a highly selective protocol for sensing DCP vapour against other vapour of relative coexisting nerve agents mimic analytes (Fig. 1.35).[132]

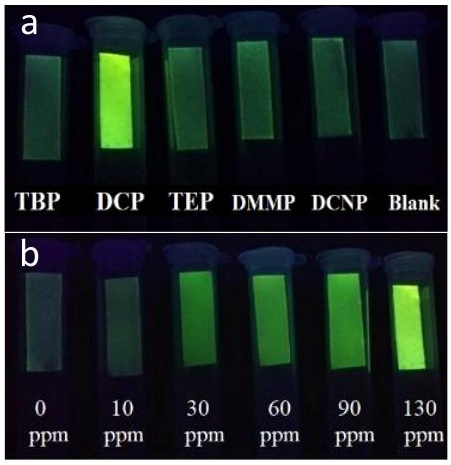

Figure 1.35: (a) Fluorescence response of the probe-coated filter papers upon exposure to various vapours of nerve agent mimic, (b) Fluorescence response of the probe-coated filter papers upon exposure to various concentration of DCP

1.8.4. Application of chemosensors in real-world sample analysis

Food safety issues and water pollution by poisonous molecules and ions have drawn attention with the development of science and technology nowadays. World health organization (WHO) stipulates the permissible acceptable concentration of aluminium in drinking water is 4.5 gm/lit and that of cyanide is 1.9 x 10^{-6} mol/L. But the toxicity of these ion in human body can cause various difficult diseases. So it is very much urgent to detect and determine the concentration level of these poisonous analytes in various real samples. In order to validate the practicality of chemosensor in real-world sample analysis, many research groups have been developed a number of new organic probes and successfully applied to monitor these analytes. Recently, A. Saravanan et al. developed a new naphthyl derivative chemosensor for recognition of Al^{3+} ions. They also determined aluminium in variety of water samples.[133] P. S. Kumar and co-workers have reported a chemoreceptor for selective ratiometric fluorescent detection of CN^-. The sensor is able to display a similar fluorescence change with extracts samples of cyanogenic food samples such as sprouting potato, bitter almond and cassava powder (Fig. 1.36).[134]

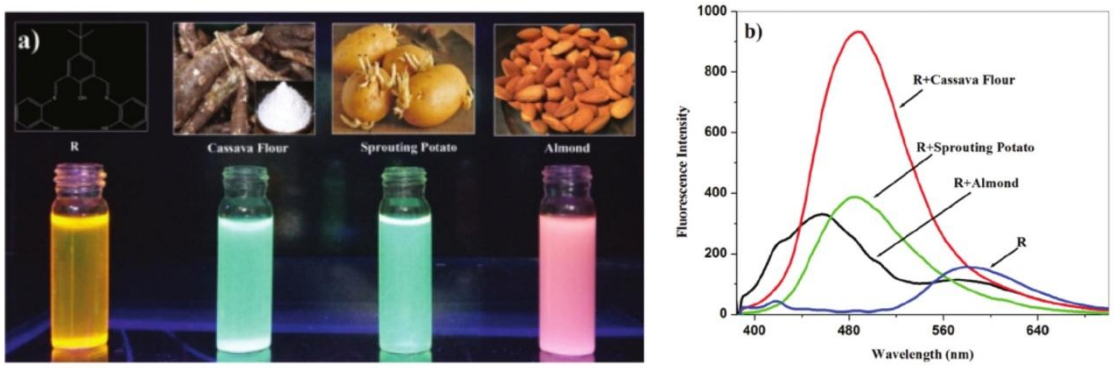

Figure 1.36: Colour changes observed for probe upon addition of extracts of various food samples under a UV lamp (left side) and fluorescence spectra of probe with extracts solutions of foods (right side).

1.8.5. Application in construction of molecular logic gates

Recently construction of molecular logic circuits has been an area of interest in chemosensor chemistry.[135-137] It may have extensive applications such as in molecular arithmetic, digital information security, drug action and construction of memory devices. A molecular logic circuit, used as a digital building block, may be designed when there is more than one chemical input that corresponds to a signal output giving rise to a logic function viz. AND, OR, NAND or INHIBIT.[138] In 2020, Saha et al. developed a Schiff base ligand H_2NPV for efficient detection of Al^{3+} ion. They also constructed two input-based INHIBIT logic gate and molecular device and interpreted with the proper sequential summary of different inputs (Fig. 1.37 & Fig. 1.38).[139]

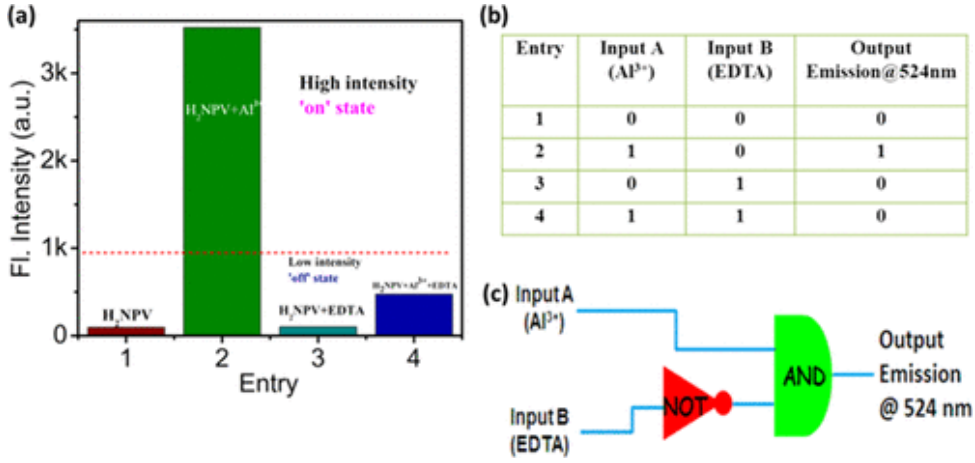

Entry	Input A (Al^{3+})	Input B (EDTA)	Output Emission@524nm
1	0	0	0
2	1	0	1
3	0	1	0
4	1	1	0

Figure 1.37. (a) The fluorescence intensity variation, (b) truth table for advance-level molecular logic gate, and (c) corresponding circuit diagram by U. Saha et al.

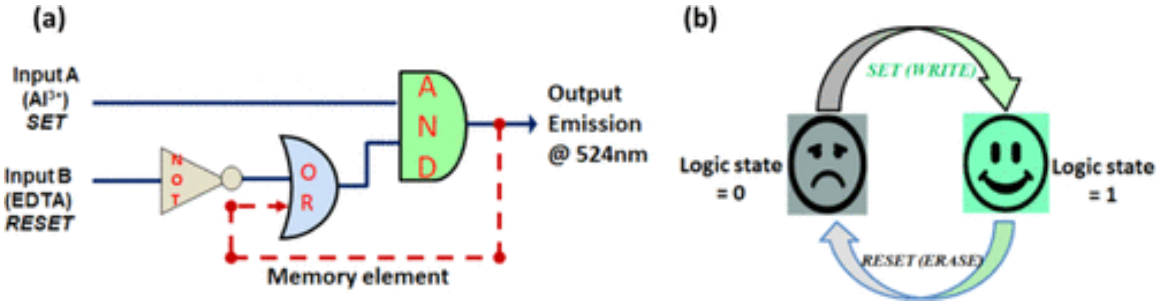

Figure 1.38. (a) Consecutive logic circuit of a memory unit and (b) schematic presentation of the reversible logic operation for the memory element with a write–read–erase–read kind of manners by U. Saha et al.

In 2022, P. Das et al. also reported construction of an INHIBIT logic circuit with three chemical inputs viz. the free ligand(HL), Zn(II) ion and EDTA and the fluorescence emission at 459 nm as a single output. Upon addition of Zn(II) ion into the solution of free probes, the emission at 459 nm at observed. On further addition of EDTA solution, no emission was observed (output off) due to formation of a stronger complex with Zn(II) and frees the probe. EDTA has been used as a chemical output via an inverter. The fig. 1.39 displays the inhibit logic gate and the relevant truth table.[140]

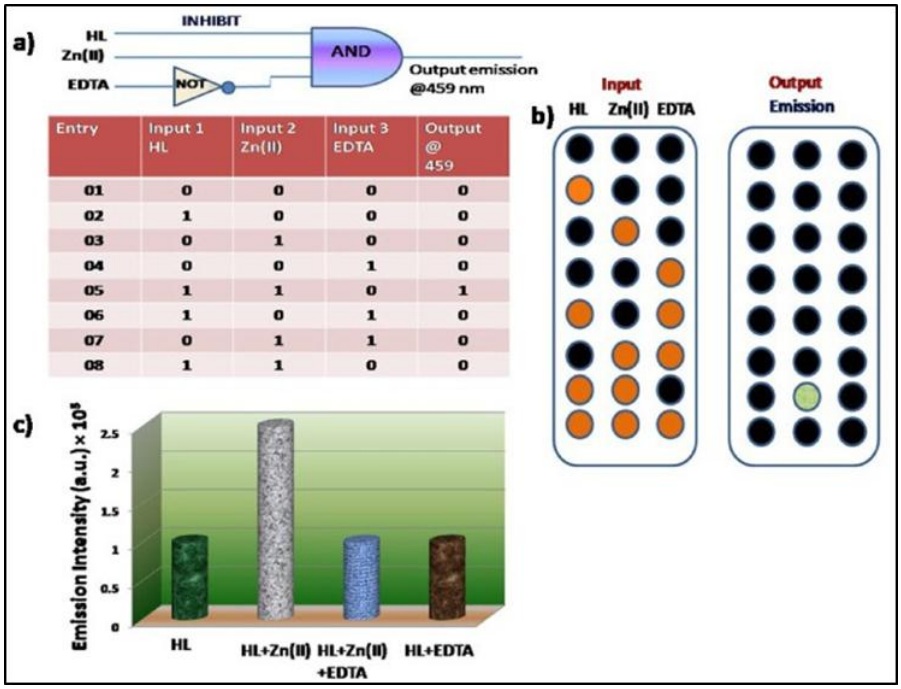

Entry	Input 1 HL	Input 2 Zn(II)	Input 3 EDTA	Output @ 459
01	0	0	0	0
02	1	0	0	0
03	0	1	0	0
04	0	0	1	0
05	1	1	0	1
06	1	0	1	0
07	0	1	1	0
08	1	1	0	0

Fig. 1.39: The logic circuit and the truth table for the chemosensor reported by P. Das et al.

1.9. Aim of my thesis

The aim of my thesis is the extension of the field of chemosensor for the detection and monitoring of various harmful ionic and neutral analytes in environment. Due to having negative impact on human beings and environment, recognition and determination of these species are highly essential and has drawn great attention of budding researchers presently. Although there are number of conventional methods, they are involved in sophisticated analytical instruments and also suffer limitation in case of online or field monitoring. My thesis presents the applications of few sensing approaches for the recognition of these toxic compounds and ions based on optical sensing. In this thesis, I will discuss some newly fabricated organic compounds for the detection of certain biologically as well as environmentally hazardous toxic compounds and ions even in µM as well as in nM range. The discussed chemosensors in this thesis binds with the targeted analyte very rapidly along with a distinct and prominent visible color change in few cases and hence have the advantage of real time, naked-eye detection. Few chemosensors discussed here are reversible in nature and can be reused potentially. More importantly, some of the fabricated chemosensors presented in this thesis can be applied in cellular imaging studies and also can be exploited for the construction of certain logic circuits and their applications can also be shown for the qualitative identification of these analytes via a simple, low cost and easy-to-handy experiment named "dip-stick method".

2.2. References

1. S. S. David and E. Meggers, *Curr. Opin. Chem. Biol*., 2008, **12**, 194–196.
2. N. R. Yamanaka, S. Tabata, Y. Shindo, K. Hotta, K. Suzuki, T. Soga and K. Oka, *Sci. Rep*., 2016, **6**, 30027.
3. E. Bonneau and P. Legault, *Biochemistry*, 2014, **53**, 579–590.
4. P. B. Tchounwou, C. G. Yedjou, A. K. Patlolla and D. J. Sutton, *Clinical and Environmental Toxicology Exs*., 2012, **101**, 133-164.
5. G. Genchi, M. S. Sinicropi, G. Lauria, A. Carocci and A. Catalano, *Res. Public Health*., 2020, **17**, 3782.
6. Z. Rahman and V.P. Singh, *Environ. Monit. Assess*, 2019, **191**, 419.
7. M. Shahid, B. Pourrut, C. Dumat, M. Nadeem, M. Aslam and E. Pinelli, *Rev. Environ. Contam. T*., 2014, **232**, 1–44.
8. H. C. Xia, X. H. Xu and Q. H. Song, ACS Sens., 2017, **2**, 178–182.
9. S. Wang, B. Zhu, B. Wang, P. Fan, Y. Jiu, M. Zhang, L. Jiang and J. T. Hou, Dyes Pigm., 2020, **173**, 107933.
10. Y. Hu, X. Zhou, H. Jung, S. J. Nam, M. H. Kim and J. Yoon, *Anal. Chem*., 2018, **90**, 3382−3386.

11. X. Liu, Y. Gong, Y. Zheng, W. Xiong, C. Wang, T. Wang, Y. Che, J. Zhao, *Anal. Chem*., 2018, **90**, 1498−1501.
12. S. K. Sheet, B. Sen and S. Khatua, *Inorg. Chem*., 2019, **58**, 3635−3645.
13. P. F. Walker, (2017) A Century of Chemical Warfare: Building a World Free of Chemical Weapons. In: Friedrich B., Hoffmann D., Renn J., Schmaltz F., Wolf M. (eds) One Hundred Years of Chemical Warfare: Research, Deployment, Consequences. Springer, Cham. https://doi.org/10.1007/978-3-319-51664-6_20.
14. Y. L. Duan and Y. S. Zheng, *Talanta*, 2013, **107**, 332–337.
15. J. Brooks, T.B. Erickson, S. Kayden, R. Ruiz, S. Wilkinson and F.M. Burkle Jr., *Confl. Health*, 2018, **12**, 12.
16. Y. J. Jang, K. Kim, O. G. Tsay, D. A. Atwood and D.G. Churchill, *Chem. Rev*., 2015, **115**, PR1-PR76.
17. V. V. Singh, K. Kaufmann, B. E. de Ávila, M. Uygun and J. Wang, *Chem. Commun.*, 2016, **52**, 3360.
18. A. Balamurugan and H. Lee, *Macromolecules*, 2016, **49**, 2568.
19. Y. J. Jang, S.V. Mulay, Y. Kim, P. Jorayeva and D.G. Churchill, *New. J. Chem*., 2017, **41**, 1653-1658.
20. A. J. Russell, J. A. Berberich, G. F. Drevon and R. R. Koepsel, *Annu. Rev. Biomed. Eng.*, 2003, **5**, 1.
21. H. S. So, S. Angupillai and Y. A. Son, *Sens. Actuators B Chem.*, 2016, **235**, 447.
22. T. Alizadeh and L. H. Soltani, *Sens. Actuators B Chem.*, 2016, **234**, 361.
23. H. Mao, Y. Yan, N. Hao, Q. Liu, J. Qian, S. Chen and K. Wang, *Sens. Actuators, B Chem.*, 2017, **238**, 239.
24. K. Kim, O. G. Tsay, D. A. Atwood and D. G. Churchill, *Chem. Rev.*, 2011, **111**, 5345.
25. F. R. Sidell and J. Borak, *Ann. Emerg. Med.*, 1992, **21**, 865.
26. T. C. Marrs, *Pharmacol. Ther*., 1993, **58**, 51.
27. K. Tuovinen, *Toxicology*, 2004, **196**, 31.
28. S. Huang, Y. Wu, F. Zeng, L. Sun and S. Wu, *J. Mater. Chem. C*, 2016, **4**, 10105.
29. M. Ehrich, in Encyclopedia of Toxicology, ed. P. Wexler, Academic Press, San Diego, CA, 1998, p. 467.
30. F. R. Sidell and J. Borak, *Ann. Emerg. Med.*, 1992, **21**, 865.
31. T. C. Marrs, *Pharmacol. Ther*., 1993, **58**, 51.
32. L. Szinicz, *Toxicology*, 2005, **214**, 167.
33. S. M. Somani, Chemical Warfare Agents, Academic, San Diego, 1992.
34. T. I. Kim, S. B. Maity, J. Bouffard and Y. Kim, Anal. Chem., 2016, **88**, 9259-9263.
35. K. Kim, O.G. Tsay, D. A. Atwood and D. G. Churchill, *Chem. Rev.*, 2011, **11**1, 5345-5403.
36. Y. C. Yang, *Acc. Chem. Res*., 1999, **32**, 109-115.
37. F. Wang, L. Wang, X. Chen and J. Yoon, *Chem. Soc. Rev.*, 2014, **43**, 4312-4324.
38. M. D. Sobsey and S. Bartram, *Forum Nutr*., 2003, **56**,396-405.
39. D. A. Jones, *Phytochem.*, 1998, **47**, 155-162.
40. M. Zagrobelny, S. Bak and B. L. Moller, *Phytochem*., 2008, **69**, 1457-1468.
41. D. G. Barceloux,*Dis.Mon.*, 2009, **55**, 336-352.
42. U. A. Patrick, N. Egwuonwn, A. A. Onunkwo, *J.SoilSci.Environ. Manage.*, 2011, **2**, 49-57.
43. I. F. Bolarinwa, C. Orfila and M. R. Morgan, *Food Chem.*, 2014,**152**, 133-139.
44. M. T. Wilson, G. Antonini, F. Malatesta, P. Sarti and M. Brunori, *J. Biol. Chem.*, 1994, **269**, 24114-24119.

45. A. V. Gourine, N. Dale, E. Liaudet, D. M. Poputnikov, K. M. Spyer and V. N. Gourine, *J. Physiol.*, 2007, **585**, 305-316.
46. O. S. Wolfbeis, *J. Mater. Chem*., 2005, **15**, 2657.
47. W. C. Mignani and F. Baldini, *Phys. Med. Biol*., 1997, **42**, 967.
48. W. C. Mahoney, A. A. Luderer, R. A. Brier and J.-N Lin, Immunoassay automation: An update guide to systems, Chan. D. W. (ed.), Academic Press, San Diego, CA, 1996, 231
49. C. Huber, I. Klimant, C. Krause and O. S. Wolfbeis, *Anal. Chem*., 2001, **73**, 2097.
50. C. Krause, T. Werner, C. Huber and O.S. Wolfbeis, *Anal. Chem*., 1999, **71**, 5304.
51. C. Huber, I. Klimant, C. Krause, T. Werner, T. Mayr and O. S. Wolfbeis, *J. Anal. Chem*., 2000, **368**, 196.
52. L. W. Burges, Review of progress in quantitative nondestructive evaluation, in D. O. Thompson, D. E. Chimenti, Plenum Press, New York, NY, 1996, **15**, 9.
53. M. Montalti, L. Prodi and N.J. Zaccheroni, *J. Mater. Chem*., 2005, **15**, 2810.
54. Z. Liu, W. He and Z. Guo, *Chem. Soc. Rev*., 2013, **42**, 1568.
55. D. Buccella, J. A. Horowitz and S. J. Lippard, *J. Am. Chem. Soc*., 2011, **133**, 4101.
56. C. J. Pedersen, *Angew. Chem. Int. Ed. Engl*., 1988, **27**, 1021.
57. F. P. Schmidtchen, Probing the design of a novel ditopic anion receptor, J. Am. Chem. Soc., 108 (1986) 8249.
58. (a) C. A. Hunter, *Angew. Chem. Int. Ed. Engl.* 2005, **43**, 5310; (b) R. Paulini, K. Muller and F. Diederich, *Angew. Chem. Int. Ed. Engl.* 2005, **44**, 1788.
59. (a) G. A. Jeffrey, *An Introduction to Hydrogen Bonding*, Oxford University Press: Oxford, 1997; (b) H. Dugas, *Bio-organic Chemistry*, Springer Verlag, New York, Inc. 1996; (c) J. M. Lehn, *Supramolecular Chemistry*, Weinhein, New York, Basel. Cambridge, Tokyo: VCH, 1995. 3.
60. (a) F. Vogtle, *Supramolecular chemistry, An Introduction;* Wiley & Sons: Chichester, 1993; (b) P. D. Beer, P. A. Gale and D. K. Smith, *Supramolecular Chemistry*, Oxford University Press, New York, 1999. (c) S. H. Gellman, *Chem. Rev.* 1997, **97**, 1231; (d) T. Schrader and A. D. Hamilton, *Functional Synthetic Receptors*, Wiley-VCH, Weinheim, 2005. (e) A. D. Hamilton, *Supramolecular Control of Structure and Reactivity* (*Perspective in supramolecular Chemistry*), Wiley, New York, 1996.
61. C. J. Pedersen, *J. Am. Chem. Soc.* 1967, **89**, 2495.
62. J.-M. Lehn, *Acc. Chem. Res*., 1978, **11**, 49-57.
63. J.-M. Lehn, *Pure Appl. Chem*., 1978, **50**, 871.
64. D. J. Cram and J.M. Cram, *Science*, 1974, **183**, 803.
65. J.-M. Lehn, *Science,* 1985, **227**, 849.
66. D. J. Cram and J. M. Cram, Container Molecules and Their Guests, Royal Society of Chemistry, Cambridge, 1994.
67. F. P. Schmidtchen and M. Berger, *Chem. Rev*., 1997, **97**, 1609.
68. M. Rigby, E. B. Smith, W.A. Wakeham, G.C. Maitland, The Forces between molecules, Clarendon, Oxford, 1986.
69. R. Dharanipragada, S. B. Ferguson and F. Diederich, *J. Am. Chem. Soc*., 1988, **110**, 1679.

70. T. Iimori, W.C. Still, A. L. Rheingold and D. L. Staley, *J. Am. Chem. Soc*., 1989, **111**, 3439.
71. J.-M. Lehn, *Angew. Chem. Int. Ed. Engl*., 1988, **27**, 89.
72. A. Halder, D. Data, P. P. Seelam, D. Bhattacharyya and A, Mitra, *ACS Omega*, 2019, **4**, 7354–7368.
73. C. Zhang, K. Ji, X. Wang, H. Wu and C. Liu, *Chem. Commun*., 2015, **51**, 8173.
74. S. Kang, J. Kim, J.-H. Park, C. K. Ahn, C.-H. Rhee and M. S. Han, *Dyes Pigm*., 2015, **123**, 125-131.
75. H. Adams, C. A. Hunter, K.R. Lawson, J. Perkins, S. E. Spey, C. J. Urch and J. M. Sanderson, *Chem. Eur. J*., 2001, **7**, 4863
76. E. J. Corey, K. B. Becker and R. K. Varma, *J. Am. Chem. Soc*., 1972, **94**, 8616.
77. G. R. Desiraju, Eds. Crystal Design: Structure and Function, Perspectivein Supramolecular Chemistry, Vols. 7, John Wiley & Sons Ltd.: New York, NY, 2003.
78. A. Sygula, F. R. Fronczek, R. Sygula, P. W. Rabideau and M. M. Olmstead, *J. Am. Chem. Soc*., 2007, **129**, 3842.
79. A. Petitjean, R. G. Khoury, N. Kyritsakas and J.-M. Lehn, *J. Am. Chem. Soc*., 2004, **126**, 6637-6647.
80. V. Blanco, M. Chas, D. Abella, E. Pia, C. Iglesias, C. Peinador, J. Quintela, Org. Lett., 2008, **10**, 409.
81. A. Singh, P. Raj, J. J. Dubowski and N. Singh, *Cryst. Growth Des*., 2018, **18**, 4320–4333.
82. S. Scheiner, Molecular interactions. From Van der Waals to strongly bound complexes, Wiley, Chichester, 1997.
83. S. L. Wiskur, H. Aıt-Haddou, J.J. Lavigne and E.V. Anslyn, *Acc. Chem. Res*., 2001, **34**, 963.
84. M.-Y. Chae and A.W. Czarnik, *J. Am. Chem. Soc.*, 1992, **114**, 9704.
85. V. Dujols, F. Ford and A. W. Czarnik, A Long-Wavelength Fluorescent Chemodosimeter Selective for Cu(II) Ion in Water, *J. Am. Chem. Soc*., 1997, **119**, 7386.
86. Z. Xu, X. Chen, H. N. Kim and J. Yoon, *Chem. Soc. Rev*., 2010, **39**, 127.
87. K. Kaur, R. Saini, A. Kumar, V. Luxami, N. Kaur, P. Singh and S. Kumar, *Coord. Chem. Rev.*, 2012, **256**, 1992.
88. J. R. Ed. Lakowicz, *Principles of Fluorescence Spectroscopy*; Plenum Publishers Corporation: New York, 1999.
89. S. J. Strickler and R. A. Berg. *J. Chem. Phys.*, 1962, **37**, 814.
90. E. Zhang, P. Ju, P. Guo, X.Hou, X. Hou, H. Lv, J. -J. Wang and Y. Zhang, *RSC Adv.*, 2018, **8**, 31658.
91. K. C. Behera, D. Mallick, B. N. Patra and B. Bag, *Spectrochim. Acta Part A*, 2022, **271**, 120934
92. (a) V. Dujols, F. Ford and A. W. Czarnik, *J. Am. Chem. Soc.*,1997, **119**, 7386; (b) A. P. de Silva, T. S. Moody and G. D. Wright, *Analyst*, 2009, **134**, 2385.
93. J. R. Ed. Lakowicz, *Principles of Fluorescence Spectroscopy*; Plenum Publishers Corporation: New York, 1999.
94. A. Weller, *Pure Appl. Chem.* 1968, **16**, 115.
95. S. Y. Kim, J.-In Hong, *Tetrahedron Lett.*, 2009, **50**, 2822-2824.
96. A. Pavel, A. Panchenko, Pavel A. Ignatov, Marina, A. Zakharko, Yurii V. Fedorov and Olga A. Fedorova, *Mendeleev Commun.*, 2020, **30**, 55–58.
97. A. Gangopadhyay and A. Mahapatra, *New J. Chem*, **43**, 11743-11748
98. Y. Jiao, B. Zhu, J. Chen and X. Duan, *Theranostics.*, 2015, **5**, 173187.
99. P. Liu, N. Liu, C. Liu, Y. Jia, L. Huang, G. Zhou, C. Li and S. Wang, 2019, **163**, 489-495
100. L. Patra, K. Aich, S. Gharami and T. K. Mondal, J. Lumin, 2018, **201**, 419-426
101. T. Iijima, A. Momotake, Y. Shinohara, T. Sato, Y. Nishimura and T. Arai, *J. Phys. Chem. A*., 2010, **114**, 1603.

102. S. Park, J. E. Kwon, S. H. Kim, J. Seo, K. Chung, S. Y. Park, D. J. Jang, B. M. Medina, J. Gierschner and S. Y. Park, *J. Am. Chem. Soc.*, 2009, **131**, 14043.
103. J. S. Wu, W. M. Liu, J. C. Ge, H. Y. Zhang and P. F. Wang, *Chem. Soc. Rev.*, 2011, **40**, 3483.
104. V. Luxami and S. Kumar, *New J. Chem.*, 2008, **32**, 2074.
105. N. Kaur, G. Jindal, Sukhvinder and S. Kumar, *New J. Chem.*, 2019, **43**, 436.
106. F. Zeng, G. Bao, B. Zhou and Y. Han, 2021, **45**, 5631-5636
107. A. S. Gupta, K. Paul and V. Luxami, *Anal. Methods*, 2018, **10**, 983.
108. S. Mabhai, M. Dolai, S. Dey, A. Dhara, B. Das and A. Jana, *New J.Chem.*, 2018, **42**, 10191.

109. J. B. Li, Y. Liu, X.J. Zheng, D. Wang, *Microchem. J.*, 2019, **150**, 104123.
110. J. Rodr´ıguez-Lavado, A. Lorente, E. Flores, A. Ochoa, F. Godoy, P. Jaque and C. Saitz, RSC Adv., 2020, **10**, 21963–21973.
111. Y. -Q. Weng, F. Yue and Y. -R. Zhong, *Inorg. Chem.*, 2007, **46**, 7749.
112. D. A. Blake, R. M. Jones, R. C. Blake, A. R. Pavlov, I. A. Darwish and H. Yu, *Biosens. Bioelec*., 2001, **16**, 799.
113. S. F. D'Souza. *Biosens.Bioelec*., 2001, **16**, 337.
114. I. Bontidean, J. Ahlqvist, A. Mulchandani, W. Chen, W. Bae, R. K. Mehra, A. Mortari and E. Csöregi, *Biosens. Bioelec*., 2003, **18**, 547.
115. S. Lee, K. Sode, K. Nakanishi, J.-L. Marty, E. Tamiya and I. Karube, *Biosens.Bioelec.*,1992, **7**, 273.
116. P. Corbisier, D. V. de Lelie, B. Borremans, A. Provoost, V. de Lorenzo, N. L. Brown, J. R. Lloyd, J. L. Hobman, E. Csöregi, G. Johansson and B. Mattiasson, *Anal. Chim. Acta*,1999**, 387**, 235.
117. E. M. Bosch, J. R. A. Sanchez, S. F. Rojas and B. C. Ojada, *Sensors*,2007, **7**, 797.
118. O. S. Wolfbeis, *J. Mater. Chem*., 2005**, 15**, 2657.
119. I. Bontidean, C. Berggren, G. Johansson, E. Csoregi, B. Mattiasson, J.R. Lloyd, K. J. Jakeman and N. L. Brown, *Anal. Chem.*,1998**, 70**, 4162.
120. N. F. Starodub, N. I. Kanjuk, A. L. Kukla and Y. M. Shirshov, *Anal. Chim. Acta.*, 1999, **385**, 461.
121. A. L. Kukla, N. I. Kanjuk, N. F. Starodub and Y. M. Shirshov, *Sens. Actuators B: Chem*., 1999, **57**, 213.
122. N. F. Starodub, N. I. Kanjuk, A. L. Kukla and Y. M. Shirshov, *Anal. Chim. Acta.*, 1999, **385**, 461.
123. G.-q. Shi and G. Jiang, *Anal. Sci*.,2002**, 18**, 1215.
124. L. Basabe-Desmonts, D. N. Reinhoudt and M. Crego-Calama, *Chem. Soc. Rev.* 2007**, 36**, 993.
125. E. M. Bosch, J. R. A. Sanchez, S. F. Rojas and B. C. Ojada, *Sensors*,2007, **7**, 797.
126. S. Das, P. P. Das, J. W. Walton, K. Ghoshal, L. Patra and M. Bhattacharyya, 2021, **45**, 1853
127. P. Das, S. S. Rajput, M. Das, S. Laha, I. Choudhuri, N. Bhattacharyya, A. Das, B. C. Samanta, M. M. Alam, T. Maity, *Journal of Photochemistry & Photobiology A*, 2022, **427**, 113817.
128. L. Hou, F. Li, J. Guo, X. Zhang, X. Kong, X. T. Cui, C. Dong, Y. Wang and S. Shuang, 2019, **7**, 4620-4629
129. S. S. Ali, A. Gngopadhyay, A. K. Pramanik, U. N. Guria, S. K. Samanta and A. K. Mahapatra, Dye Pigm, 2019, **170**, 107585
130. J. Zhao, J. Zhang, B. Hu, C. Gao, Z. Li, Z. Sun and J. You, *Spectrochim. Acta A*, 2023, **286**, 121965

131. S. D. Padghan, L. –C. Wang, W. –C. Lin, J. –W. Hu, W. –C. Liu and K. –Y. Chen, *ACS Omega*, 2021, **6(8)**, 5287-5296
132. H. Xu, H. Zhang, L. Zhao. C. Peng, G. Liu and T. Cheng, *New J. Chem*, 2020, **44**, 10713-10718
133. A. Saravanan, S. Shyamsivappan, N. K. Kalagatur, T. Suresh, N. Maroli, N. Bhuvanesh, P, Kolandaivel and P. S. Mohan, *Spectrochim. Acta A*,2020, **241**, 118684
134. P. S. Kumar, P. R. Lakshmi and K. P. Elango, *New J. Chem*, 2019, **43**, 675-680
135. P. A. De Silva, N. H. Q. Gunaratne, C. P. McCoy, *Nature*, 1993, **364**, 42–44.
136. J. Qin, Z. Yang, *J. Photochem. Photobiol.*, 2016, **324,** 152–158.
137. W. T. Huang, Y. Shi, W.Y. Xie, H.Q. Luo, N.B. Li, *Chem. Commun.* 2011, **47**, 7800–7802.
138. W. Yang, G. Zhang, W. Weng, B. Qiu, L. Guo, Z. Lin and G. Chen, *RSC Adv.*, 2014, **4**, 58852.
139. U. Saha, B. Das, M. Dolai, R. J. Butcher, and G. S. Kumar, *ACS Omega*, 2020, **5(29)**, 18411-18423
140. P. Das, S. S. Rajput, M. Das, S. Laha, I. Choudhuri, N. Bhattacharyya, A. Das, B. C. Samanta, M. M. Alam and T. Maity, *Journal of Photochemistry & Photobiology A*, 2022, **427**, 113817.

General instrumental techniques and methods of analysis

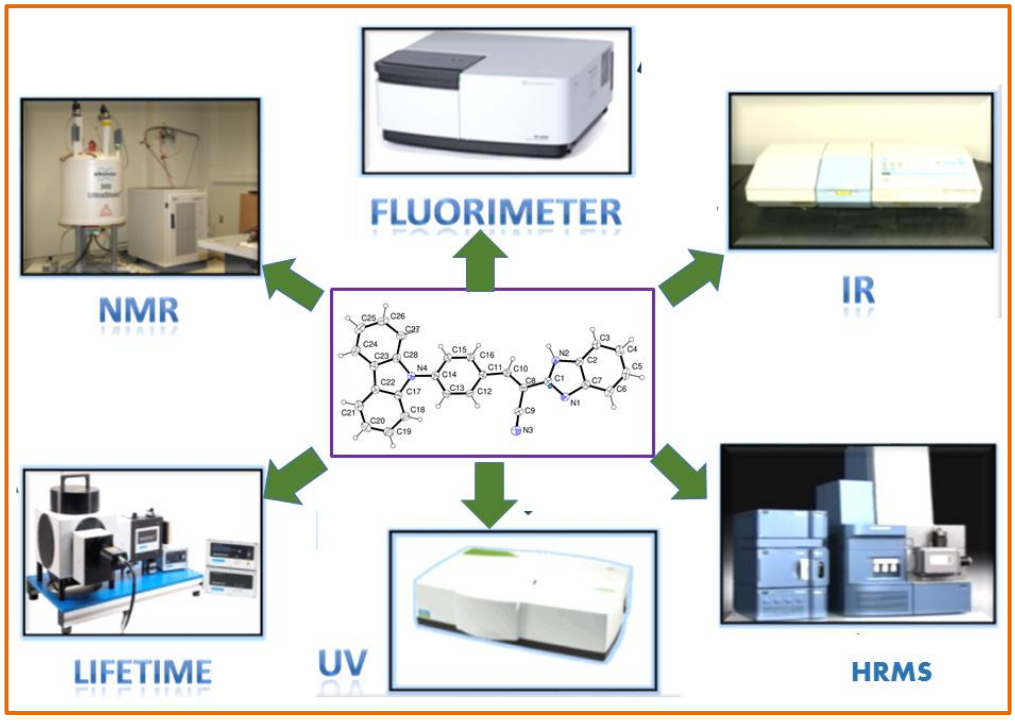

2.1. Introduction

This chapter includes the various instrumentation techniques which have been employed for the characterization of all synthesized probes as well as for all the complexes and adducts fabricated throughout the thesis-work. In this chapter, we also describe some methods like calculation of detection limit, quantum yield and binding constant which are essential in order to evaluate the efficiency of sensors more accurately. The chemical structures of the synthesized probes here have been thoroughly characterized by elemental analysis, ^{1}H NMR, ^{13}C NMR, HRMS, IR, while some other spectral as well as photophysical studies like UV-Vis, fluorimetric techniques, lifetime decay measurements are also recorded for studying their optical features. Single crystal X-ray diffraction studies are also executed to gain more information for the single crystals we obtain from some of our works.

2.2. Reagents for synthesis

Solvents used for the synthesis and analysis of the probes throughout my thesis have been purchased from Merck chemicals, India and used as received. DMSO-d_6 and $CDCl_3$ solvent for NMR spectroscopic studies have been bought from Sigma Aldrich and used in its current form. All organic compounds including methyl picolinate, 4-hydroxy-2H-chromen-2-one, 9H-carbazole, 4-fluorobenzaldehyde, 2-aminothiophenol, malononitrile, 8-hydroxy quinoline, o-phenylenediamine and ethyl cyanoacetate are purchased from Sigma Aldrich, USA and used without further purification. Anhydrous sodium sulphate, calcium chloride, potassium carbonate, phosphoryl chloride, acetyl chloride, thionyl chloride, tri-n-butyl phosphate, triethyl phosphate, acetic acid, hydrochloric acid and other metal salts as well as some toxic molecules used for competitive analytes are purchased from Merck chemicals, Germany. Silica gels and aluminum oxide (basic) are purchased from various commercial sources.

2.3. Several Physiochemical procedures

Characterization of the purified synthesized probes was carried out using these different techniques thoroughly.

2.3.1. ^{1}H NMR Spectroscopy

To confirm the chemical structure of a newly fabricated chemosensor, ^{1}H as well as ^{13}C NMR spectroscopies are the most effective analytical techniques. Nuclear magnetic resonance is a phenomenon which involves the interaction between an oscillating magnetic field of electromagnetic radiation and the magnetic energy of the hydrogen nucleus or some other type of nuclei when these are settled in an external static magnetic field. Among the group of spectroscopic techniques, the NMR spectroscopy needs electromagnetic wave with lowest irradiation energy for excitation. The sample absorbs electromagnetic energy in radio-wave region at various frequencies since absorption depends upon the type of certain nuclei or proton contained in the sample compound.

This method is nondestructive in nature and provides molar response which allows structure elucidation as well as quantification simultaneously thereby supplying significant information about the chemical structure of the desired compounds. In this technique, the protons in inorganic or organic molecule are exposed to a powerful field.[1] Under the influence of that external magnetic field the different protons will precess at different frequencies. When these precessing protons are exposed with steadily changing radio frequencies, protons undergo transition from low-energy parallel state to high-energy anti-parallel state. This type of transition only happens when the transition energy and the energy of the radiation are well matched. At the certain value of the field strength, the energy required to spin the protons matches the energy of the radiation and then absorption happens and a signal is noticed. Such a spectrum is known as nuclear magnetic resonance spectrum. In this spectrum, applied magnetic field strengths for each type of protons is measured and the absorption peaks are plotted. The total number of signals obtained at different applied magnetic field strengths indicates the different sets of equivalent protons present in the investigated molecule. The location of the signals in the NMR spectrum provide us about the nature of protons adjacent to some electron releasing or electron attracting group.

When a compound is placed in a magnetic field strength, the electrons begin to circulate thereby introducing secondary magnetic fields. This rotation of electrons about the proton itself generates a field in such a manner that the proton opposes the applied magnetic field. When the induced field is in opposite direction with the external magnetic field, then the proton is said to be shielded and the corresponding protons are said to be shifted to upfield region. Again, if the

induced field and the external applied field are in the same direction, the corresponding proton is said to be deshielded and shifted to downfield region. Such shifts are known as chemical shifts. The signal for tetramethylsilane (TMS) is considered as a reference for determining chemical shifts of an assortment of protons in a compound. Clearly, the NMR signal for a specific proton in a compound will be noticed at different field strengths compared to a signal from tetramethylsilane (TMS). This change in the absorption position of the proton with respect to TMS signal is referred as chemical shift. It is determined in equivalence frequency and denoted as δ value.

$$\delta = (\nu_{sample} - \nu_{TMS})/\text{operating frequency in per sec.}$$

The unit of δ is expressed in perts per million (ppm). Solvents used for this techniques should be free of proton so that it does not produce any absorption of its own in NMR spectrum. Conventionally deuterated solvents like DMSO-d_6 and $CDCl_3$ are used conveniently as deuterium is effectively NMR silent in the operating frequency range of proton NMR.

In an NMR spectrum, total number of peaks represent equivalent sets of protons. The size or the area of each peak provides information about the number of each set of protons present in the investigated compound and the area under an NMR signal is directly proportional to the number of equivalent protons giving rise to signal. The splitting of a signal is owing to the different surroundings of the absorbing proton with respect to the nearby protons. Significantly the separation between the midpoints of the two adjacent peaks in a multiplet is usually constant and is called the coupling constant. The unit of coupling constants are expressed in Hz.

In case of NMR titration, inferences about the stability of the host-guest complex can be drawn by calculating the association constant through the analysis of the chemical shift values. By simply plotting the chemical shift versus host-guest mole ratio, we can get information about the exact stoichiometry of a receptor molecule when the binding constant is large and exchange is fast. When broad range of association constants is considered and dynamic exchange between the free host and the complex is fast on the NMR time scale, the Job's experiment is usually adopted for the stoichiometry of the complex. When it is slow on the NMR time scale, the stoichiometry of the complex is apparent.[2]

Each and every ^1H NMR spectrum of all the newly fabricated probes and the other associated compounds were recorded on a Bruker 300 MHz instrument.

2.3.2. ^{13}C NMR Spectroscopy

^{13}C is a comparatively new technique. There are significant and prominent differences between the ^{1}H and ^{13}C spectra both in the form of recording as well as in manifestation. The nuclear spin quantum number is expressed by I and its value for ^{12}C is equal to zero. Therefore, being non-magnetic, it does not produce any NMR signal, while ^{13}C possess a spin quantum number equal to ½ making it NMR active. Its natural abundance is only 1.11%. Every C^{13} resonance strongly couples with the directly attached proton and also couples with the protons which are two to four bonds away from it. The value of the coupling constants differs accordance to the distance between ^{13}C and the proton consequently.

For almost all organic compounds, complete ^{13}C spectra observe in the range of 0-200 ppm. TMS is taken as the common internal reference which is used for ^{13}C NMR.

All the ^{13}C NMR spectrum of the developed compounds throughout the thesis was recorded on a Bruker 300 MHz instrument.

2.3.3. Infrared Spectroscopy (IR)

IR spectrum is an important technique which provides sufficient and significant information about the structure of newly fabricated probes. Unlike ultraviolet spectrum which contains moderately few peaks, this procedure provides a spectrum including a huge number of absorption bands that gathered a lot of information about that particular chemical structure. The absorption of infra-red radiation causes various bands in a molecule to stretch and bend with respect to one another. The most significant infra-red region is observed from 2.5 μ to 15 μ in which molecular vibrations can be detected and measured. The absorption of IR radiations of a particular compound can be articulated either in terms of wave number (ν) or in terms of wavelength (λ).

Mostly, IR spectra of molecules are recorded and plotted as percentage transmittance versus wavenumber. The correlation between wave number and wavelength is as follows:

Wave number =1/wavelength in cm

IR band intensity is either expressed in terms of transmittance (T) or absorbance (A).

$$A = \log_{10}(1/T)$$

The absorption of IR radiation leads in an excitation of molecule from a lower to the higher vibrational level. Now each vibrational level consists a number of strictly spaced rotational levels. All the bonds present in a molecule are not IR active but only those bonds which produce a change

in dipole moment during vibration will absorb in the IR region. Such vibrational transitions are called IR-active transitions and the corresponding compounds will be referred as IR-active molecule. Thus Infrared (IR) spectroscopy is also considered as vibrational-rotational spectroscopy.

All the IR data in this thesis works were recorded on a RX-1 PerkinElmer spectrophotometer with samples prepared as KBr pellets.

2.3.4. High resolution mass spectrometry (HRMS)and Elemental analysis

High resolution mass spectrometry technique is one of the most essential and vital analytical tool to analyze the chemical structure of newly synthesized compounds, in this case, newly fabricated chemosensors as well as chemodosimeters. This spectrometry provides the most accurate information about the molecular mass of the studied compound and also its elemental composition.

In this method, sample compounds are bombarded with a beam of electrons with high energy. Consequently, the molecules are ionized and broken up into numerous fragments. Some of them are positive ions. Each variety of an ion possess a particular m/z ratio i.e., mass to charge ratio. The charge for most ions is one and thus m/z ratio is basically equal to the molecular mass of the ion. A distinct signal is observed for each value of m/z which corresponds to the mass of the particular fragment. The intensity of each signal in HRMS spectrum corresponds to the relative abundance of the fragment producing the signal. The largest peak in the structure is called the base peak and its intensity is taken as 100.

Similarly, elemental analysis is also proved to be useful method which determines the percentage presence of C, H and N in an investigated molecule. So in this thesis, all HRMS mass spectral data were monitored on Waters (Xevo G2 Q-TOF) mass spectrometer and elemental analysis was performed in a 2400 Series-II CHN analyzer, Perkin Elmer, USA.

2.3.5. UV-Vis absorption spectroscopy

In order to investigate the sensing capability, the change in absorption spectra of the fabricated probes were meticulously studied upon addition of specific guest analytes into the probe solution. It is of utmost importance and a common technique in order to explore the sensing characteristics of chemosensors.

This technique is often referred as Electronic spectroscopy since electrons promote from the ground level to the higher energy level. For ultra-violet and visible spectrum, electronic

excitation is studied in between 200-700 nm and leads to the promotion of electrons to the higher energy molecular orbital. Compounds which are able to absorb energy in the visible range, will appear colored to the human eye and any specific change in the absorption spectrum of such compound results in distinct change of color. The wavelength of specific radiation absorbed can be denoted as energy or frequency.

In the absorption spectrum or UV-Vis plot, the wavelength (nm) in 'nm' is taken in the x-axis and the quantity of light absorbed by the compound (a. u.) is taken in the y- axis as a function of the former. It generally consists of a number of absorption bands. There are two well-known laws explaining the absorption changes by the compounds. These are:

(i) Lambert's law and (ii) Beer's law.

By combining these two laws, the Beer-Lambert law can be expressed as:

$$\mathbf{I(\nu) = I_0(\nu)10^{-\varepsilon(\nu)cl}}$$

Where $I(\nu)$ and $I_0(\nu)$ are transmitted light and the intensity of incident light respectively at the frequency ν,$\boldsymbol{\varepsilon}$ is the molar extinction coefficient at ν frequency which can be denoted in the unit of L (liters)$mol^{-1}cm^{-1}$, l is the path length (cm) of the absorbing medium and c is the concentration of solution in moles $litre^{-1}$.

In order to measure absorption spectra accurately, baseline of the solvent in which the studied compound is dissolved, was carried out at first so that one can easily eliminate any contribution of the solvent in the absorption spectra of the probe itself. This technique is called as baseline correction. After baseline correction, the samples of desired concentration were taken in quartz cuvette and the absorption spectrum measurement was recorded. In my thesis work, Perkin Elmer Lambda 750 spectrophotometer was used to record all the electronic spectra.

2.3.6. Fluorescence Spectroscopy

The emission spectral changes of the developed probes were also studied and analyzed to further gain knowledge about the sensing characteristics of chemosensors as well as chemodosimeter and to discover the sensing pattern of the particular probe.

The principles of photoluminescence or fluorescence processes are described by briefly studying Jablonski diagram which ascribed a variety of processes that happen between absorption and emission of light. This technique explains the various molecular processes which happen in the excited level of the studied molecule.[3] The Jablonski diagram is depicted in Figure 2.1. They

are represented as S_0, S_1 and S_2 which implies singlet, ground, first and second electronic states respectively. Each of these electronic energy levels can consist of a number of vibrational energy levels, expressed as by 0, 1, 2, etc. Electronic transitions take place in about 10^{-15} sec thereby making the displacement of the nucleus irrelevant. This is described in Frank-Condon principle. The excited vibrational levels are not populated at room temperature. As a result, absorption as well as emission occurs mostly from or to the lowest vibrational energy levels. Absorption of light energy by the fluorophore promotes excitation to some higher vibrational states of either S_1 or S_2. When the excited molecules come back from S_2 to S_1, the phenomenon is called internal conversion (IC). But the emission from the S_1 to S_0 level, emission of light occurs and the phenomenon is phrased as fluorescence. Conversion of S_1 state to T_1 state is termed as intersystem crossing (ISC) due to change in spin. Emission from the triplet ground state to singlet ground state is called phosphorescence.[4] As this transition is forbidden, the rate constants for such emission are much lower than those for fluorescence.

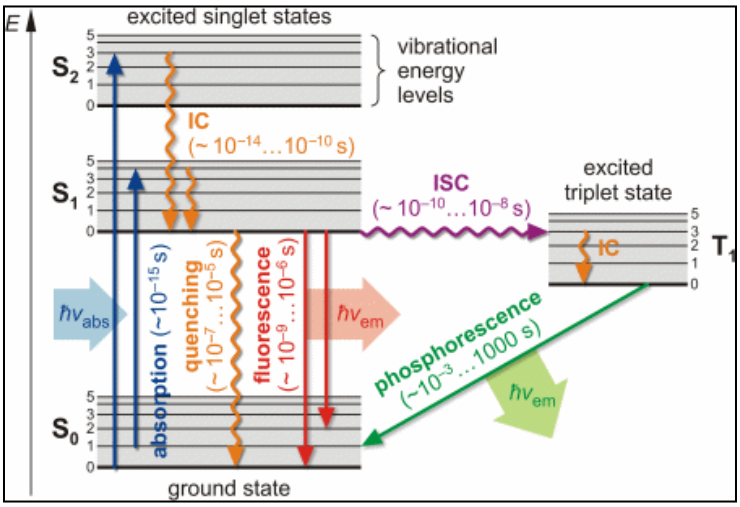

Figure 2.1: A schematic of Jablonski diagram showing the excitation and de-excitation processes involved in photoluminescence.

For a typical measurement of fluorescence, the sample solutions of desired concentration were placed in quartz cuvette and the fluorescence emission spectra were monitored without any baseline correction as in this method contribution in the photo-luminescence spectra from the solvent molecule is assumed to be negligible. All the fluorescence spectral studies were performed with the aid of Shimadzu RF-6000 fluorescence spectrophotometer at room temperature (298 K), reported in this thesis.

2.3.7. Fluorescence lifetime measurement

Fluorescence lifetime of a fluorophore is the characteristic average time in its excited state and the decay curve plotted against time of a particular emission wavelength, exciting at a specific wavelength. Commonly, a fluorescent compound displays a single exponential decay and their intensity and time are related by the following equation:

$I(t) = I(0) \exp(-kt)$

Where, I(t) and I(0) are the fluorescence intensity at a given time t and the original stage (t = 0) respectively; k signifies rate constant describing the fluorescence decay. Both radiative and non-radiative decays affect the rate constant, k of fluorescence decay.

Radiative decay rate constant is expressed by k_r which is characterized by lifetime τ_r and a non-radiative decay rate constant is symbolized by k_{nr}, characterized by lifetime τ_{nr}. So, the equation of lifetime is formulated as:

$k = k_r + k_{nr} = 1/\tau_r + 1/\tau_{nr} = 1/\tau$ and $I(t) = I(0) \exp(-t/\tau)$

One can get the overall fluorescence lifetime (τ) value, by fitting a single exponential decay to the experimental fluorescence decay plot.

For a typical lifetime measurement, the sample solutions of desired concentration were situated in quartz cuvette and the fluorescence spectra were monitored. The lifetime measurement of developed sensor is a significant tool to investigate further about these probes. All the lifetime decay measurement throughout the thesis work was successfully done using time-correlated single photon counting set up from Horiba Jobin-Yvon. The emission decay data were then collected on a Hamamatsu MCP photomultiplier (R3809) and were resolved by using IBH DAS6 software. The goodness of fit was appreciated by χ^2 criterion and visual observation of the residuals of the fitted function to the data. In general, fluorescence posseses a lifetime of a few nanoseconds (ns), while spin-forbidden phosphorescence shows a lifetime in the order of microsecond (μs) to millisecond (ms).

2.3.8. Single crystal X-ray diffraction method

Single crystal X-ray diffraction technique is a non-destructive analytical tool that provides more detailed information about the internal lattice of crystalline substances such as unit cell dimensions, bond-angles, bond-lengths and details of site-ordering. This technique involves

single-crystal refinement, the data collection from the X-ray analysis and data interpretation and refined to get the crystal structure.

In 1912, Scientist Max von Laue first discovered that crystalline substances act as three-dimensional diffraction gratings for X-ray wavelengths similar to the spacing of planes in a crystal lattice. This technique has been appeared as a familiar procedure for the study of crystal structures as well as atomic spacing. X-ray diffraction process is based on constructive interference of a crystalline sample and monochromatic X-rays. A cathode ray tube is used to generate these X-rays and then filtered to produce monochromatic beam and directed towards the studied compound. The interaction between the incident rays and the investigated compound produces constructive interference when conditions match Bragg's Law ($n\lambda=2d\sin\theta$). The wavelength of electromagnetic radiation to the diffraction angle and the lattice spacing in a crystalline sample are related by this law. Diffracted X-rays are then detected, processed and counted. The orientation of the centered crystal and the detector, all possible diffraction directions of the lattice can be controlled by changing the geometry of the incident rays.[5]All diffraction procedures are associated with the generation of X-rays in an X-ray tube. The angle between the incident and diffracted beams is a vital component of all diffraction.

To execute this experiment, single crystals were mounted on glass fibers very carefully with epoxy cement as explained in relevant thesis work. X-ray analysis was performed using Apex II CCDC diffractometer with fine-focus sealed tube graphite-monochromated Mo Kα radiation (λ = 0.71073 Å) at room temperature. The crystal data was processed with SAINT and corrected for absorption using SADABS.[6] The crystal structures were then solved by direct method using the program SHELXTL[7] and was refined by full-matrix least squares technique on F2 using anisotropic displacement parameters for all non-hydrogen atoms. According to riding model, hydrogen atoms were included in the refinement process. Moreover, the Mercury 3.0 software was also employed for the analysis of bond distances and angles of the crystal.

2.4. Theoretical calculation

In order to get more important information about a molecular assemble, quantum mechanical calculations have been achieved. Density functional theory (DFT) is carried out for the theoretical explanation of the optimized electronic structure. Full geometrical optimizations of some chemosensors, chemodosimeters and their corresponding complex or adduct are performed using DFT method at B3LYP level using 6-31-G(d) basic set. Additionally, the vibrational frequency

calculations on the optimized geometries were carried out to assure that optimized structural geometries represent the local minima and there were only positive eigen values. Based on B3LYP optimized geometries, the vertical electronic excitations were computed using TDDFT (time-dependent density functional theory) method in selected solvent using the conductor like polarizable continuum formalism (CPCM). All theoretical calculations were successfully performed with the Gaussian09 program package with the aid of the Gauss View visualization program.

2.5. Instrumentation segment of the spectroscopic methods

2.5.1. NMR technique

The work function of nuclear magnetic resonance spectrophotometer involves the use of a radio-frequency, a magnet, a detector and an amplifier. The detection system is employed to note down that energy is being transferred from the radio-frequency ray to the nucleus. The sample under investigation is taken in a glass tube which is placed in between the two pole faces of a magnet. A light source in radio-frequency region is made to fall on the sample. It can be accomplished by feeding energy into a coil placed around the sample tube. If the nuclei in the sample resonates with the light source, a signal is detected. Energy is driven from the source through nuclei to the detector coil. The output from the detector can be directed to a cathode ray oscillograph or to a strip of chart recorder after amplification.

The instrumentation technique is displayed in Figure 2.4.

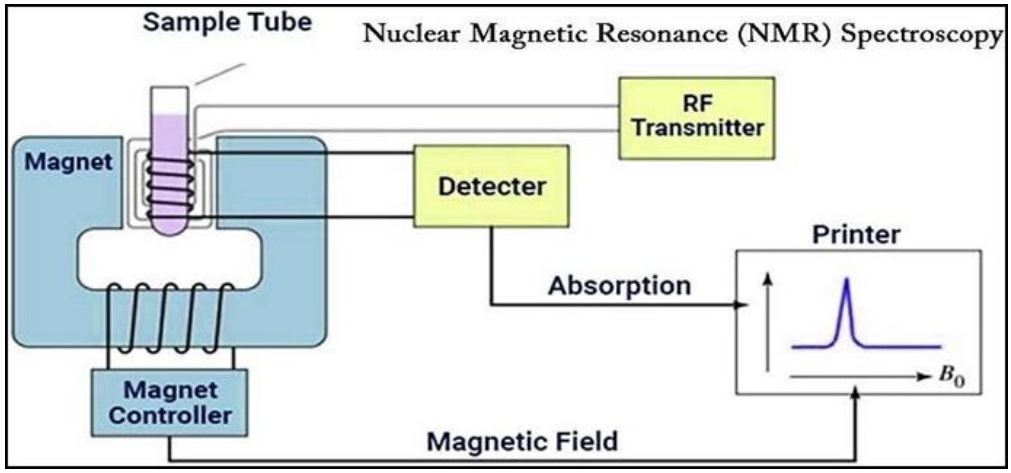

Figure 2.2: Schematic of instrumentation of NMR spectroscopy.

2.5.2. HRMS technique

The mass spectrometer device consists of three main parts:

(a) Ion source. The foremost and a crucial step of achieving a mass spectrum is to ionize the investigated compound. In this technique, sample molecule is bombarded by a beam of light with high for the fabrication of ion in mass spectrometer. An electrically heated tungsten filament is used as the source of bombarding electrons. A few milligram of the sample undergoes in its vapor phase under the operating pressure of 10^{-6} mm. The vapor is allowed to pass through a slit into the ion chamber in this device. Here this vapor is bombarded by a flow of electrons generated by a tungsten filament. As a result of bombardment, the compound generally loses one electron to produce a parent ion radical. But if the energy of the bombarding electron is near equal to 70 eV, the excess energy is utilized in fragmenting the parent ion. This produces the daughter ions or fragment ions. (b) Mass analyser. The cationic ions produced in the ion chamber are accelerated by pertaining an acceleration potential. Theses ions then pass through the mass analyser or the mass filter. Here the fragmented ions are identified on the basis of their m/z ratio and their mass to charge ratio is calculated. (c) Ion detector. The ions which are segregated by the mass analyser, are detected and measured electrically. The ions go through the collecting slit one after the other and fall on the detector. The instrumentation method is depicted in Figure 2.6.

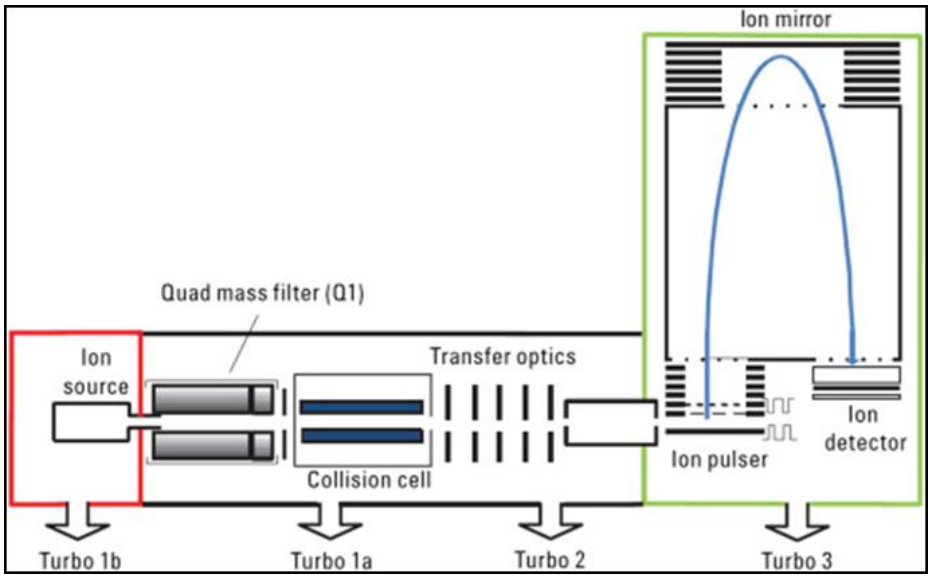

Figure 2.4: Schematic of instrumentation of High resolution mass spectrometry.

2.5.3. IR technique

In common IR devices, the source of Infra-red light used for scanning of an organic compound is Nernst glower which basically a rod containing the sintered mixture of the oxides of Ytterbium, Zirconium and Erbium. The rod is electrically heated to 1500°C to generate Infra-red radiations. The rod of Silicon carbide may also be used to produce Infra-red radiations. Optical prisms or gratings is taken to generate monochromatic light. For prism material, quartz or glass cannot be selected since they absorb light strongly via most of the IR-region. Potassium chloride or certain alkali metal halides are generally used as cell containers or for prism materials as these materials are transparent to most of the IR region under consideration. Light from the source is first split into two beams. One of the beams is passed through the sample solution under examination and is referred as the sample beam. The other beam is termed as the reference beam. When the reference beam goes through the sample solution, its intensity is reduced due to the absorption of certain frequencies that makes a difference in the intensities of these two beams. Intensities of the bands can be monitored as a linear function T (transmittance) against the respective wave-number.
The instrumentation technique is shown in Figure 2.5.

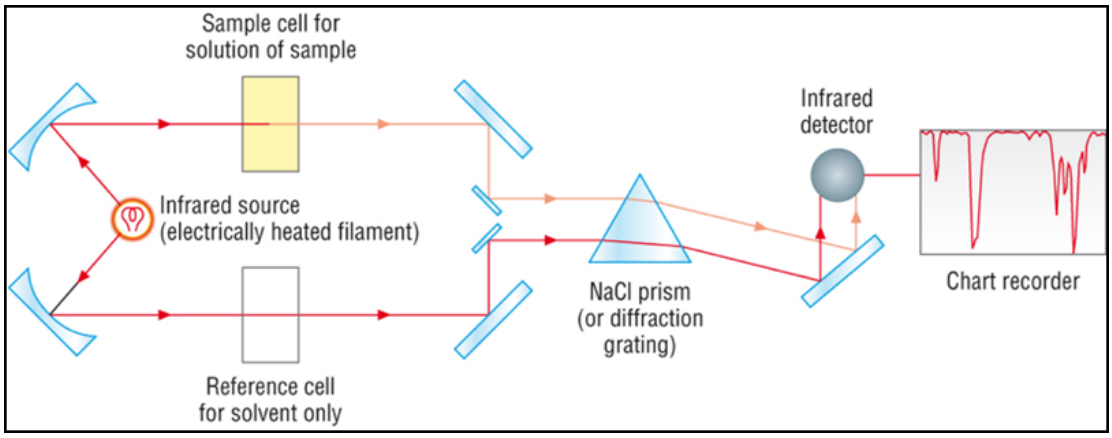

Figure 2.3: Schematic of instrumentation of IR spectroscopy.

2.5.4. UV-Vis technique

Spectrophotometer is used to detect the percentage transmittance of light radiation when light with constant intensity and frequency range is passed through the sample taken in solution state. Thus, the device compares the intensity of the transmitted light with that of the light transmitted through the pure solvent.

The modern UV-Vis spectrometer involves few key parts viz. the source of light, an amplifier, a monochromator filter, a detector and the data recording devices. Hydrogen-deuterium discharge lamp and tungsten Filament lamp are used as the most popular sources of light. These two lamps associated with whole frequency range of the UV-Vis region. Almost all spectrophotometers are double beam instruments. The light used in primary stage is divided into two beams of equal intensity by a beam splitter. One of which passes though the reference and the other through the sample. A schematic representation is shown below in Figure 2.5. which presents the detailed instrumentation of an ultra-violet spectrophotometer.

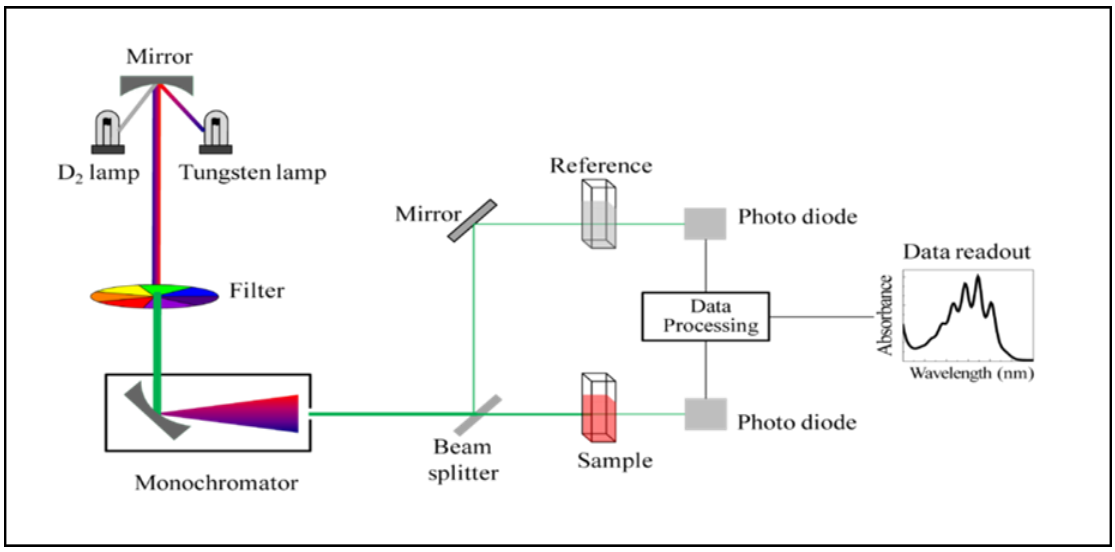

Figure 2.5: Schematic presentation of different parameters involved in absorption spectra measurement

2.5.5. Fluorescence emission measurement technique

A fluorimeter is a machine use to measure the intensity as well its distribution throughout the wavelength range visible to human eye. Upon excitation by a certain wavelength of light generally from ultra violet region of the spectrum the fluorophore undergoes radiative relaxation and consequently emits light in visible rang which is then detected, quantified as well as represented digitally by a detector-computer assembly. Modern fluorimeters are able to detect the emission from a fluorescent compound in very minute concentrations.

The basic segments of a fluorometer includes an excitation source, an excitation monochromator, a cuvette as sample chamber, an emission monochromator and a detector. In most of the cases,

commercial instruments use the right angle detector approach as it minimizes the background noise. In normal instrumentation mode, the studied compound is excited with polarized light and the intensity of the emitted florescence by that compound is recorded by a polarizer analyser. A schematic representation of the fluorimeter instrument is depicted in Figure 2.6 which describes the detailed instrumentation.

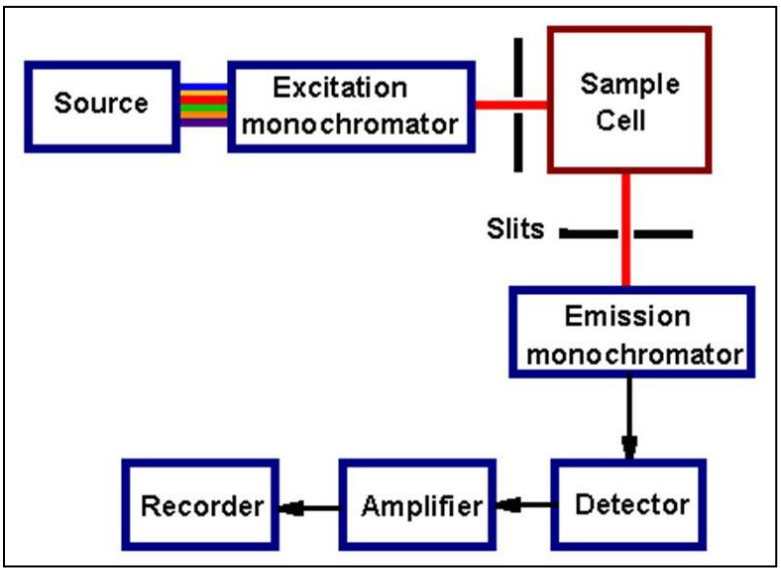

Figure 2.6: Schematic diagram of a fluorometer.

2.5.6. Fluorescence lifetime technique

This instruments measure the life time of a certain fluorophore in its excited state over the course of many events. To reconstruct the fluorescence lifetime decay profile, a technique known as time-correlating single photon counting or TCSPC is used. This method compares the timing of a pulsed excitation source, like a LED or a laser, with the timing of the arrival of single photons on a detector. It needs many a repetition of pulses of excitation source and photons detected to achieve a required statistical data precision. The instrumentation associated with TCSPC-fluorescence lifetime machine is depicted schematically in the following diagram (Figure 2.7).

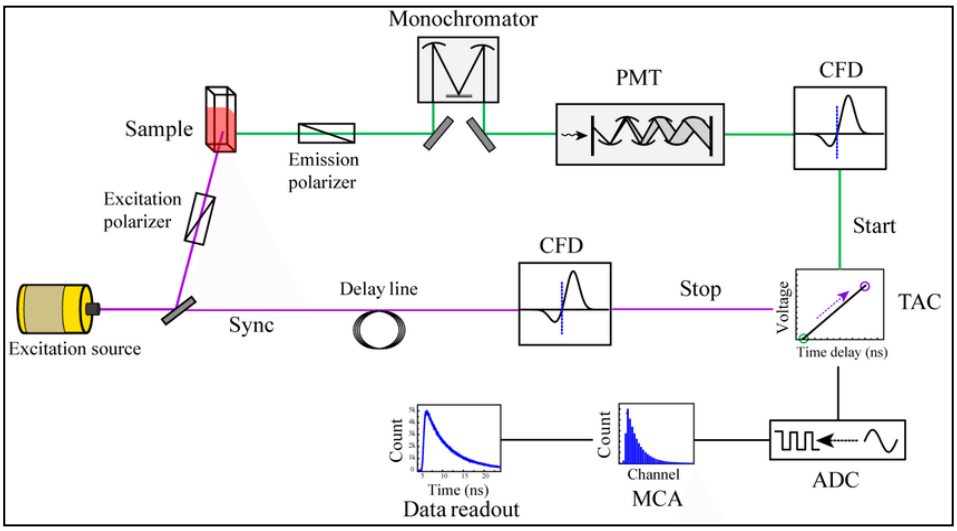

Figure 2.7: Schematic diagram of instrumentation of a time-correlated single photon counting

2.6. Some complementary essential techniques to study the chemosensors

2.6.1. Determination of limit of detection of synthesized chemosensors

The limit of detection or LOD value is a very significant term in the field of chemodosimeter and chemosensors. The lower LOD value of a probe signifies the greater sensitivity of the sensor towards the guest analytes in a minute level. Especially, in case of harmful analytes, the low LOD value of sensor is very much desirable as it indicates that the corresponding probe is able to detect such toxic analytes in concentration levels much lower than its permissible values as recommended by WHO. However, one needs very trace amount of those analytes which is environmental friendly and important for human health also.

The detection limit was determined based on the emission titration of the fabricated probe. To calculate the S/N ratio, the fluorescence intensity of the receptor itself was recorded by 10 times and the standard deviation of blank measurements was measured. So in my thesis work, the LOD value of the developed probes were calculated from the following equation.

$DL = K \times Sb_1/S$

Where K = 2 or 3 (we take 3 in this case); S is the slope of the calibration curve and Sb_1 indicates the standard deviation of the blank solution.

2.6.2. Determination of association constant of synthesized chemosensors

The association constant of a sensor actually is a parameter that determines the stability of a complex which is formed through the interaction between the probe and the specific analyte. The value of association constant (K_a) was determined from the fluorescence intensity data using the Benesi-Hildebrand equation which is formulated as below.

$$1/(F\text{-}F_o) = 1/\{K_a(F_{min}–F_o)\ [M^{n+}]^x\} + 1/[F_{min}\text{-}F_o]$$

Here the emission in absence of, at intermediate and at infinite concentration of metal ion are expressed bythe symbol F_0, F and F_{min} respectively. K_a implies association constant or binding constant and $[M_n]$ is the concentration of the guest analyte (in maximum case, the metal with which the probe binds to). From the plot of $1/ (F\text{-}F_0)$ against $[M_n]^{-1}$ for sensor, the value of K_a has been calculated from the ratio of intercept and slope of Benesi-Hildebrand curve. The plot of $1/(F\text{-}F_0)$ vs. $1/[M_n]$ shows a straight line suggesting the 1:1 complexation of the receptor with the corresponding guest analyte.

2.6.3. Fluorescence quantum yield measurement

Photoluminescence quantum yield of a fluorescence molecule can be defined as the proficiency of converting absorbed light into emitted light, i.e.,

Quantum Yield = number of emitted photons /number of absorbed photons

Quantum yield is also called alternatively as quantum efficiency (QE) or fluorescence efficiency. Quantum yield of a luminescent particle may vary between 0 and 1. Higher value of quantum yield signifies the brighter emission. Quantum yield of a sample is determined by comparising its emission with a reference dye with known quantum yield or measuring it an absolute quantum yield. In order to measure the typical Quantum yield, the absorbance of both the reference dye and studied sample were recorded. After that, fluorescence emission spectra were carried out using the maximal excitation wavelengths and then the integrated areas of the spectra were measured further. The quantum yields were then determined by using the following equation:

$$\Phi X = \Phi S \times \left(\frac{I_x}{I_s}\right) \times \left(\frac{A_s}{A_x}\right) \times \left(\frac{n_x}{n_s}\right)^2$$

Where, s & x designate the standard solution and the unknown solution respectively, I is the integrated area under the fluorescence spectra and φ indicates quantum yield, n is the refractive index of the solvent and A is the absorbance.

According to the position of the absorbance peaks in each case, the reference dye was selected throughout my thesis work. All the absorption and emission spectra for measuring the quantum yield were carried out using Perkin Elmer Lambda 750 spectrophotometer and Shimadzu RF-6000 fluorescence spectrophotometer respectively.

2.7. References

1. B. Diehl, NMR Spectroscopy in Pharmaceutical Analysis, 2008, Chapter 1, 1-41.

2. M. T. Blanda, J. H. Horner and M. Newcomb, *J. Org. Chem.*, 1989, **54**, 4626.

3. A. Jablonski, *Z. Phys*., 1935, **94**, 38.

4. J. R. Lakowicz, *Plenum Press*,**1983**, 496.

5. C. P. Gomez and R. A. Jacobson, John Wiley & Sons, Inc., 2012.

6. Bruker. APEX2, SAINT and SADABS. Bruker AXS Inc., Madison, Winconsin, USA. 2009.

7. G. M. Sheldrick. *ActaCryst.* 2008, **A64**, 112.

Fabrication of a new coumarin based fluorescent “turn-on” probe for distinct and sequential recognition of Al^{3+} and F^- along with its application in live cell imaging

Fabrication of a new coumarin based fluorescent "turn-on"probe for distinct and sequential recognition of Al^{3+} and F^- along with its application in live cell imaging

Abstract

A new coumarin based fluorescent switch PCEH is fabricated which displays high selective sensing towards Al^{3+} among other metal cations at physiological pH. On gradual addition of Al^{3+}, PCEH shows a brilliant "turn-on" emission enhancement in MeOH/H_2O (4/1, v/v) solution. This new fluorescent switch is proven to be a reversible probe by gradual addition of F^- into the PCEH-Al^{3+} solution. Detection limit as well as binding constant values are calculated to be in the order of 10^{-9} M and 10^4 M^{-1} respectively. We have also explored its potential as a biomarker in the application of live cell imaging using breast cancer cells (MDA-MB-231 cell).

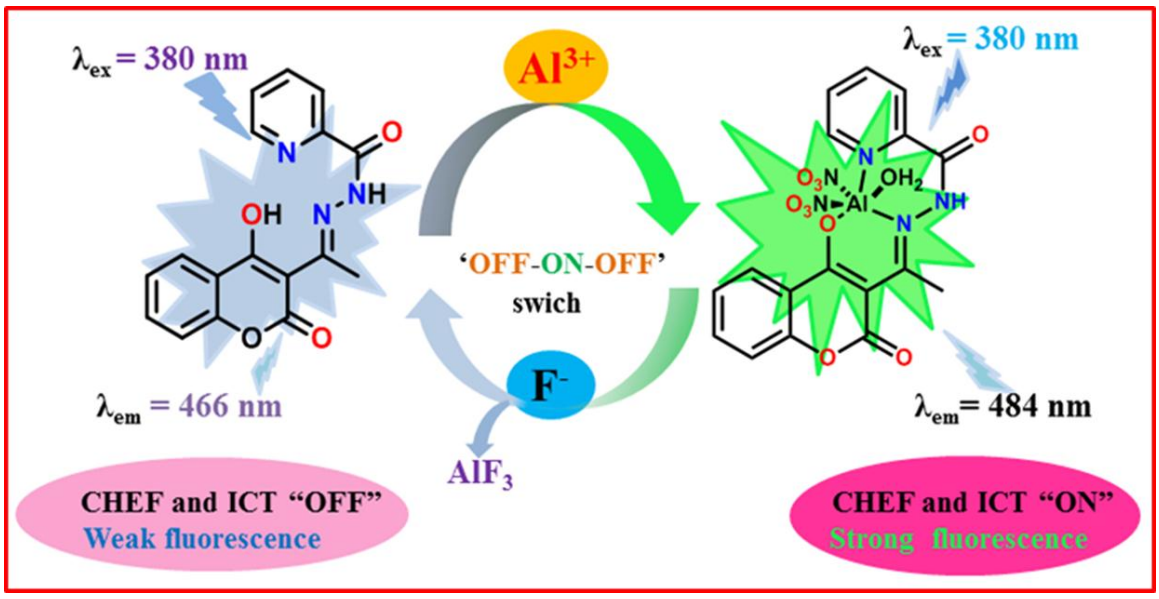

3.1. Introduction

Fluorescent molecular switches which can distinctly detect specific metal cations just by turning on their photophysical properties have been a tremendous source of attraction of the budding researchers over the last few years.[1-3] The interest in the fabrication of these fluorescent molecules is at peak owing to their huge need for the recognition and identification of lethal heavy metal ions present in the environment and also in living organisms.[4,5] This interest has stimulated the fabrication of a significant number of fluorescent sensors for cations which consists of a variety of organic fluorophores, for instance coumarin.[6,7] fluorescein[8,9] pyrene[10,11] and boron-dipyrromethene.[12,13] Recently the fluorescent switches procured from Schiff bases have drawn a huge deal of attention for the recognition of metal ions due to their inexpensive and easy synthetic route, compelling complexation capability, fast and immediate response and elevated sensitivity.[14-17] Due to the C=N isomerization, Schiff base fluorescent probes exhibit a weak fluorescence whereas after binding with the metal ions, the probes show a noteworthy emission enhancement along with a noticeable color alteration owing to the inhibition of C=N isomerization. Aluminium is the third most plentiful metallic element of all elements present in the earth's crust and being the most plentiful metallic elements, aluminum ions have been widely utilized in water purification systems, cosmetics, food packaging, food additives and electronic devices.[18-22] Aluminium is widely used in our daily life such as pharmaceutical manufacturing, food processing and purifying and industrial fabrication.[23,24] It has extensive applications in the textile, food, dye production and paper industries along with the production of household tools. Nevertheless, the extensive use of Al^{3+} ions in our daily life in diverse forms has created a threat to damage the ecological atmosphere. Unnecessarily excessive amount of Al^{3+} can result in acute inhibition in bone development that sometimes leads to diseases like osteoporosis, osteomalacia etc. Advance research leads to the fact that too much Al^{3+} will cause memory loss thereby leading to life-menacing diseases like Alzheimer's, Parkinson's, dementia.[25-27] Excessive presence of aluminium can cause severe damage in our nervous system which eventually results into other dangerous diseases such as gastrointestinal problems, kidney malfunction, headaches, lateral sclerosis, hypochromic anaemia etc.[28-30] Further studies confirmed that large concentration of aluminium ions could result in soil acidification thereby inhibiting the growth of plants.[31,32] The World Health Organization (WHO) has stated that the maximum permissive limit of Al^{3+} for daily intake is about 3-10 mg.[33-35] So because of the different harmful effects of excessive presence of aluminium in

environment, industry as well as in human body, it is of utmost importance to develop some easy noteworthy technique in order to distinctly recognize Al^{3+} to control its effect. The fluorescence-based method has confirmed to be one of the most suitable and fast and facile strategies rather than the former traditional analytical methods for the determination of Al^{3+} which includes atomic emission spectroscopy (AES) and atomic absorption spectroscopy (AAS), laser-ablation microprobe mass analysis (LAMMA) and coupled plasma mass spectroscopy (ICP-MS) and also those methods involved difficult sample treatment, the unnecessary usage of chemicals and luxurious measurement apparatus.[36] Due to their elevated hydration capability, low coordination capacity and also the absence of spectral properties, distinct recognition of Al^{3+} ions continue to be a grand challenge.[37-39] Hence, the design and fabrication of new Schiff base probes with an emissive moiety for the selective and sensitive sensing of metal ions is of immense importance for environmental, industrial and biological systems.

3.2. Prior works

To date, there are many reports of fluorescent sensors for distinct recognition of Al^{3+} ions with various fluorophore moieties have been reported in the literature.[40-47] Again, Singh et al. developed a silatrane-based Schiff base-functionalized probe which is able to detect Al^{3+} ions with excellent detection limit of 10^{-7} M, while Aydin et al. designed a hydrazide-based "turn-on" swich to detect Al^{3+} ion only and showed a limit of detection (LOD) value of 6.47 nM.[48,49] Recently in 2021, Das et al. fabricated a pyridine-pyrazole hydrazide-based highly sensitive probe for solely detecting Al^{3+} ion with a good detection limit of 4.78 µM.[50] Liu et al. synthesized a Schiff base fluorescent "off-on-off" reversible swich to recognize Al^{3+} with detection limit of 10^{-8} M.[51] Lv et al. and Jiang et al. both reported a "turn-on" fluorescent receptor for the Al^{3+} in 2019. Hwang et al. fabricated a simple Schiff base sensor which selectively binds with Al3+ with a very little detection limit of 290 nM and executed live cell imaging studies.[52] Another interesting report on aluminum sensors is found by Balamurugan et al. They synthesized a phenazine fluorophore based sensors which displays AIE effect selectively for Al^{3+} ion.[53] Again in 2018, Guchhait group fabricated a CHEF sensing mechanism based fluorogenic probe for nanomolar range detection of Al^{3+} and studied its crystal structure and also its application in breast cancer cell imaging.[54] A few fluorescent probes were synthesized with a coumarin framework though, because of its low LOD values, high costing values etc.

3.3. Present work

Here in this article, we have established a simple design and fabrication of a fluorescent "turn on" switch (PCEH) based on coumarin framework and precisely for recognising only Al^{3+} among other cations with a good detection limit and a brilliant binding constant. So, in this study PCEH displays a "turn-on" emission response towards Al^{3+} and also exhibits its reversible nature via F^- titration.

3.4. Results and discussions

3.4.1. Synthesis of PCEH

The synthetic route towards the probe, PCEH was shown in scheme 3.1. Compound 1 and 2 were synthesized according to the reported procedures in literature.[55,56] ^1H and ^{13}C NMR spectroscopy along with ESI mass spectrometry confirm the chemical structure of PCEH (Fig. A3.1-A3.4, Appendix). Reflux condensation of compound 1 and 2 in ethanol for 5 h affords the desired fluorescent probe, PCEH with yield of 85%.

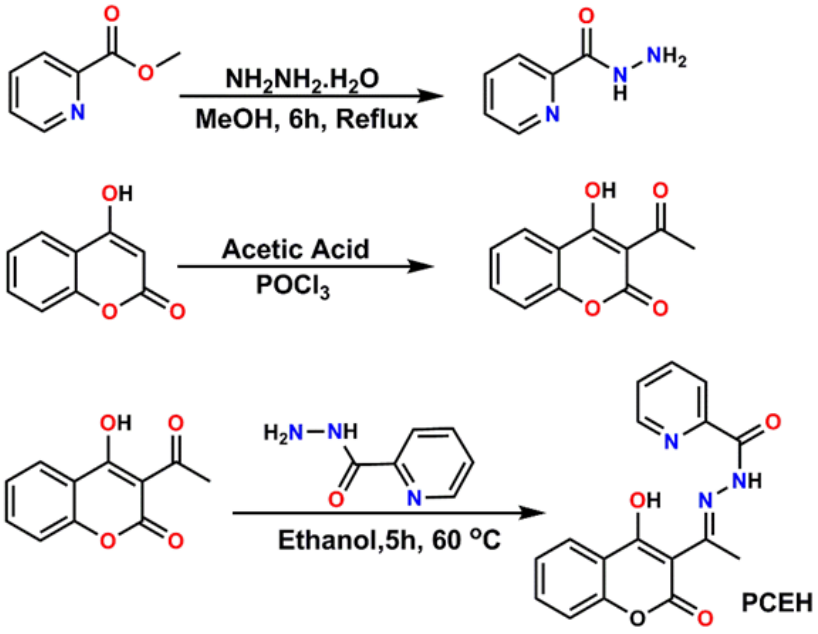

Scheme 3.1: Synthetic scheme of the probe, PCEH.

3.4.2. ^1H NMR and HRMS analysis of PCEH

^1H NMR titration of the probe (PCEH) was carried out in DMSO-d_6 solvent upon addition of 1 equivalent of Al^{3+}. From the NMR titrtation data, it was noticed that the singlet peak at δ 15.3 ppm

for -OH group in the free probe is vanished upon addition of 1eq. Al^{3+}, indicating the participation of –OH group in complex formation. All the aromatic protons are also observed in the expected region. (See appendix). We have also recorded the HRMS of PCEH. The HRMS of PCEH shows a peak at m/z 346.0648, probably for $[M+Na]^+$.

3.4.3. Cation sensing studies using UV-Vis spectroscopy

The absorbance properties of PCEH were studied in MeOH/H_2O (4/1, v/v) solution at 25°C under physiological pH (10 mM HEPES buffer, pH=7.2). The UV-Vis spectrum of PCEH (10 μM) in MeOH/H_2O (4/1, v/v) shows a moderate absorbance band at 372 nm with two shoulders at 281 and 392 nm. Gradual incremental addition of Al^{3+} into the solution of PCEH displays an increase of the former absorbance peak at 372 and 392 nm and a new absorbance band at 386 nm was noticed along with a small shoulder at 372 nm supporting the coordination of Al^{3+} to PCEH (Fig. 3.1). To establish the selectivity of the probe, the absorption spectral changes of the probe were recorded in presence of other metal cations such as Na^+, Mg^{2+}, Mn^{2+}, Ba^{2+}, Bi^{3+}, La^{3+}, Ce^{3+}, Ga^{3+}, In^{3+}, Fe^{3+}, Cr^{3+}, Co^{2+}, Ni^{2+}, Hg^{2+}, Zn^{2+}, Cu^{2+}, Pb^{2+} and Cd^{2+}. There is no significant absorbance change observed for any other metals except only for Al^{3+} (Fig. 3.1)

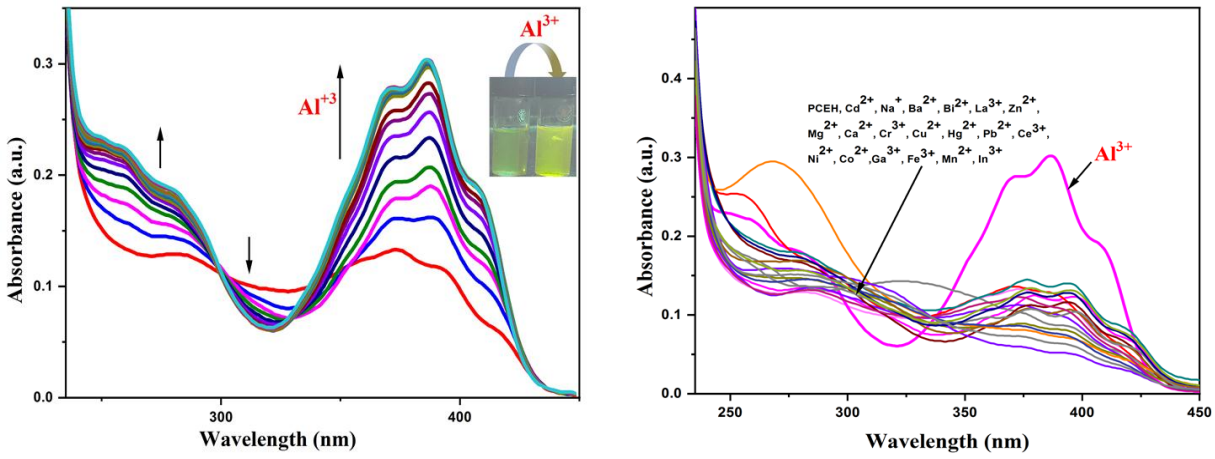

Figure 3.1: Change in UV-Vis spectrum of PCEH (10 μM) upon addition of Al^{3+} (20 μM) in MeOH/H_2O (4/1, v/v) (HEPES buffer, pH=7.2). (left side) and change in UV-Vis spectrum upon addition of different metal ions (40 μM) in MeOH/H_2O (1/1, v/v) using HEPES buffered solution at pH=7.2 (right side).

3.4.4. Cation sensing studies using emission spectroscopy

The fluorescent probe, PCEH exclusively exhibits an emission band with weak emission intensity with the maxima (F_0) appearing at 466 nm (λ_{ex}, 380 nm) in MeOH/H_2O (4/1, v/v). The emission quantum yield is of the probe (PCEH) is very low (φ = 0.01). Upon incremental addition of Al^{3+} to the PCEH solution, a sharp emission enhancement was observed showing another hump at 484 nm along with the hump at 466 nm (φ = 0.31) (Fig. 3.2). This emission enhancement falls under a strong "OFF-ON" category of emission property. Further on addition of F^- to the solution of PCEH-Al^{3+}, the emission intensities at 484 nm as well as 466 nm reverted back to the original intensity of the probe which clearly reflects the fact that PCEH has returned to its free form (Fig. 3.2) thereby making the probe a reversible fluorescent switch. Thus PCEH can be utilized as an "OFF-ON-OFF" fluorescence signaling probe. The changes in emission property of the probe, PCEH was also observed in presence of a group of metal ions such as Na^+, Mg^{2+}, Mn^{2+}, Ba^{2+}, Bi^{3+}, La^{3+}, Ce^{3+}, Ga^{3+}, In^{3+}, Fe^{3+}, Cr^{3+}, Co^{2+}, Ni^{2+}, Hg^{2+}, Zn^{2+}, Cu^{2+}, Pb^{2+} and Cd^{2+} to reveal the distinct sensitivity of PCEH towards only Al^{3+} in MeOH/H_2O (4/1, v/v). It is noted that none of the abovementioned metal ions resulted in any noteworthy changes in the emission profile (Fig. 3.3).

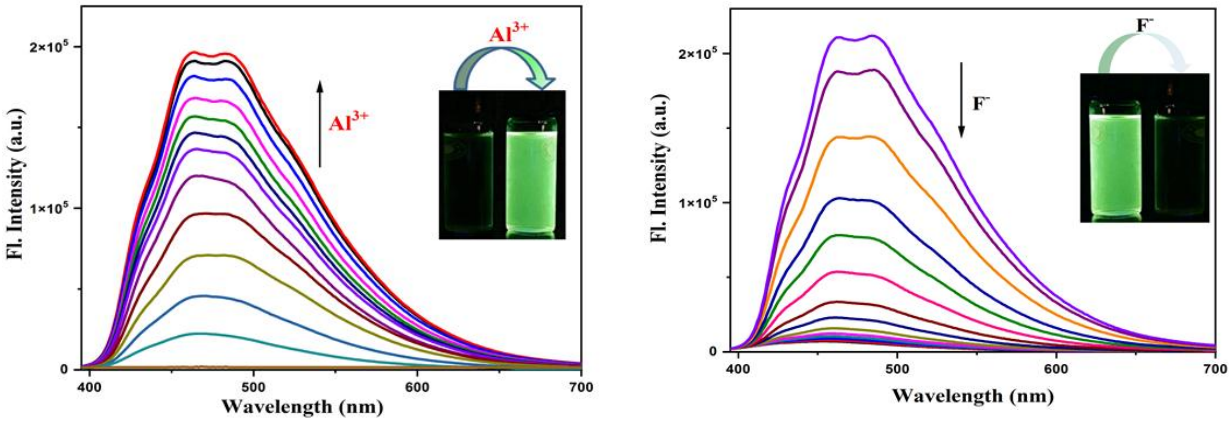

Figure 3.2: Change in emission spectra of PCEH (10 µM) upon gradual addition of (a) Al^{3+} (20µM) in MeOH/H_2O (4/1, v/v) (HEPES buffer, pH=7.2). (Inset shows the change in colour under UV-radiation) (left side) and change in emission spectra of PCEH-Al^{3+}(10 µM) upon gradual addition of F^- (20 µM) in MeOH/H_2O (4/1, v/v) (HEPES buffer, pH=7.2). (Inset shows the change in colour underUV-radiation) (right side).

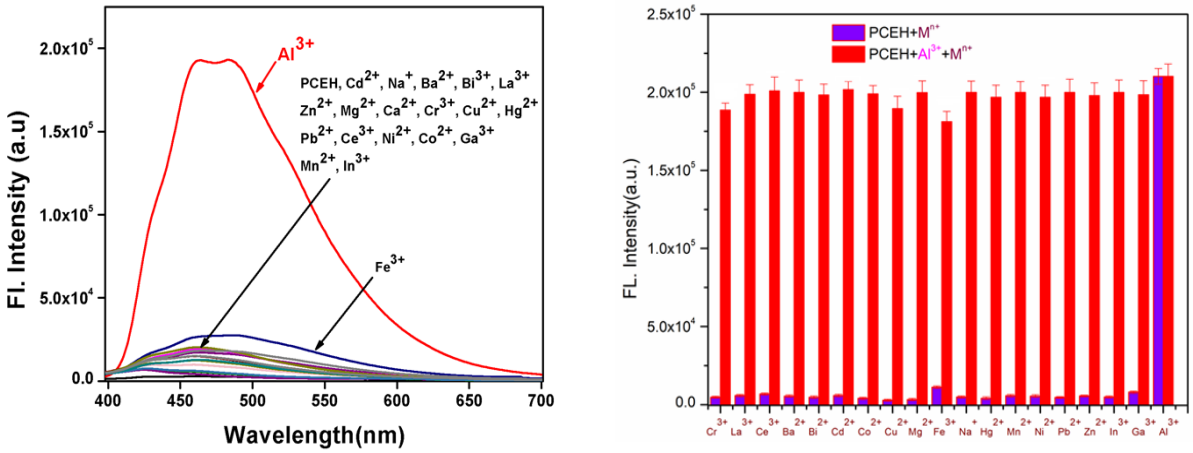

Figure 3.3: Change in emission intensity of PCEH (10 µM) upon addition of different metal ions in MeOH/H_2O (4/1, v/v) using HEPES buffered solution at pH = 7.2 (left side) and bar diagram illustration of the relative emission intensity of HMCP upon addition of various metals (10 µM) in MeOH:H_2O (4:1, v/v) (HEPES buffer, pH=7.2) (violet bars) and Al^{3+} (20 µM) in presence of other metal ions (red bars) (right side).

Now to facilitate the estimation the stoichiometry of the complex of PCEH with Al^{3+}, Job's plot analysis was executed where the maxima shows the mole fraction at 0.5 for Al^{3+}, which corresponds to the 1:1 complex formation of PCEH and Al^{3+} (Fig. 3.4). The detection limit of PCEH for Al^{3+} was calculated to be $(2.64\pm0.11)\times10^{-9}$ M which was found from the emission spectral change of PCEH upon incremental addition of Al^{3+} following the equation, LOD = K × SD/S where 'SD' is the standard deviation of the blank solution of the probe and 'S' in the slope of the curve (Fig. 3.5).

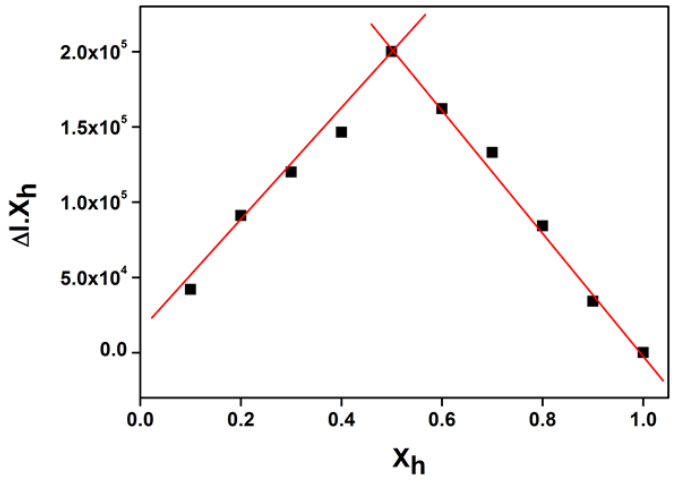

Figure 3.4: Job's plot of HMCP for Al^{3+}

This low detection limit value evidently signifies to the fact that PCEH has much effectiveness in detecting Al^{3+} in a very minute level and compared with other previously reported probes in Table A1(Appendix). The association constant (K_a) of PCEH for Al^{3+} was also determined using Benesi-Hildebrand equation and found to be (9.47± 0.45)×10^4 M^{-1} (Fig. 3.5), indicating that PCEH-Al^{3+} complexation is adequately stable.

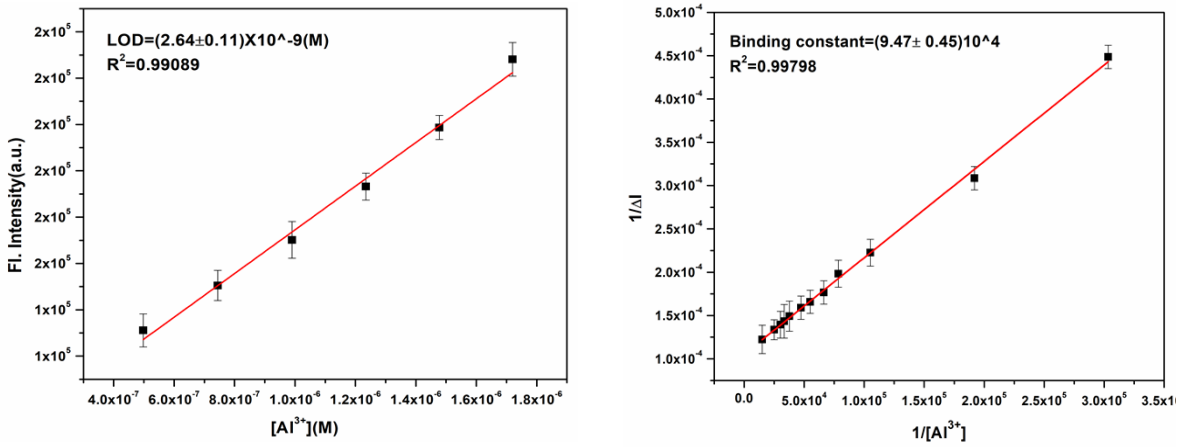

Figure 3.5: Linear response curve of PCEH at 484 nm depending on the Al^{3+} concentration (left side) and determination of binding constant of PCEH at 484 nm depending on the Al^{3+} concentration using Benesi-Hildebrand equation (right side).

The pH titration study of PCEH was carried out and the titration indicated to the fact that the new fluorescent probe, PCEH does not experience any major change in the emission profile at 473 nm thereby revealing that the probe, PCEH is independent of pH. Now upon addition of Al^{3+} in the solution of PCEH, the emission intensity increases rapidly within the pH range of 3-7 and achieving the highest intensity at pH 7.2 thus stating the fact that PCEH is competent in detecting Al^{3+} at neutral pH (Fig. 3.6). But on further enhancement of pH, the emission intensity gets decreased thus indicating that in the pH range of 8-12, PCEH cannot detect Al^{3+}. In the basic region, the deprotonation of the -OH group may cause the dissociation of the probe which eventually results into the incapacity of PCEH in sensing Al^{3+}. Hence the probe PCEH can detect Al^{3+} in the neutral pH range with an excellent efficacy.

3.4.5. Fluorescence lifetime decay studies of PCEH with Al^{3+}

To comprehend the excited state stability of this fluorescent switch, the lifetime measurements were also carried out. The fluorescence lifetime of the free probe (PCEH) measured at λ_{em} = 484

nm was found to be 1.42 ns which fits well with a mono-exponential decay pattern whereas the average lifetime of PCEH-Al^{3+} displays a prominent increase of 5.14 ns due to the stable complexation of PCEH with $Al^{3+}$and the pattern of this decay was found to be a bi-exponential one. On the other hand, after addition of F^-, the lifetime of PCEH-Al^{3+} again decreases and found to be 2.31 ns owing to the fact that the addition of F^- to PCEH-Al^{3+} solution is responsible for the reverting back of the emission intensity of free PCEH (Fig. 3.6). An interference experiment was then carried out by studying the fluorescence intensity of PCEH (10 μM) in presence of other metal ions (20 μM) in order to study the specific selectivity of the probe. It is observed from the experiment that the emission enhancement of PCEH is noticeably specific towards Al^{3+} (Fig. 3.3) and no noteworthy change was observed in presence of the other metal cations except Fe^{3+}, Cr^{3+} and Cu^{2+}.

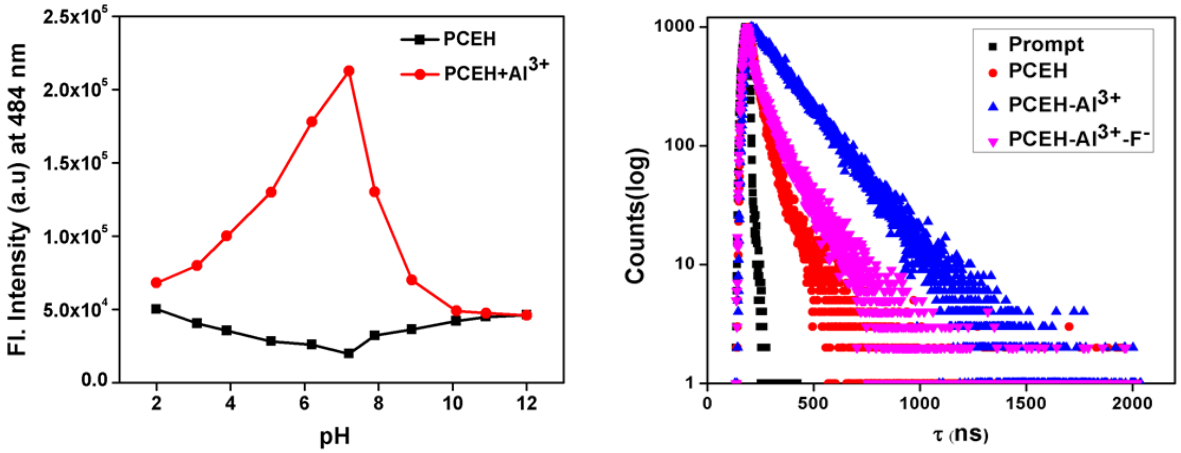

Figure 3.6: pH study of PCEH for Al^{3+} (left side) and lifetime decay profile of PCEH and PCEH-Al^{3+} (right side).

3.4.6. Reversibility and time dependent study

An efficient chemosensor must have two essential features, reversibility and reusuability in its sensing action. So to examine the reversibility, a solution of PCEH was prepared inaq. MeOH solution (4/1, v/v). Upon the addition of Al^{3+} ion to the PCEH solution, we observed that it displays a 'turn on' emission. Subsequently, the addition of F^- ion to PCEH:Al^{3+} solution gives turn off emission as aluminum ion is removed from the solution due to formation of stable AlF_3, releasing a free probe. This observation implies that the sensing capability of the probe PCEH is reversible. To further demonstrate the reversibility, the experiment was carried out using aq. MeOH solution

of PCEH for second time. Upon further addition of Al^{3+} ion to the solution gives a 'turn on' emission and sequential addition of F^- ion displays turn off fluorescence. For every cycle, a increase in fluorescence intensity of PCEH solution in addition of Al^{3+} ion and a decrease in fluorescence intensity of PCEH:Al^{3+} complex in addition of F^- ion was observed for four cycle, with slight loss of fluorescence intensity (Fig.3.7). Hence due to the reversible nature, our probe can be used for monitoring Al^{3+} ion in real sample with high efficiency.

A fast fluorescence response chemosensor is always preferable in practical application. Time dependent study has been performed in order to interpret the instance fluorescence response of the probe PCEH. At different time interval, the fluorescence intensity was recorded with different concentration of Al^{3+} (10 µM, 20 µM, 30 µM). Fig. 3.7 revealed that our present probe PCEH can detect Al^{3+} within 0-10 second after addition. After 10 second of Al^{3+} addition, the fluorescence emission intensity at 484 nm almost reached its saturation level, which implies completion of the reaction. Hence PCEH can be considered as a proficient and reliable probe for recognition of Al^{3+} ion within minimal time (0-10 sec).

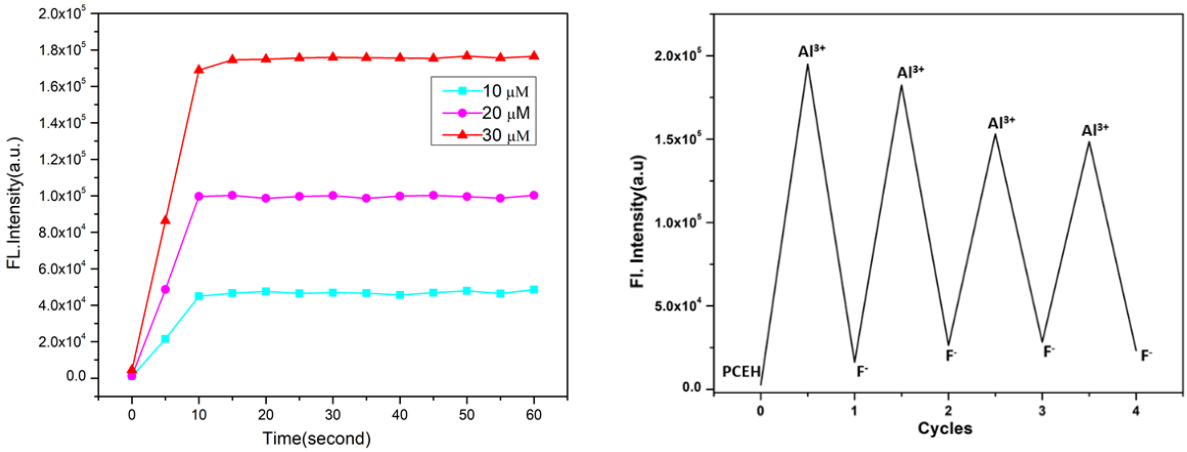

Figure 3.7: Time dependent fluorescence response study of PCEH (20 µM) with different concentration of Al^{3+} ion (10-30 µM) in MeOH/H_2O solution (4/1, v/v) at 484 nm (left side) and the fluorescence 'ON-OFF' repetitive cycle upon sequential addition of Al^{3+} and F^- ion at 484 nm (λ_{ex} = 380 nm) in MeOH:H_2O (4/1, v/v) solution (right side).

3.4.7. Probable sensing mechanism of PCEH towards Al^{3+}

The "turn-on" emission enhancement of the probe (PCEH), upon addition of Al^{3+} may be accredited to the CHEF (Chelation induced fluorescence) as well as ICT (Internal Charge Transfer)

process. When aluminum gets coordinated to the probe, it forms a stiff binding pattern which accordingly increases the rigidity of the complex thus resulting in the sharp enhancement in emission intensity. The red shift of ~18 nm in the emission maximum, after addition of Al^{3+} may be attributed to the ICT (Internal charge transfer) mechanism. The probable binding mechanism is confirmed by comparing ^{1}H-NMR spectra of PCEH and PCEH:Al^{3+} complex (Fig. 3.8). Upon addition of Al^{3+}, the peak at 15.57 ppm corresponding to the phenolic –OH group disappeared in the ^{1}H-NMR spectrum of PCEH, which implies the participation of –OH group in the complex formation. Again, the proton signals of –NH group and pyridine moiety shifted downfield, suggesting the N atom of pyridine unit and imine group might coordinate to the central Al^{3+} ion. Furthermore, HRMS of PCEH:Al^{3+} (Fig. A3.5, Appendix) and Job's plot analysis significantly indicate the formation of 1:1 complex between PCEH and Al^{3+} ion. On the basis of the aforesaid informations, a probable binding mode of PCEH with Al^{3+} is shown in the diagram below (Fig. 3.9), which was consistent with previous reported works.[57] In Table 1, a comparison of the probe, PCEH was displayed with other probes which include the testing conditions, selectivity, sensitivity etc.

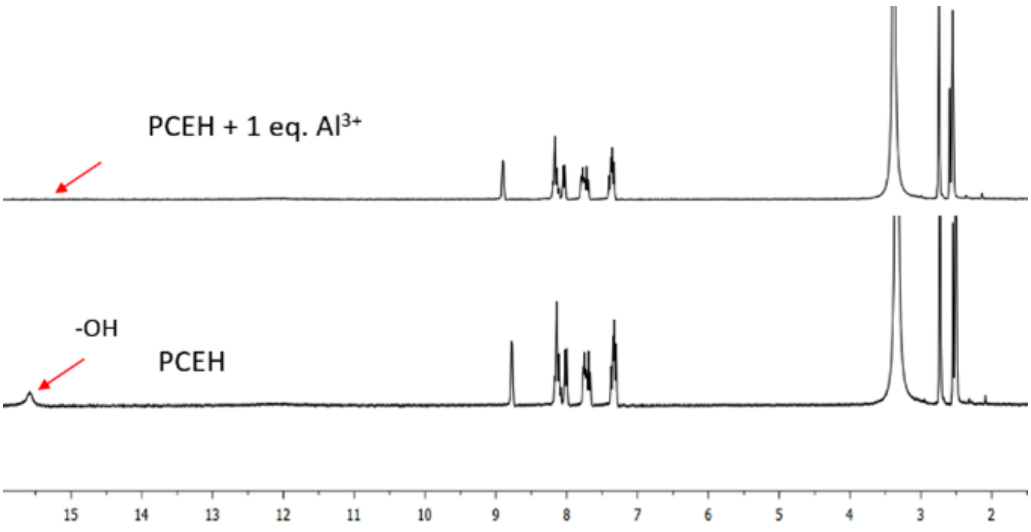

Figure 3.8: Comparison of ^{1}H-NMR spectra of PCEH and PCEH:Al^{3+} complex in DMSO-d_6.

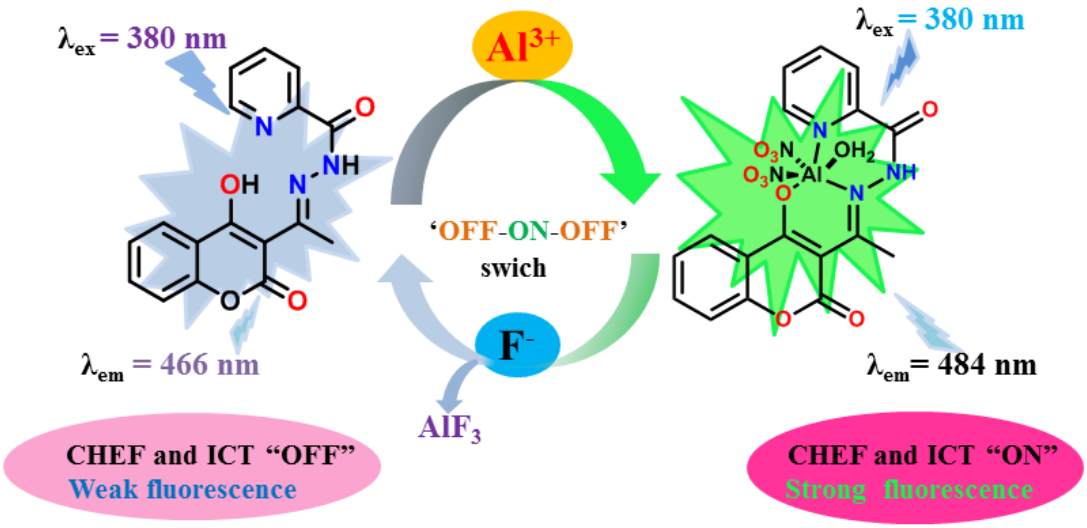

Figure 3.9: Probable sensing mechanism of PCEH with Al^{3+}.

3.4.8. Practical application as Dip-stick experiment: detection of Al^{3+} using TLC plate

We have executed a proficient method known as dipstick experiment to exhibit some luminous applications of this new fluorescent probe where the probe can behave as a fluorescent portable kit displaying its sensing property towards distinct metal ions in solid state too. Without the aid of any instruments, one can get vital qualitative information on detecting $Al^{3+}$from using this experiment. So to perform this experiment, few thin-layer chromatography (TLC) plates were arranged andthey are dipped into PCEH solution (2×10^{-4} M) in MeOH and then kept for some time so the solvent gets evaporated. Then the TLC plates are immersed into Al^{3+} (2×10^{-3} M) solution and then the solvent was evaporated again in order to dry. These dried test strips were again dipped into F^- solution (2×10^{-3} M), and allow them to dry in order to evaporate the solvent. The distinct color change of TLC plates from colorless to cyan color in the case of Al^{3+} and from cyan to almost colorless in presence of F^- ion was observed under UV light (Fig. 3.10). This experiment helps one to thoroughly and easily study the detection of Al^{3+} by naked eye.

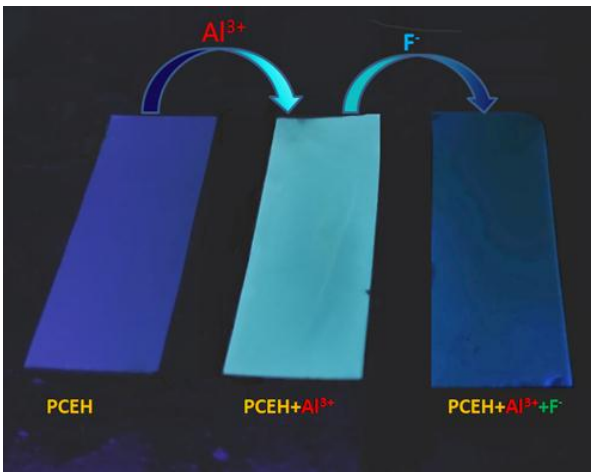

Figure 3.10: Pictures of TLC plates immersed in MeOH/H_2O (4/1, v/v) solution, after addition of (a) Al^{3+}-MeOH solution and (b) F^--MeOH solution under UV chamber. [PCEH] = 2×10^{-4} M, [Al^{3+}] = 2×10^{-3} M, [F^-] = 2×10^{-3} M.

3.4.9. Application in biological field via live cell imaging in human breast cancer cells

From the MTT experiment it can be stated that the probe, PCEH has a very negligible toxicity at lower concentrations towards human breast cancer (MDA-MB-231) (Fig. 3.11). The IC_{50} value of PCEH is found to be 178 µM and therefore we have preferred the dose for the experiment to be 15 µM as the chosen dose should be less than the IC_{50} value (Fig. 3.11).

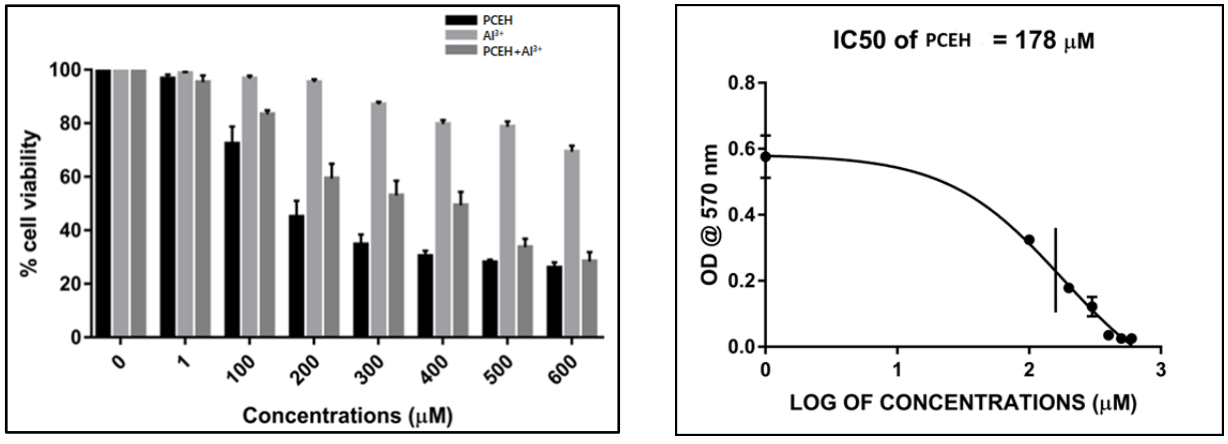

Figure 3.11: MTT assay of PCEH, Al^{3+} and PCEH-Al^{3+} complex in MDA-MB-231 cell line (left side) and IC_{50} dose of the probe (PCEH) in breast cancer cell; calculated to be 178 µM (right side).

Now the fluorescence imaging study under microscope disclosed that the treatment of the breast cancer cells with PCEH itself shows no fluorescence while upon incubating the MDA-MB-231 cells with 15μM of Al^{3+} and PCEH a bright blue fluorescence in the intracellular region was observed (Fig. 3.12). So we can conclude the observation by indicating to the fact that the probe, PCEH can easily go through the cell membrane in order to bind with the intracellular Al^{3+} ion. Additionally, when F^- ion solution (15μM) is added to the former solution, the bright blue fluorescence induced by Al^{3+} ion is almost diminished inside the human breast cancer cells. Further, there is no physical change noticed of the cells in bright field images after incubation with Al^{3+} and F^- ion signifying that the MDA-MB-231 cells are viable and PCEH is not toxic at that specific concentration (Fig. 3.12). Therefore, our probe can be served as a cell membrane-penetrable fluorescence kit that has efficient biological application in living cells organisms for detecting Al^{3+} and F^- ion.

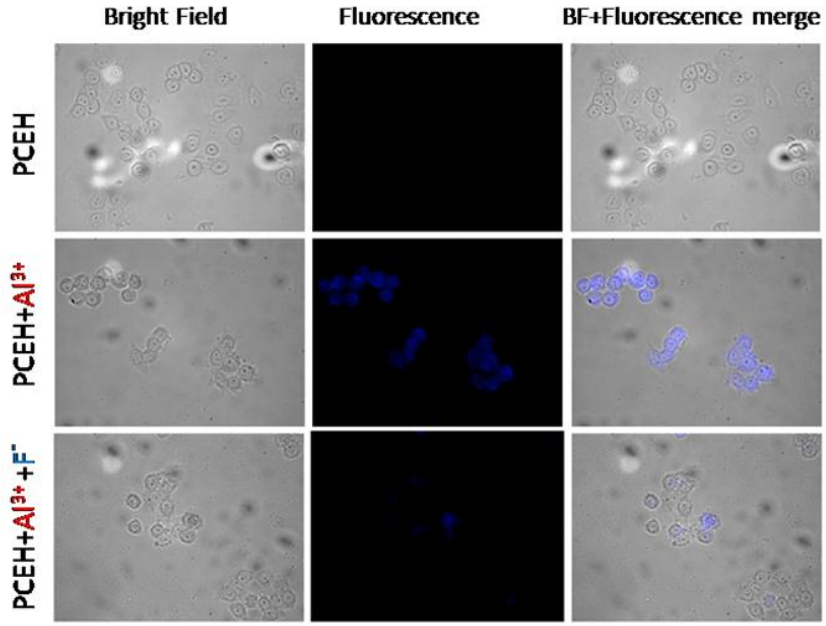

Figure 3.12: Fluorescence image of MDA-MB-231 cells after incubation with 15 μM PCEH and PCEH-Al^{3+} and PCEH-Al^{3+}-F^-. DAPI is used to stain the nucleus.

3.5. Experimental

3.5.1. *Material and instrumentations*

All the reagents and organic chemicals used in this synthesis are purchased from Aldrich. All spectroscopic grade solvents were from other commercial sources and used with no additional

refinement.^{1}H and ^{13}C NMR spectra were recorded on Brucker 300 MHz instrument and DMSO-d_6 was used as solvent using TMS as an internal standard. The chemical shifts are reported as □ in units of parts per million (ppm). HRMS mass spectra were confirmed on Waters (Xevo G2 Q-TOF) mass spectrometer. Elemental analysis was carried out in a 2400 Series-II CHN analyzer, PerkinElmer, USA. A PerkinElmer Lambda 750 spectrophotometer was used to obtain absorbance spectra and emission property was measured using Shimadzu RF-6000 fluorescence spectrophotometer at room temperature (298 K). Lifetimes were measured using a time-resolved spectrofluorometer from IBH, UK.

3.5.2. Synthesis of pyridine-2-carboxylic acid [1-(4-hydroxy-2-oxo-2H-chromen-3-yl)-ethylidene]-hydrazide (PCEH)

Pyridine-2-carboxylic acid hydrazide(**2**) (0.17 g, 1 mmol) was added to the ethanolicsolution of 3-acetyl-4-hydroxy-chromen-2-one(**1**) (0.25 g, 1mmol) and the mixture was refluxed for about 5 h. After completion of the reaction, orange precipitation was obtained which was subjected to column chromatography furthermore to yield pure orange solid. Yield was, 0.274 g, 85%.

Anal. Calc. for $C_{17}H_{13}N_3O_4$(PCEH): Calc. (%) C,63.16; H,4.05; N,13.00. Found (%), C,63.96; H 3.95; N,12.87.

^{1}H NMR (300 MHz, DMSO-d_6): δ(ppm) 2.73(s, 3H),7.33-7.30 (m, 2H),7.36(d,J=7.2,1H), 7.77-7.66 (m, 3H),8.01 (d, J = 6.0, 1H), 8.14(t, J= 9Hz, 1H), 8.77 (s, 1H), 15.58 (s, 1H),

^{13}C NMR (75 MHz, $CDCl_3$): δ(ppm): 97.64, 116.48, 119.91, 123.05, 123.41, 124.74, 125.02, 126.34, 128.63, 129.70, 132.52, 133.95, 134.18, 136.55, 137.45, 149.58, 150.75, 153.79, 154.59, 161.04, 162.32, 173.64,181.36.

IR data (KBr) (cm^{-1}): 3512, υ(O-H);3165, υ(Ar-H), 1657,υ(C=N).

HRMS: calculated for $C_{17}H_{13}N_3O_4$ $[M+Na]^+$, (m/z) = 346.08; found = 346.0648.

3.5.3. General Method for UV-Vis and Fluorescence Titration

UV-Vis titration, stock solution of the probe, PCEH (10 μM) was prepared in [($MeOH/H_2O$), 4/1, *v/v*] (at 25°C) using HEPES buffered solution. Deionized water was used to make all the solutions

of guest cations using their chloride salts (1×10^{-5} M) using HEPES buffer at physiological pH. Solutions of different concentrations of the probe and all the cations were prepared separately and then the spectra of these solutions were recorded by means of UV-Vis method. Similarly, for fluorescence titrations, stock solutions were prepared using similar methods and then the spectra were recorded with the help of fluorescence method.

3.5.4. Live cell imaging studies

3.5.4.1. Cell cytotoxicity assay

Cell cytotoxicity assay was performed on triple negative breast cancer cell line MDA MB-231 with aluminum nitrate(Al^{3+}), PCEH and PCEH-Al^{3+} complex according to the following procedure as described by S. Gharami et al. [48]. MDAMB-231 cells were seeded in 96 well plate at a density of 5×10^3 cells per well followedby incubation at 37°C for 24 h at a 5% CO_2 atmosphere. The cells were treated with individual doses of free PCEH, Al^{3+} and PCEH-Al^{3+} complex (0, 1, 100, 200, 300, 400,500, 600 µM) along with control for 24 h. The probe PCEH was dissolved in DMSO while Al^{3+} was used by dissolving in aqueous medium maintaining the final concentration of DMSO below 1%. 10 µL of MTT solution (5 mg/mL) was added to each well after 24 h treatment. Subsequently, the plates were incubated under dark condition in a CO_2 incubator at 37 °C for 3 h. Then 100 µl DMSO was added to each well to solubilize theformazan crystals and the plates were shaken briefly before quantification at 570 nm with the help of a multi-mode reader (SpectraMax i3x, Molecular devices). IC_{50} value of PCEH was determined by plotting a non-linear regression curve between the log of concentration of PCEH and O.D value at 570 nm.

3.5.4.2. Cell bio-imaging

In a six well plate containing 22×22 mm glass cover slips positioned at
the bottom of the well, the MDA MB 231 cells were seeded and allowed to adherer overnight. 15 µM of the probe, PCEH as well as PCEH-Al^{3+} complex was added to the respective well containing cells along with a separate control. After that, fixation of the cells was done with methanol and washed with 0.5% phosphate buffer saline tween (PBST) twice and then with 1 × PBS thrice. The cover slips were then mounted on a glass slide by glycerol and were observed under a fluorescence microscope (Leica DM4000 B, Germany) at 40x magnification.

3.6. Conclusions

Herein, we report the fabrication of a new coumarin based fluorescent reversible switch which selectively detects $Al^{3+}$with a sharp "turn-on" emission response at 484 nm with a cyan colored fluorescence under UV-radiation. On addition of F^- into the probe-metal solution, the emission intensity reverts back to the original intensity of the probe itself thereby establishing the fact that the probe is reversible in nature. The probe displays significant selectivity towards Al^{3+} over other metal cations with satisfactorily low LOD values of the order of 10^{-9} Min physiological pH. The probe also shows its potential in biological applications through behaving as a biomarker tool in breast cancer cell lines (MDA-MB-231 cell).

3.7. Notes and references

1 M. H. Chua, H. Zhou, Q. Zhu, B. Z. Tang and J. W. Xu, *Mater Chem Front.*, 2021, **5**, 659

2 J. Yin, Y. Hu and J. Yoon, *Chem. Soc. Rev.*, 2015, **44**, 4619

3 Y. Jeon and J. Yoon, *Inorg. Chim. Acta*, 2012, **381**, 2

4 K. Rurack, *SpectrochimActa Part A*, 2001, **57**, 2161.

5 B. Valeur and I. Leray, *Coord. Chem. Rev.*, 2000, **205**, 3.

6 D. Cao, Z. Liu, P. Verwilist, S. Koo, P. Jangjili, J. S. Kim and W. Lin, *Chem. Rev.*, 2019, **119**, 10403

7 K. C. Ko, J. S. Wu, H. J. Kim, P. S. Kwon, J. W. Kim, R. A. Bartsch, J. Y. Lee and J. S. Kim, *Chem. Commun.*, 2011, **47**, 3165.

8 X. Chen, T. Pradhan, F. Wang, J. S. Kim and J. Yoon. *Chem. Rev.*, 2012, **112**, 1910.

9 S. C. Burdette, G. K. Walkup, B. Spingler, R. Y. Tsien and S. J. Lippard, *J. Am. Chem. Soc.*, 2001, **123**, 7831.

10 E. Manandhar and K. J. Wallace, *Inorg. Chim. Acta*, 2012, **381**, 15.

11 S. Karuppannan and J. C. Chambron, *Chem. Asian J.*,2011, **6**, 964.

12 E. V. Antina, N. A. Bumagina, A. I. V'yugin and A. V. Solomonov, *Dyes Pigm.*, 2017, **136**, 368.

13 X. Peng, J. Du, J. Fan, J. Wang, Y. Wu, J. Zhao, S. Sun and T. Xu, *J. Am. Chem. Soc.*, 2007, **129**, 1500.

14 H. Tian, X. Qiao, Z. Zhang, C. Xie, Q. Li and J. Xu, *Spectrochim. Acta PartA*, 2019, **207**, 31-38.

15 S. Pramanik, S. K. Manna, S. K. Pathak, D. Mondal, K. Pal and S. Mukhopadhyay, *New J. Chem.*, 2020, **44**, 13259.

16 X. B. Li, J. Y. Chen and E. J. Wang, *Aust. J. Chem.*, 2015, **68**, 156.

17 L. Wang, W. Qin and W. Liu, *Anal. Methods.*, 2014, **16**, 1167.

18 S. Das, M. Dutta and D. Das, *Anal. Methods.*, 2013, **55**, 6262.

19 Y. Qiao, Z. Li, M. H. Yu, Z. Chang and X. H. Bu, *CrystEngComm*, 2021, **23**, 8087.

20 H. Xu, W. Chen, L. Ju, and H. Lu, *Spectrochim. Acta Part A*, 2021, **247**, 119074.

21 Z. Li, W. Chen, L. Dong, Y. Song, R. Li, Q. Li, D. Qu, H. Zhang, Q. Yang and Y. Li, *New J. Chem., 2020*, **44**, 3261.

22 D. Anu, P. Naveen, R. Rajamanilandan and M. V. Kaveri, *J. Photochem. Photobiol. A*, 2021, **405**, 112921.

23 P. Ghorai, K. Pal, P. Karmakar and A. Saha, *Dalton Trans.*, 2020, **49**, 4758.

24 J. Y. Xie, C. Y. Li, Y. F. Li, Y. J. Fu, S. X. Nie and H. Y. Tan, *Dyes Pigm.*, 2017, **136**, 817.

25 G. D. Fasman, *Coord. Chem. Rev.*, 1996, **194**, 125.

26 D. R. C. McLachlan, *Environmetrics*, 1995, **6**, 233.

27 J. R. Walton, *J InorgBiochem.*, 2007, **101**, 1275.

28 S. Polizzi, E. Pira, M. Ferrara, M. Bugiani, A. Papaleo, R. Albera and S. Palmi, *Neurotoxicology*, 2002, **23**, 761.

29 J. R. Cannon and J. T. Greenamyre, *Toxicol. Sci.*, 2011, **124**, 225.

30 B. Wang, W. Xing, Y. Zhao and X. Deng, *Environ. Toxicol. Pharmacol.*, 2010, **29**, 308.

31 J. Barcelo and C. Poschenrieder, *Environ. Exp. Bot.*, 2002, **48**, 75.

32 C. S. Cronan, W. J. Walker and P. R. Bloom, *Nature*, 1986, **324**, 140.

33 K. Tiwari, M. Mishra and V. Singh, *RSC Adv.*, 2013, **3**, 12124.

34 Y. Xu, L. Yang, H. Wang, Y. Zhang, X. Yang, M. Pei and G. Zhang, *J. Photochem. PhotobiolA, 2020*, **391**, 112372.

35 A. Saravanan, S. Shyamsivappan, N. K. Kalagatur, T. Suresh, N. Maroli, N. Bhuvanesh, I. P. Kolandaivel and P. S. Mohan, *SpectrochimActa Part A*, 2020, **241**, 118684.

36 M. R. Awual, S. Suzuki, T. Taguchi, H. Shiwaku, Y. Okamoto and T. Yaita, *Chem. Eng. J.*, 2014, **242**, 127.

37 Z. Zuo, Y. Tang, F. Lei, R. Jin, P. Yin, Y. Li and Q. Niu, *Spectrochim. Acta Part A*, 2020, **242**, 118712.

38 V. Kumar, A. Kumar, U. Diwan, S. K. Srivastava and K. K. Upadhyay, *Sens. Actuators, 2017*, **207**, 650.

39 J. Wang and Y. Pang, *RSC Adv.*, 2014, **4**, 5845.

40 S. Mabhai, M. Dolai, S. K. Dey, S. Maiti Choudhury, B. Das, S. Dey, A. Jana and D. R. Banerjee, *New J. Chem.*, 2022, **46**, 6885.

41 S. Zhang, Y. Gu, Z. Shi, N. Lu and H. Xu, *Anal. Methods.*, 2021, **13**, 5360.

42 D. Das, R. Alam and M. Ali, *Analyst*, 2022, **147**, 471.

43 S. Gharami, K. Aich, P. Ghosh, L. Patra, N. Murmu, T. K. Mondal, *J. Photochem. Photobiol. A*, 2020, **390**, 112294.

44 W. Luo, Z. Yuwen, H. Li and S. Pu, *New J. Chem.*,2022, **46**, 2411.

45 S. O. Tümay, A. Şenocaka and A. Mermer, *New J. Chem.*, 2021, **45**, 18400.

46 S. Bhogal, P. Sharma, P. Rani, K. Kaur and A. K. Malik, *J. Fluoresc.*, 2022, **32**, 359-367.

47 Z. Wang, L. Shu, X. Luo, Y. Tu, J. Lv, G. Liu, C. Fan and S. Pu, *J. Fluoresc.*, 2022, **32**, 2213.

48 G. Singh, Priyanka, A. Singh, P. Satija, Sushma, Pawan, Mohit and J. Singh, *New J. Chem.*, 2021, **45**, 7850-7859

49 D. Aydin, I. B. Gunay, S. N. K. Elmas, T. Savran, F. N. Arslan, G. Sadi and I. Yilmaz, *New J. Chem.*, 2020, **44**, 12079-12089.

50 B. Das, M. Dolai, A. Ghosh, A. Dhara, A. Das Mahapatra, D. Chattopadhyay, S. Mabhai, A. Jana, S. Dey and A. Misra, *Anal. Methods*, 2021, **13**, 4266-4279

51 Y. Liu, Y. Zhang, M. Sheng, Y. Kang, B. Jia, W. Li and Y. Fu, *Spectrochim. Acta Part A*, 2023, **287**, 122085

52 I. H. Hwang, Y. W. Choi, K. B. Kim, G. J. Park, J. J. Lee, L. Nguyen, I. Noh and C. Kim, *New J. Chem.*, 2016, **40**, 171-178.

53 G. Balamurugan, S. Velmathi, N. Thirumalaivasan and S. P. Wu, *Analyst*, 2017, **142**, 4721-4726.

54 S. Gharami, K. Aich, D. Sarkar, P. Ghosh, N. Murmu and T. K. Mondal, *New J. Chem.*, 2019, **43**, 1857.

55 Z. Liu, Q. Zhang, H. Liu, W. Liu, X. Wang, H. Zhao and S. Zhang, *Russian J. Org. Chem.*, 2020, ***56*(12)**, 2222.

56 S. Goswami, S. Das, K. Aich, D. Sarkar, T. K. Mondal, C. K. Quah, and H. K. Fun, *Dalton Trans.*, 2013, **42**, 15113.

57 H. Liu, T. Liu, J. Li, Y. Zhang, J. Li, J. Song, J. Qu and W. Y. Wong, *J. Mater. Chem.*, 2018, **6**, 5435.

APPENDIX

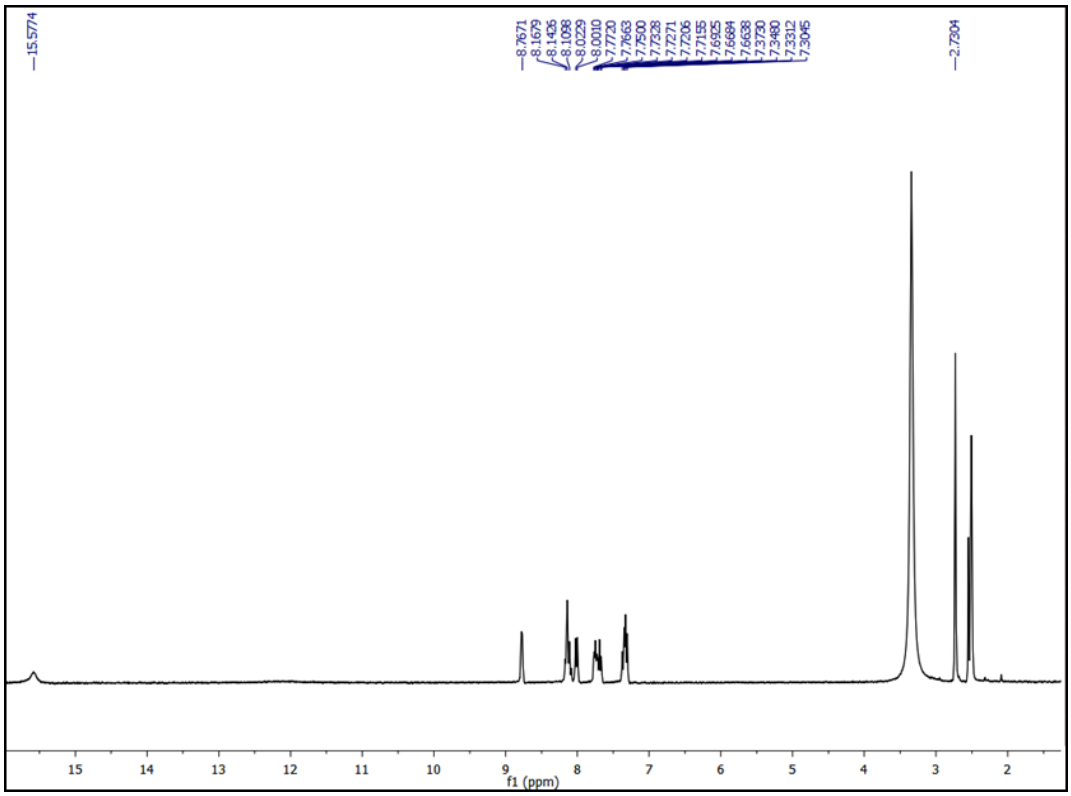

Fig. A3.1: ^{1}H NMR (300 MHz) spectra of the probe (PCEH) in DMSO-d_6

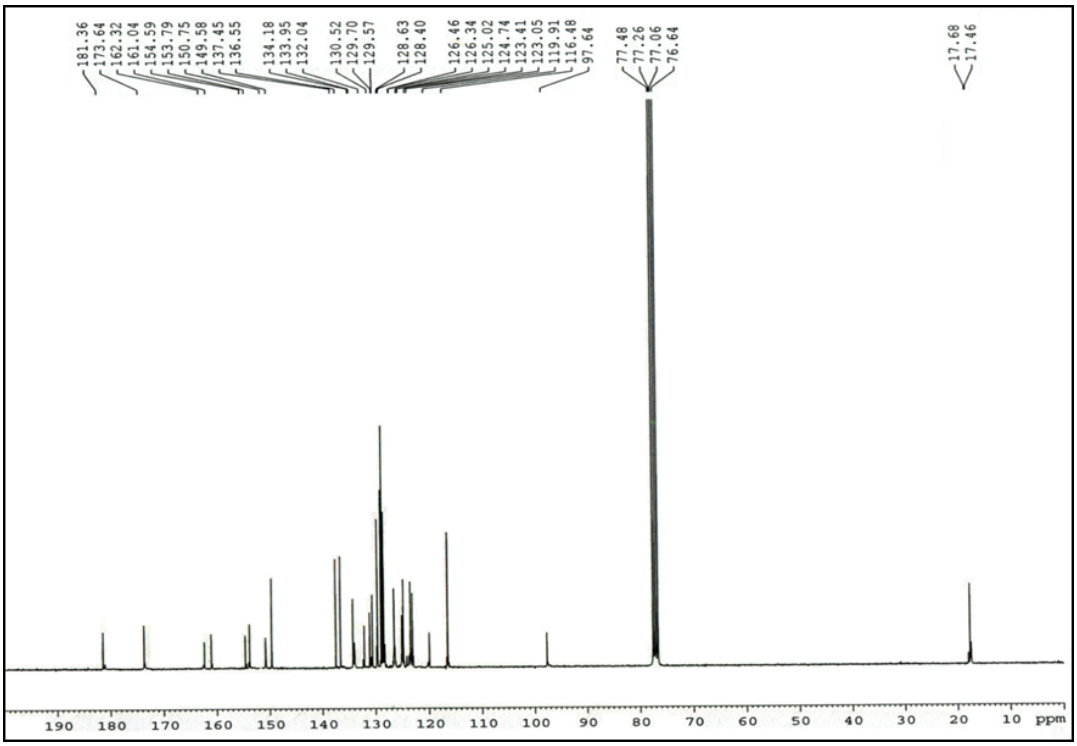

Fig. A3.2: ^{13}C NMR (75 MHz) spectra of the probe (PCEH) in $CDCl_3$

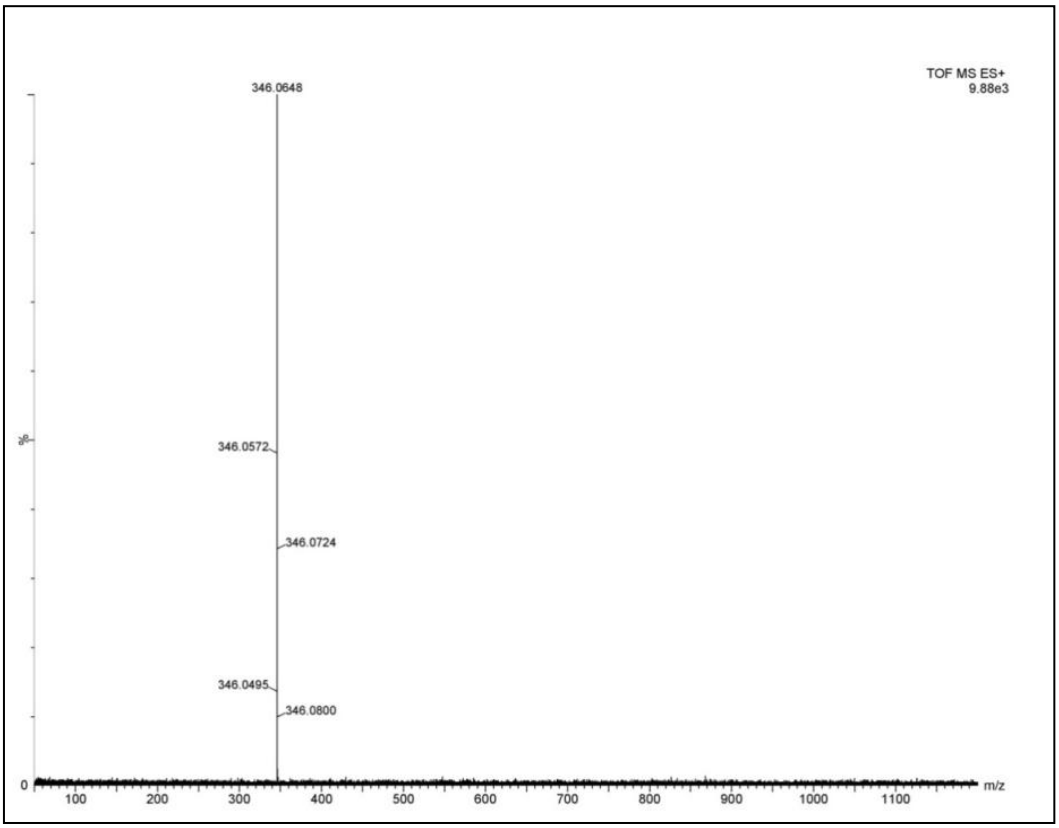

Fig. A3.3: HRMS of the probe (PCEH)

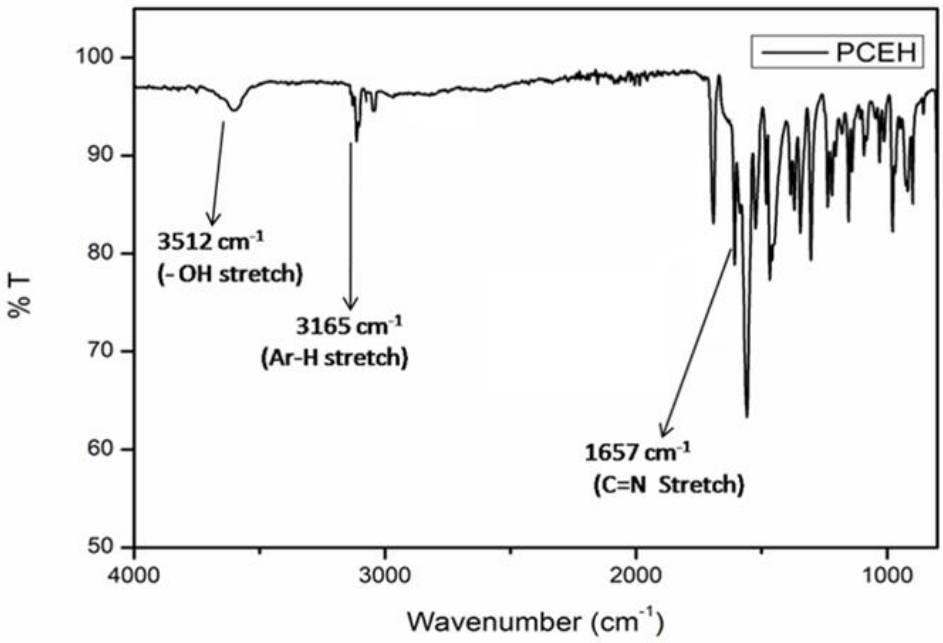

Fig. A3.4: IR- Spectra of PCEH

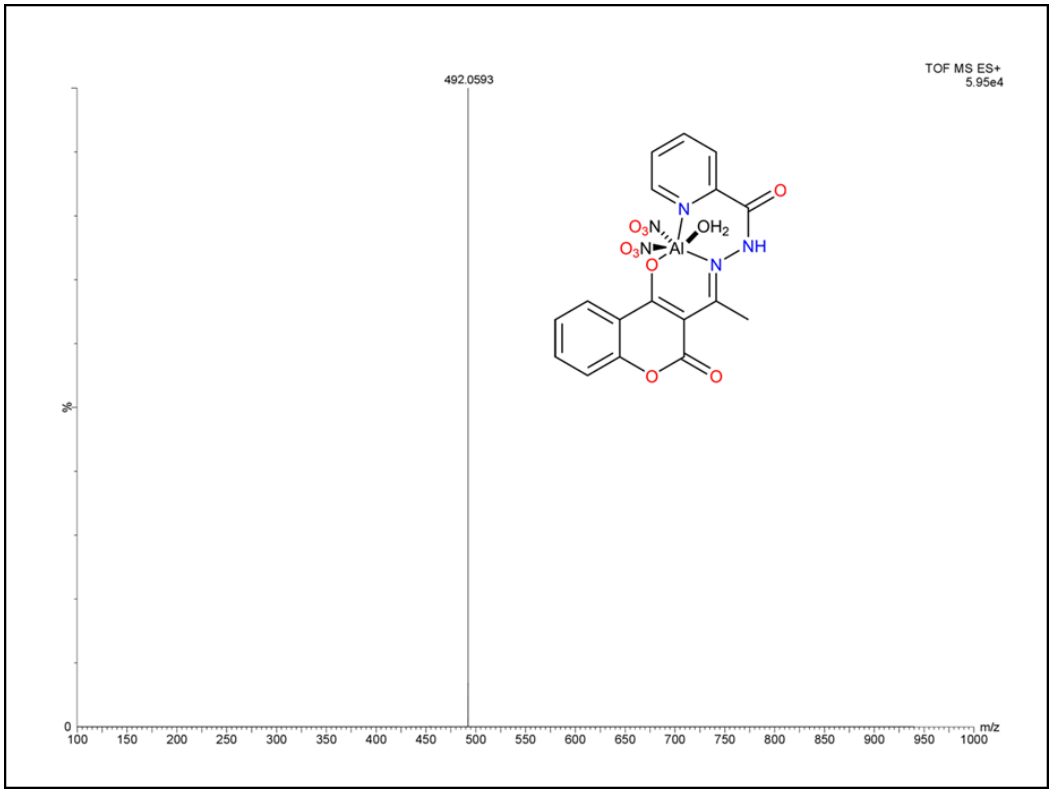

Fig. A3.5: HMRS of PCEH:Al^{3+} complex

Table A3.1: Comparison of sensor PCEH towards Al^{3+} with previously reported receptors.

Chemoreceptors	Testing Condition	Detection limit	Test Strips	References
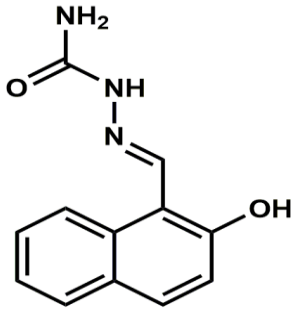	EtOH/H_2O,(1/9, v/v, pH=5.3, 25^0C)	6.75×10^{-8} M	No	**[1]**
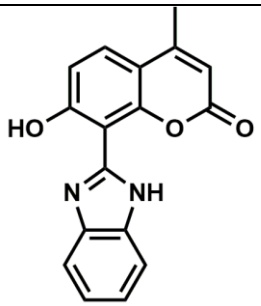	ACN:H_2O(2:1, v/v, pH= 7.2), HEPES Buffer	0.62 µM	No	**[2]**
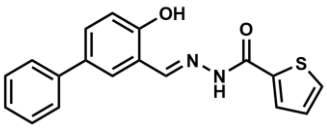	Acetonitrile-Water(4:1, v/v, pH=7.2)	0.5×10^{-9} M	Yes	**[3]**
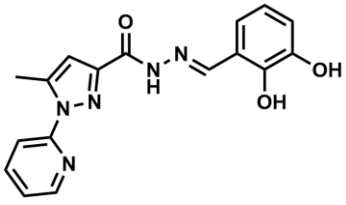	CH_3OH-H_2O (9:1, v/v)	4.78 µM	Yes	**[4]**
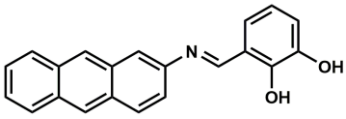	H_2O	0.397 µM	No	**[5]**

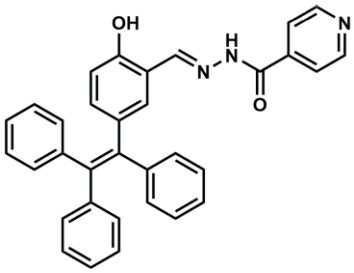	MeOH-H_2O (9:1, v/v), Tris Buffer, pH=7.4	1.587×10^{-7} M	No	**[6]**
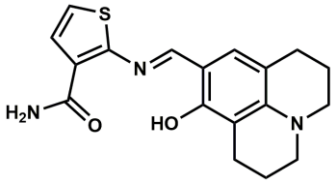	MeCN-DMF (1:3, v/v)	1.4 µM	Yes	**[7]**
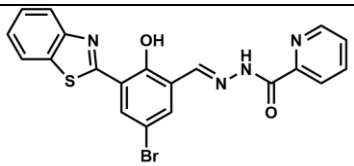	H_2O-MeOH (1:1, v/v, pH= 6.0)	31.2 nM	No	**[8]**
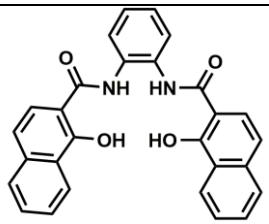	DMF	5.0×10^{-6} M	No	**[9]**
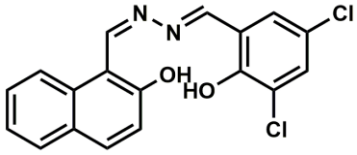	DMSO-H_2O (99:1, v/v, pH =7-8)	0.04 µM	No	**[10]**
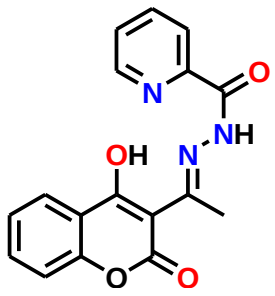	MeOH-H_2O (4:1, v/v)	2.64×10^{-9} M	Yes	**Present Work**

References

1. L. Hou, W. Liang, C. Deng, C. Zhang, B. Liu, S. Shuang and Y. Wang, *RSC Adv*., 2020, **10**, 21629-21635.
2. M. B. Maity, B. Dutta, A. Rahaman, N. Sahu, D. P. Mandal, S. Bhattacharjee and C. Sinha, *J. Mol. Struct*., 2022, **1250**, 131870.
3. A. Biswas, R. Naskar, D. Mitra, A. Das, S. Gharami, N. Murmu and T. K. Mondal, *New J. Chem*., 2022, **46**, 21968.
4. B. Das, M. Dolai, A. Ghosh, A. Dhara, A. D. Mahapatra, D. Chattopadhyay, S. Mabhai, A. Jana, S. Dey and A. Misra, *Anal. Methods*, 2021, **13**, 4266-4279.
5. N. Mudi, M. Shyamal, P. K. Giri, S. S. Samanta, R. Ramirtz-Tagle, *Photochem. Photobiol. Sci*., 2023, **22**, 1491-1503.
6. W. Wang, L. Lu, W. Song, X. Wang, T. Sun, J. Zhu and J. Wang, *J. Lumin*., 2021, **233**, 117911.
7. J. S. Heo, D. Gil and C. Kim, *J. Fluoresc*., 2022, **32**, 825-833.
8. J. Wang, L. Feng, J. Chao, Y. Wang and S. Shuang, *Anal. Methods*, 2019, **11**, 5598.
9. N. Ahfad, G. Mohammadnezhad, S. Meghdabi and H. Farrokhpour, *Spectrochim. Acta A Mol*., 2020, **228**, 117753.
10. J. A. Anshori, D. Ismalah, A. F. Abror, A. Zainuddin, I. W. Hidayat, M. Yusuf, R. Maharani and A. T. Hidayat, *RSC Adv*., 2022, **12**, 2972.

Modulation in the binding sites for adaptable DNA interactive probe efficient at chromo-fluorogenic meticulous recognition of Al^{3+} and its live cell bioimaging

Modulation in the binding sites for adaptable DNA interactive probe efficient at chromo-fluorogenic meticulous recognition of Al^{3+} and its live cell bioimaging

Abstract

Herein, a chromone based simple reversible fluorescent "turn-on" probe HMCP [6-(Hydroxymethyl)-N'-((6-methyl-4-oxo-4H-chromen-3-yl)methylene)picolinohydrazide] was successfully introduced to detect Al^{3+} over a group of other coexisting metal cations in methanol at pH 7.2. The "turn on" emission response along with the effective enhancement in fluorescence intensity upon addition of Al^{3+} can be attributed to the inhibition of photo-induced electron transfer (PET) and C=N isomerization as well as initiation of Chelation-enhanced-fluorescence (CHEF). The sensor HMCP binds Al^{3+} in 1:1 stoichiometry with a brilliant binding constant and good detection limit in the order of 10^3 M^{-1} and 10^{-7} M. The binding mode of interaction of HMCP with Al^{3+} was supported by ^{1}H-NMR titration, HRMS, Job's plot analysis, theoretical calculations and also by molecular logic gate applications. DNA binding study was also executed to elucidate possible bioactivity and found that HMCP interacts with DNA more effectively over other analogues. Furthermore, the applicability in live cell imaging study indicated that HMCP is highly efficient to detect exogenous Al^{3+} in living cells. In addition, real sample analysis and dip-stick experiment provide a wide range of practical application of the probe conveniently.

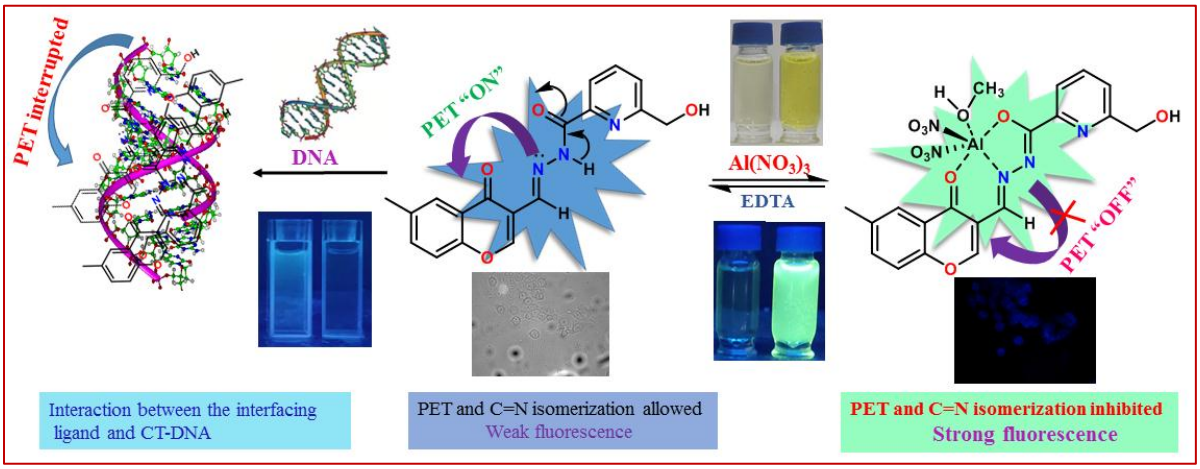

4.1. Introduction

Materials owing multitasking application are important and an emerging field in modern science nowadays. A schiff base is such kind of materials. Its low cost, user-friendliness and time management pattern leads to endeavors towards sustainable development in pharmacy, medicine, molecular memory storage, chemical synthesis and analysis, photochromic materials and in colorimetric and fluorometric chemosensor.[1-6] Several analytical scientific techniques have been developed for recognition of metal ions including spectrometry, chromatography, spectrophotometry, titrimetry and electrochemical strategies.[7,8] The above mentioned methods are complicated, time and cost consuming. Among various techniques utilized, fluorescence signaling method is one of the first preference as it is reliable, simpler, rapid as well as profoundly sensitive for the recognition of environmentally and biologically important metal ions.[9,10]

Aluminum is the third most abundant metal of all elements (after oxygen and silicon) and the most plentiful (8.3 % by weight) metallic element in the earth's crust. The extensive use of aluminum in our daily life in diverse forms, for example, cosmetics, food packaging, medicine, water purification systems, food additives and electronic devices has increased the probability of human exposure to aluminum, leading to a serious concern in recent years.[11] In addition, the concentration of Al^{3+} in soil and water resources dramatically increases due to acid rain and thus inhibits growth of plant and aquatic ecosystem.[12-20] As directed by the WHO (World Health Organization) the weekly permissible intake limit of Al^{3+} by human beings is around 7 mg/Kg of body weight.[21] On the other hand, long-term intake of excess Al^{3+} by humans could cause major health diseases, for example, Alzheimer's, Parkinsonisn, kidney stone, osteoporosis, cardiac arrest, anemia, headache, rickets, dementia and many more.[22-27] Doctors refers to Al^{3+} as the 'silent killer' in human body because of possible connection to the brain.[28] So because of the negative impact of excessive presence of Al^{3+} in human body and environment, it is of great importance to develop some noteworthy tool with improved properties in order to distinctly recognise Al^{3+} to regulate its effect.

DNA is one of the most important biomacromolecule in living beings that records the hereditary statistics. It controls the biosynthesis of various enzyme and proteins via replication and transcription. Therefore, DNA is the prime intracellular target of most of the hazardous substance and drugs. In general, duplex DNA binds with small molecule through various noncovalent interaction.[29] Due to the non-fluorescent nature of DNA, the main physiochemical experiments to investigate the interaction of small molecule with DNA are absorption and emission spectroscopy.

The interactions of small molecule with DNA are of great demand and encourage further application in DNA molecular probe as well as in chemotherapeutic reagents.[30-32]

Again, construction of semiconductors based on the molecular logic gate functions is of specific interest, extensively used in modern computing, in which the relationship between the input and output might be demonstrated by the truth table, "1" denotes an active input/output and "0" as inactive one. Since, de Silva et al. had developed molecular AND logic circuit for the first time,[33] many research groups settled molecular logic gate to use in different application.[34,35] For application in data storage, many molecular logic gates have been constructed based on specific recognition property of cation and anion detection.[36]

4.2. Prior works

To date, many research groups have been reported fluorescent sensors based on different fluorophore unit for distinct recognition of Al^{3+} in the literature. For example, S. L. Hu et al. developed a simple pyrazoline-based fluorescent probe that exhibited fluorescence quenching pattern for Al^{3+} in aqueous solution.[37] Zhang et al. developed a naphthalimide-based highly sensitive sensor (NPP) which detects Al^{3+} with significance enhancement in fluorescence intensity and detection limit is determined to be 39 nM while, Wang et al. fabricated tetrastyrene based fluorescence probe (L) showing low detection limit of 1.587×10^{-7} M for Al^{3+} in methanol-water (9/1, v/v) mixed solvent. Both the probes show strong fluorescence emission in living cells.[38,39] Recently, Hwang et al. reported a simple Schiff base probe which selectively binds with aluminum with a very little detection limit of 290 nM and shows live cell imaging studies [40]. In the year of 2022, Das et al. reported a chromone-based fluorescent switch for multi-analyte detection and displayed a prominent 'turn-on' fluorescence response for Al^{3+} (LOD= 6.9 µM) in aqueous medium.[41] Liu et al. synthesized a chromone derivative for sole detection of Al^{3+} in EtOH with detection limit of 0.214 µM.[42]

4.3. Present work

Considering the HSAB (Hard and Soft Acids and Bases) principle, the hard acid Al^{3+} always prefer to bind with hard coordination sphere of donor atoms like "O" or "N" at suitable position to form stable chelate complex, we intend to introduce a chromone based very simple and low cost novel probe HMCP. The probe HMCP shows higher sensitivity over its analogues towards Al^{3+} in

methanol at pH 7.2 based on PET and C=N isomerization as well as CHEF mechanism. Upon titration with EDTA, probe, HMCP shows reversible nature due to dissociation of HMCP-Al^{3+} complex followed by formation of stable complex Al (EDTA). Experimental outcomes are well verified with theoretical calculations. The possible bioactivity of HMCP was also examined by DNA binding studies. Cell imaging using breast cancer cells as well as real sample analysis have been also carried out to display some extensive potential practical utilization of the probe (HMCP).

4.4. Results and discussions

4.4.1. Synthesis of HMCP and its analogues

The synthetic ways towards the probe, HMCP and its analogues (MCMP & MCMB) were depicted in scheme 4.1. 6-(Hydroxymethyl)picolinohydrazide, picolinohydrazide and benzohydrazide were synthesized using the reported literatures procedures.[43-45] Reflux condensation of 6-methyl-4-oxo-4H-chromene-3-carbaldehyde and 6-(Hydroxymethyl)picolinohydrazide in ethanol medium for 4 hr affords the desired compound HMCP with a high yield (86%). In the same way, the analogues MCMP and MCMB were fabricated through the reflux condensation of 6-methyl-4-oxo-4H-chromene-3-carbaldehyde with picolinohydrazide and 6-methyl-4-oxo-4H-chromene-3-

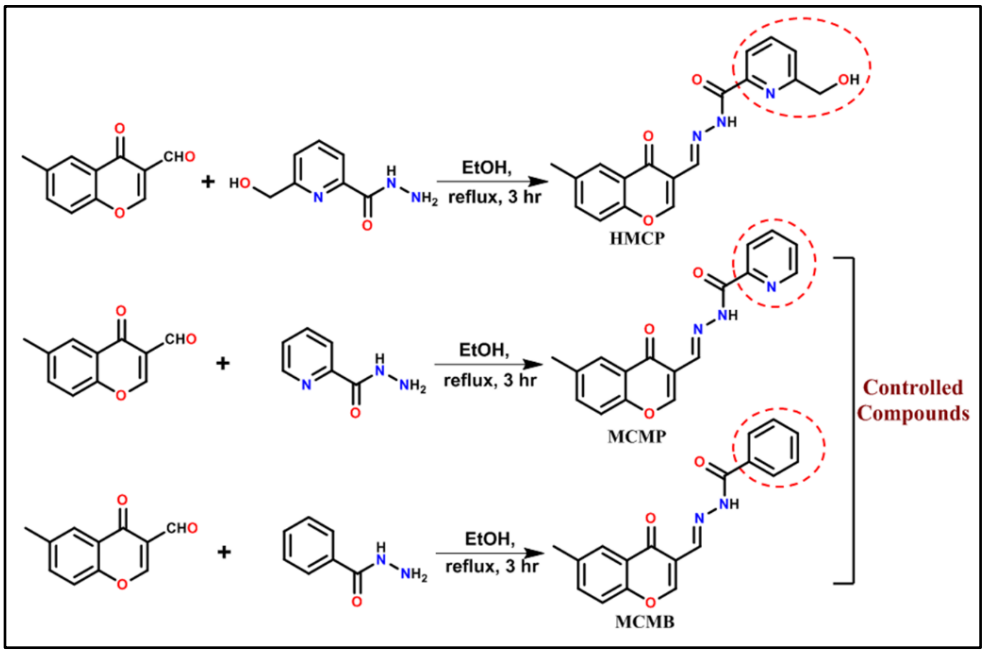

Scheme 4.1: Synthetic scheme of the investigated probe, HMCP and its analogues (MCMP & MCMB).

carbaldehyde with benzohydrazide in ethanol for 3 hr with the yield of 83% and 85% respectively. The chemical structures of HMCP, MCMP and MCMB were confirmed by ^{1}H-NMR, ^{13}C-NMR along with ESI mass spectrometry (Fig. A4.1-A4.9, Appendix).

.4.4.2. ^{1}H NMR and HRMS analysis of HMCP and its analogues (MCMP and MCMB)

We recorded ^{1}H-NMR titration of the probe (HMCP) upon addition of 1equivalents of Al^{3+} in DMSO-d_6 solvent. From the NMR spectral data, it was confirmed that the signal at δ 12.98 ppm can be assigned to the proton of the –NH-C=O unit. Upon interaction with Al^{3+} ion, the proton of the amide moiety was gradually shortened and meanwhile a new peak appeared at 9.23 ppm, indicating the conversion of amide unit into an imidic acid tautomer (–(N=C(OH))-). Moreover, the peak at 6.78 ppm for imine proton shifted slightly downfield, thereby confirming the participation of imine nitrogen atom in complex formation and all the aromatic protons are observed in the expected region (See appendix). We have also carried out the HRMS of HMCP. The HRMS of HMCP shows a peak at m/z 360. 0491, probably for $[HMCP + Na]^{+}$. Similarly, the chemical structure of MCMP and MCMB were characterized by ^{1}H-NMR and HRMS spectra. The HRMS of MCMP and MCMB shows characteristic peaks at m/z 308. 0941 and m/z 307.1206, probably for $[MCMP+H]^{+}$ and $[MCMB+H]^{+}$ respectively.

4.4.3. Al^{3+} sensing studies of HMCP and its analogues using UV-Vis spectroscopy

In order to investigate in depth, the interaction of HMCP towards Al^{3+}, UV-Visible and emission studies were carried out in methanol at 25°C under physiological pH (10 Mm HEPES buffer, pH=7.2). The sensor HMCP displays a moderate absorbance band at 315 nm along with a shoulder peck at 283 nm. Upon incremental addition of Al^{3+} into the solution of HMCP, the intensity of the former absorbance peaks at 315 and 283 nm were gradually decreased and simultaneous emergence of a new absorption band at 424 nm along with two closely situated bands at 408 nm and 448 nm were noticed with formation of a distinct isosbestic point at 351 nm (Fig. 4.1). The appearance of new absorption bands at 424 nm along with two small shoulders at 408 nm and 448 nm and distinct color change supports the complexation of Al^{3+} to HMCP. To establish the

selectivity of the probe (HMCP), UV-Visible spectrum of HMCP were recorded in presence of other metal cations such as Na^{+}, Mg^{2+}, Mn^{2+}, Ba^{2+}, Bi^{3+}, La^{3+}, Ce^{3+}, Ga^{3+}, In^{3+}, Fe^{3+}, Cr^{3+}, Co^{2+}, Ni^{2+}, Hg^{2+}, Zn^{2+}, Cu^{2+}, Pb^{2+} and Cd^{2+}, but there is no significant absorbance change observed for any other metal cations except only for Zn^{2+} and Cu^{2+} (Fig. 4.1). The absorption spectrum of MCMP and MCMB were also studied. The probe MCMP itself shows a strong absorption band at 313 nm along with a small shoulder at 281 nm. In presence of Al^{3+}, the absorption intensity at 313 nm and 281 nm gradually decreases followed by the appearance of a new absorption band 422 nm with two closely situated small humps (Fig. 4.2). Similarly, upon addition of Al^{3+} into the probe solution of MCMB, the absorption band at 310 nm for free probe MCMB gradually decreases along with the appearance of new band at 412 nm with a small hump at 398 nm were observed (Fig. 4.2). These outputs confirm the coordination of Al^{3+} to the analogues (HMCMP & MCMB). Two distinct isosbestic points at 347 nm and 354 nm were also noticed for MCMP and MCMB respectively. In presence of other metal ions, absorption spectra of analogues were recorded and it was noted that none of the abovementioned metal ions resulted in any noteworthy changes in the emission profile the analogues shows no significant spectral change in the absorption spectrum except Zn^{2+} and Cu^{2+}. Therefore, HMCP and its analogues (MCMP and MCMB) are highly selective towards Al^{3+}.

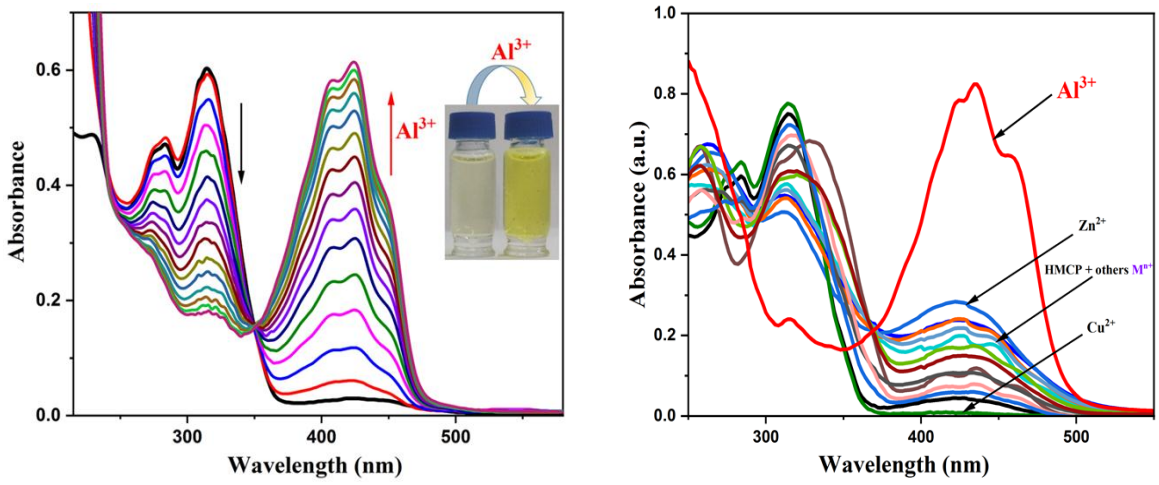

Figure 4.1: Change in UV-Vis spectrum of HMCP (10 μM) upon successive addition of Al^{3+} (0-20 μM) in MeOH (left side) and different metal ions, 40 μM) in MeOH at pH=7.2 (right side).

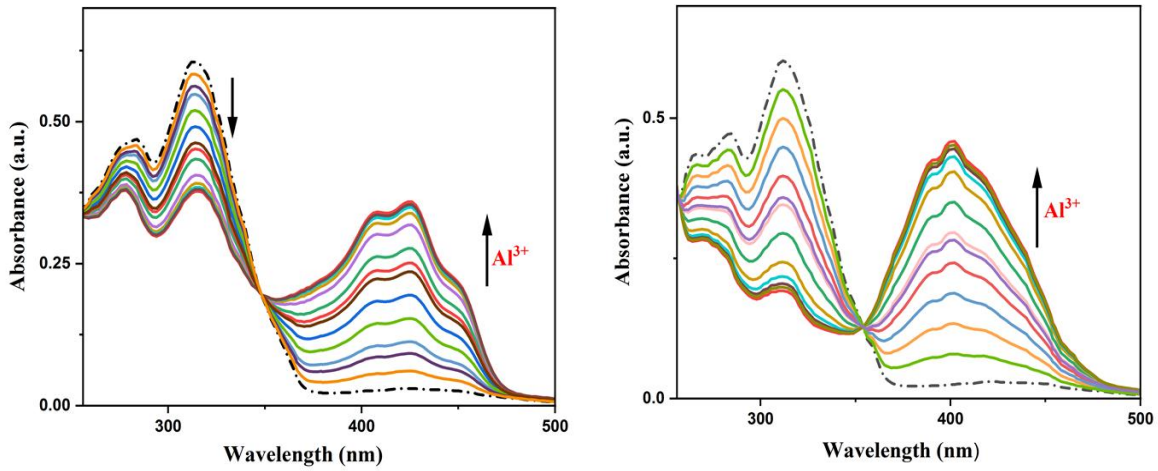

Figure 4.2: Change in UV-Vis spectrum of MCMP (10 μM) upon incremental addition of Al^{3+} (0-20μM) in MeOH (left side) and change in UV-Vis spectrum of MCMP (10 μM) upon addition of Al^{3+} (0-20μM) in MeOH (right side).

4.4.4. Al^{3+} sensing studies of HMCP and its analogues using emission spectroscopy

Fluorescent spectral pattern revealed that upon excitation at 351 nm, probe, HMCP displays a broad centered emission band at 471 nm with very low intensity. This very low fluorescence intensity can be ascribed to the combined effects of PET and C=N isomerization via non-radiative decay processes of excited state. Sequential incremental addition of Al^{3+} into the probe solution resulted in a significant enhancement in the fluorescence intensity (~14 fold) at around 496 nm with an increase in the quantum yield (φ) from 0.03 to 0.21(Fig. 4.3). The "turn-on" emission response of HMCP towards Al^{3+} should be explained to the strong binding affinity of Al^{3+} with HMCP, which prohibited both the C=N isomerization and PET processes in the receptor and initiated increasing rigidity in the complex resulting in chelation enhanced fluorescence (CHEF). The change in the fluorescence properties of HMCP was examined in presence of other coexisting metal ions, but there is hardly any change in the fluorescence intensity of HMCP (Fig. 4.4). Therefore, the receptor, HMCP is highly efficient to detect Al^{3+} fluorimetrically with a significant emission enhancement followed by prominent fluorescence color change from colorless to intense cyan. This fluorescence enhancement falls under a strong "OFF-ON" category of fluorescence property. Further on sequential addition of EDTA to the solution of HMCP-Al^{3+}, the fluorescence intensities at 484 nm as well as 466 nm reverted back to the original emission intensity of the probe (HMCP) itself which clearly establish the fact that HMCP has returned to its free state (Fig. 4.3)

thereby making the sensor a reversible fluorescent switch. Hence, HMCP can be served as an "OFF-ON-OFF" fluorescence signaling sensor.

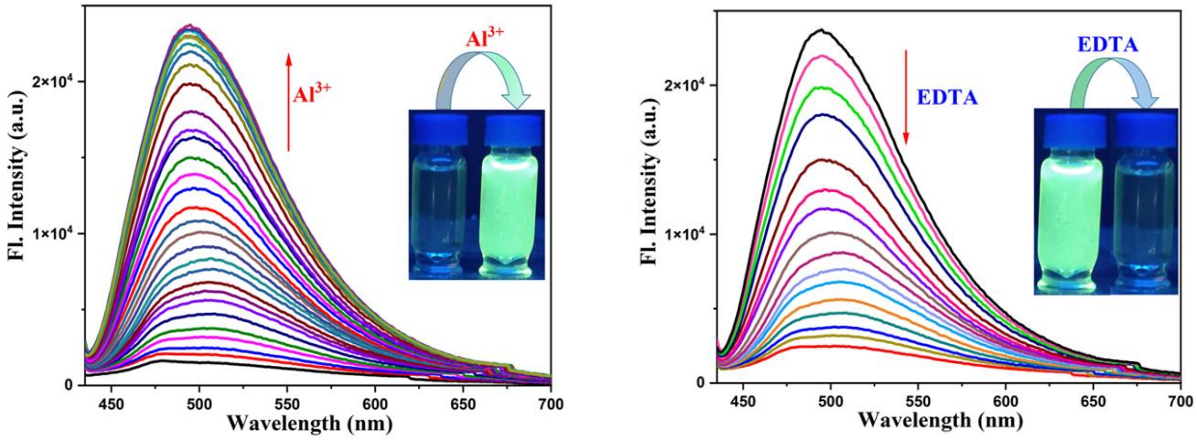

Figure 4.3: Change in emission spectra of HMCP (10 μM) upon gradual addition of Al^{3+} (0-20 μM) (Inset shows the change in colour under UV-radiation (left side) and upon incremental addition of EDTA (0-20 μM) into PCEH:Al^{3+} complex solution (right side). (Inset shows the change in colour under UV-radiation).

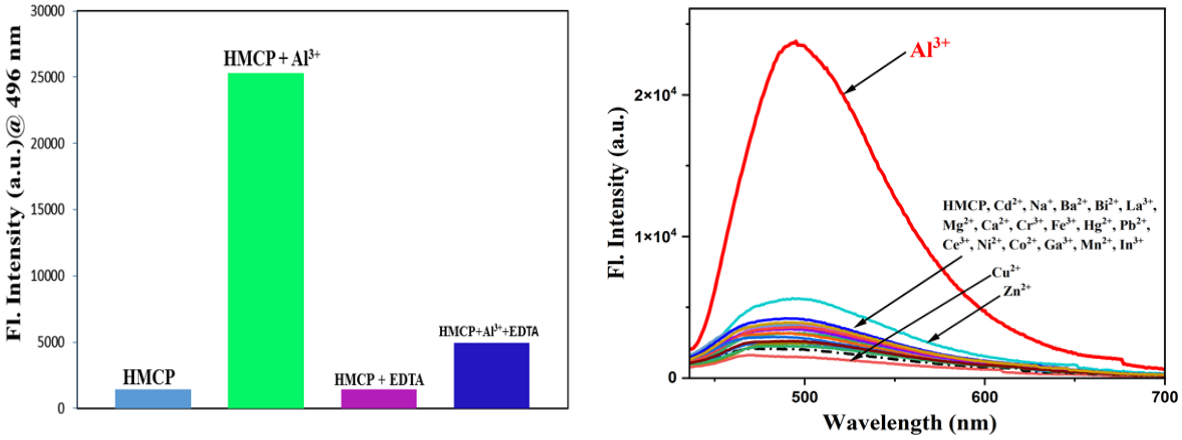

Figure 4.4: Fluorescence intensity variation (left side) and change in emission intensity of HMCP (10 μM) upon addition of different metal ions (40 μM) in MeOH at pH=7.2 (right side).

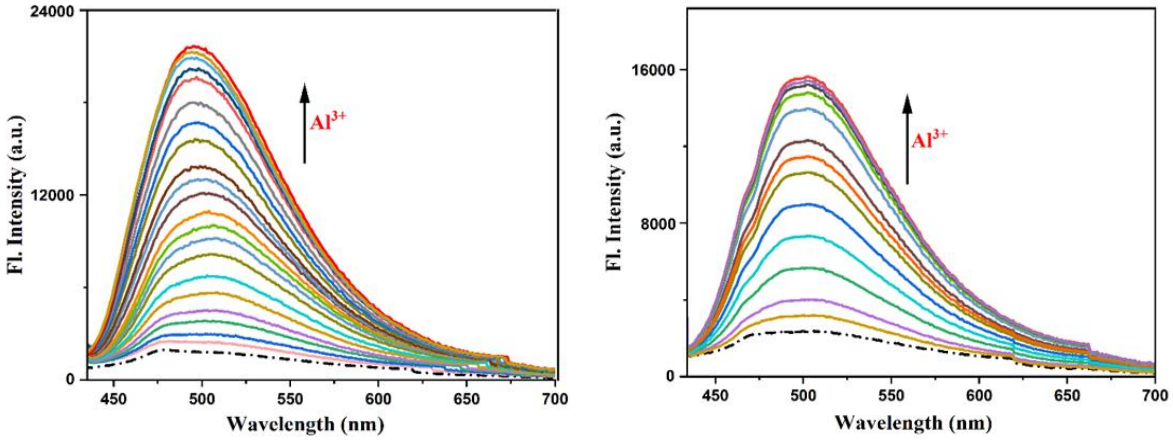

Figure 4.5: Change in emission intensity of MCMP (10 µM) upon gradual addition of Al^{3+} (0-20µM) in methanol (left side) and change in emission intensity of MCMB (10 µM) upon gradual addition of Al^{3+} (0-20µM) in methanol (right side).

From the fluorescence spectral change, the detection limit of HMCP for Al^{3+} was determined following the equation, LOD = K × SD/S where 'SD' is the standard deviation of the blank solution of the probe and 'S' in the slope of the curve and found to be (3.12±0.12) $x10^{-7}$ (M) (Fig. 4.6). This low detection limit value evidently demonstrates to the fact that HMCP is highly efficient in detecting Al^{3+} in a very minute concentration. The binding affinity (K_a) of HMCP for Al^{3+} was also calculated using Benesi-Hildebrand equation and found to be (9.34± 0.45) $x10^3$ M^{-1} (Fig. 4.6), which signifies that HMCP-Al^{3+} complexation is notably stable.

Table4.1: Fluorescence intensity enhancement of HMCP and its analogues (10 µM) upon addition of Al^{3+} (20 µM).

Compound	Emission intensity enhanced in presence of Al^{3+}	Excitation at respective isosbestic point
HMCP	~ 14 fold	351 nm
MCMP	~ 12 fold	347 nm
MCMB	~ 9 fold	354 nm

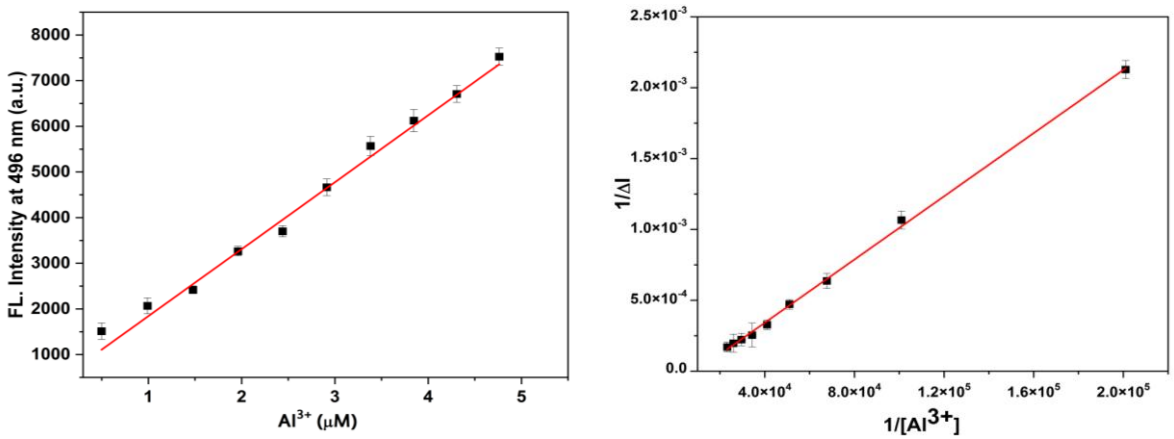

Figure 4.6: Linear response curve of HMCP at 496 nm depending on the Al^{3+} concentration (left side) and determination of association constant of HMCP at 496 nm depending on the Al^{3+} concentration using Benesi-Hildebrand equation (right side).

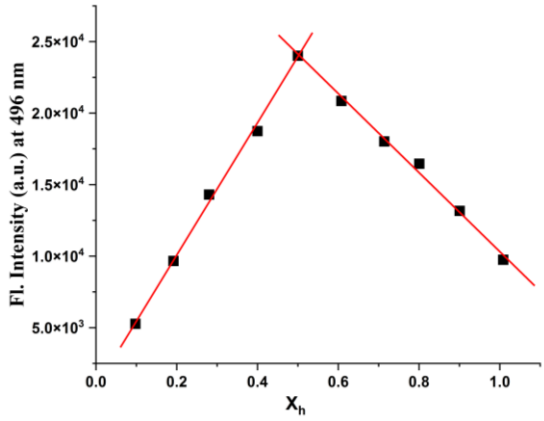

Figure 4.7: Job's plot of HMCP for Al^{3+}

To better comprehend the excited state stability of this fluorescent switch, the lifetime of HMCP and HMCP-Al^{3+} were also measured. The fluorescence lifetime of the free probe (HMCP) shows a mono-exponential decay pattern and was found to be 1.12 ns while HMCP-Al^{3+} complex exhibit a bi-exponential one measured at (λ_{em} = 484 nm) with lifetime value 4.24 ns. The increase in life time is attributed to the decrease in non-radiative decay due to the structural rigidity of the complex over comparatively more flexible free probe. On the other hand, after addition of EDTA, the lifetime of HMCP-Al^{3+} again decreases and found to be 1.53 ns suggesting the dissociation of the complex to the free HMCP (Fig. 4.8).

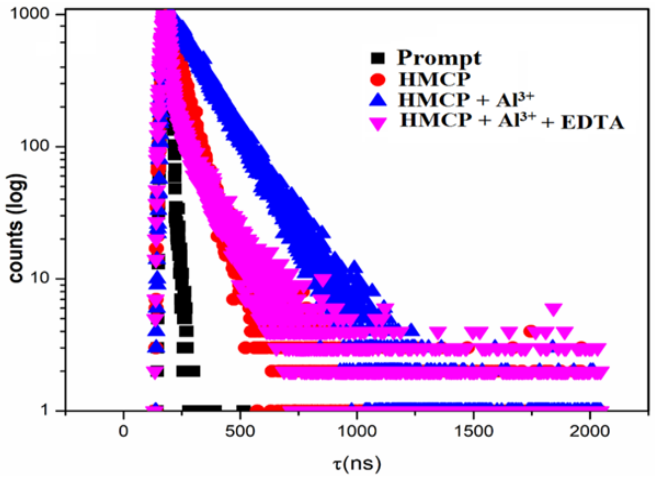

Figure 4.8: Lifetime decay profile of HMCP and HMCP-Al^{3+}.

In order to investigate the specificity of the probe towards Al^{3+}, fluorescence intensity of the probe solution containing other metal cations were recorded separately before and after addition of Al^{3+} ion. It is observed from the competitive experiment that the fluorescence enhancement of HMCP upon addition of Al^{3+} is not significantly affected by the presence of other metal cations. Therefore, HMCP is highly specific towards Al^{3+}. An ideal chemosensor must have two essential properties, recyclability and reusability in its sensing action. To examine the reversibility nature, a solution of HMCP was prepared in MeOH solution. Fig. 4.9b revealed that upon the addition of Al^{3+} ion to the HMCP solution, a 'turn on' emission was observed. Subsequently, the addition of EDTA solution into HMCP-Al^{3+} complex solution gives "turn off" emission as the complex is dissociated due to formation of stable Al(EDTA) complex, releasing a free receptor. This observation signifies that the sensing capability of the probe HMCP is reversible. To further confirm the reversible nature, the experiment was performed using MeOH solution of HMCP for second time. Upon further addition of Al^{3+} ion to the solution gives again a 'turn on' emission and sequential addition of EDTAion shows turn off emission response. Thus a increase in emission intensity of HMCP solution upon addition of Al^{3+} ion and a quenching in fluorescence intensity of HMCP-Al^{3+} complex in presence of EDTA was observed for four cycle, with little loss in sensing efficacy (fig.4.9b). Such reversibility and regeneration are important for the design of devices to recognize Al^{3+}.

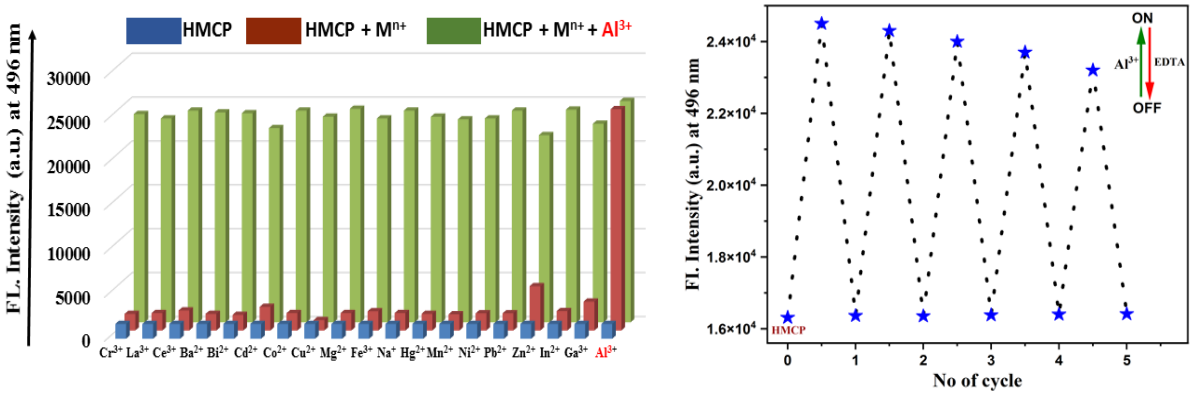

Figure 4.9: Bar diagram illustration of the relative emission intensity of HMCP upon addition of various metals (10 µM) inMeOH (red bars) and Al^{3+} (20 µM) in presence of other metal ions (blue bars) (left side) and the fluorescence 'OFF-ON-OFF' repetitive cycle upon each sequential addition of $Al^{3+}$and EDTA ion at 496 nm (λ_{ex} = 351 nm) in MeOH solution (right side)**.**

A rapid fluorescence response chemosensor is always highly preferable for practical purpose. Time dependent experiment has been executed in order to interpret the instance emission response of the sensor HMCP. At different time interval, the emission intensity was monitored in presence of different concentration of Al^{3+} (5 µM, 10 µM, 15 µM). Fig.4.10 disclosed that our investigated probe HMCP is highly efficient to detect Al^{3+} within very short time span (0-10 second) after addition of Al^{3+} ion. After 10 second of Al^{3+} addition, the emission intensity at 496 nm almost reached its saturation level, which signifies completion of the reaction. Hence HMCP can be served as a powerful and reliable sensor for the recognition of aluminum ion within minimal time period (0-10 sec).

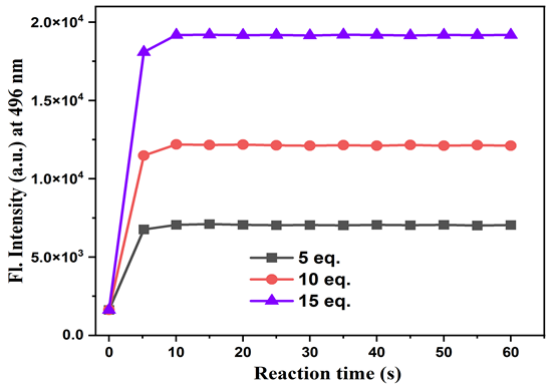

Figure 4.10. Time dependent fluorescence response study of HMCP (10 µM) at different concentration of Al^{3+} ion (5-15 µM) in MeOH/H_2O solution (4/1, v/v) at 496 nm.

4.4.5. Probable sensing mechanism of HMCP

The enhancement in the emission intensity of HMCP and its analogues in presence of Al^{3+} is possibly accredited to the combined effect of two important mechanism PET and C=N isomerization, which was on in the free probes, but after binding with Al^{3+} ion these two mechanism was inhibited and rigidity in the complex was introduced that accounts for the enhancement in fluorescence intensity. In addition, due to the presence of several oxygen and nitrogen donor centres, it was anticipated that the probes and its analogues have strong affinity for chelation with hard acid Al^{3+} according to the HSAB (Hard and Soft Acids and Bases) principle. The nature of binding mode of the chemosensor HMCP was investigated via ^{1}H-NMR titration study. The signal at δ 12.98 ppm can be assigned to the proton (H_b) of the –NH-C=O unit. Upon interaction with Al^{3+} ions, the H_b proton of the amide unit was gradually shortened and meanwhile a new peak noticed at 9.23 ppm due to the conversion of amide into an imidic acid tautomer (–(N=C(OH))-).[45] Furthermore, the peak at 6.78 ppm for imine proton (H_a underwent a slight down-field shift, thereby confirming the participation of imine nitrogen atom in complex formation. The HRMS spectrum of HMCP exhibits a peak at m/z 360.0491, possibly for $[HMCP+Na]^+$, whereas the the HMCP-Al^{3+} complex exhibits a peak at m/z 542.0648 indicating the formation of mononuclear complex of HMCP and Al^{3+}. The binding stoichiometry of HMCP to Al^{3+} was further supported by Job's plot experiment. Therefore, ^{1}H-NMR, HRMS, FT-IR and Job's plot analysis gave strong evidence for the proposed binding mode as depicted in fig. 4.13.

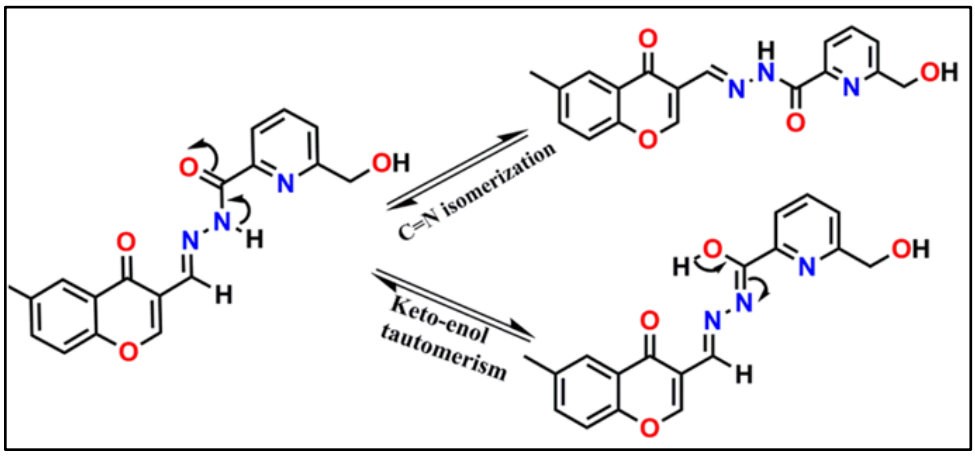

Figure 4.11: Keto-enol tautomerism and C=N isomerization process in the probe

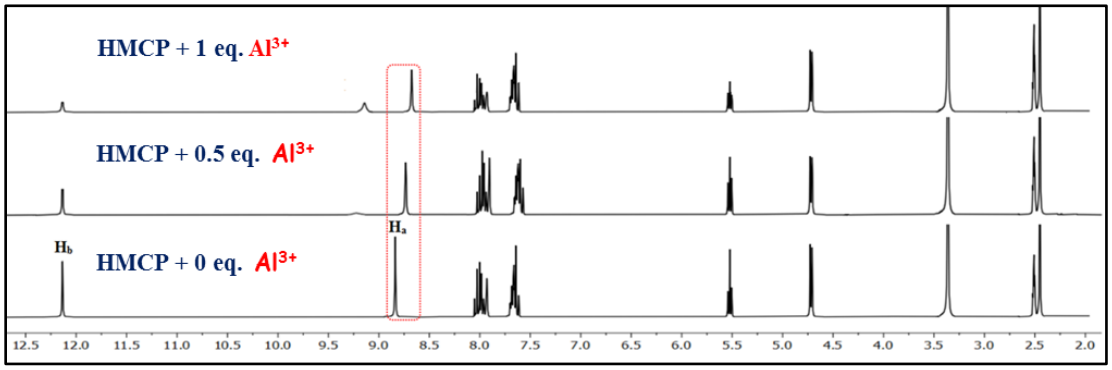

Figure 4.12: ^{1}H-NMR titration sensing mechanism of HMCP upon addition of different concentration of Al^{3+}.

The cyan fluorescence response of MCMB in presence of Al^{3+} established the fact that the pyridinium nitrogen atom of HMCP and MCMB do not participate in the complex formation and further supported the binding mechanism as depicted in Fig. 4.13. The higher emission intensity enhancement of HMCP and MCMP compared to MCMB upon addition of Al^{3+} can be attributed to the -I effect of pyridine moiety which more favoured the enol form of both HMCP and MCMB (Table 4.1). Again, the large emission intensity enhancement of HMCP compared to MCMP in presence of Al^{3+} is due to the presence of additional aliphatic hydroxyl group which increases the solubity of HMCP through H-bonding, thereby displaying higher emission intensity.

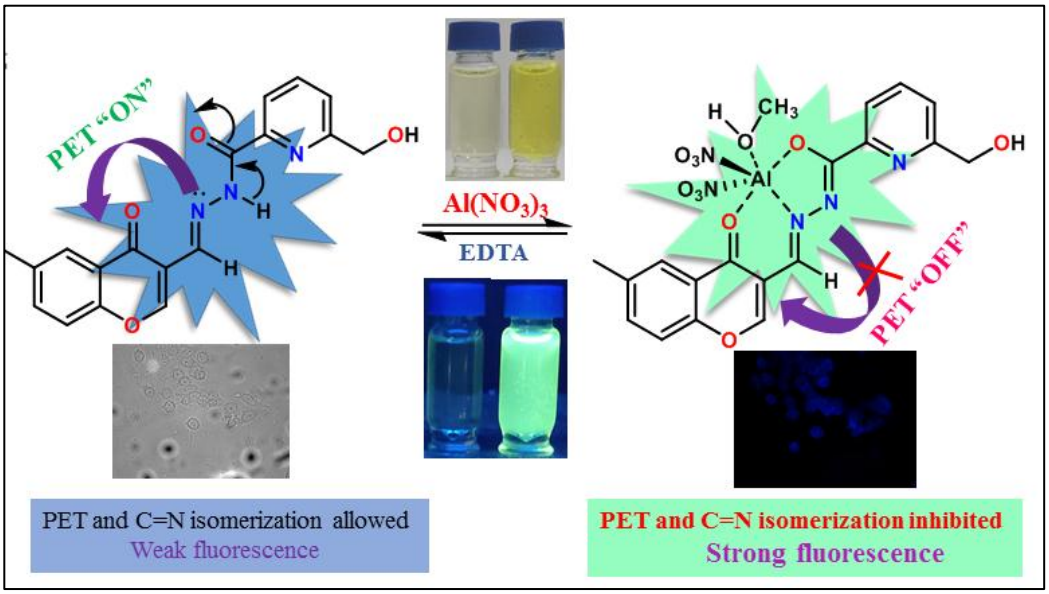

Figure 4.13: Probable sensing mechanism of HMCP with Al^{3+}.

4.4.6. DNA binding study

The DNA binding experiment with sensor is immensely demandable for design and development of new targeted drugs. Ligand can bind with DNA through various non-covalent interaction. The affinity of the HMCP and its analogues toward ct-DNA were examined through the change in absorption and emission spectral change. Generally, the change in absorption spectra with appearance of new peak at new location are observed when a complex is developed by the interaction of small molecule/ligand with ct-DNA. The absorption spectra of HMCP was recorded upon addition of ct-DNA. Fig. 4.15 revealed that upon incremental addition of ct-DNA into the probe HMCP solution, the inherent absorption band of HMCP at 315 nm gradually diminishes along with appearance of two new absorption band at 356 nm and 266 nm, where ct-DNA absorption is insignificant, suggesting the existence of an effective interaction between the π electron cloud of the interfacing sensor HMCP and the base pairs of DNA along with the H-bonding.[47]

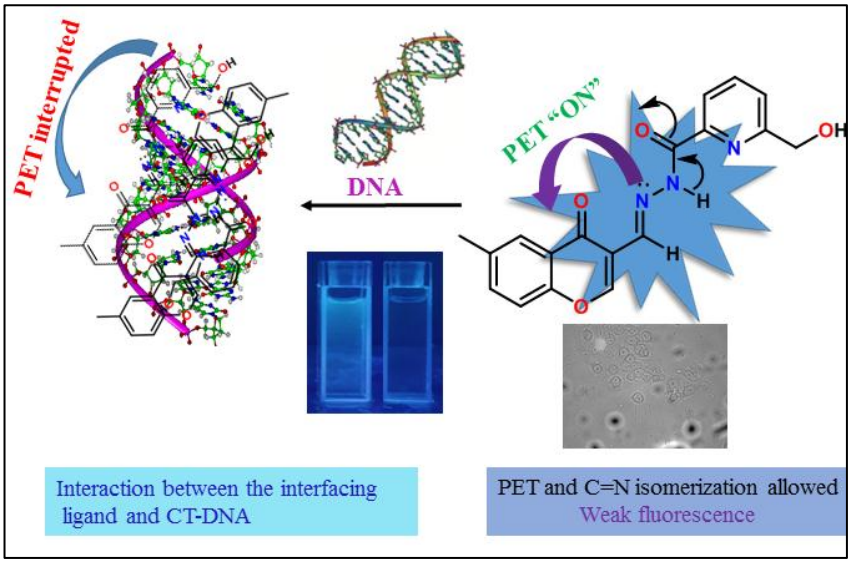

Figure 4.14: Probable sensing mechanism of HMCP toward ct-DNA.

Upon excitation at 331 nm, the sensor HMCP displays an emission band at 471nm. After successive addition of ct-DNA into the solution of HMCP, about 8-fold enhancement in the fluorescence intensity was detected at 476nm (Fig. 4.15). This significant rise in fluorescence intensity with distinct fluorescence color change on association with ct-DNA implies an effective

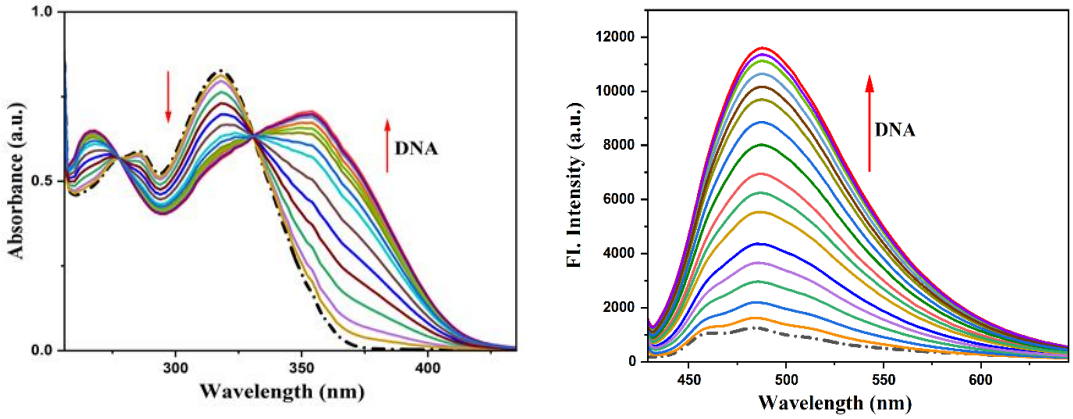

Figure 4.15: Change in UV-Vis spectrum of HMCP (10 μM) upon addition of ct-DNA (0-20 μM) in MeOH (left side) and change in emission spectra of HMCP (10 μM) upon addition of ct-DNA(0-20 μM) in MeOH (right side).

interaction of the sensor HMCP with DNA. The turn on fluorescence response can be attributed to the PET process, which is interrupted upon binding with DNA due to the interaction of lone pair of imine nitrogen of HMCP with the π electron clouds of DNA. The "turn-on" emission enhancement of MCMP and MCMB upon addition of ct-DNA were also recorded and outcomes are summarized in table 4.2. The higher enhancement in the fluorescence intensity for HMCP compared to MCMP may due to the presence of aliphatic –OH group in HMCP which initiated additional H-bonding interaction followed by stronger binding with DNA compared to that of MCMP. Again, the higher emission intensity of MCMP compared to MCMB may be due to the presence of additional lone pair of electron on pyridinium nitrogen atom that provide extensive interaction with DNA base pairs compared to that of MCMB.

Table 4.2: Comparison of emission intensity enhancement of HMCP and its analogues upon addition of ct-DNA

Compound	Emission intensity enhanced by DNA
HMCP	~ 8 fold
MCMP	~ 4.5 fold
MCMB	~ 1.6 fold

4.4.7. Molecular logic gate

The emission properties of the sensor HMCP compelled us to investigate its application in numerous logic gates by successive addition of inputs like metal cations such as Al^{3+} and anionic species (EDTA and recording their fluorescence at 496 nm as the output. Inputs are denoted as "1" for their presence and their absence are assumed as "0". Outputs are denoted as "1" when the fluorescence intensity is above a certain threshold value (25% of maximum). When no input is present, no characteristic fluorescence is noted and is considered by "0" (off state). From the truth table, it is observed that HMCP shows the emission intensity output signal in such a manner with Al^{3+} (Input A) that is seems to realise the needs of "AND" operation and "NOT" operation with EDTA (Input B) (Fig. 4.16). Furthermore, when both inputs (Al^{3+} and EDTA) are present, the output emission intensity decreases, indicating the off state according to the truth table. These data are related to an "INHIBIT" logic gate via a particular arrangement of logical functions AND and NOT.

Entry	Input A (Al^{3+})	Input B (EDTA)	Output Emission@ 494 nm
1	0	0	0
2	1	0	1
3	0	1	0
4	1	1	0

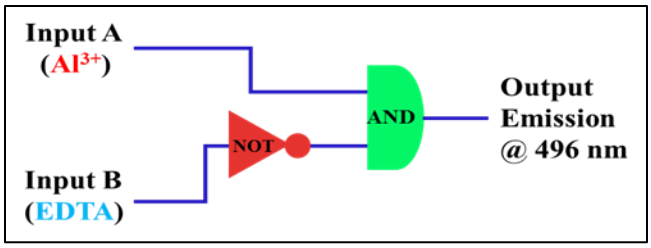

Figure 4.16: Truth table for advance-level molecular logic gate and corresponding circuit diagramme

4.4.8. Molecular memory device

The techniques of data storing are well equipped and can be combined by successive logic circuits. All these circuits bring the following response loop. Here one of the output signal is assumed as the input of the memory device and is considered as the "memory element". The function of the memory device is built on a binary logic; either 1 or 0 alternates the two crisp states. In our device, for the establish of a suitable mimic of the memory component, we consider Al^{3+} and EDTA as the set (S) and reset (R) inputs respectively and the fluorescence intensity at 496 nm as the output signal. In memory device function, input A(Al^{3+}) considered as set (S) and it seems binary state 1. However, written data get erased under reset input (EDTA) and binary state "0" is recorded. 'So,

by applying a binary logic function, we have successfully established a consecutive logic circuit displaying "Write-Read-Erase-Read" features (Fig. 4.17). It is worth mentioning that the write-erase cycles could be reversed repeatedly for several times with the same complex solution without significant decrease in the fluorescence intensity. Thus, the circuits developed by this manner exhibit comparable conduct to the logic memory devices of conventional semiconductors and it is considered as the better technique for set up of molecular microprocessors of integrated circuits that can be possibly explored in the near future.

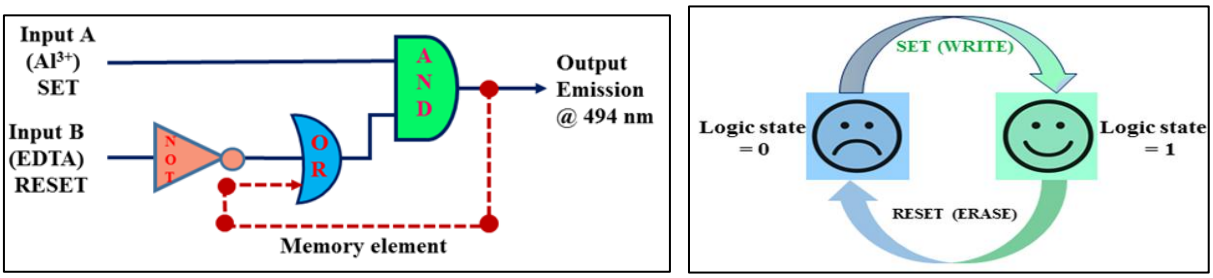

Figure 4.17: Consecutive logic gate of a memory unit (left side) andschematic presentation of the reversible logic operation for the memory element with a write-read-erase-read kind of manners (right side).

4.4.9. Practical application as Dip-stick experiment: detection of Al^{3+} using TLC plate

For qualitative identification of Al^{3+}, we have carried out a proficient experiment known as dip-stick experiment where the sensor can act as a fluorescent portable kit, exhibiting its sensing capability towards the specific metal ion in solid state too without the aid of any sophisticated instruments. In order to execute this experiment, few thin-layer chromatography (TLC) plates were prepared and they are immersed into the solution of HMCP (2×10^{-4} M) in MeOH and then dried by evaporating the solvent. After that, the dried probe-coated TLC plates are immersed into Al^{3+} solution (2×10^{-3} M) and then the solvent was evaporated again in order to dry. The visual colour change of the probe-loaded TLC plate in absence and presence of Al^{3+} was prominent and distinguishable in day light and under UV light (Fig. 4.18). This method helps one to thoroughly and easily study the identification of Al^{3+} by naked eye.

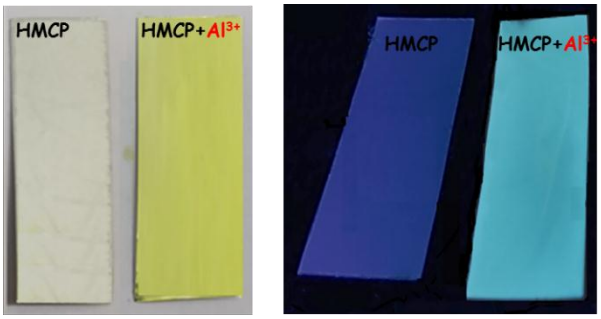

Figure 4.18: Pictures of TLC plates immersed in MeOH solution before and after dipped into Al^{3+}-solution in normal light (left side) and under UV chamber (right side). [HMCP] = 2×10^{-4} M, [Al^{3+}] = 2×10^{-3} M.

4.4.10. Real sample analysis

In order to validate the practical utility of our approach, the feasibility of probe was investigated in the detection of aluminium ion in different water samples (tap and lake water) through fluorescence method according to the previously reported methods.[48,49] The samples were first filtered and then used for further experiment. These natural water samples were not measured. Now various concentrations of Al^{3+} ion were mixed into these natural water samples and the probe HMCP was successfully employed for the determination of aluminium content in these real water samples. From the experimental outcomes as summarized in table 4.3, it is concluded that the sensor HMCP is highly proficient to detect the concentration of Al^{3+} from contaminated natural water samples with excellent recovery (97-100.5%).

Table 4.3: Recovery experiment for various natural water samples using the proposed methods

Source	Water samples studied	Amount of standard Al^{3+} spiked (µmol)	Total Al^{3+} found (µmol)[b]	Recovery (%)
Tap water (Department of Chemistry)	Tap water 1	5	4.94 ± 0.04	98.8
	Tap water 2	10	9.95 ± 0.06	99.5
	Tap water 3	15	15.03 ± 0.35	100.2
Lake water (Jadavpur University campus)	Lake water 1	5	4.9 ± 0.07	98.6
	Lake water 2	10	9.65± 0.05	96.5
	Lake water 3	15	14.97 ± 0.06	99.8

[b]Relative standard deviations were calculated based on three times of measurement.

4.4.11. Application in biological field via live cell imaging in human breast cancer cells

From the MTT experiment it can be concluded that the receptor, HMCP has a negligible toxicity at lower concentrations towards human breast cancer (MDA-MB-231) (Fig. 4.19).

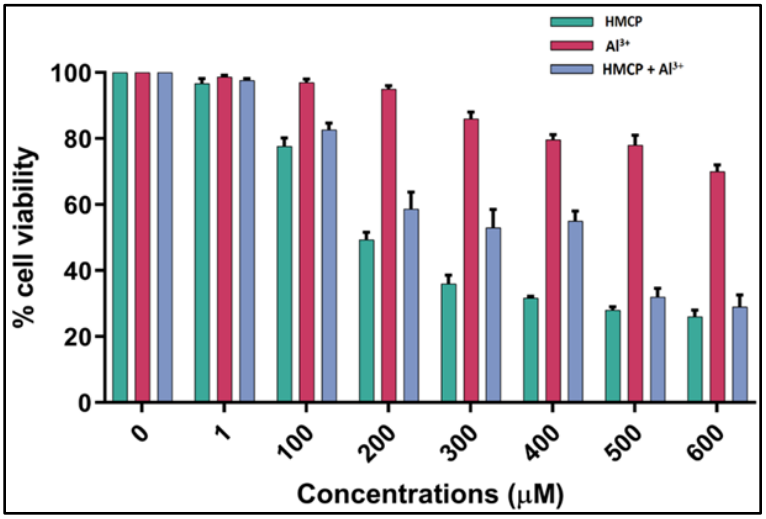

Figure 4.19: MTT assay of HMCP, Al^{3+} and HMCP-Al^{3+} complex on human breast cancer cell lines.

The IC_{50} value of HMCP is determined and found to be 189.6 μM and therefore we have preferred the dose to execute this experiment to be 15 μM as the chosen dose should be less than the IC_{50} value (Fig. 4.20).

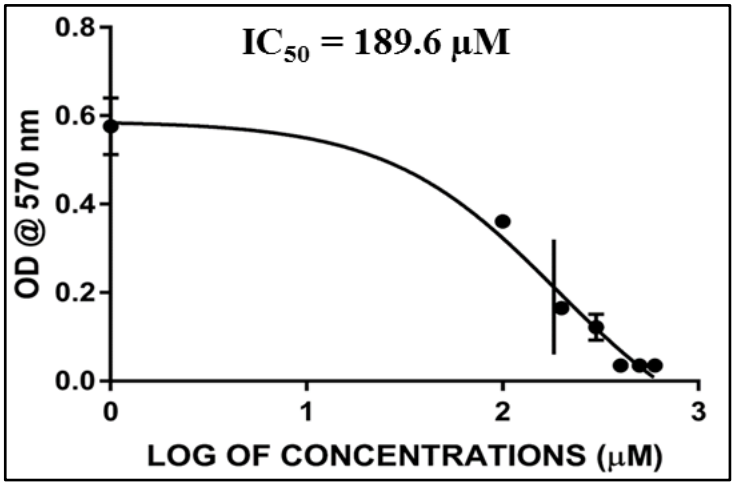

Figure 4.20: IC_{50} dose of the probe (HMCP) in human breast cancer cells.

Now the fluorescence imaging experiment under microscope revealed that the treatment of the breast cancer cells with HMCP itself exhibits no fluorescence while upon incubating the MDA-MB-231 cells with 15µM of aluminum and HMCP a bright blue emission in the intracellular region was noticed (Fig. 4.21). This experiment established the fact that the sensor, HMCP can easily penetrate cell membrane in order to bind with the intracellular aluminum ion. Further, there is no physical change observed for the studied cells in bright field images after incubation with Al^{3+} ion implying that the MDA-MB-231 cells are viable and HMCP is not toxic at that specific concentration (Fig. 4.21). Therefore, our present probe has a chance to serve as a cell membrane-penetrable fluorescence kit that has proficient biological application in living cells organisms for analyzing Al^{3+} ion.

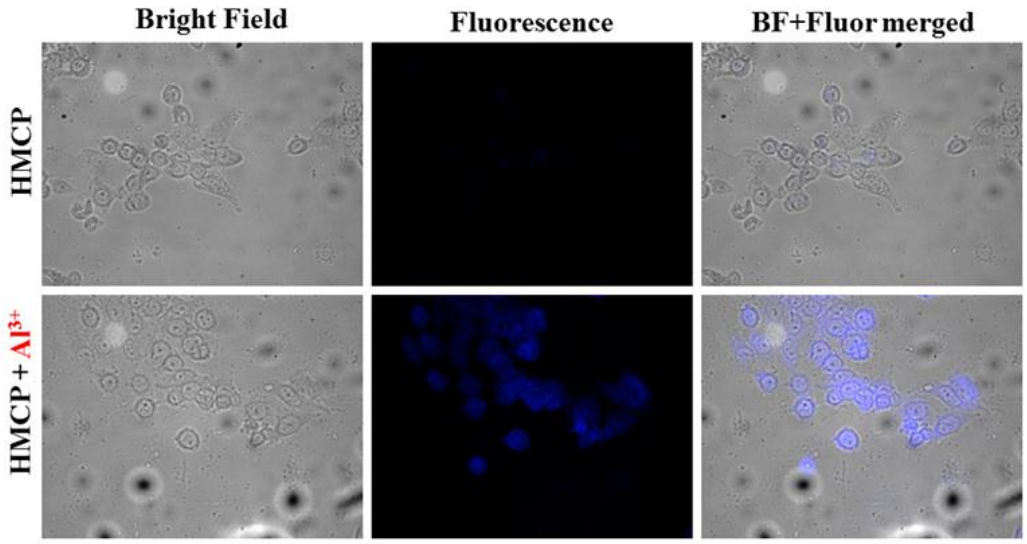

Figure 4.21: Fluorescence image of breast cancer cells after incubation with 15 µM HMCP and HMCP-Al^{3+} complex. DAPI is used to stain the nucleus.

4.4.12. Theoretical calculations

In order to understand the structural changes of HMCP upon binding with Al^{3+}, DFT calculations were executed by B3LYP/6-31+G(d) method using Gaussian 09 program. Figure 4.23 represent the optimized structures of HMCP and complex. The fig. A4.10 and fig. A4.11displays the contour plots of some selected molecular orbitals (HOMOs) of HMCP and HMCP-Al^{3+} complex respectively.

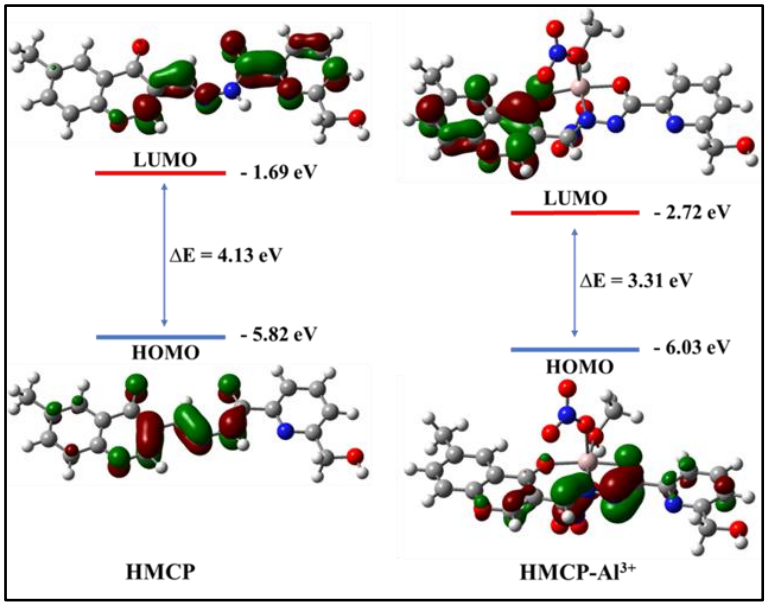

Figure 4.22: HOMO-LUMO energy gap of HMCP before and after addition of Al^{3+}.

The HOMO-LUMO energy gap of HMCP was 4.13 eV, while for HMCP-Al^{3+} complex, the HOMO-LUMO energy gap is decreased to 3.31eV (Fig. 4.22). This effective change in HOMO-LUMO energy gap is well supported with the bathochromic shift in the absorption spectrum upon addition of Al^{3+} into the probe solution. To interpret the electronic spectra, vertical electronic transitions were determined by time dependent density functional theory (TDDFT) calculation (solvent correction is incorporated by CPCM model and MeOH is chosen as solvent) and summarized in Table A4.2, (Appendix). The calculated vertical excitations of HMCP shows strong transitions at 335 nm (f=0.7610) due to HOMO→LUMO. However for HMCP-Al^{3+}, HOMO→LUMO transition shifted to 380 nm (f= 0.0868) (Table A4.2, Appendix).

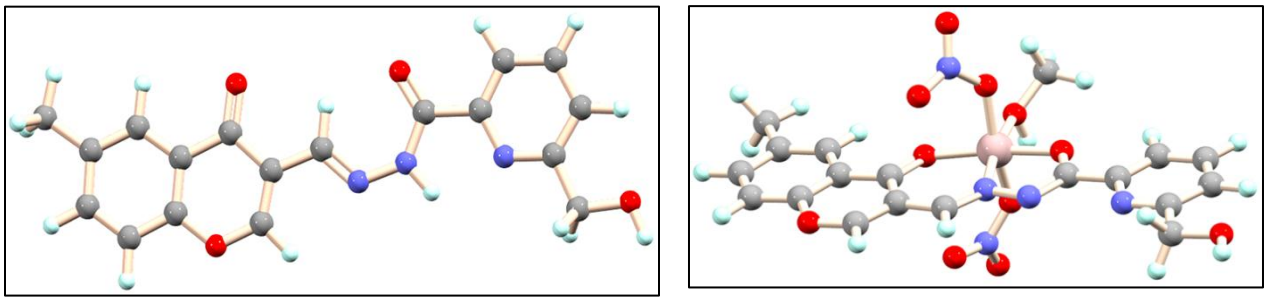

Figure 4.23: Optimized structure of HMCP (left side) and optimized structure of HMCP-Al^{3+}complex (right side) calculated by DFT/B3LYP/6-31+G(d) method.

4.5. Experimental

4.5.1. Reagent and methods

All the reagents and organic compounds used in this synthesis are purchased from sigma-aldrich. All the other solvents and inorganic salts used in the synthetic procedures were purchased from available commercial sources. DMSO-d_6 and $CDCl_3$ were used as solvent for the NMR spectra without further distillation. Thin layer chromatography (TLC) was carried out using Merck 60 F_{254} plates with a thickness of 0.25 mm. A PerkinElmer Lambda 750 spectrophotometer was used to obtain absorbance spectra and emission property was measured using Shimadzu RF-6000 fluorescence spectrophotometer at room temperature (298 K). Lifetimes were measured using a time-resolved spectrofluorometer from IBH, UK.

4.5.2. Synthesis of 6-(Hydroxymethyl)-N'-((6-methyl-4-oxo-4H-chromen-3-yl)methylene)picolinohydrazide (HMCP)

6-(Hydroxymethyl)picolinohydrazide(0.167 g, 1mmol) was added to the ethanolic solution of 6-methyl-4-oxo-4H-chromene-3-carbaldehyde(0.19 g, 1mmol) and the mixture was then refluxed for about 7 hours. After completion of the reaction, white precipitation was obtained which was purified by column chromatography furthermore to yield desired product (HMCP). Yield was, 0.29 g, 86%.

^{1}H NMR data (300 MHz, DMSO-d_6): δ (ppm): 2.45 (s, 3H), 4.72 (d, J = 5.88 Hz, 2H), 5.52 (t, J = 6 Hz, 1H), 7.61-7.69 (m, 3H), 7.92-8.05 (m, 3H), 8.83 (s, 1H), 12.13 (s, 1H).

^{13}C NMR (75 MHz, DMSO-d_6): δ(ppm): 22.1, 50.21, 103.9 110.4, 112.1, 116.7, 121, 123.6, 126.8, 127, 131, 132.6, 140, 144.7, 147.9, 148.8

HRMS: Calculated for $C_{18}H_{15}N_3NaO_4$ $[M + Na]^+$ (m/z) = 360. 0690; found = 360. 0491.

4.5.3. Synthesis of (E)-N'-((6-methyl-4-oxo-4H-chromen-3-yl)methylene) picolinohydrazide (MCMP)

Picolinohydrazide (0.14 g, 1mmol) was added to the ethanolic solution of 6-methyl-4-oxo-4H-chromene-3-carbaldehyde (0.19 g, 1mmol) and the reaction mixture was refluxed for about 8 hours. After completion of the reaction, white product was appeared which was then subjected to column chromatography furthermore to get pure white solid. Yield was, 0.25 g, 83%.

^{1}H NMR data (300 MHz, DMSO-d_6): δ (ppm): 2.46 (s, 3H), 7.65 (s, 1H), 7.67-7.71 (m, 2H), 7.93 (d, J = 7.77 Hz, 1H), 8.03-8.14 (m, 2H), 8.80 (d, J = 6.87 Hz, 2H), 10.13 (s, 1H), 12.36 (s, 1H).

^{13}C NMR (75 MHz, DMSO-d_6): δ(ppm) 23.2, 51.2, 102.9, 103.9, 110.4, 112.1, 116.7, 121, 123.6, 126.8, 127, 131.8, 132.6, 140, 144.6, 146.8, 147.9

HRMS: Calculated for $C_{17}H_{14}N_3O_3$ $[M + H]^+$ (m/z) = 308.1030; found = 308. 0941.

4.5.4. Synthesis of (E)-N'-((6-methyl-4-oxo-4H-chromen-3-yl)methylene) benzohydrazide (MCMB)

The ethanolic mixture of Benzohydrazide(0.14 g, 1mmol) and 6-methyl-4-oxo-4H-chromene-3-carbaldehyde (0.19 g, 1 mmol) was refluxed carefully for about 7 hours. After completion of the reaction, white precipitation was obtained which was subjected to column chromatography furthermore to yield pure final product. Yield was, 0.26 g, 85%.

^{1}H NMR data (300 MHz, DMSO-d_6): δ (ppm): 2.46 (s, 3H), 7.51-7.71 (m, 6H), 7.93 (d, J = 6.9 Hz, 2H), 8.64 (s, 1H), 8.82 (s, 1H), 11.94 (s, 1H).

^{13}C NMR (75 MHz, DMSO-d_6): δ(ppm) 21.3, 50.2, 102.9, 103.9, 110.2, 112.1, 113.7, 121, 123.6, 126.8, 127.4, 131.8, 132.5, 140, 144.7, 145.8, 147.9

HRMS: Calculated for $C_{18}H_{15}N_2O_3$ $[M + H]^+$ (m/z) = 307.1077; found = 307.1206.

4.5.5. General Method for UV-Vis and Fluorescence Titration

4.5.5.1. UV-Vis Method

In order to record UV-vis spectrum, stock solution of the sensor, HMCP (10 μM) was prepared in MeOH (at 25°C). The solutions of all the competitive cations were prepared in the order of 1×10^{-5} M, in deionized water. Solutions of a different concentrations containing HMCP and all the metal cations were prepared separately. The UV-Vis spectra of these sample solutions were monitored.

4.5.5.2. Fluorescence Method

In order to record fluorescence spectra, stock solution of the present probe, HMCP (10 μM) was prepared as the same as that used for UV-vis method. The solutions of the guest metal ions, in the order of 1×10^{-5} M, were prepared using deionised water. Different concentrations of sample solutions containing the probe HMCP and metal ions were prepared separately. The spectra of these solutions were monitored by means of fluorescence technique.

4.5.5.3. Job's Plot experiment

For this experiment, a series of sample solutions containing HMCP (10 μM) and Al^{3+} (20 μM) were prepared in such a way that the sum of the volume of total metal cation and HMCP remained constant (4 mL) in MeOH at pH 7.2. Job's plots were then plotted as the function of emission intensity change at 496 nm versus mole fraction of Al^{3+}.

4.5.6. Live cell imaging studies

4.5.6.1. Cell cytotoxicity assay

AGS cells were studied for cytotoxicity with aluminium nitrate (Al^{3+}), HMCP and HMCP-Al^{3+} complex according to the following procedure as reported by Gharami et al. [50]. Cells were seeded in 96-well plates at a density of 5×10^3 cells per well and cultivated in CO_2 incubator for 22 h. Different doses (10, 25, 50, 75, 100, 125, 150, 175) μM of free HMCP, Al^{3+} and HMCP-Al^{3+} complex were introduced into the cells separately along with control for 24 h. Now aluminum was used by dissolving in aqueous medium while the sensor (HMCP) was dissolved in DMSO although the final concentration of DMSO while treating of studied cells was maintained below 1%. After 24 h treatment, Methyl tetrazolium dye (MTT) (5 mg/ml) solution was mixed to each well (10 μl/well). The well plates were then incubated in the dark at 37°C for 2 h. To each well 100 μl DMSO was mixed and allowed to settle for 1 h in a vortex shaker. Now cell viability efficiency was evaluated by recording absorbance at 570 nm for each well using a microplate reader (Tecan, infinite M200). Untreated cells were considered as 100% viable. IC_{50} value of free probe HMCP only was calculated by plotting a non-linear regression between the log of concentration of HMCP and O.D value at 570 nm.

4.5.6.2. Cellular bio-imaging

AGS cells were grown on 22×22 mm glass cover slips positioned at the bottom of six well plates for overnight. Then the cells were treated with the probe, HMCP and HMCP-Al^{3+} complex with 15 μM each for 1 h. IC_{50} value for HMCP was determined and found to be 189.6 μM. Based on the IC_{50} value, the dosage of 15 μM was selected. After the treatment, the cells were then fixed with methanol and washed with 0.5% phosphate buffer saline tween (PBST) twice and then with 1 × PBS thrice. The cover slips then were mounted on a glass slide and were observed under a fluorescence microscope (Leica DM4000 B, Germany) at 20x magnification.

4.5.7. Computational methodology

Full geometry optimizations were performed using the density functional theory (DFT) method at the B3LYP[51] level for the ligand and complex. All calculations were carried out with Gaussian 09 program package.[52] The calculations were aided by the Gauss View visualization program. All elements except aluminium were assigned 6-31+G(d)[53] basis set. The vibrational frequency calculations were executed to certain that the optimized geometries show the local minima and there were only positive eigen values. time-dependent density functional theory (TDDFT) formalism[54,55] were employed to compute vertical electronic excitations based on B3LYP optimized geometries in methanol using conductor-like polarizable continuum model (CPCM).[56]

4.6. Conclusions

In conclusion, we have designed and successfully fabricated a chromone based OFF-ON-OFF reversible chemosensor HMCP, which is more efficient to detect Al^{3+} ion compared to its analogues. The affinity of HMCP towards Al^{3+} over a group of other coexisting metal ions was accredited to the HSAB principle where hard centre N and O atom in the probe prefer to bind with hard acid Al^{3+} ion. The detection limit was determined based on fluorescence change and found to be 3.12±0.12) $x10^{-7}$ (M). The "turn-on" chromo-fluorogenic response after binding with Al^{3+} was due to the restriction of C=N rotation and inhibition of PET process along with the initiation of chelation-enhanced-fluorescence (CHEF). The proposed binding mode of HMCP to Al^{3+} was supported by ^{1}H-NMR titration, HRMS, Job's plot analysis as well as DFT calculation. DNA binding studies was also performed to elucidate higher bioactivity of HMCP over its analogues. In addition, the synthesized probe HMCP may have been utilised in selective detection of Al^{3+} in real water sample analysis. Moreover, cellular imaging studies were also conducted to establish Al^{3+} bio-sensing ability of HMCP in living cells (MDA-MB-231).

4.7. Notes and references

1. R. Emas, The Concept of Sustainable Development: Definition and Defining Principles. In Brief for GSDR; Florida International University, 2015; pp 1−3.
2. A. Frio, R. Janeiro, S. M. Viana, C. S. Valladares and B. P. Duarte, *Rev. Bras. Geocienc*. 2001, 6.
3. K. Brodowska and E. Łodyga-Chruscińska, *Chemik*, 2014, **68**, 129−134.
4. S. Kumar, D. N. Dhar and P. N. Saxena, *J. Sci. Ind. Res*., 2009, **68**, 181− 187.
5. A. M. Abu-Dief and I. M. A. Mohamed, *J. Basic Appl. Sci*., 2015, **4**, 119−133.

6. P. G. Cozzi, *Chem. Soc. Rev*., 2004, **33**, 410−421.
7. D. T. Quang and J. S. Kim. *Chem. Rev*., 2010, **110**, 6280−6301.
8. F. J. Hayes, H. B. Halsall, and W. R. *Anal. Chem*., 1994, **66**, 1860−1865.
9. B. Valeur and I. Leray, *Coord. Chem. Rev*., 2000, **205**, 3−40
10. L. Prodi, F. Bolletta, M. Montalti and N. Zaccheroni, *Chem. Rev*., 2000, **205**, 59−83.
11. G. C. Woodson, *Bone*, 1998, **22**, 695−698.
12. C. S. Cronan, W. J. Walker and P. R. Bloom, *Nature*, 1986, **324**, 140−143
13. T. P. Flaten, *Brain Res. Bull*., 2001, **55**, 187−196.
14. G. Berthon, *Coord. Chem. Rev*., 1996, **149**, 241−280.
15. M. G. Soni, S. M. White, W. G. Flamm, G. A. Burdock, *Regul. Toxicol. Pharmacol*., 2001, **33**, 66−79.
16. E. Gauthier, I. Fortier, F. Courchesne, P. Pepin, J. Mortimer and D. Gauvreau, *Environ. Res*., 2000, **84**, 234−246.
17. G. D. Fasman, *Coord. Chem. Rev*., 1996, **149**, 125−165.
18. D. Krewski, R. A. Yokel, E. Nieboer, D. Borchelt, J. Cohen, S. Kacew, J. Lindsay, A. M. Mahfouz and V. Rondeau, *J. Toxicol. Environ. Health, Part B*, 2009, **10**, 1−269
19. G. C. Woodson, *Bone*, 1998, **22**, 695−698.
20. J. Barcelo and C. Poschenrieder, *Environ. Exp. Bot*., 2002, **48**, 75−92.
21. WHO. Guidelines for Drinking-Water Quality, 4th ed.; World Health Organization, 2017.
22. T. P. Flaten, *Brain Res. Bull*., 2001, **55**, 187−196
23. G. Berthon, *Coord. Chem. Rev*., 1996, **149**, 241−280.
24. M. G. Soni, S. M. White, W. G. Flamm and G. A. Burdock, *Regul. Toxicol. Pharmacol*., 2001, **33**, 66−79
25. E. Gauthier, I. Fortier, F. Courchesne, P. Pepin, J. Mortimer and D. Gauvreau, *Environ. Res*., 2000, **84**, 234−246.
26. G. D. Fasman, *Coord. Chem. Rev*., 1996, **149**, 125−165.
27. D. Krewski, R. A. Yokel, E. Nieboer, D. Borchelt, J. Cohen, S. Kacew, J. Lindsay, A. M. Mahfouz and V. Rondeau, *J. Toxicol. Environ. Health Part B*, 2009, **10**, 1−269.
28. B. Das, M. Dolai, A. Ghosh, A. Dhara, A. Das Mahapatra, D. Chattopadhyay, S. Mabhai, A. Jana, S. Dey and A. Misra, *Anal. Methods*, 2021, **13**, 4266
29. C. V. Kumar and E. H. Asuncion, *J. Am. Chem. Soc*., 1993, **115**, 8547−8553
30. X. Chen, L. Zhang, K. Zhou, E. Davies, K. Sugden, I. Bennion, M. Hughes and A. Hine, Opt. Lett., 2007, 32, 2541-2543
31. W. A. Durai and Dr. A. Ramu, Chemistry Select, 2020, **5**, 4778-4785
32. S. K. Sheeta, B. Sena, R. Thounaojamb, K. Aguanb and S. Khatua, *J. Photochem. Photobiol. A*, 2017, **332**, 101-111
33. A. P. de Silva, Molecular Logic-Based Computation; Royal Society of Chemistry: Cambridge, UK, 2012.
34. S. Erbas-Cakmak, S. Kolemen, A. C. Sedgwick, T. Gunnlaugsson, T. D. James, J. Yoon and E. U. Akkaya, *Chem. Soc. Rev*., 2018, **47**, 2228−2248.
35. J. Andreasson and U. Pischel, *Chem. Soc. Rev*., 2018, **47**, 2266−2279.
36. B. Das, S. Dey, G. P. Maiti, A. Bhattacharjee, A. Dhara and A. Jana, *New J. Chem*., 2018, **42**, 9424−9435.

37. S. L. Hu, J. J. Song, G. Y. Wu, C. X. Cheng and Q. Gao, *Spectrochim. Acta Part A*, 2015, **136**,1188-1194.
38. S. Zhang, Y. Wang and H. Xu, 2022, **275**, 121193
39. J. Wang, L. Feng, J. Chao, Y. Wang and S. Shuang, *Anal. Methods.*, 2019, **11**, 5598
40. I. H. Hwang, Y. W. Choi, K. B. Kim, G. J. Park, J. J. Lee, L. Nguyen, I. Noh and C. Kim, *New J. Chem.*, 2016, **40**, 171-178.
41. A. Das and G. Das, *New J. Chem*., 2022, **46**, 19002-19008
42. C. Liu, L. Liu, T. Li, K. Liu and Z. Yang, *Inorganica Chim. Acta*, 2020, **502**, 119327
43. N. Behera and V. Manivannan, *J. Photochem. Photobiol. A Chem*., 2018, **353**, 77–85.
44. A. Maji, R. Naskar, D. Mitra, S. Gharami, N. Murmu and T. K. Mondal, *J. Fluoresc*., 2023, **33**, 2403-2414
45. J. Wang, L. Feng, J. Chao, Y. Wang and S. Shuang, *Anal. Methods*., 2019, **11**, 5598
46. S. Gharami, K. Aich, D. Sarkar, P. Ghosh, N. Murmu and T. K. Mondal, *New J. Chem*., 2019, **43**, 1857-1863.
47. U. Saha, B. Das, M. Dolai, J. Butcher, G. Suresh Kumar, 2020, **5(29)**, 18411-18423
48. S. O. Tümay, A. Şenocak and A. Mermer, *New J. Chem*., 2021, **45**, 18400-18411
49. A. Saravanan, S. Shyamsivappan, N. K. Kalagatur, T. Suresh, N. Maroli, N. Bhuvanesh, P. Kolandaivel and P. S. Mohan, *Spectrochim. Acta A*, 2020, **241**, 118684
50. S. Gharami, K. Aich, D. Sarkar, P. Ghosh, N. Murmu, and T. K. Mondal, *New J. Chem.*, 2019, **43**, 1857-1863
51. A. D. Becke, *J. Chem. Phys*. 1993, **98**, 5648−5652.
52. Gaussian 09, Revision D.01, M. J. Frisch, G. W. Trucks, H. B. Schlegel, G. E. Scuseria, M. A. Robb, J. R. Cheeseman, G. Scalmani, V. Barone, B. Mennucci, G. A. Petersson, H. Nakatsuji, M. Caricato, X. Li, H. P. Hratchian, A. F. Izmaylov, J. Bloino, G. Zheng, J. L. Sonnenberg, M. Hada, M. Ehara, K. Toyota, R. Fukuda, J. Hasegawa, M. Ishida, T. Nakajima, Y. Honda, O. Kitao, H. Nakai, T. Vreven, J. A. Montgomery, Jr., J. E. Peralta, F. Ogliaro, M. Bearpark, J. J. Heyd, E. Brothers, K. N. Kudin, V. N. Staroverov, R. Kobayashi, J. Normand, K. Raghavachari, A. Rendell, J. C. Burant, S. S. Iyengar, J. Tomasi, M. Cossi, N. Rega, J. M. Millam, M. Klene, J. E. Knox, J. B. Cross, V. Bakken, C. Adamo, J. Jaramillo, R. Gomperts, R. E. Stratmann, O. Yazyev, A. J. Austin, R. Cammi, C. Pomelli, J. W. Ochterski, R. L. Martin, K. Morokuma, V. G. Zakrzewski, G. A. Voth, P. Salvador, J. J. Dannenberg, S. Dapprich, A. D. Daniels, Ö. Farkas, J. B. Foresman, J. V. Ortiz, J. Cioslowski and D. J. Fox, Gaussian, Inc., Wallingford CT, 2009.
53. F. Furche and R. Ahlrichs, *J. Chem. Phys.*, 2002, **117**, 7433.
54. R. Bauernschmitt and R. Ahlrichs, *Chem. Phys. Lett*., 1996, **256**, 454−464.
55. R. E. Stratmann, G. E. Scuseria and M. J. Frisch, *J. Chem. Phys*., 1998, **109**, 8218−8224.
56. M. E. Casida, C. Jamorski, K. C. Casida and D. R. Salahub, *J. Chem. Phys*., 1998, **108**, 4439−4449

APPENDIX

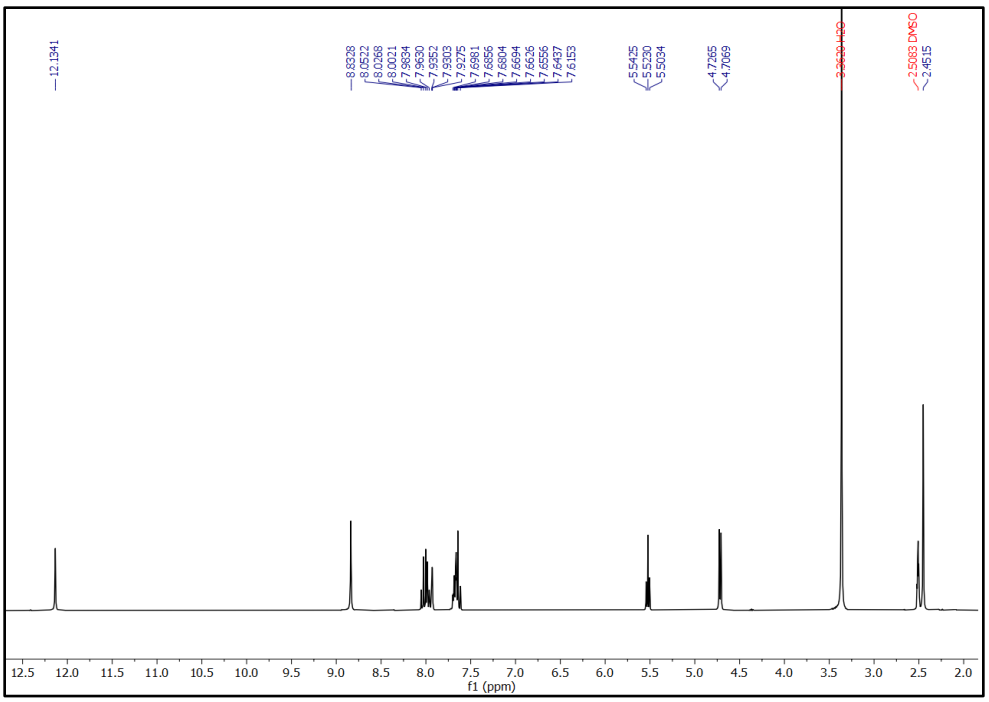

Fig. A4.1: ^{1}H NMR (300 MHz) spectra of the probe (HMCP) in DMSO-d_6

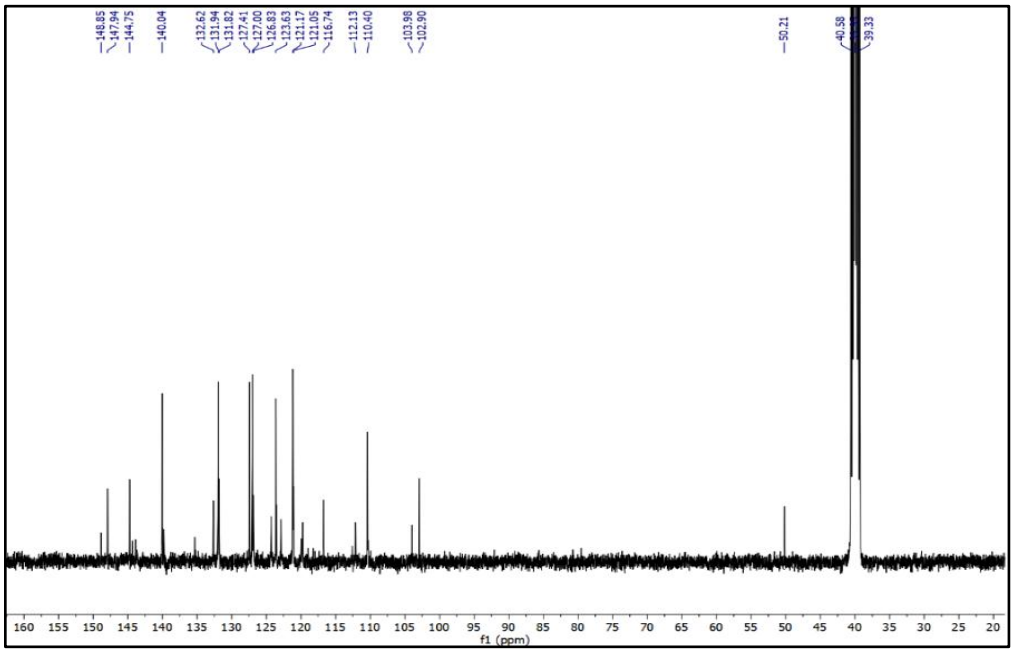

Fig. A4.2: ^{13}C NMR (75 MHz) spectra of the probe (HMCP) in DMSO-d_6

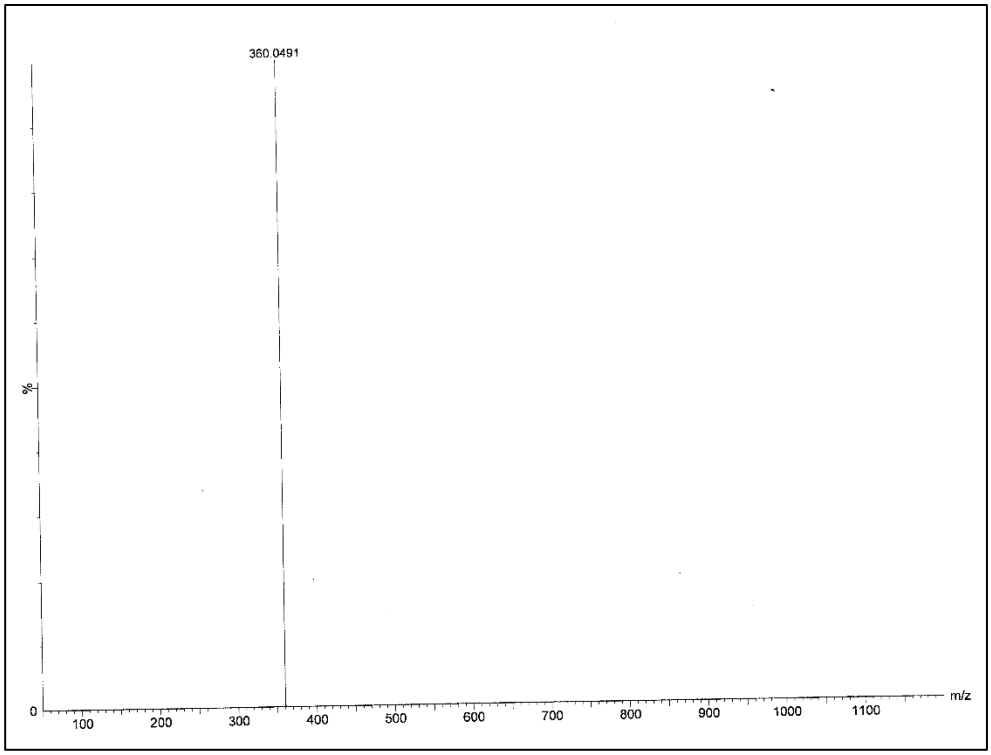

Fig. A4.3: HRMS of the probe (HMCP)

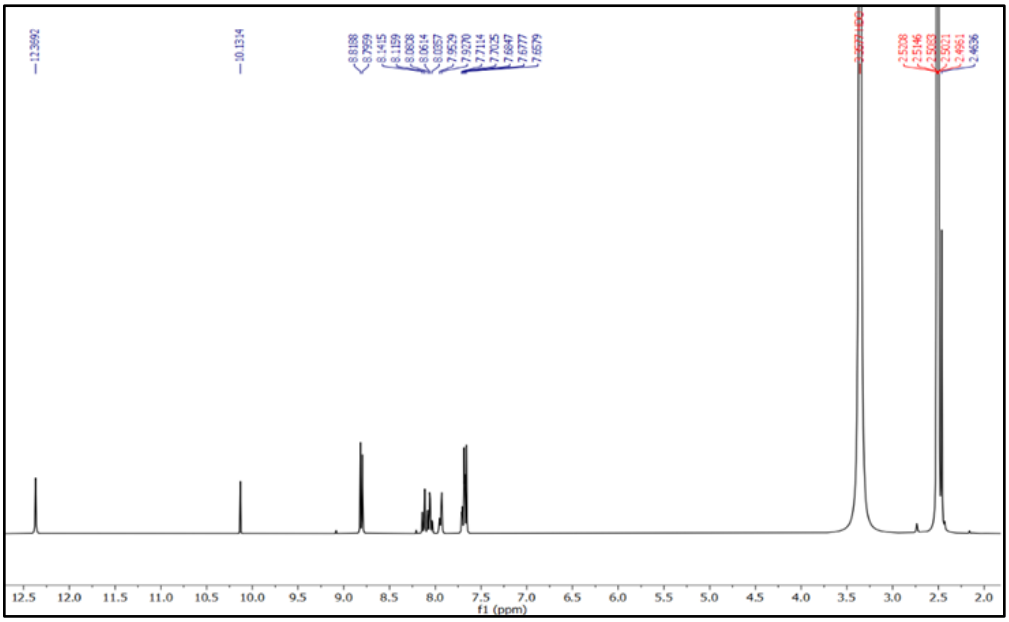

Fig. A4.4: ^{1}H NMR (300 MHz) spectra of the probe (MCMP) in DMSO-d_6

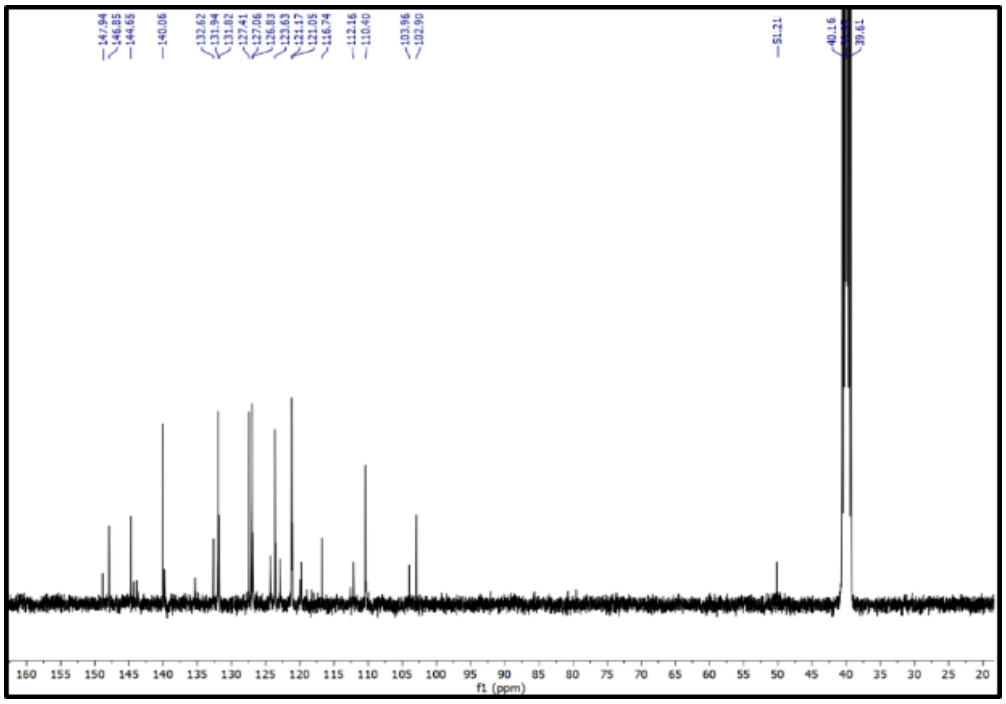

Fig. A4.5: ^{13}C NMR (75 MHz) spectra of the probe (MCMP) in DMSO-d_6

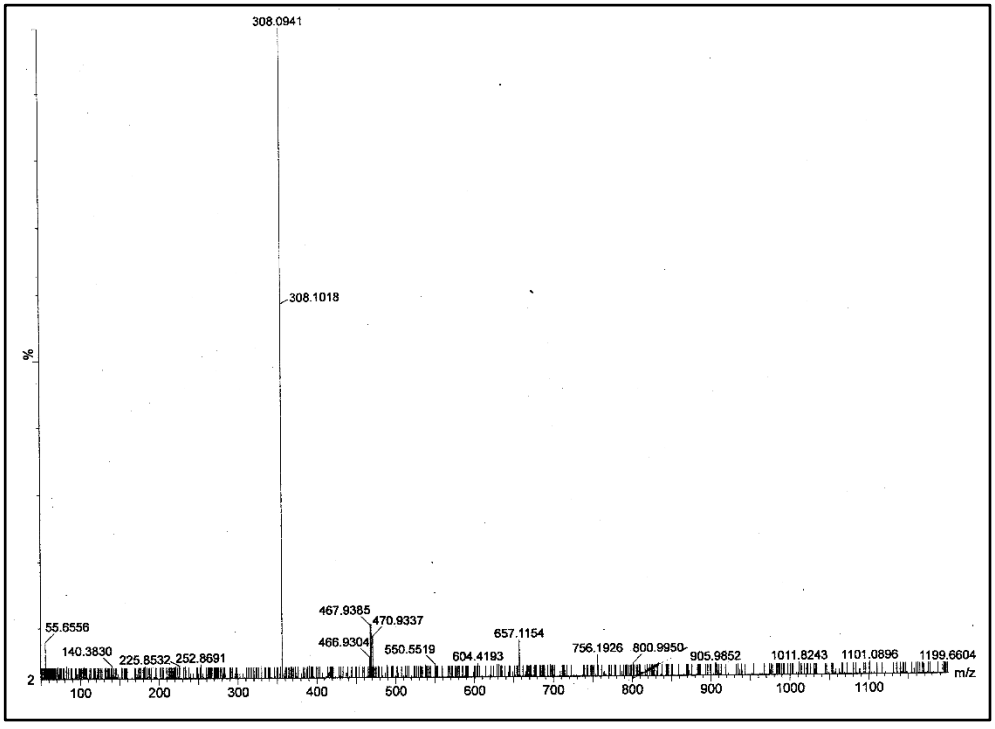

Fig. A4.6: HRMS of the probe (MCMP)

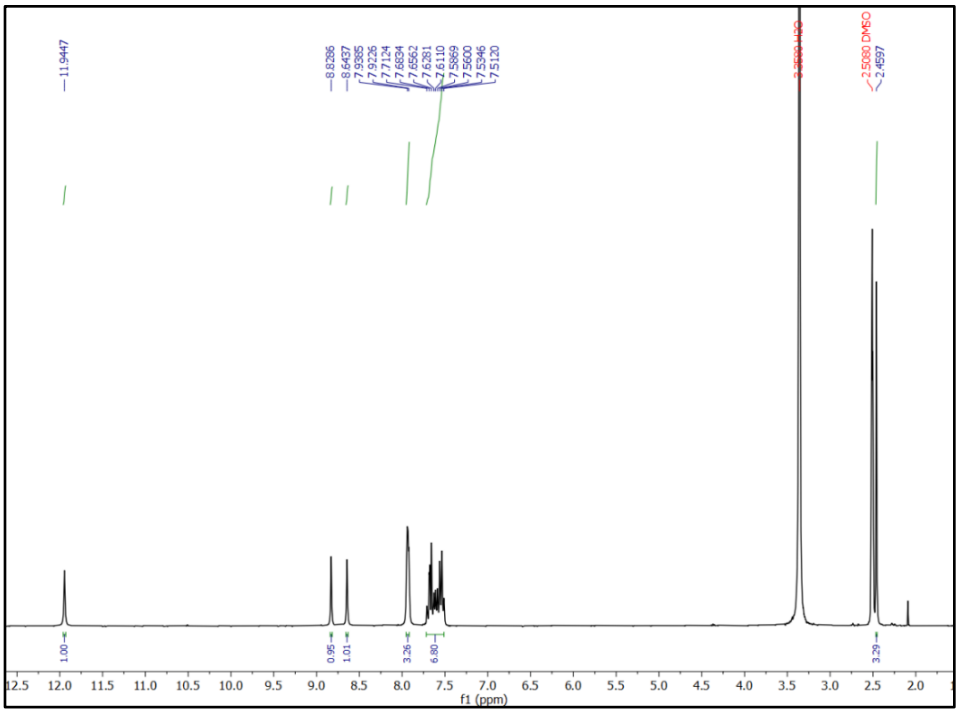

Fig. A4.7: ^{1}H NMR (300 MHz) spectra of the probe (MCMB) in DMSO-d_6

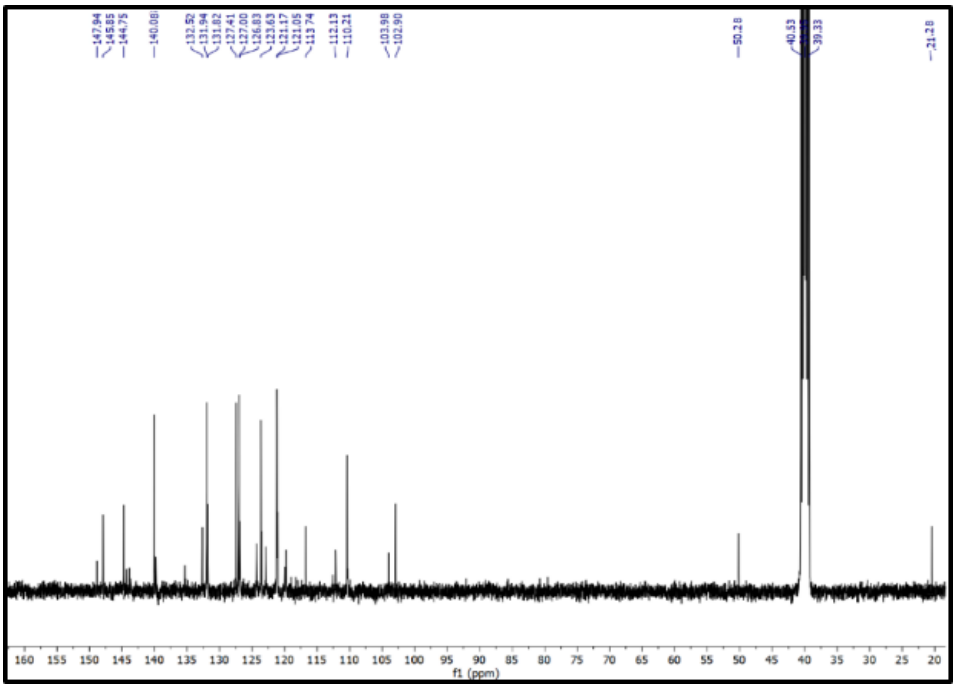

Fig. A4.8: ^{13}C NMR (75 MHz) spectra of the probe (MCMB) in DMSO-d_6

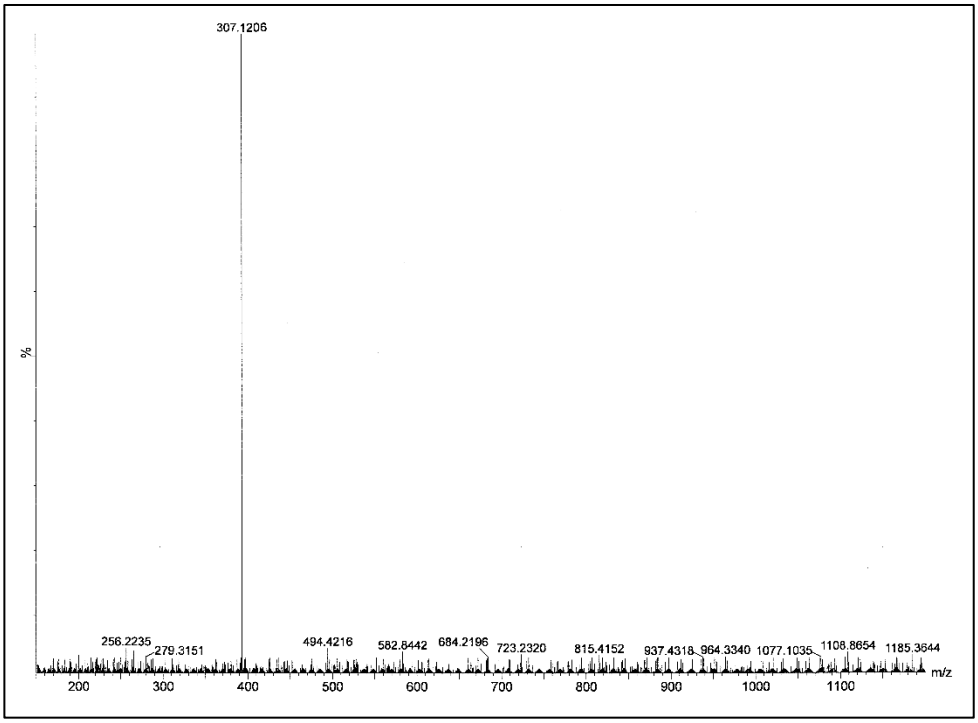

Fig. A4.9: HRMS of the probe (MCMB)

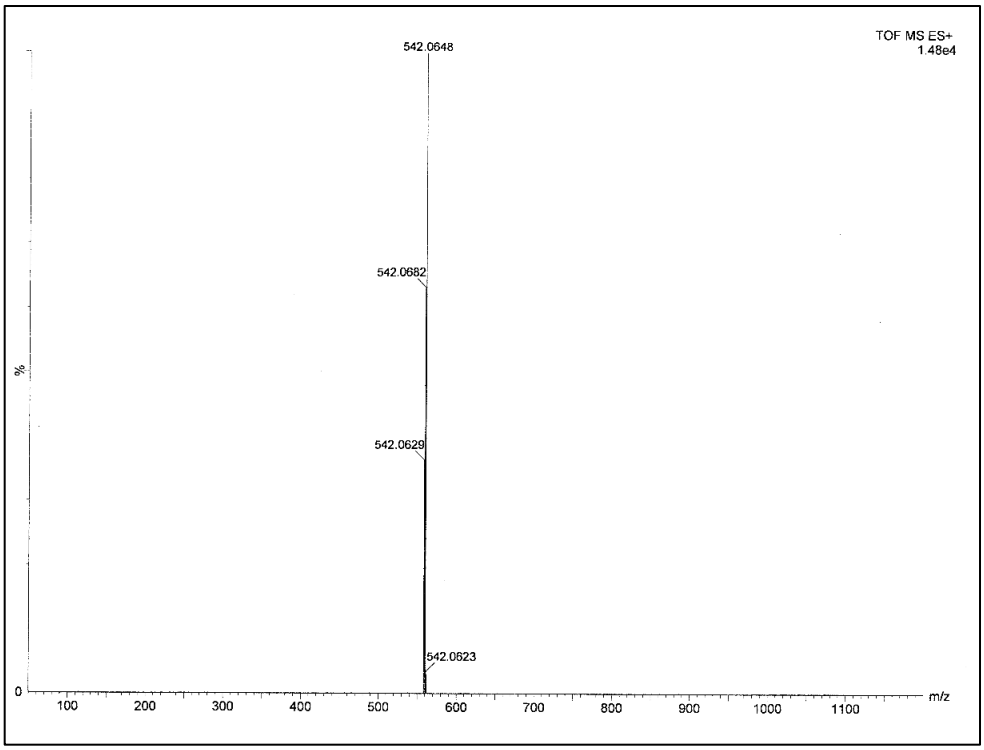

Fig. A4.10: HRMS of HMCP-Al^{3+} complex

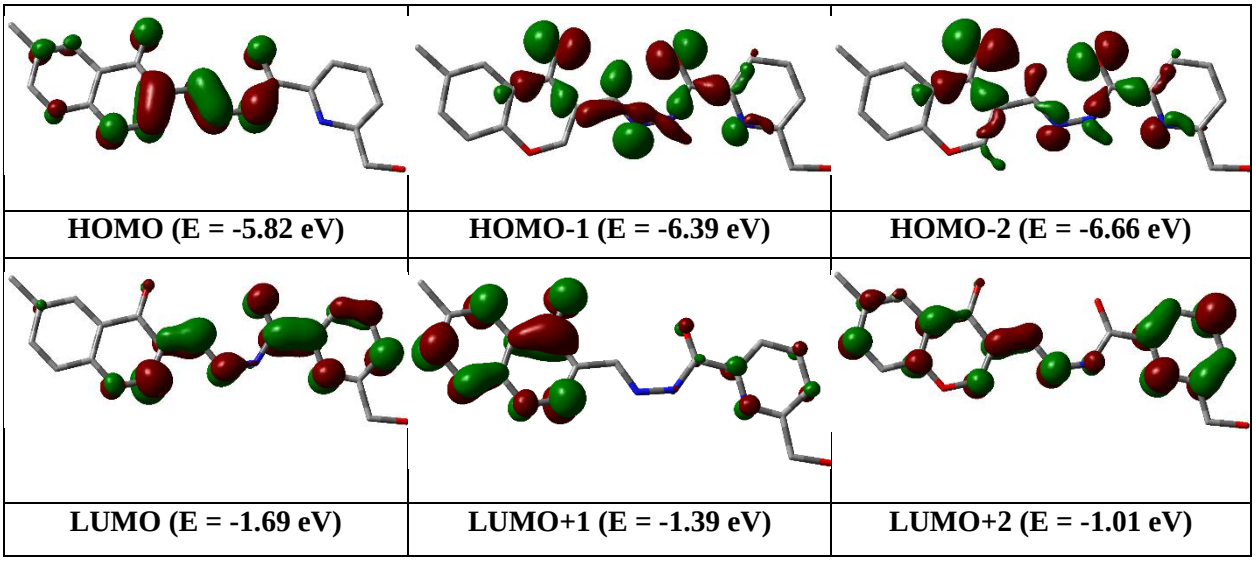

Fig. A4.10: Contour plots of some selected molecular orbitals of HMCP

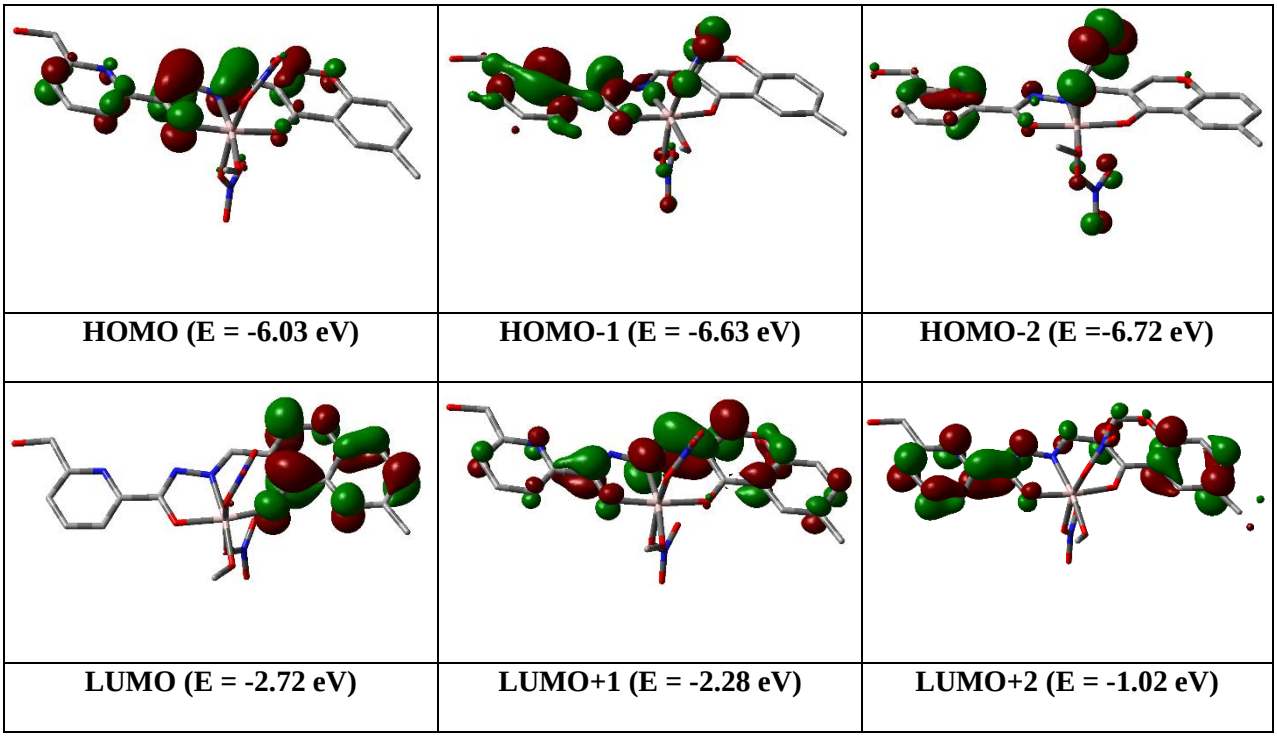

Fig. A4.11: Contour plots of some selected molecular orbitals of HMCP-Al^{3+} complex

Table A4.1. Energy and compositions of some selected molecular orbitals of HMCP and HMCP-Al^{3+}

MO	Energy (eV)	
	HMCP	**HMCP-Al^{3+}**
LUMO+5	0.74	-0.45
LUMO+4	0.02	-0.59
LUMO+3	-0.63	-0.73
LUMO+2	-1.01	-1.02
LUMO+1	-1.39	-2.28
LUMO	-1.69	-2.72
HOMO	-5.82	-6.03
HOMO-1	-6.39	-6.63
HOMO-2	-6.66	-6.72
HOMO-3	-6.69	-6.80
HOMO-4	-7.09	-6.85
HOMO-5	-7.13	-7.33

Table A4.2. Vertical electronic transitions calculated by TDDFT/B3LYP/CPCM method for HMCP and HMCP-Al^{3+} in methanol

Compounds	λ (nm)	E (eV)	Osc. Strength (f)	Key excitations	Character	$\lambda_{expt.}$ (nm) (ε, $M^{-1}cm^{-1}$)
HMCP	335.44	3.6962	0.7610	(96%) HOMO→LUMO	π → π*	314 (60408)
	309.01	4.0124	0.0650	(91%) HOMO→LUMO+1	π → π*	283 (47192)
	277.95	4.4607	0.0637	(86%) HOMO→LUMO+2	π → π*	
HMCP-Al^{3+}	380.93	3.2547	0.0868	(97%) HOMO→LUMO	π → π*	424 (61475)
	352.17	3.5206	0.8959	(96%) HOMO→LUMO+1	π → π*	407 (58289)
	310.88	3.9881	0.1218	(66%) HOMO-3→LUMO	π → π*	

A novel AIE active carbazole-benzothiazole based chemodosimeter for chromogenic and fluorogenic recognition of CN^-

A novel AIE active carbazole-benzothiazole based chemodosimeter for chromogenic and fluorogenic recognition of CN^-

Abstract

A novel colorimetricand fluorescent sensing probe (E)-3-(4-(9H-carbazol-9-yl)phenyl)-2-(benzo[d]thiazol-2-yl)acrylonitrile (CBTA) was synthesized and characterized by spectroscopic techniques. CBTA displayed "turn off" fluorescence in the presence of cyanide with relatively high selectivity compared to others anions such as Br^-, Cl^-, I^-, NO_3^-, SO_4^{2-}, SCN^-, CO_3^{2-}, N_3^- , OH^- , HCO_3^- , $H_2PO_4^-$, HPO_4^{2-}, F^-, ACO^-, PO_4^{3-} in DMSO:H_2O medium (40:60, v/v, HEPES buffer, pH=7.2). The "turn off" fluorescence response mechanism can be attributed to intra-molecular charge transfer (ICT) process, which is blocked by nucleophilic attack of cyanide ion at the cyano vinyl group of the probe. The LOD is found to be 3.57×10^{-8} M. The interaction involved behind the sensing of cyanide was investigated by Job's plot analysis, ^{1}H-NMR and mass spectroscopic studies. DFT and TDDFT has also been employed to verify the experimental outcomes. Moreover, test strips experiment provides a wide application prospect of the receptor for detecting poisonous cyanide in environment and biological system.

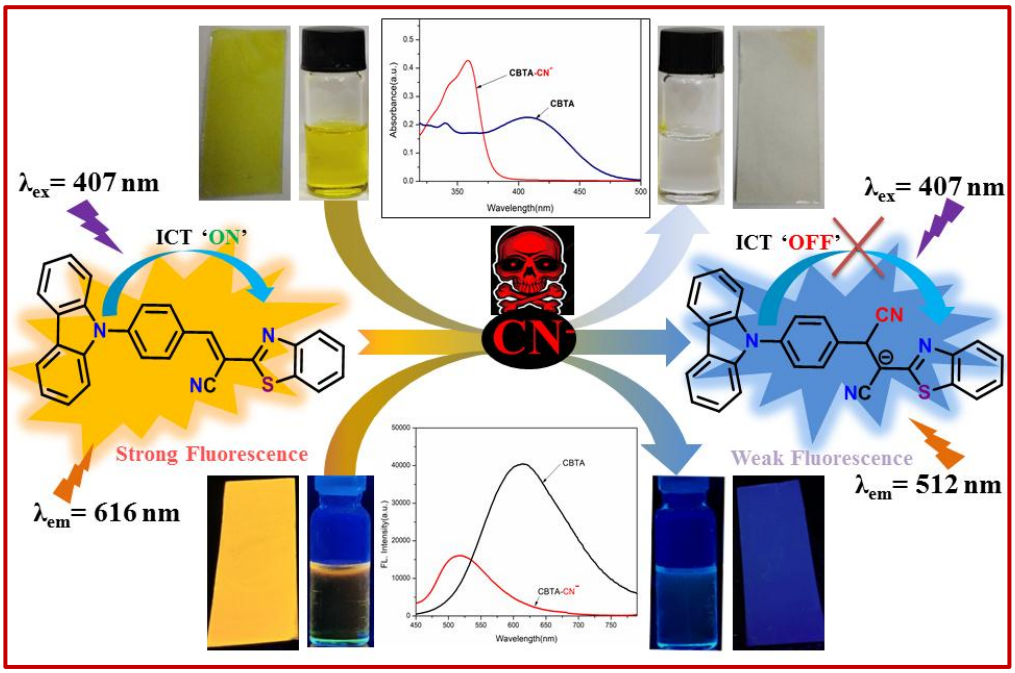

5.1. Introduction

The development of new molecular probe for the detection of anions is of great interest because of their vital important roles in a broad range of medicine, catalysis, life science and the environment.[1] Additionally food safety issues and water pollution by poisonous anions has drawn an attention with the development of science and technology nowadays.[2-6] Cyanide is one of the most well-known toxic anion, even at a lower concentration, which can be lethal to human beings, animal and environment. Cyanide is currently extensively used in many industrial processes such as electroplating, petrochemicals, photography, steel production, gold mining, metallurgy and the synthesis of resign and fibre due to its critical role in multi-functional reaction.[7] World health organization (WHO) stipulates the permissible acceptable concentration of cyanide in drinking water is 1.9×10^{-6}mol/L.[8] By the way, cyanide is present in some insects, fruits, seeds, roots where it is released through the hydrolysis process of cyanogenic glycosides.[9-14] Cyanide binds to the iron ion in cytochrome c oxidase and blocks the electron transport in metabolism and inhibits the production of ATP in cells, resulting the biological system inefficient to provide sufficient energy to heart, central nervous system and other vital organs ultimately.[15,16] Considering the above fact, development of simple, efficient and rapid detection tools with high selectivity and sensitivity towards cyanide is an ongoing hot topic to prevent harmful affect in human body from contaminated food and environment.

5.2. Prior works

To date, fluorescence molecular probes capable of detecting CN^- have been reported based on fluorescence resonance energy transfer (FRET),[17-19] intra-molecular charge transfer (ICT),[20,21] twisted intra-molecular charge transfer (TICT),[22] excited state intra-molecular proton transfer (ESIPT),[23,24] photo-induced electron transfer (PET).[25,26] Recently several groups have been reported detection methods by utilizing nucleophilic addition reaction of cyanide directly involved in the development of covalent bond formation and showing anti-interference ability, high selectivity.[27-38] Compared with the traditional sophisticated analytical tools such as spectrophotometry, voltammetry, chromatography, potentiometric methods, optical molecular probes based on colorimetric and fluorometric responses towards CN^- are of great preference in virtue of their convenience, simple, tenability, low cost, high selectivity and rapid response.[39]

Particularly, naked-eye optical sensor is very much impressive. Since tang et. el. discovery of AIE phenomenon in 2001, several research groups have been published a growing number of AIE active fluorescence probes[47-50] for their wide application in optoelectronics, environmental monitoring, biological imaging as well as in the construction of the green energy devices and chemosensors.[39-46] The active AIE effect is mainly due to the restriction of molecular motion. Therefore the fabrication of AIE active fluorescence probes for recognition of CN^- in the aqueous medium is now a recent trends depending on the special features of AIE active molecules.[51-52] So far, with the intra-molecular charge transfer (ICT) process developed, several plenty of typical donor-π-acceptor (D-π-A) type sensor have been reported to recognize trace CN^- ions, which inhibits the ICT process by nucleophilic attack at the subunits (such C=C and C=N) and causes obvious color and spectral changes.[53-65] Keeping in mind the unique nucleophilicity of CN^- ions, cyanide can be recognized by the donor-π-acceptor (D-π-A) type molecular probe that considered as a colorimetric and fluorimetric sensor.

5.3. Present work

We herein have successfully fabricated AIE active chemodosimeter CBTA consist of a donor-π-acceptor (D-π-A) skeleton in which carbazole acts as a donor moiety and benzothiazole acts as an acceptor unit. The probe can be served as a new dual-modal colorimetric and fluorescent sensor for distinct detection of cyanide ions among all others relative anions based on ICT mechanism and exhibited high sensitivity and selectivity in 60% aqueous DMSO solution. The sensing mechanism could be ascribed to the nucleophilic attack by cyanide ion to the vinyl group of the receptor that leads to the cut off in the ICT process, causing the spectroscopic changes followed by the obvious color changes that could be distinguished by the naked eye in the ambient light as well as under UV lamp.

5.4. Results and discussions

5.4.1. Synthesis of CBTA

The chemodosimeter (CBTA) was synthesized via the condensation of 4-(9H-carbazol-9-yl)benzaldehyde and 2-(benzo[d]thiazol-2-yl)acetonitrile in absolute ethanol solvent under reflux condition (scheme-1). The chemical structure of CBTA has been confirmed by ^{1}H-NMR, ^{13}C-NMR, IR-spectroscopy, mass-spectral analysis (Fig. A5.1-A5.4, Appendix).

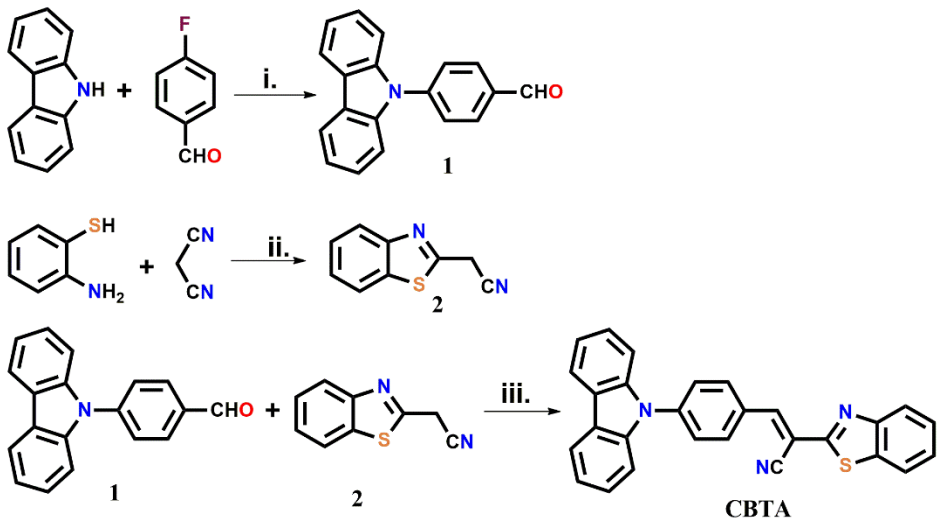

Scheme 5.1: Synthetic route of the probe, CBTA. (i) KOtBu, DMF, 100^0C,12 h; (ii) EtOH, Acetic acid, stirring for 12 hr, room temperature, (iii) EtOH, Piperidine, reflux, 7h

5.4.2. Spectral characterization and analysis of CBTA and CBTA-CN^- adduct

^{1}H-NMR spectrum of CBTA is recorded in DMSO-d_6 which exhibits that the resonance signal of aromatic protons appears at around 8.42-7.35 ppm (16H) and the proton signal at 8.57 ppm corresponds to vinylic proton in the free CBTA. Upon addition of cyanide into probe solution, the all aromatic protons shifted to an upfield region at around 7.88-6.81 ppm (16 H) due to the formation of negative charge in CBTA-CN^- adduct, while the vinylic proton shifted to around 5.43 ppm, indicating the conversion of Sp^2 carbon to SP^3 carbon and confirms the formation of the CBTA-CN^- adduct. The HRMS of CBTA shows a peak at m/z 428.12 possibly for probe itself whereas upon addition of cyanide solution, a new peak at 455.13 (m/z) observes that indicating the formation of CBTA-CN adduct.

5.4.3. Aggregation-induced Emission Enhancement (AIEE) effect of CBTA

AIEE behavior of CBTA was studied by fluorescence spectra. As water is an undesirable solvent, the addition of H_2O to DMSO facilitate the aggregation of CBTA. The fluorescence changes of CBTA is shown by modifying the DMSO to water proportion in the solvent system. The fluorescence intensity gradually decreases as volume proportion of water of H_2O-DMSO solution increases from 0% to 40%. After that a dramatic enhancement in fluorescence intensity is observed

and achieved maximum intensity at 60% of water content with a red shift of 16 nm along with large enhancement of the fluorescence intensity about 6 fold compared to the fluorescence intensity in pure DMSO solvent (Fig. 5.1). It is suggested that aggregation of the probe, CBTA is started after near about 40% of water fraction in solvent situation. All these findings show that our probe is AIEE active. The free intra-molecular single bond rotation in the free probe that quenches the emission intensity via non-radiative decay is responsible for not viewing AIEE activity in the solution phase. But in the aggregate state where this rotation is forbidden, displays high fluorescence intensity with red shift. The large enhancement in fluorescence intensity with red shift may be ascribed by the electronic transition (π-π^*) inside the probe.

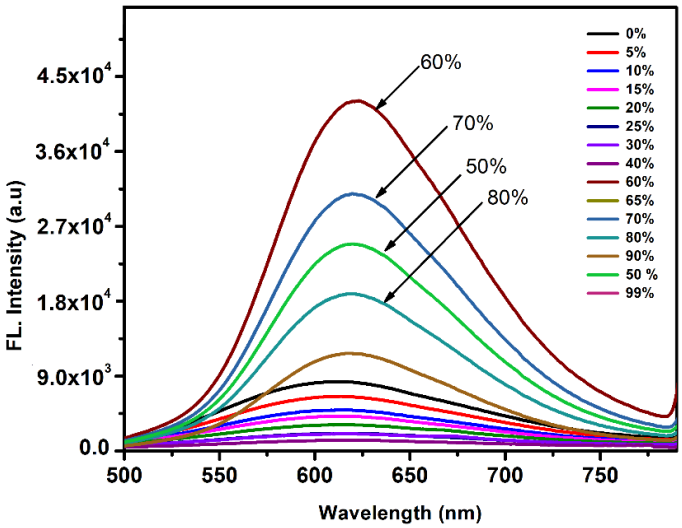

Figure 5.1: Emission spectra of CBTA (20 µM) in DMSO/water mixtures(v/v) with different water fraction (f_w) (excitation=409 nm).

5.4.4. Sensing performance of CBTA

In order to observe the sensing ability of CBTA, the UV-Vis spectra of the probe were performed in presence and absence of various chosen anions (F^-, Cl^-, ACO^-, NO_3^-, SCN^-, CO_3^{2-}, HCO_3^-, HSO_4, SO_4^{2-}, $H_2PO_4^-$, HPO_4^{2-}, CN^-) in DMSO-H_2O (40:60, v/v, HEPES buffer, pH=7.2) solution at room temperature. Upon addition of CN^-, the solution color changes instantly from yellow to colorless in ambient light (Fig. 5.3(a)). Furthermore, an intense bright orange-yellow fluorescence change to light blue was clearly observed by naked eye after addition of CN^- solution under UV lamp, which is noticeably different from that orange-yellow fluorescence upon addition of several anions

(Fig. 5.3(b)). Fig. 5.1 and Fig. 5.2 displayed the absorption and emission spectra of CBTA upon addition of various chosen anions respectively. As shown in Fig. 5.1, the probe shows an absorption band at 410 nm along with two small humps at 339 nm and 293 nm in the absorption spectrum of CBTA. The absorption peaks at 293 and 339 nm are attributed to the local π-π* electronic transition inside the probe, while the one at 410 nm may be accredited due to the intramolecular charge transfer (ICT) process from the carbazole moiety to the electron deficient benzothiazole units. Upon gradual addition of CN^-, the absorption peaks at 293 nm and 410 nm are decreased along with the appearance of a new peak at 353 nm. However, upon addition of the other anions except CN^-, the absorption spectra remain almost unaltered relative to that of free receptor. The spectral data are in well agreement with the phenomenon shown in Fig. 5.3(a). The fluorescence spectra of CBTA shows emission peak at 616 nm upon excitation at 407 nm, which is assigned to ICT process (Fig. 5.2). Upon addition of each chosen anions (2.0 equiv.) except for CN^-, only negligible change is noticed in the fluorescence spectra (Fig. 5.2). However, the

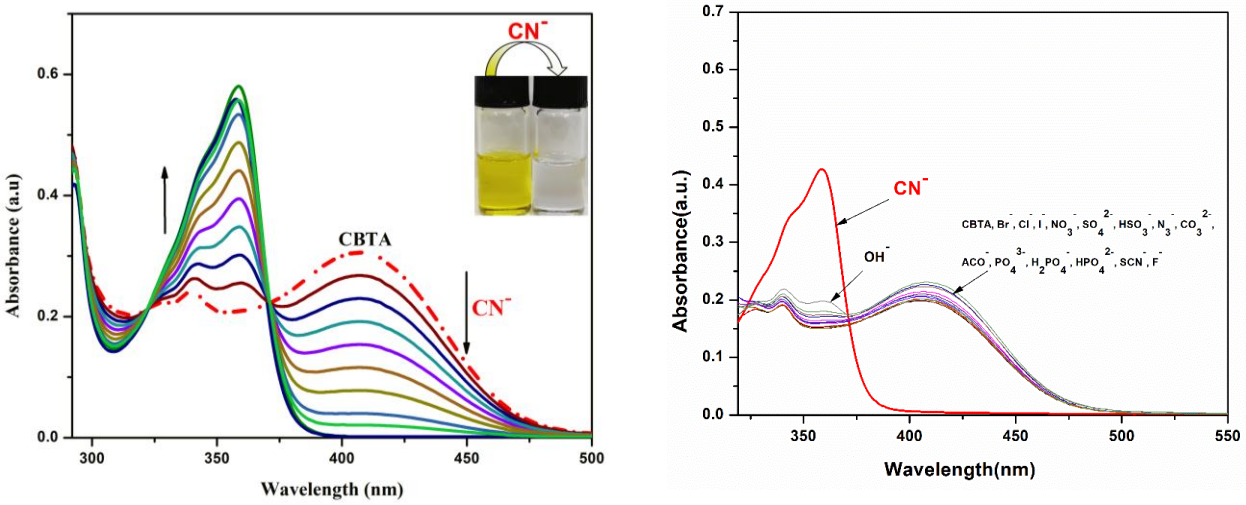

Figure 5.1: Change in UV-Vis spectrum of CBTA (20 μM) upon addition of CN^-(40 μM) in DMSO/H_2O (40:60, v/v) (HEPES buffer, pH=7.2). (Inset shows the change in colour in sunlight) (left side) and UV-Vis change of CBTA (10 μM) upon addition of different anions, i.e. Br^-, Cl^-, I^-, NO_3^-, SO_4^{2-}, SCN^-, CO_3^{2-}, N_3^-, OH^-, HCO_3^-, $H_2PO_4^-$, HPO_4^{2-}, F^-, ACO^-, $PO_4^{3-}$and CN^- (40 μM) in DMSO/H_2O (40:60, v:v) using HEPES buffered solution at pH=7.2 (right side) .

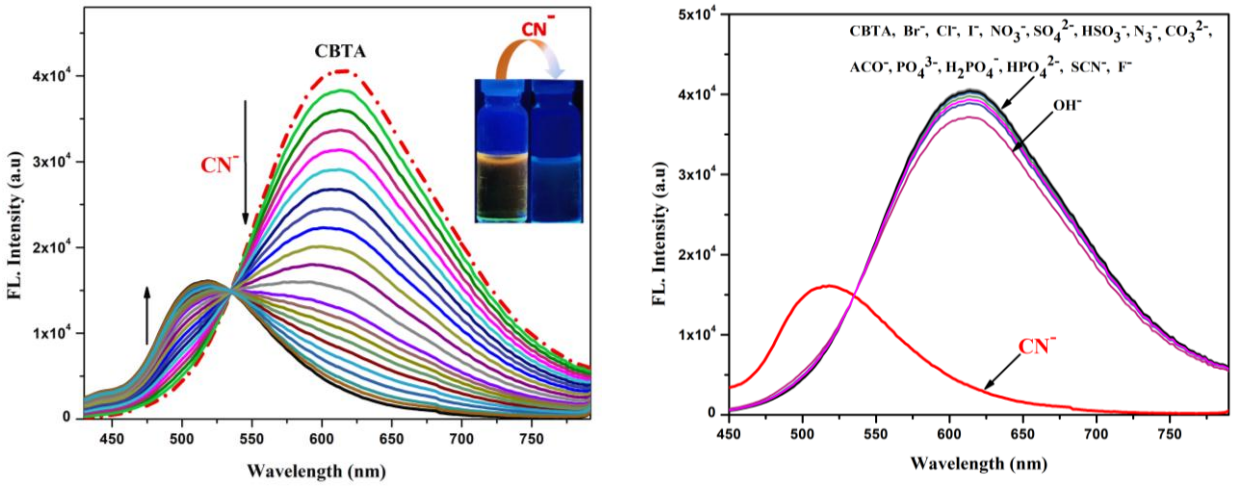

Figure 5.2: Change in emission spectra of CBTA (20 µM) upon gradual addition of CN^-(40 µM) in DMSO/H_2O (40:60, v/v) (HEPES buffer, pH=7.2) (left side) (Inset shows the change in colour underUV-radiation) and Change in emission spectrum of CBTA (20 µM) upon addition of different anions (40 uM) in DMSO-H_2O (40:60, v/v, HEPES buffer, pH=7.3) solution (right side).

The change in the absorption spectra of CBTA after addition of CN^- of different concentration were recorded in 60% aq. DMSO solution (Fig. 5.1). In the absorption spectral changes, it is clearly observed that the absorption bands at 293 nm, 339 nm and 410 nm consecutively attenuate along with a progressive raise of new absorption peak at 358 nm upon successive addition of CN^- (0-2 equiv.). Upon incremental addition of CN^-, the emission band at 616 nm decreases gradually along with the appearance of small new emission band at 512 nm upon excitation at 407 nm (Fig.5.2), suggesting that CBTA could be served as a potential candidate to quantitatively monitor CN^- ion. To illustrate the efficiency and selectivity of the present probe (CBTA) towards CN^- ion, the limit of detection (LOD) of probe for cyanide ion is calculated and found to be (7.68±0.29) $x10^{-8}$ (M) which was established from the fluorescence titration data of the CBTA upon addition of CN^- using the equation, LOD = K×(SD/S), where SD and S stand for the standard deviation and the slope of the linear response curve respectively (Fig. 5.4). From the mole ratio plot of CBTA, it can be stated that after addition of almost 7 µM of CN^-, no significant changes in emission intensity at 616 nm is displayed thereby signifying to the fact that the saturation has taken place (Fig. 5.4). In addition, the kinetics study was also performed to monitor the reaction time of the probe with CN^- and fluorescence spectra were recorded depending on time. This experiment shows that the

fluorescence intensity of the probe at 616 nm and absorbance at 410 nm rapidly decreases as reaction progresses and CBTA-CN^- adduct forms and finally reaches its minimum and stable value within 22s, indicating the completion of the reaction (Fig. 5.5). These observations clearly suggest that cyanide can result in the color change of CBTA solution as well as the attenuation of fluorescence intensity, implying CBTA may be used as a potential candidate in portable device for rapid CN^- recognition.

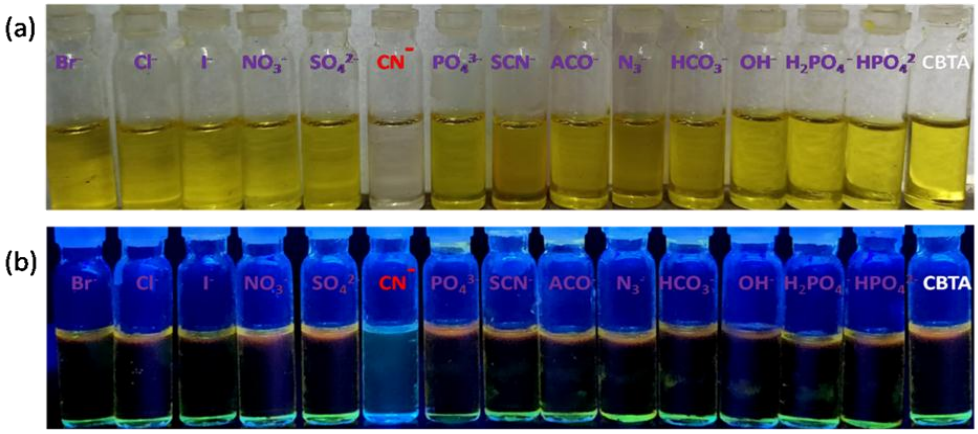

Figure 5.3: Color variations upon addition of different anions (40µM) to the sensor CBTA (20 µM) under sunlight(a) and under UV light(b).

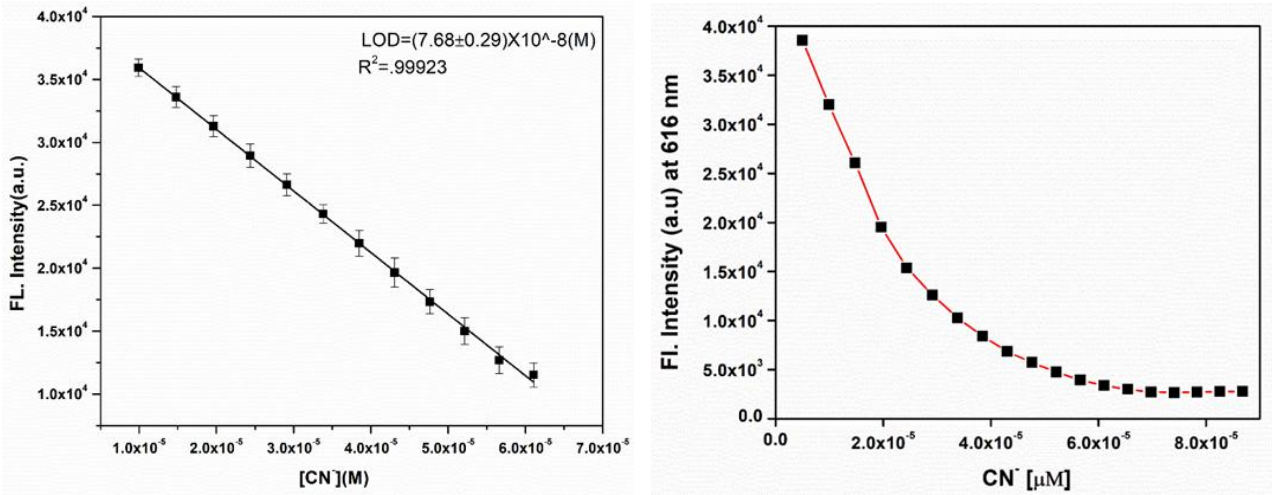

Figure 5.4: Linear response curve of CBTA at 616 nm depending on the CN^-concentration; Mole ratio plot of CBTA for CN^-

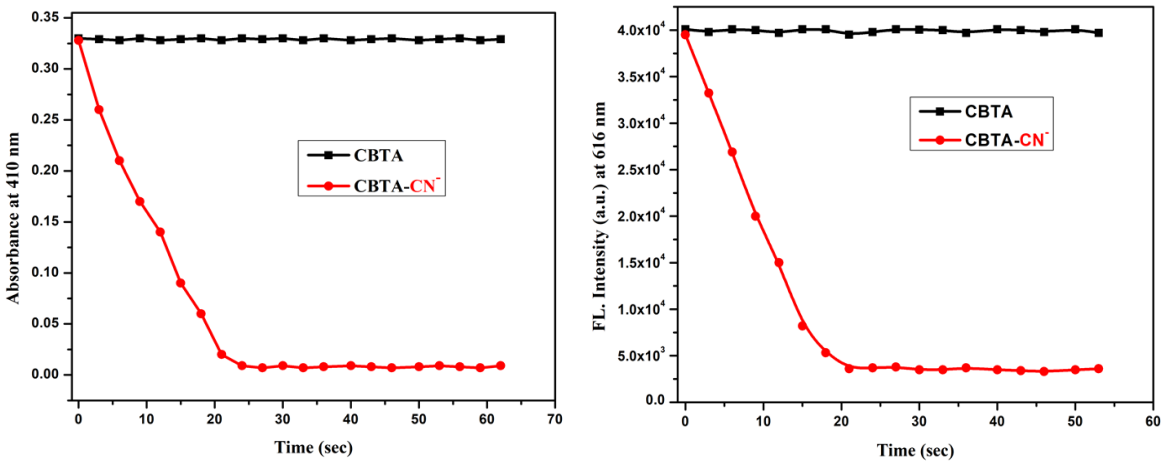

Figure 5.5: The time-dependent absorbance (left side) and FL.Spectrum (right side) of CBTA towards CN^- in DMSO-H_2O (40:60, v/v, pH= 7.2).

To confirm the specific selectivity of CBTA to CN^-, a competition experiment was executed upon addition of CN^- to CBTA solution containing other common anions in DMSO/H_2O (40:60, v/v). As observed in Fig. 5.6, it is almost unchanged in CN^- induced fluorescence intensity in the presence of all other anions which can also be referred as binary competitive system "Target + anion" in the same solution phase, indicating efficient CN^- signalling aptitude and higher anti-interference capability of CBTA-CN^- system.

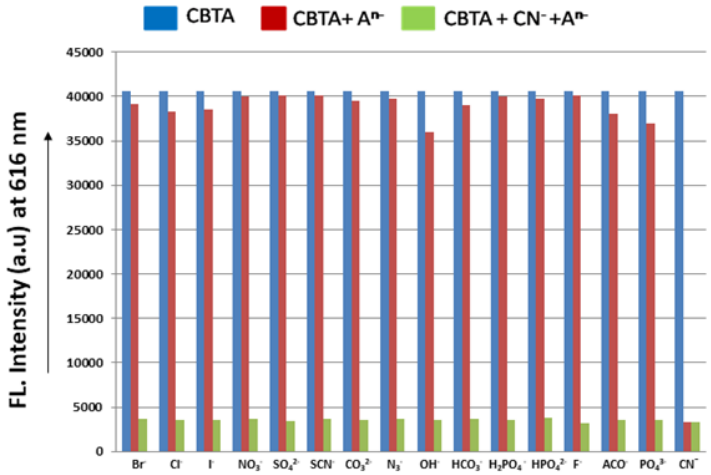

Figure 5.6: Competitive experiments of CBTA (20 µM) for CN^- (40 µM) in presence of common anions (40 µM) in 60% aqueous DMSO mixture.

To investigate the dependence of the CBTA towards pH, we recorded emission spectra of CBTA and CBTA-CN^- in DMSO-H_2O (40:60, v/v) solution with different pH values (2.0-12.0). For the

free receptor, emission of the solution remains almost unaltered within the pH rang of 0 to 9 and after that, emission intensity slightly decreases with increase in pH The maximum emission quenching of CBTA in presence of CN^- ion was observed at pH 7.2 suggesting the probe is suitable to show maximum sensing ability at neutral pH condition (Fig. 5.7).

Time resolved fluorescence technique (TRPL) is also studied to examine the excited state behaviour of the fabricated probe (CBTA) and the cyanide adduct (CBTA-CN). The fluorescence decay curves of CBTA and cyanide adduct are obtained by using the mono-exponential functions with good χ^2 values (Fig. 5.7). For CBTA, τ=6.1 ns (χ^2=1.16), and for CBTA-CN adduct, τ=1.38 ns (χ^2 = 1.14). Radiative rate constant K_r and total non-radiative rate constant K_{nr} have been calculated using the equation $\tau^{-1} = K_r + K_{nr}$ and $K_r = \varphi_f/\tau$ (Table A5.3, Appendix). The change in the value of τ, K_r and K_{nr} supports the adduct formation of CN^- with the probe CBTA to form a new very weak fluorogenic compound CBTA-CN which has lower life-time than the free probe itself.

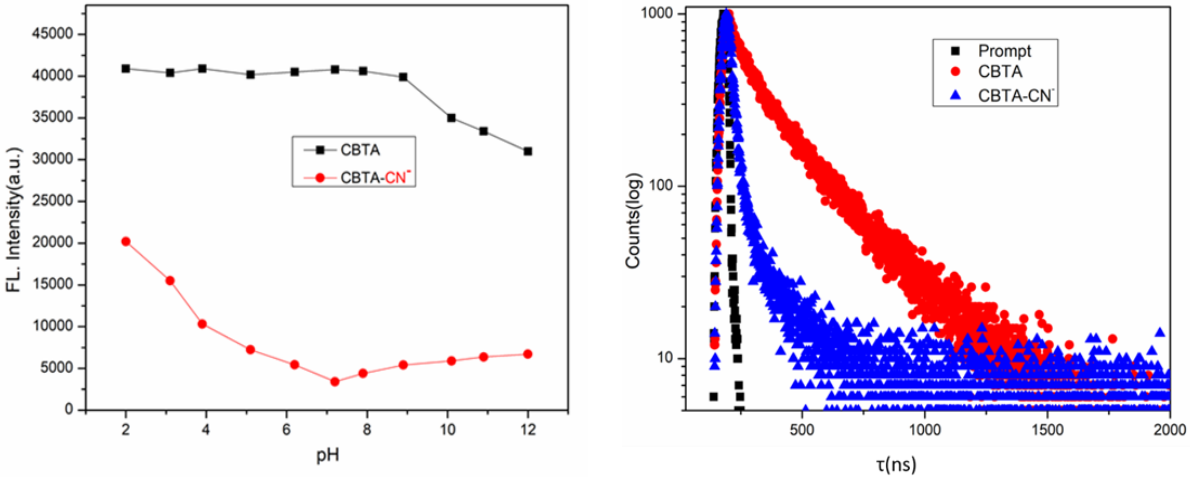

Figure 5.7: pH study of CBTA for CN^- (left side) and lifetime decay profile of CBTA and CBTA-CN^- adduct (right side).

5.4.5. Possible sensing mechanism

The possible interaction mechanism of the probe, CBTA towards CN^- is investigated by ^{1}H-NMR spectroscopy. In ^{1}H-NMR spectrum of free CBTA, the resonance signal of aromatic protons appears at around 8.42-7.35 ppm (16H), whereas after addition of 1.0 equivalent of CN^-, the protons shifted to an upfield region at around 7.88-6.81 ppm (16 H) due to development of negative charge in CBTA-CN^- adduct, clearly indicating the break-down of conjugation between benzothiazole and phenyl carbazole units. However, in the resonance spectra of CBTA-CN adduct, the proton signal at 8.57 ppm, corresponds to vinylic proton in the free CBTA, disappeared

together with the appearance of a new upfield signal at around 5.43 ppm (Fig. 5.9) confirms the formation of the CBTA-CN adduct. The formation of CBTA-CN-specie is also supported by HRMS spectroscopy. The mass spectrum shows a peak at 428.12 (m/z) that corresponds to the probe itself (Fig. A5.3). However, a new peak at 455.13 (m/z) confirms the formation of CBTA-CN adduct (Fig. A5.6). In addition to estimate the exact stoichiometry of the adduct formation, Jobs plot analysis was carried out (Fig. 5.10). The minimum intensity showed at 0.5 mole fraction of CN^-, indicating 1:1 adduct formation of CBTA with CN^- which is also supported by the observed peak at 455.13 (m/z) in the mass spectroscopy of the adduct (Fig. A5.6). These outcomes reveal the nucleophilic addition of cyanide at the cyano vinyl position accompanied with the conversation of sp^2 hybridized carbon to sp^3 hybridization (Fig. 5.8).

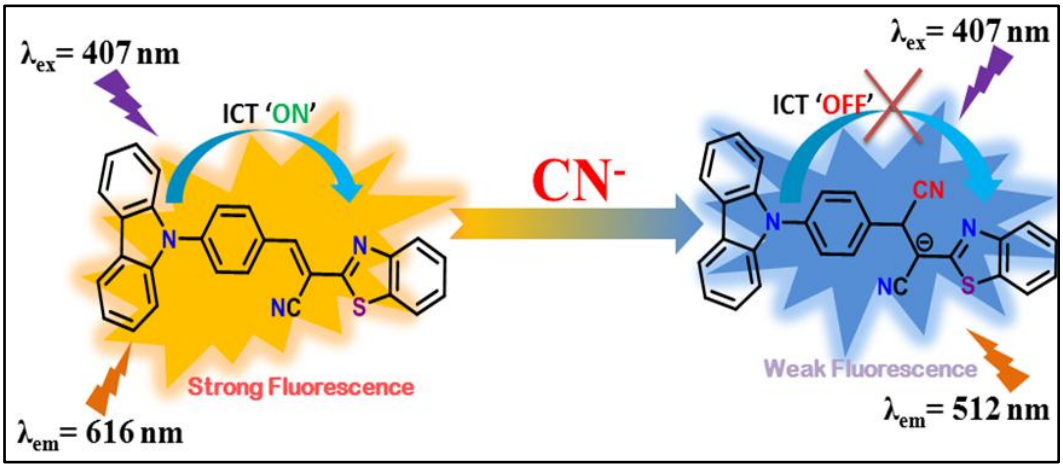

Figure 5.8: Proposing the sensing mechanism of CBTA with CN^-

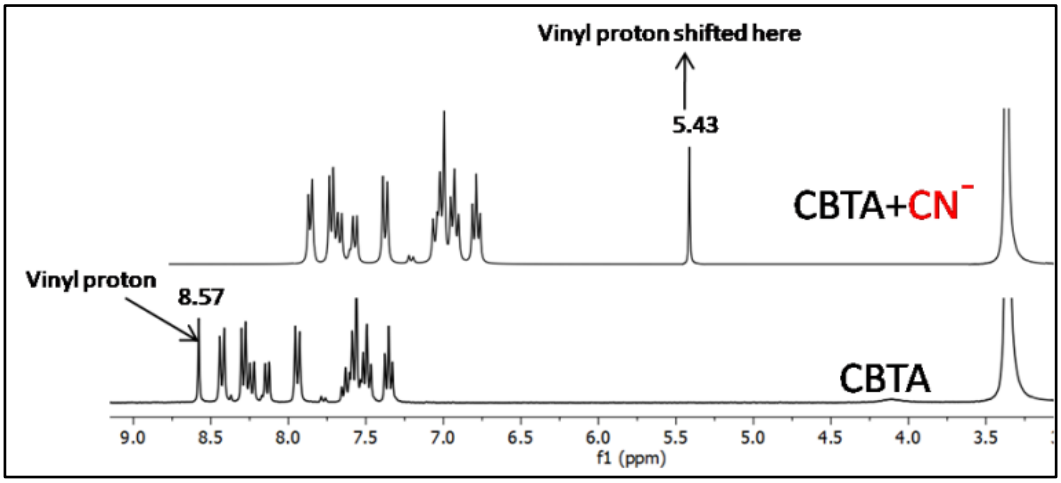

Figure 5.9: ^{1}H-NMR spectrum of CBTA and CBTA-CN^- in DMSO-d_6.

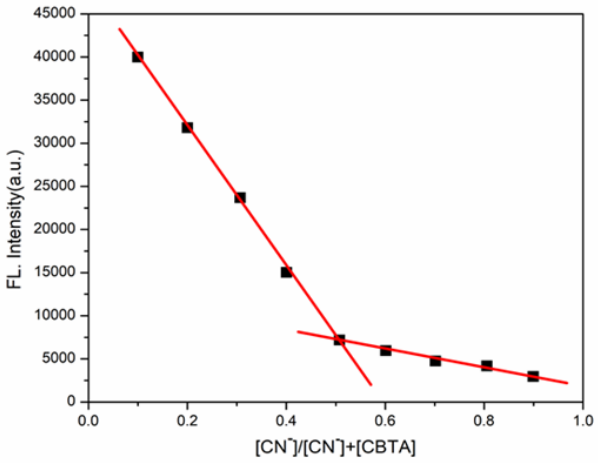

Figure 5.10: Job's plot of CBTA for CN^-

5.4.6. Dip-stick experiment: Detection of CN^- using TLC plate

For visual detection of CN^- ion, we have performed a proficient portable method called dip-stick in which the probe can act as a fluorescent portable kit showing its sensing property towards CN^- in solid state too. So to execute this experiment, few thin-layer chromatography (TLC) plates were prepared and they were dipped into CBTA solution (2×10^{-4} M) in DMSO and then kept for some time so as to evaporate the solvent in air. A fluorescence colour change observed when strips are immersed into aqueous solution (2×10^{-3} M) of cyanide and dried. This colour change can be easily visualised by naked eyes when exposed in ambient light as well as under UV light (Fig. 5.11). As CN^- shows different colours under UV light upon reaction with the receptor (CBTA) present in the test strips, we can easily distinguish it qualitatively.

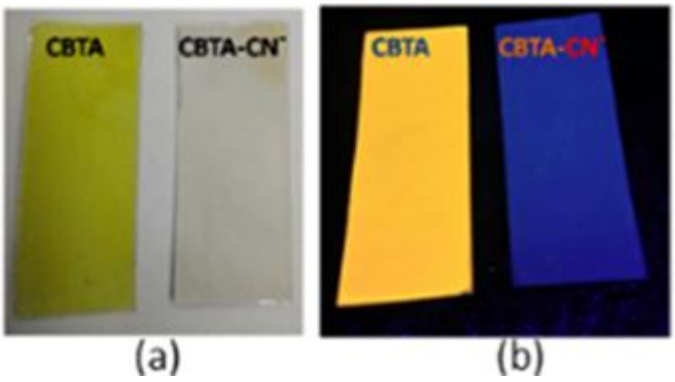

Figure 5.11: Pictures of TLC plates after immersion in 60% (v/v) aqueous DMSO solution of CBTA and in CBTA-CN^- under sunlight (a) and UV chamber (b). [CBTA] = 2×10^{-4} M, [CN^-] = 2×10^{-3} M. Excitation wavelength of the UV light is 380 nm.

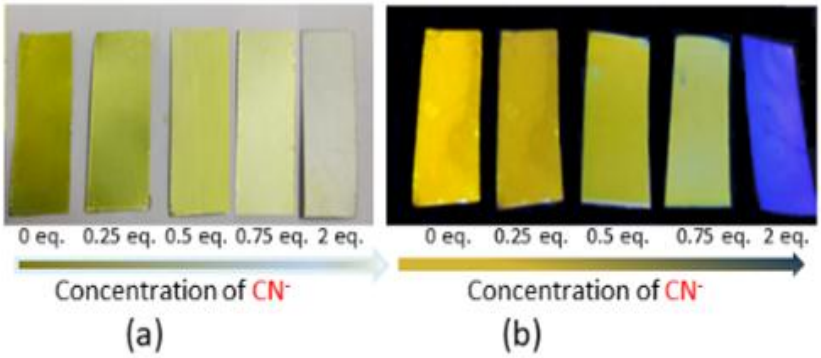

Figure 5.12: Pictures of TLC plates after immersion in 60% (v/v) aqueous DMSO solution of CBTA in presence of different CN^- concentration under sunlight (a) and UV chamber(b). [CBTA] = 2×10^{-4} M, [CN^-] = 2×10^{-3} M. Excitation wavelength of the UV light is 380 nm.

5.4.7. Photosensitivity Study

For fluorescence based detection application, a sensor having high photo-stability with displaying steady analytical signals is highly desired. Therefore, in order to photostability evaluations, sensor CBTA and CBTA-CN adduct were used over 60 min in day light under optimal conditions according to the previously reported procedure.[66] As depicted in Fig. 5.3, sensor CBTA and CBTA-CN adduct have highly photostable relative fluorescence responses throughout the experimental time (60 min) with slight signal change. This experimental results shows that receptor CBTA has highly photostable "turn-off" fluorescence signal response after nucleophilic addition of CN^-, making it compatible for the spectrofluorimetric analysis of real samples.

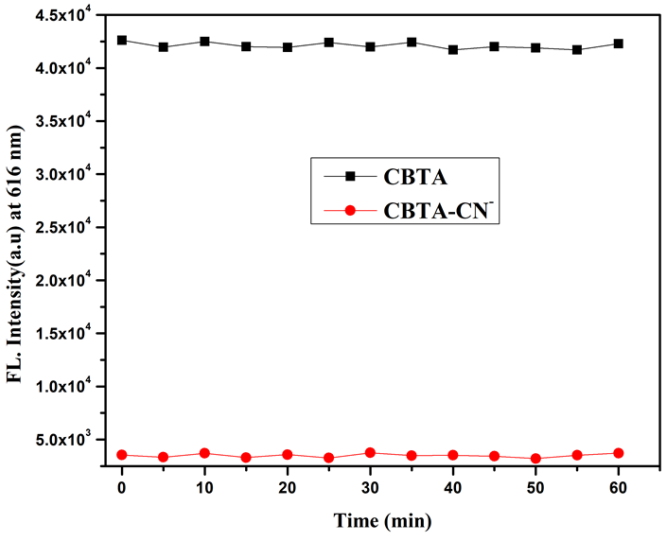

Figure 5.13: Photostability study of CBTA and CBTA-CN^- adduct.

5.4.8. Real sample analysis

As cyanide from different sources could possibly be dumped into water and pollute the water resources, so it is very much urgent to detect the concentration level in these wastewater. In order to validate the practicality of our approach, we have analyzed natural water resources (tap, pond, river) for sensing of CN^- according to the previously reported procedure.[67-71] As result shown in Table 5.1, cyanide in these natural water resources were not measured. Now different concentrations of cyanide ion were added into these natural water samples and the sensor CBTA was employed to recover the concentrations of cyanide. From Table 1, it is concluded that the probe is highly efficient to detect the concentration of cyanide from contaminated water samples with good recovery (97-100.5%). Therefore, this experiment established that our probe CBTA is capable of determining quantitatively cyanide concentration levels in the natural water resources.

Table 5.1: Recovery experiment for various natural water samples using the proposed methods

Source	Sample	CN^- added(mol/lit)	CN^- recovery(mol/lit)	Recovery(%)
Tap water	Tap water 1	0	Not detected	
	Tap water 2	4.00×10^{-4}	$(3.96\pm0.04)\times10^{-4}$	99
	Tap water 3	3.00×10^{-3}	$(2.93\pm0.03)\times10^{-3}$	97
Pond water	Pond water 1	0	Not detected	
	Pond water 2	4.00×10^{-4}	$(3.94\pm0.03)\times10^{-4}$	98.5
	Pond water 3	3.00×10^{-3}	$(2.97\pm0.02)\times10^{-3}$	99
River water	River water 1	0	Not detected	
	River water 2	4.00×10^{-4}	$(4.02\pm0.06)\times10^{-4}$	100.5
	River water 3	3.00×10^{-3}	$(2.94\pm0.04)\times10^{-3}$	98

"Relative standard deviations were calculated based on three times of measurement."

5.4.9. Computational study

In order to interpret the interaction mechanism of the chemodosimeter (CBTA) for the recognition of CN^-, geometry optimization of CBTA and CBTA-CN were performed by DFT/B3LYP/6-31+G(d) method using the Gaussian 09 program. The optimized structures of CBTA and CBTA-CN are displayed in Fig. 5.14. Fig. A5.7 and Fig. A5.8 (Appendix) displayed the contour plots of some selected molecular orbitals including HOMO and LUMO of CBTA and CBTA-CN

respectively. The HOMO-LUMO energy gap of CBTA (2.52 eV) is considerably increased in CBTA-CN^- (3.65 eV) which implies the shifting of high energy band in the adduct thereby correlating the appearance of a new band at shorter wavelength for the CBTA-CN^- adduct which is supported by the changes in UV-visible spectra. In order to obtain insight about the electronic transitions, the time dependent density functional theory (TDDFT) was performed to the optimized geometries of the compounds and summarized in Table A1(Appendix). The low energy transition for CBTA at 491 nm ($\lambda_{expt.}$, 410 nm) corresponds to HOMO → LUMO transition while for CBTA-CN^-, the low energy band shifted to 340 nm ($\lambda_{expt.}$, 353 nm) (Table A5.1, Appendix).

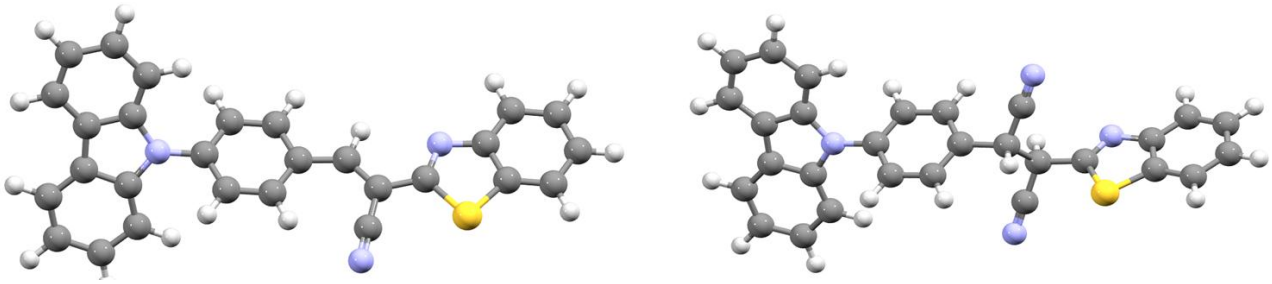

Figure 5.14: Optimized structure of CBTA (left side) and CBTA-CN^- adduct (right side) calculated by DFT/B3LYP/6-31+G(d) method.

5.5. Experimental section

5.5.1. Materials and instrumentations

All the reagents and organic chemicals and solvents used in this synthesis such as 9H-carbazole, 4-fluorobenzaldehyde, 2-aminothiophenol, malononitrile, piperidine, potassium tert-butoxide, dimethyl formamide and ethanol are purchased from Sigma Aldrich and used without further purification. All spectroscopic grade solvents were from other commercial sources and used with no additional refinement. ^1H and ^{13}C NMR spectra were recorded on Brucker 300 MHz instrument and DMSO-d_6 was used as solvent using TMS as an internal standard. The chemical shifts are reported as δ in units of parts per million (ppm). HRMS mass spectra were confirmed on Waters (Xevo G2 Q-TOF) mass spectrometer.Elemental analysis was carried out in a 2400 Series-II CHN analyzer, Perkin Elmer, USA. A Perkin Elmer Lambda 750 spectrophotometer was used to obtain absorbance spectra and emission property was measured using Shimadzu RF-6000 fluorescence

spectrophotometer at room temperature (298 K). Lifetimes were measured using a time-resolved spectrofluorometer from IBH, UK.

5.5.2. UV-Vis and fluorescence method

For UV-Vis titrations, stock solution of the probe, CBTA (10 μM) was prepared in [(DMSO/H_2O), 40:60, *v/v*] (at 25°C) using HEPES buffered solution. Deionized water was used to make all the solutions of guest anions using their sodium salts (1×10^{-5} M) and the solution of cyanide ion using tetra butyl ammonium cyanide salt using HEPES buffer at physiological pH. Solutions of different concentrations of the receptor and all the anions were prepared separately and then the spectra of these solutions were recorded with the help of UV-Vis method. Similarly, for fluorescence titrations, stock solutions were prepared using similar procedures and then the spectra were recorded by means of fluorescence method.

5.5.3. pH solution preparation method

For pH study, stock solution of the probe, CBTA (10 μM) was prepared in [(DMSO/H_2O), 40:60, v/v] (at 25°C) using HEPES buffer solution. The pH is adjusted by using aqueous solution of 1M HCl and 1M NaOH. Solutions of probe and different concentration of acids and bases were prepared separately with adjusting pH and the spectra of these solutions were recorded via fluorescence technique. Similar study was executed while recording the pH titration of probe (CBTA) in presence of CN^-.

5.5.4. Determination of fluorescence Quantum Yields (Φ) of CBTA and its complex with CN^-

The luminescence quantum yield was determined using coumarin-153 as reference dye. The compounds and the reference dye were excited at the similar wavelength and the emission spectra were then studied. The area of the emission spectrum was integrated and the quantum yield is determind according to the following equation:

$$\phi_S/\phi_R = [A_S / A_R] \times [(Abs)_R /(Abs)_S] \times [n_S^2/n_R^2]$$

Here, ϕ_S and ϕ_R are the luminescence quantum yields of the sample and reference dye, respectively. A_S and A_R are the area under the emission spectra of the sample and the reference respectively, $(Abs)_S$ and $(Abs)_R$ are the respective optical densities of the sample and the reference solution at the wavelength of excitation, and n_S and n_R stand for the values of refractive index for the respective solvent used for the sample and reference.

The quantum yields of CBTA and CBTA-CN are determined using the above mentioned equation and the values are found to be 0.205 and 0.015 respectively.

5.5.5. Synthesis of (E)-3-(4-(9H-carbazol-9-yl)phenyl)-2-(benzo[d]thiazol-2-yl)acrylonitrile (CBTA)

4-(9H-carbazol-9-yl)benzaldehyde[72]and 2-(benzo[d]thiazol-2-yl)acetonitrile[73] were synthesized by following the procedure reported previously. 2-(Benzo[d]thiazol-2-yl)acetonitrile (0.09 gm, 0.52 mmol) and piperidine (0.52mmol) were added to the stirred ethanolic solution of 4-(9H-carbazol-9-yl)benzaldehyde (0.141 gm, 0.52 mmol) and the whole mixture was stirred under refluxing condition for 8 hours in inert atmosphere. After completion of the reaction, the reaction mixture is allowed to cool and the yellow precipitation was collected through filtration. The product is purified by column chromatography to get the final product. Yield was, 0.363 g, 85%.

^{1}H NMR (300 MHz, DMSO-d_6): δ(ppm) 8.57 (s, 1H), 8.42 (d, 2H, J=8.5 Hz), 8.22-8.3 (m,3H), 8.13 (d, 1H, J=7.9Hz), 7.93 (d, 2H, J=8.4 Hz), 7.56-7.63 (m, 4H), 7.49 (t, 2H, J=8 Hz), 7.35 (t, 2H, J= 7.4 Hz).

^{13}C NMR (75 MHz, DMSO-d_6): δ(ppm) 49.0, 105.9, 110.4, 116.6, 121.2, 123.0, 123.7, 127.0, 127.7, 131.3, 132.6, 134.8, 139.9, 140.6, 147.6, 153.3, 163.6.

HRMS: calculated for $C_{28}H_{18}N_3S$ $[MH]^+$, (m/z) = 428.1221; found = 428.1207.

5.5.6. Theoretical study

All the calculations were performed with Gaussian 09 program package[74]. Density functional theory (DFT) helped carry out the full geometry optimizations at the B3LYP[75,76] level for the compounds. The calculations were aided by the Gauss View visualization program. All elements

were assigned 6-31+G(d)[77] basis set. The vibrational frequency calculations were executed to assure that the optimized geometries stand for the local minima and there were only positive eigen values. Vertical electronic excitations based on B3LYP optimized geometries were computed using the time-dependent density functional theory (TDDFT) formalism[78-80] in methanol using conductor-like polarizable continum model (CPCM).[81-83]

5.6. Conclusions

In summary, a novel carbazole-based colorimetric and fluorometric sensor (CBTA) has been designed and successfully developed that displayed cyanide selective fluorescence 'ON-OFF' property. The receptor CBTA exhibited highly selectivity, good sensitivity, rapid interaction time (within 22 s) and low LOD (7.68±0.29) $x10^{-8}$ M for CN^- detection in 40% (v/v) DMSO-H_2O mixture which is very much lower than WHO recommended value (1.9 x 10^{-6} M) accompanied the visual color changes from light yellow to colorless over other co-existing competitive anions. The quenching phenomenon of fluorescence intensity of the probe upon addition of CN^- ion was explained to intra-molecular charge transfer (ICT) process which is blocked by the nucleophilic attack of CN^-, resulting in the discontinuance of π-conjugation that causes the observed photophysical changes and the findings were also supported by DFT calculations. Moreover, the excellent test strips response in the solid state helps us to detect CN^- quantitatively without any sophisticated equipment. Therefore, the chemodosimeter CBTA can be served as a promising alternative for the selective recognition of cyanide in mixed DMSO-H_2O medium.

5.7. Notes and references

1. J. M. Holloway, R.A. Dahlgren, B. Hansen and W.H. Casey, *Nature.*, 1998, **395**, 785.
2. D. Cheng, H. H. Ngo, W. Guo, S. W. Chang, D. D. Nguyen, Y. Liu, Q. Wei and D. Wei, *J. Hazard. Mater.*, 2020, **387**, 121682.
3. M. E. Mahmoud, M. F. Amira, S. M. Seleim and A. K. Mohamed, *J. Hazard Mater.*, 2020, **381**, 120979.
4. I. Zwolak, *Biol. Trace Elem. Res.*, 2020, **193**(1), 44-63.
5. B. Zuo, Q. Deng, H. Shao, B. Cao, Y. Fan, W. Li and M. Huang, *ACS Appl. NanoMater.*,2021, **4(2)**, 1831-1840.
6. B. Zuo, W. Li, X. Wu, S. Wang, Q. Deng and M. Huang, *Chem.Aian. J.*, 2020, **15(8)**, 1248-1265.
7. F. Wang, L. Wang, X. Chen and J.Yoon, *Chem. Soc. Rev.*, 2014, **43**, 4312-4324.
8. M. D. Sobsey and S. Bartram, *Forum Nutr.*, 2003, **56**,396-405.
9. D. A. Jones, *Phytochem.*, 1998, **47**, 155-162.

10. M. Zagrobelny, S. Bak and B. L. Moller, *Phytochem.*, 2008, **69**, 1457-1468.
11. D. G. Barceloux,*Dis.Mon.*, 2009, **55**, 336-352.
12. U. A. Patrick, N. Egwuonwn, A. A. Onunkwo, *J. Soil Sci. Environ. Manage.*, 2011, **2**, 49-57.
13. I. F. Bolarinwa, C. Orfila and M. R. Morgan, *Food Chem.*, 2014,**152**, 133-139.
14. L. D. Tivana, J. D. C. Francisco, F. Zelder, B.Bergenstahl and P. Dejmek, *Food Chem.*, 2014, **158**, 20-27.
15. M. T. Wilson, G. Antonini, F. Malatesta, P. Sarti and M. Brunori, *J. Biol. Chem.*, 1994, **269**, 24114-24119.
16. A. V. Gourine, N. Dale, E. Liaudet, D. M. Poputnikov, K.M. Spyer and V.N. Gourine, *J.Physiol.*, 2007, **585**, 305-316.
17. S. H. Park, N. Kwon, J. H. Lee, J. Moon and I. Shin, *Chem. Soc. Rev.*, 2020, **49**, 143-179.
18. X. Lv, J. Liu, Y. Zhao, M. Chen, P. Wang and W. Guo, *Org. Biomol. Chem.*, 2011, **9**, 4954-4958.
19. A. Ishizaki, T. R. Calhoun, G. S. Schlaucohen and G. R. Fleming, *Phys. Chem. Chem. Phys.*, 2010, **12**, 7319-7337.
20. K. Xiong, F. Huo, C. Yin, Y. Yang, J. Chao, Y. Zhang and M. Xu, *Sens. Actuat. B Chem.*, 2015, **220**, 822-828.
21. Z. Liu, X. Wang, Z. Yang and W. He, *J. Org. Chem.*, 2011, **76**, 10286-10290.
22. S. Goswami, S. Paul and A. Manna, *Tetrahedron Lett.*, 2014, **55,** 3946-3949.
23. A. C. Sedgwick, L.Wu, H. H. Han, S. D. Bull, X. P. He, T. D. James, J. L. Sessler, B. Z. Tang, H. Tian and J. Yoon, *Chem. Soc. Rev.*, 2018, **47**, 8842-8880.
24. W. H. Ding, D. Wang, X. L. Zheng, W. J. Ding, J. Q. Zheng, W. H. Mu, W. Cao and L. P. Jin, *Sens. Actua. B Chem.*, 2015, **209**, 359-367.,
25. M. Jamkratoke, V. Ruangpornvisuti, G. Tumcharern, T. Tuntulani and T Tomapatanaget, *J. Org. Chem.*, 2009, **74**, 3919-3922.
26. C. R. Wade and F. P. Gabbai, *Inorg. Chem.*, 2010, **49**, 714-720.
27. Q. Zou, F. Tao, Z. Xu, Y.Ding, Y. Tian and Y. cui, Anal. Methods., 2019, **11**, 5553-5561.
28. H. Wu, M. Chen, Q. Xu, Y. Zhang, P.Liu, W. Li and S. Fan, *Chem. Commun.*, 2019, **55**, 15137-15140.
29. K. Vongnam, K. Chansaenpak, M. Sukwattanasinitt, P. Rashatasakhon, ChemistrySelect., 2020, **5**, 4303-4306.
30. R. Dalapati, S. Nandi, S. Biswas, *Dalton Trans.*, 2020, **49**, 8684-8692.
31. D. Tamilarasan, R. Suhasini, V. Thiagaranjan and R.Balamurugan, *Eur. J. Org. Chem.*, 2020, **2020**, 993-1000.
32. H. Fang, W. J. Qu, H. H. Yang, J. X. He, H. Yao, Q. Lin, T. B. Wei and Y. M. Zhang, *Dyes Pigm.*, 2020, **174**, 108066.
33. G. Sun, W. Chen, Y. Liu, X. Jin, Z. Zhang and J. Su, *Dyes Pigm.*, 2020, **176**, 108224.
34. A. Popczyk, Y. Cheret, A. El-Ghayoury, B. Sahraoui and J. Mysliwiec, *Dyes. Pigm.*, 2020, **177**, 108300.
35. L. Hou, F. Li, J. Guo, X. Zhang, X. Kong, X. T. Cui, C. Dong, Y. Wang and S. Shuang, *J. Mater. Chem. B.*, 2019, **7**, 4620-4629.

36. X. Zhao, Y. Sun, Y. Zhu, H. Chen, Z. Wang, S. Zhao, D. Cao and G. Liu, *J. Photochem. Photobiol. A Chem.*, 2018, **367**, 83-88.
37. A. Ozdemir and S. Erdemir, *J. Photochem. Photobiol. A Chem.*, 2020, **390**, 112328.
38. T. S. Reddy and M.S. Choi, *J. Photochem. Photobiol. A Chem.*, 2018, **351,** 108-114.
39. J. Mei, N. L. C. Leung, R. T. K. Kwok, J. W. Y. Lam and B. Z. Tang, *Chem.Rev.*, 2015, **115**, 11718-11940.
40. Y. Hong, J.W.Y. Lam and B. Z. Tang, *Chem. Soc. Rev.*, 2011, **40**, 5361.
41. H. T. Feng, Y. X. Yuan, J. B. Xiong, Y. S. Zheng and B. Z. Tang, *Chem. Soc. Rev.*, 2018, **47**, 7452-7476.
42. N. Zhao, C. Ma, W. Yang, W. Yin, J. Wei and N. Li,*Chem. Commun.*, 2019, **55**, 8494-8497.
43. X. Wei, M. Zhu, H. Yan, C. Lu and J. Xu, *Chem. Eur. J.*, 2019 ,**25,** 12671-12683.
44. G. Jin, R. He, Q. Liu, M. Lin, Y. Dong, K. Li, B. Z. Tang, B. Liu and F. Xu, Theranostics., 2019, **9**, 246-264.
45. Y. Li, K. Xu, Y. Si, C. Yang, Q. Peng, J. He, Q. Hu and K. Li, Dyes Pigm., 2019, **171**, 107682.
46. J. Shi, Q. Deng, C. Wan, M. Zheng, F. Huang and B. Tang, *Chem. Sci.*, 2017, **8**, 6188-6195.
47. M. H. Chua, K. W. Shah, H. Zhou and J. Xu, *Molecules.*, 2019, **24**(15), 2711.
48. T. Ghosh, S. Mitra, S. K. Maity and D. K. Maiti, *Nano Mater.*, 2020, **3(4),** 3951-9.
49. K. Santhiya, S. K. Sen and R. Natarajan, *Dyes Pigms.*, 2021, **185**, 108891.
50. Y. Wang, H. Liu, Z. Chen and S. Pu, *Spectrochim. Acta A.*, 2021, **245**, 118928.
51. Y. Liu, A. Qin and B. Z. Tang, *Prog. Polym. Sci*., 2018, **78**, 92.
52. S. Bozkurt and E. Halay, *Tetrahedron.*, 2020, **76**, 131647.
53. E. Keles, B. Aydınerand Z. Seferoğlu, Curr. Org. Chem., 2023, **20**, 61.
54. D. Jothi, S. Munusamy, S. M. kumar, S. Enbanathan and S. K. Iyer, RSC Adv., 2022, **12**, 8570.
55. A. Tigreros and J. Portilla, Eur. J. Org. Chem. 2022, e202200249.
56. X. Yang, X. Chen and X. Lu, *J. Mater. Chem. C.*, 2016, **4**, 383-390.
57. H. Tavallali, G. Deilamy-Rad, A. Parhami and S. Kiyani, *Spectrochim. Acta A.*, 2014, **121**, 139-146.
58. T. D. Ashton, K. A. Jolliffe and F. M. Pfeffer, *Chem. Soc. Rev.*, **44**, 4547-4595.
59. N. H. Evans and P. D. Beer, *Angew. Chem. Int. Ed.*, 2014, **53,** 11716-11754.
60. A. Liu, R. Ji and S.L.Shen, *New. J. Chem.*, 2017, **41**, 10096-10100.
61. Y. Feng, S. Li and D. Li, *Sens. Actuat. B Chem.*, 2017, **254**, 282-290.
62. Y. Ge, P. Wei and T. Wang, *Sens. Actuat. B Chem.*, 2018, **254**, 314-320.
63. Y. Wang, W. Shu and B. Han, *New. J. Chem.*, 2017, **41**, 9262-9267.
64. X. Chen, L. Wang, X. Yang and L. Tang, *Sens. Actuat. B Chem.*, 2017, **241**, 1043-1049.
65. W. C. Lin and J. W. Hu, Anal. Chim. Acta., 2015, **893**, 91-100.
66. S. OğuzTümay, A. Şenocak and A. Mermer, *New J. Chem.*, 2021, **45**, 18400-18411.
67. S. Cheng, A. Li, X. Pan, H. Wang, C. Zhang, J. Li and X. Qi, *Anal. Bioanal. Chem.*, 2021, **413**, 4441-4450.
68. X. Pan, S. Cheng, C. Zhang and X. Qi, *Anal. Bioanal., Chem.*, 2020, **412**, 6959-6968.
69. J. Li, X. Qi, W. Wei, Y. Liu, X. Xu, Q. Lin and W. Dong, *Sens. Actuat. B Chem.*, 2015, **220**, 986-991.
70. L. Li, T. Yang, J. yang and X. Zhang, *Sens. Actuat. B Chem*., 2022, **353**, 131038

71. R. Bhaskar and S. Sarveswari, Inorg. *Chem. Commun*., 2019, **102**, 83-89
72. B. Patil, J. Lade, S. Chiou, Y. Cheng, Y. Lin, Y. Jadhav, P. Chetti, C. Chang and A. Chaskar, *Org. Electron*., 2021, **92**, 106090.
73. L. Patra, K. Aich, S. Gharami and T. K. Mondal, *J. Lumin*., 2018, **201**, 419-426.
74. Gaussian 09, Revision D.01, M. J. Frisch, G. W. Trucks, H. B. Schlegel, G. E. Scuseria, M. A. Robb, J. R. Cheeseman, G. Scalmani, V. Barone, B. Mennucci, G. A. Petersson, H. Nakatsuji, M. Caricato, X. Li, H. P. Hratchian, A. F. Izmaylov, J. Bloino, G. Zheng, J. L. Sonnenberg, M. Hada, M. Ehara, K. Toyota, R. Fukuda, J. Hasegawa, M. Ishida, T. Nakajima, Y. Honda, O. Kitao, H. Nakai, T. Vreven, J. A. Montgomery, Jr., J. E. Peralta, F. Ogliaro, M. Bearpark, J. J. Heyd, E. Brothers, K. N. Kudin, V. N. Staroverov, R. Kobayashi, J. Normand, K. Raghavachari, A. Rendell, J. C. Burant, S. S. Iyengar, J. Tomasi, M. Cossi, N. Rega, J. M. Millam, M. Klene, J. E. Knox, J. B. Cross, V. Bakken, C. Adamo, J. Jaramillo, R. Gomperts, R. E. Stratmann, O. Yazyev, A. J. Austin, R. Cammi, C. Pomelli, J. W. Ochterski, R. L. Martin, K. Morokuma, V. G. Zakrzewski, G. A. Voth, P. Salvador, J. J. Dannenberg, S. Dapprich, A. D. Daniels, Ö. Farkas, J. B. Foresman, J. V. Ortiz, J. Cioslowski and D. J. Fox, Gaussian, Inc., Wallingford CT, 2009.
75. A. D. Becke, *J. Chem. Phys.*, 1993, **98**, 5648.
76. C. Lee, W. Yang and R. G. Parr, *Phys. Rev. B.*, 1988, **37**, 785.
77. F. Furche and R. Ahlrichs, *J. Chem. Phys.*, 2002, **117**, 7433.
78. R. Bauernschmitt and R. Ahlrichs, *Chem. Phys. Lett.*,1996, **256**, 454.
79. R. E. Stratmann, G. E. Scuseria and M. J. Frisch, *J. Chem. Phys.*,1998, **109**, 8218.
80. M. E. Casida, C. Jamorski, K. C. Casida and D. R. Salahub, *J. Chem. Phys.*,1998, **108**, 4439.
81. V. Barone and M. Cossi, *J. Phys. Chem. A.*, 1998, **102**, 1995.
82. M. Cossi and V. Barone, *J. Chem. Phys.*, 2001, **115,** 4708.
83. M. Cossi, N. Rega, G. Scalmani and V. Barone, *J. Comput. Chem.*, 2003, **24**, 669.

APPENDIX

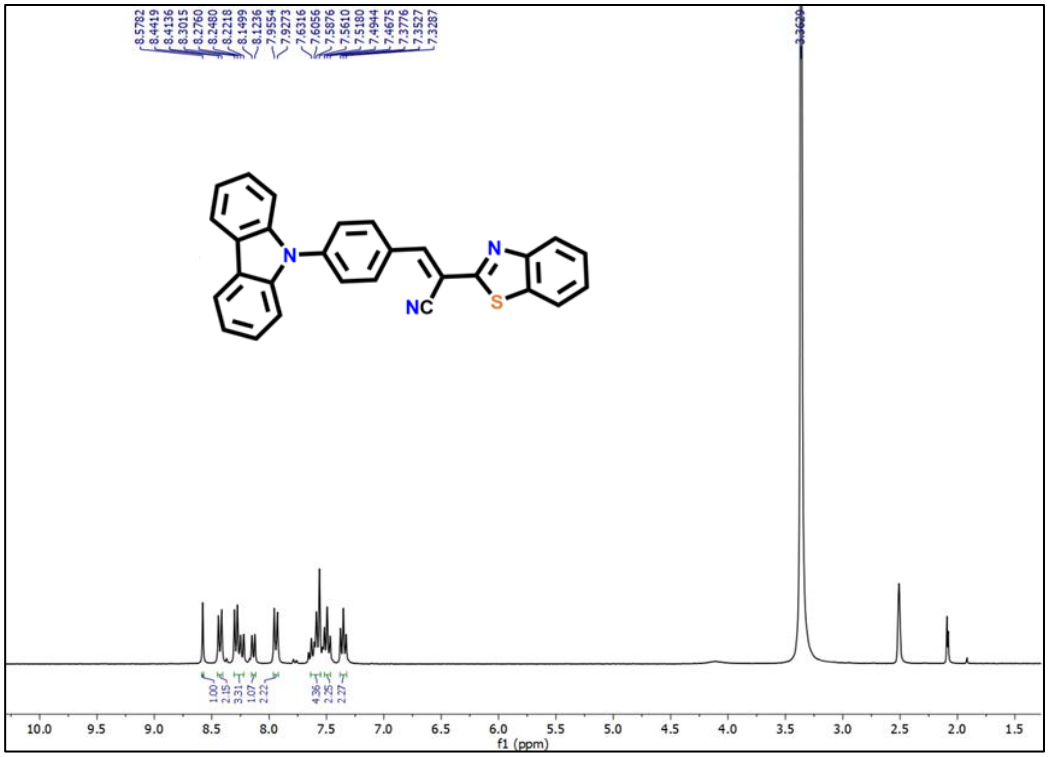

Fig. A5.1: ^{1}H NMR (300 MHz) spectrum of the probe (CBTA) in DMSO-d6

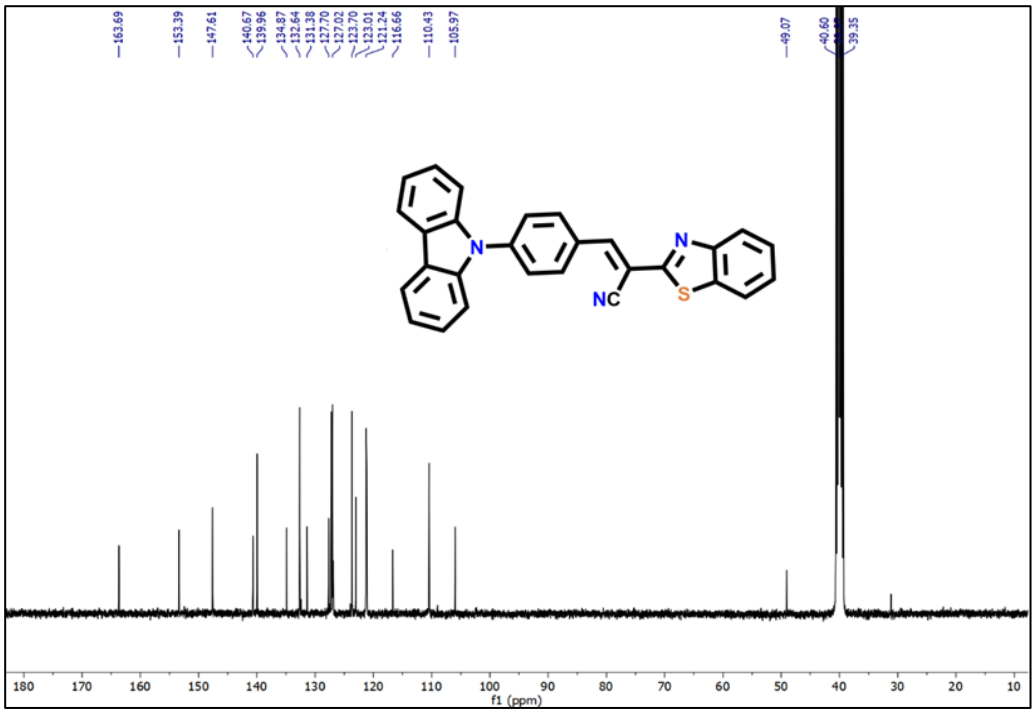

Fig. A5.2: ^{13}C NMR (75 MHz) spectrum of the receptor (CBTA) in DMSO-d_6

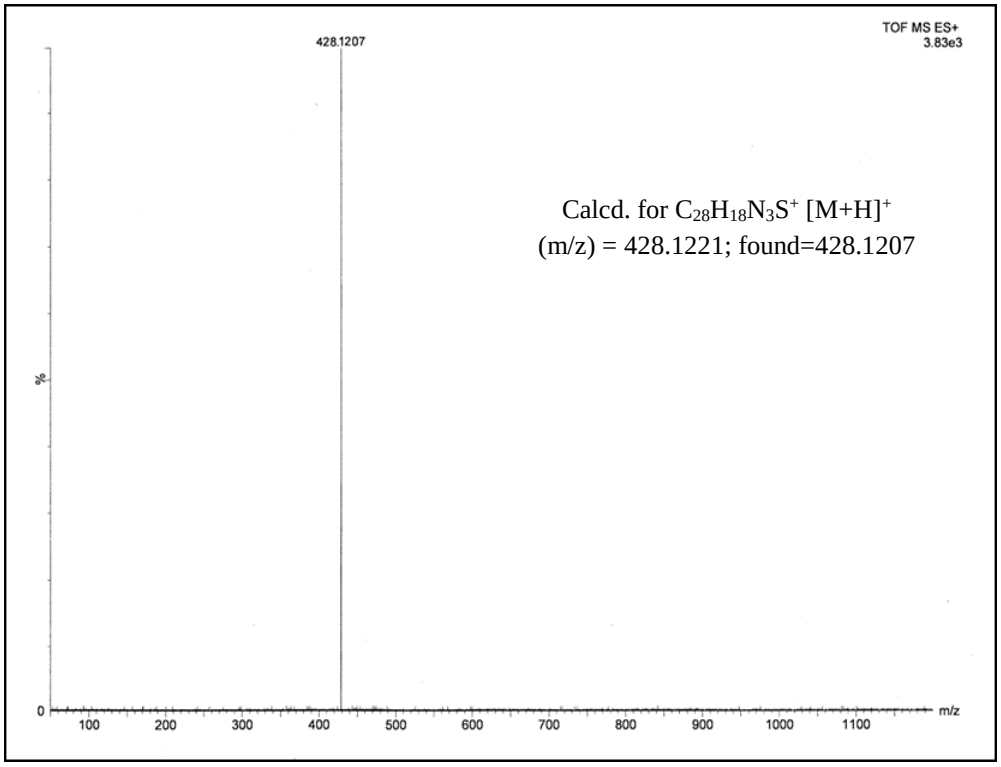

Fig. A5.3: HRMS of the receptor (CBTA)

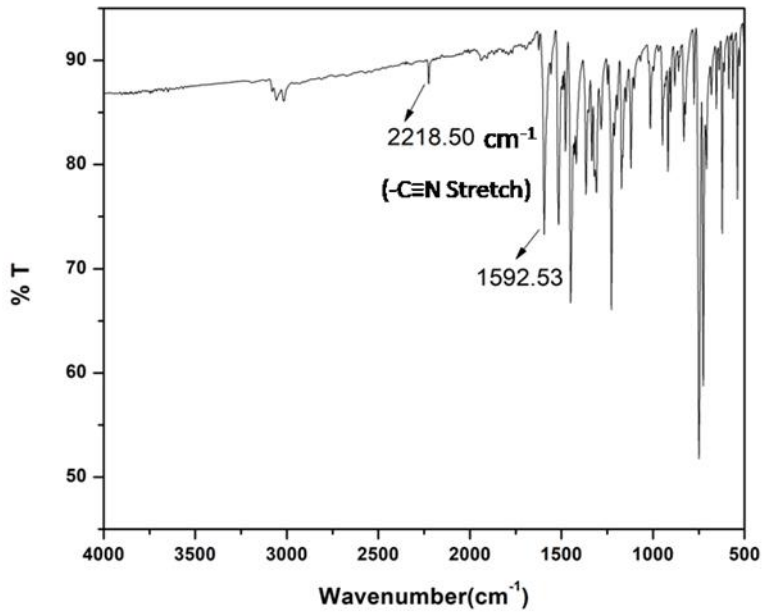

Fig. A5.4: IR Spectrum of CBTA

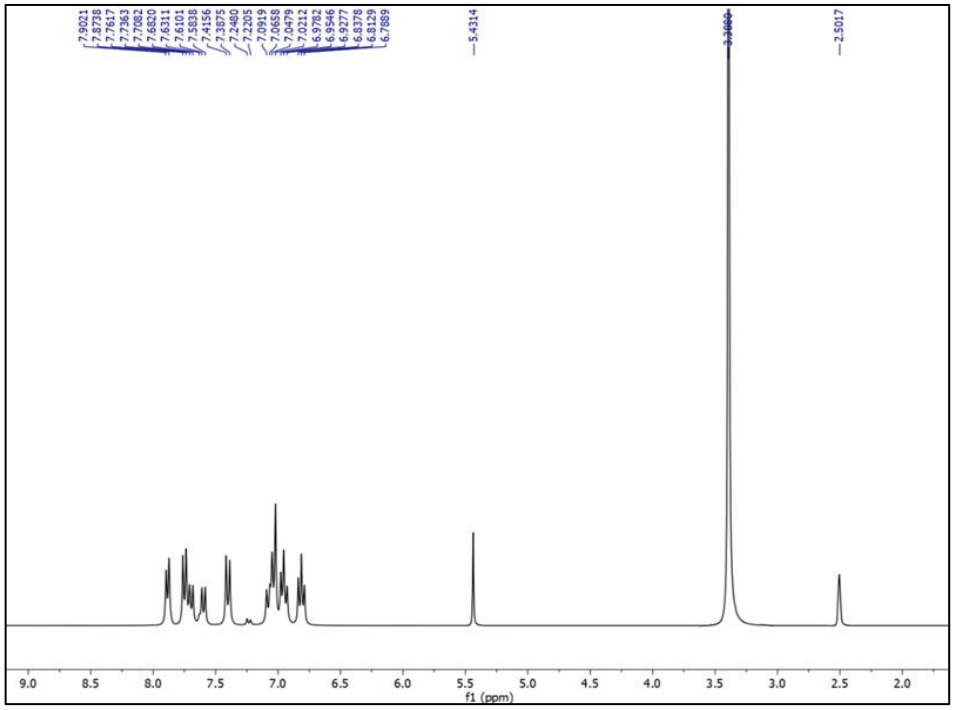

Fig. A5.5: ^{1}H NMR (300 MHz) spectra of the CBTA-CN^{-} adduct in DMSO-d_6.

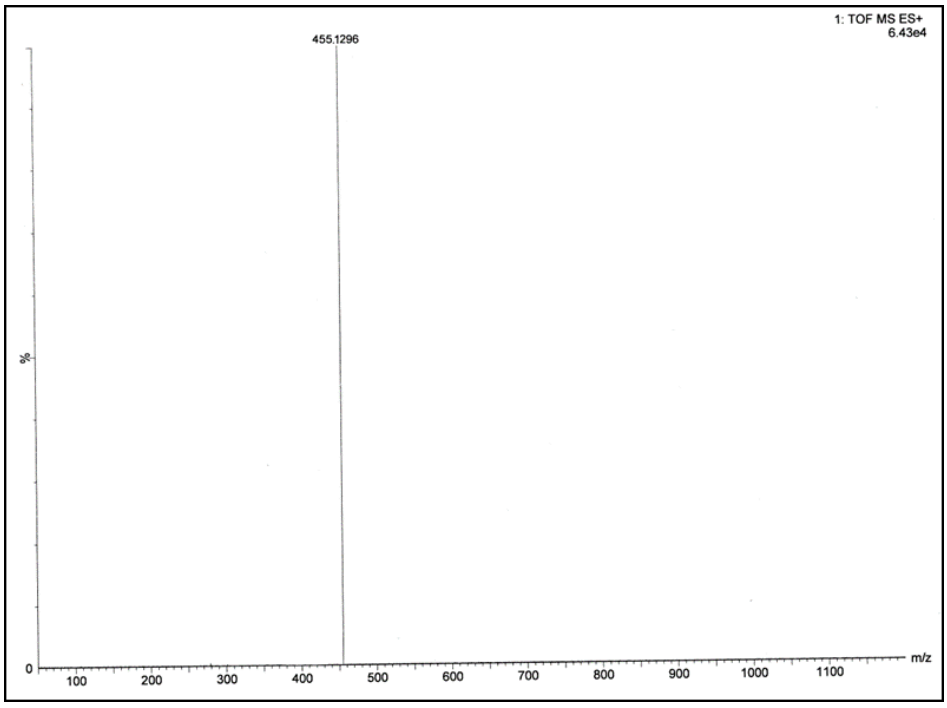

Fig. A5.6: HRMS of the CBTA-CN^{-} adduct.

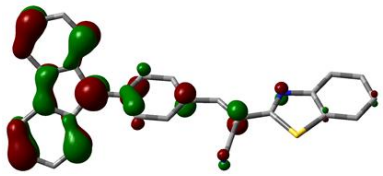

HOMO (E = -5.55 eV)

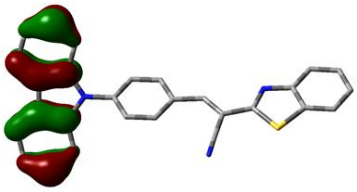

HOMO-1 (E= -5.97eV)

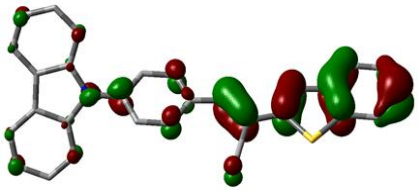

HOMO-2 (E= -6.24eV)

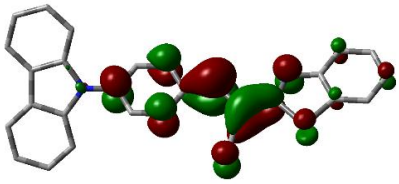

LUMO (E = -2.61eV)

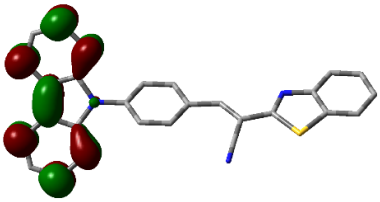

LUMO+1 (E= -0.9 eV)

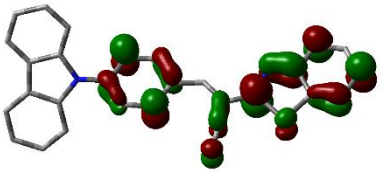

LUMO+2 (E= -0.75 eV)

Fig. A5.7: Contour plots of some selected molecular orbitals of CBTA.

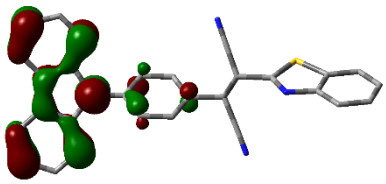

HOMO (E= -5.53 eV)

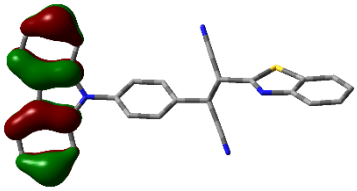

HOMO-1 (E= -5.87eV)

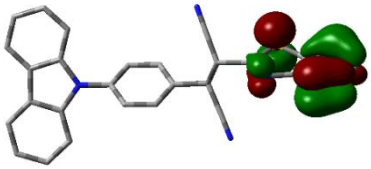

HOMO-2 (E= -6.79 eV)

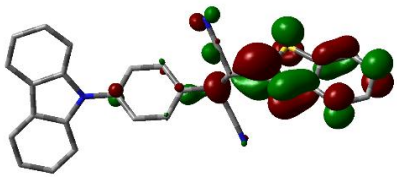

LUMO (E= -1.64 eV)

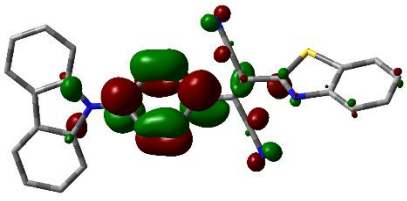

LUMO+1 (E= -1.02eV)

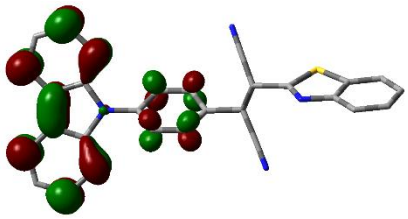

LUMO+2 (E= -0.8 eV)

Fig. A5.8: Contour plots of some selected molecular orbitals of CBTA-CN^-

Table A5.1. Vertical electronic transitions of CBTA and CBTA-CN^- calculated by TDDFT/CPCM method

Compd.	λ (nm)	E (eV)	Osc. Strength (f)	Key excitations
CBTA	491.45	2.5228	0.7330	(99%)HOMO→LUMO
	377.35	3.2857	0.5544	(97%)HOMO-2→LUMO
	293.33	4.2268	0.2105	(85%)HOMO-6→LUMO
	359.31	3.4506	0.0842	(97%)HOMO-3→LUMO
	272.04	4.5576	0.1642	(72%)HOMO-1→LUMO+1
	242.34	5.1161	0.6343	(62%)HOMO→LUMO+6
	231.79	5.3491	0.1404	(41%)HOMO-4→LUMO+1 (35%)HOMO-1→ LUMO+7
CBTA-CN^-	340.06	3.6459	0.1186	(95%)HOMO → LUMO
	308.11	4.0241	0.1946	(51%)HOMO → LUMO+2 (41%) HOMO→LUMO+1
	260.43	4.7608	0.4729	(84%)HOMO-3 → LUMO
	243.46	5.0926	0.1665	(63%)HOMO-4 → LUMO
	240.62	5.1528	0.4896	(27%)HOMO-4 → LUMO (46%)HOMO → LUMO-7
	214.97	5.7675	0.1842	(26%)HOMO-5→ LUMO+1 (19%)HOMO-3 → LUMO+3 (25%)HOMO→ LUMO+10

Table A5.2: Determination of quantum yield (φ) of sensor CBTA at different water fraction (f_w)

Sensor	**DMSO:$H_2$0 (v/v)**	**Water fraction(f_w)**	**Quantum Yields(φ)**
CBTA	100:0	0%	0.07
	60:40	40%	0.081
	50:50	50%	0.146
	40:60	60%	0.205
	30:70	70%	0.184
	20:80	80%	0.131
	10:90	90%	0.082

Table A5.3: Fluorescence lifetime data

DMSO(Solvent)	Quantum yield(φ)	τ(ns)	$K_r(10^8 \times S^{-1})$	$K_{nr}(10^8 \times S^{-1}$
CBTA	0.205	6.1	0.336	1.303
CBTA-CN^-	0.015	1.38	0.1086	7.137

Table A5.4: Sensor CBTA towards CN^- compared to others previously reported receptors

Probe	Solvent System	Detection limit	Reaction time	Reference
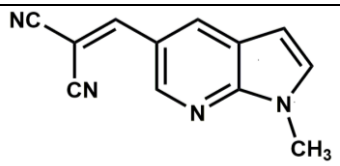	THF/H_2O(9:1)	2×10^{-6} M		[1]
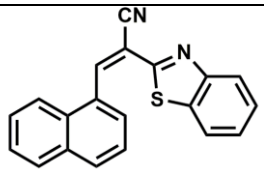	DMF	0.07 µM		[2]
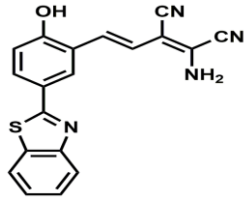	DMSO/H_2O (7:3)	1.4×10^{-7} M		[3]
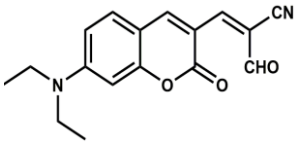	CH_3CN	0.328µM		[4]
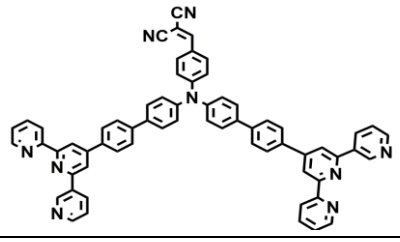	H_2O/THF(9:1)	3.83×10^{-6} M		[5]
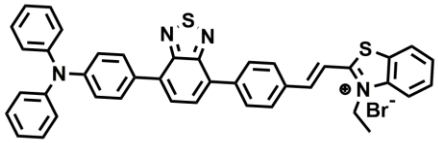	H_2O/THF(8:2)	1.3×10^{-7} M		[6]
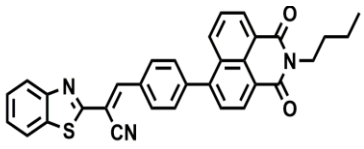	THF	0.034 µM		[7]

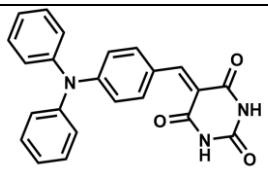	DMSO/H_2O (1:99**)**	2.95×10^{-8} M		[8]
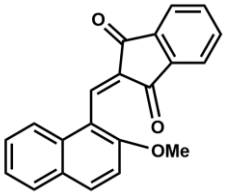	H_2O-DMF (9:1,v/v)	1.15-1.2 nM	10-30 sec	[9]
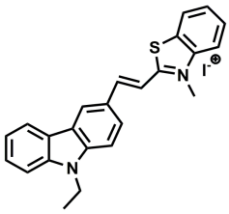	DMSO	0.94 μM		[10]
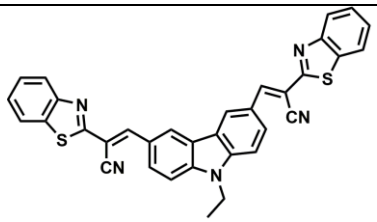	DMSO-H_2O (4/1,v/v)	3.75 nM	9-10 min	[11]
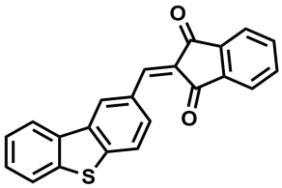	DMSO/H_2O (1:99,v/v)	2.26×10^{-7}M	15 sec	[12]
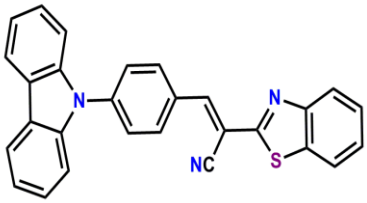	DMSO/H_2O (40:60,v/v)	7.68×10^{-8} M	22 sec	**This work**

References

1. K. Y. Chen and W. C. Lin, *Dyes Pigm.*, 2015, **123**, 1-7.
2. K. W. Kulig, Cyanide Toxicity, U.S. Department of Health and Human Services, Atlanta GA, 1991.
3. S. Malkondu, S. Erdemirand, S.Karakurt, *Dyes Pigm.*, 2020, **174**, 108019.
4. L. Yuan, W. Lin, Y. Yang, J. Song and J. Wang, *Org. Lett.*, 2011, **13,** 3730-3733.
5. Y. Li, Z. Gu, T. He, X. Yuan, Y. Zhang, Z. Xu, H. Qiu, Q. Zhang and S. Yin, *Dyes Pigm.*, 2020, **173**, 107969.
6. B. Zhai, Z. Hu, C. Peng, B. Liu, W. Li and C. Gao, *Spectrochim. Acta A.*, 2020, **224,** 117409.
7. T. S. Reddy, H. Moon and M. S. Choi, *Spectrochim Acta A.*,2021, **252**, 119535.
8. B. Zuo, L. Liu, X. Feng, D. Li, W. Li, M. Li, M. Huang and Q. Deng, *Dyes Pigm.*, 2021, **193**, 109534
9. N. Maurya and A. K. Singh, *Sens. and Actuat. B Chem.*, 2017, **245**, 74–80.
10. J. Chao, Z. Li, Y. Zhang, F. Huo, C. Yin, Y. Liu, Y. Li and J. Wang, *J. Mater. Chem.B.*, 2016, **4**, 3703-3712.
11. L. Patra, K. Aich, S. Gharami and T. K. Mondal, *J. Lumin.*, 2018, **201**, 419-426
12. Q. Zou, J. Du, C. Gu, D. Zhang, F. Tao and Y. Cui, *J. Photochem. Photobiol.A.Chem.*, 2021, **405**, 112993

Efficient solid and solution state emissive reusable solvatochromic fluorophore for colorimetric and fluorometric detection of CN^-

Efficient solid and solution state emissive reusable solvatochromic fluorophore for colorimetric and fluorometric detection of CN^-

Abstract

A novel organic receptor CPI [(E)-3-(4-(9H-carbazol-9-yl)phenyl)-2-(1H-benzo[d]imidazol-2-yl)acrylonitrile] was rationally designed and successfully fabricated for selective and sole recognition of CN^- ion over others competitive anions through an obvious chromogenic and ratiometric emission change in DMSO.The distinct and prominent color change upond addition of CN^- can be attributed to the typical ICT process, which is induced due to the deprotonation of acidic-NH proton in imidazole moiety. The sensor displayed strong solvatochromic effect in commonly used organic solvents such as n-hexane, toluene, diethyl ether, DCM, THF, DMF and DMSO. The chemical structure of the sensor has been characterized by single crystal X-ray diffraction, ^{1}HNMR, ^{13}CNMR, IR and mass spectroscopy. Significantly, the probe can function as a fluorescence based sensor for the efficient detection of low-level water in organic solvents. The solid state emission propertiesof CPI was successfully applied to recognise cyanidein solid state platform with naked eye visualized distinct color change. The probe can be made reusable by adding TFA into the CN^- treated probe solution. The detection limit of CPI towards CN^- was determined to be 4.48 $\times 10^{-8}$ M. More importantly, the sensor is capable for detecting CN^- in food samples and has been employed for wastewater treatment. Besides,the easy-to-prepare CPI-coated test strips provide a simple, reusable and easy-to-handy protocol for qualitative identification of CN^- conveniently. Finally, density functional theory and time-dependent density functional theory were performed to verify the experimental outcomes theoretically.

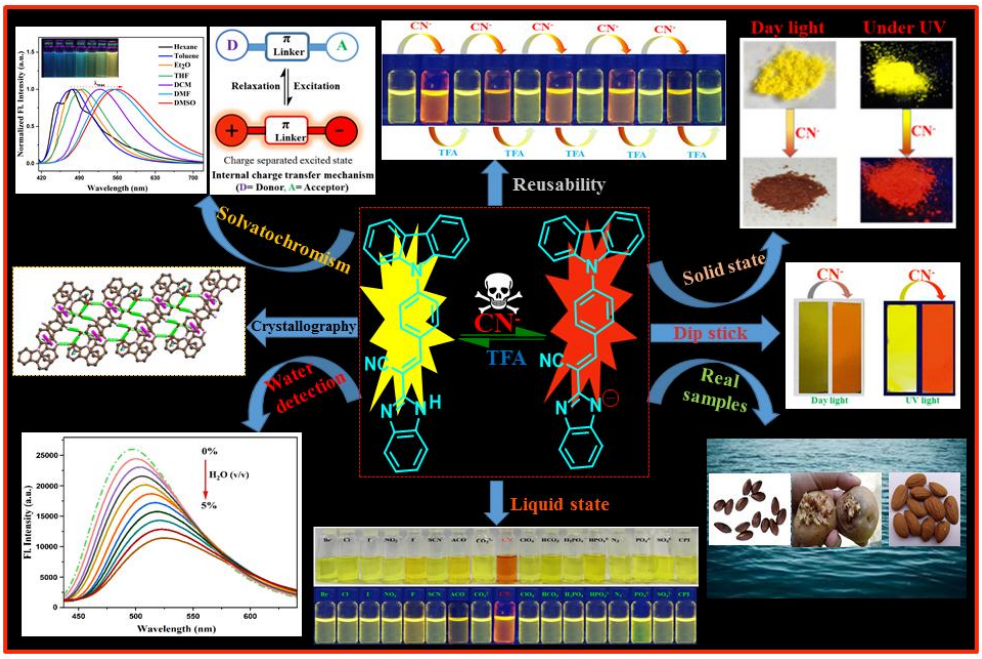

6.1. Introduction

Many researchers have paid attention to the development of anionic chemosensors recently due to its broad application in many fields including chemical, biology, medicine and technological proceses.[1-6] Among various anions, cyanide ion is one of the deadliest poisonous anion towards human being. Even trace amount of CN^- ion can affect human health in many ways and it may lead to several health risks because of its excellent binding affinity towards Fe^{3+} ion in cytochrome c oxidase, eventually leading to the incapability to produce ATP in cells which subsequently results in respiratory arrest and death ultimately.[7-10] Some insects and food samples like sprouting potatoes, bitter almonds, apple seeds as well as cassava contain cyanide and it reaches to the environment through the hydrolysis process of cyanogenic glycosides.[11-14] Despite of its toxicity, due to critical role of cyanide in multi-functional reaction,[15] cyanide has been being extensively used in many industrial production like petrochemicals, electroplating, steel production, photography, metallurgy, gold mining, synthesis of resign, fibre etc. Therefore, water pollution and food safety issues by toxic cyanide cause a massive threat to human health and environment nowadays.[16-18] The maximum intake of CN^- ion as per guideline approved by WHO and USEPA, is 1.9 µM (200 µg/L).[19] In view of its vital role in industries and toxicity, the development of new method to monitor trace amount of CN^- ion in biological and environmental sample is one of the most sensitive hotspots among researchers. In the last few decades, numerous type of chemosensors based on co-ordination,[20-22] sonogashira cross-coupling,[23-25] nucleophilic addition reaction,[26,27] hydrogen-bonding interactions[28,29] and many other mechanisms have been reported for sole detection of poisonous cyanide. However, these methods have many limitations such as complicated synthetic steps, poor sensitivity and selectivity, using of sophisticated instruments, irreversible functionality, high temperature or long reaction time for identification of cyanide ion. Furthermore, colorimetric and fluoremetric techniques possess numerous benefits such as high sensitivity, low-cost, easy operation and visual color change. Therefore, fabrication of simple, low-cost and high efficiency chromogenic and fluorogenic chemosensors for recognising CN^- ion in ppm and ppb levels are greatly needed in the modern analytical world. Solvatochromism, which is the characteristic ability of a chemical substance like ionic liquids,[39] fluorescent dyes,[40] MOFs,[41] hybrid materials[42] to change color by varying solvent polarity and widely used in many biological

and chemical research fields[43] to explore bulk and local polarity in macro system like biological membranes or the conformation and binding sides of proteins. For instance, water as the common impurity in organic solvent can decrease the reactivityof organometallic compounds and hinder many reactions in chemical and industrial processes and hence lower the yields. Thus detection as well as control of low-level water in organic solvents has drawn much attention in recent years. In past, several techniques have been proposed for sensitive detection of water including proton transfer,[47] intramolecular charge transfer(ICT),[48] water-triggered reaction of the Schiff base,[49] photo-induced electron transfer,[50] water-induced inter-polymer π-stacking aggregation,[51] etc. Fluorescence based water sensors have been widely fabricated and applied owing to their reasonable selectivity and sensitivity. More interestingly, solid state emitting property of fluorophores has drawn much attention[52-54] for their widespread application in organic solid state lasers,[55] organic light emitting diodes,[56,57] fluorescent sensors,[58,59] flat panel displays[60] etc.

6.2. Prior works

Usually, the anionic chemosensors should possess more reactive functional group containing acidic hydrogen, for examples, urea, imidazole, thiourea, hydrazine, amides, pyrrole, phenols, oximes, indoles and hydrazones and they should be employed as an interaction site for sensing of anions through deprotonation mechanism.[30-38] Presently, solvatochromic dyes are extensively used as optical sensors in the field of molecular sensor. For example, Yi et al. introduced a new terpyridyl-based naphthalimide derivatives for DMSO solvent.[44] Kim et al. prepared a solvatochromic dye based on polydiacetylene (PDA) for TFA sensor.[45] On the other hand, Zhang et al. reported a cyanostilbene derivative dye for water.[46] Therefore, the development of solvatochromic dye is highly challenging and impressive work in chemosensor chemistry. Although several fluorescence dyes have been reported, but the reports for water determination are still quite limited. Hence, development of simple and easy-to-fabricate fluorescence dye with excellent detection capability to monitor trace-level water in organic solvent is highly desired nowadays. To our best knowledge, several chemosensors have been reported to monitor cyanide ion which are based on deprotonation mechanism, but majority of them have some abridgements, for example, lack of solvatochromism or they are limited only in colorimetric response and incapable of solid state sensing or else they could not be functioned in reversible way etc.

6.3. Present work

Taking these above factors into account, we have successfully introduced a simple and easy-to-make D-π-A type carbazole-benzimidazole based solid state emitting solvatochromic fluorophore for chromogenic and fluorogenic recognition of poisonous cyanide against other competitive anions. In presence of CN^- ion, our synthesized probe has found to undergo deprotonation of –NH fragment and consequently accumulated electron density on the imidazole moiety which as a result led to both absorption and ratiometric fluorescence change. The distinct and prominent color change upon addition of CN^- in both liquid and solid state can be distinguished by naked eyes. The other coexisting competitive anions had no significant impact in the CN^- ion identification response and hence the present probe (CPI) can solely detect CN^- ion very sensitively.

6.4. Results and discussions

6.4.1. Synthesis of CPI

The sensor, CPI was synthesized via a simple one step condensation reaction between compound 1 and compound 2 (scheme 6.1). The chemical structure of CPI was characterized by ^{1}H-NMR, ^{13}C-NMR, IR spectroscopy and ESI mass spectrometry (Fig. A6.1-A6.4, Appendix).

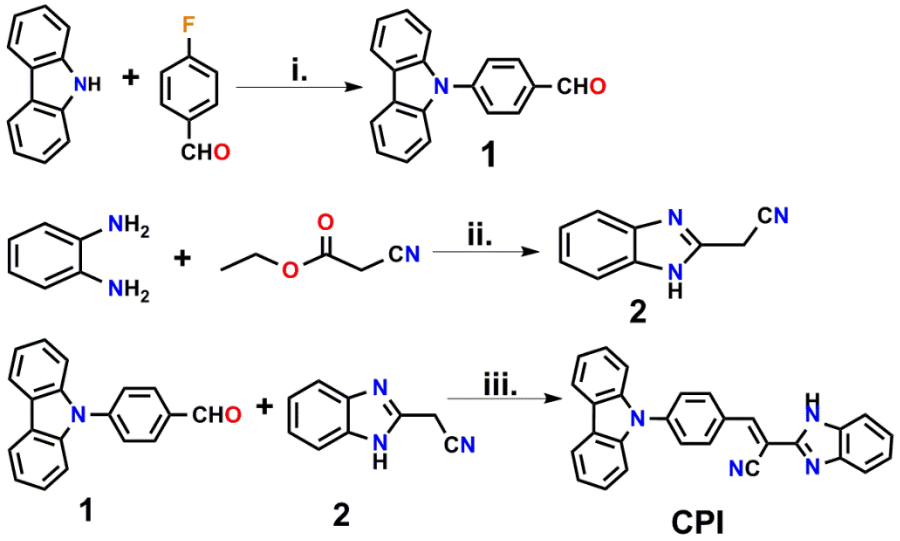

Scheme 6.1: Synthetic route of the probe, CPI (i) KOtBu, DMF, 100^{0}C,12 h; (ii I_2, 180-200 ^{0}C, reflux for 2 hr; (iii) EtOH, Piperidine,reflux, 7hr.

6.4.2. Crystal Structure

Crystal structure of CPI was determined by single crystal X-ray diffraction method. Single crystals of CPI were grown by slow evaporation methanol solvent. CPI was crystallized in the orthorhombic crystal system with *Pbca* space group. Detailed crystallographic data and X-ray bond parameters are summarized in electronic supplementary information (Tables A6.1 and Table A6.2). The ORTEP diagram with numbering scheme is depicted in Fig. 6.1.

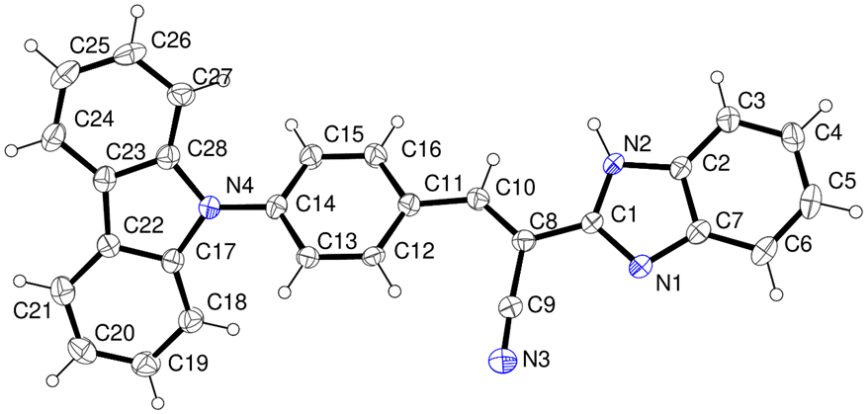

Figure. 6.1: ORTEP plot of the organic probe CPI with 35% ellipsoidal probability (selected bond distances (Å): N1-C1, 1.364(4); N1-C7, 1.383(4); N2-C1, 1.312(4); N2-C2, 1.386(4); N3-C9, 1.140(5) and C8-C9, 1.434(5).

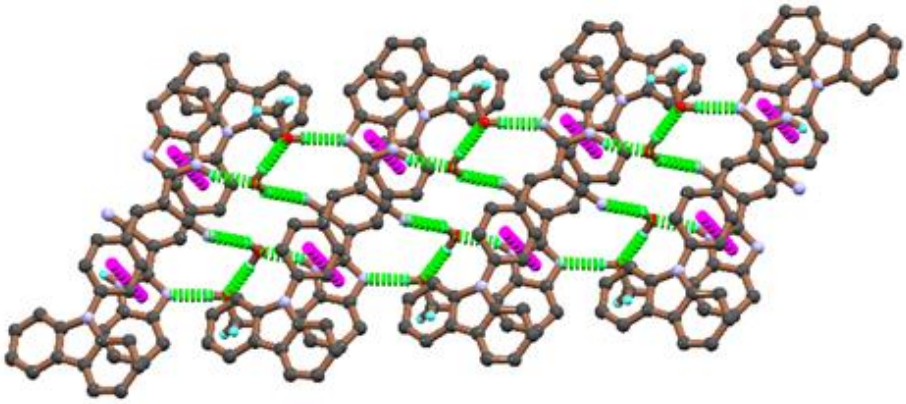

Figure 6.2: 1D supramolecular structure formed by H-bonding between N1-H1…O1, O1-H1A…O2 and O2-H2…N2 (●●●) and π–π interactions between the imidazole unit with the phenyl ring of adjacent molecule (●●●).

Crystal of CPI forms 1D supramolecular architecture via intermolecular H-bonds through methanol and water molecules. In addition, the crystal packing is stabilized by π–π interactions between the imidazole ring with the phenyl ring of adjacent molecule (Fig. 6.2). Strong H-bonding interactions are found to be between N1-H1…O1, O1-H1A…O2 and O2-H2…N2 with H…A(acceptor) distances of 1.95(4) Å, 1.93 Å and 1.94 Å respectively.

6.4.3. Solvatochromic behaviour of CPI

As the investigated sensor comprised of an electron donating unit(D) and an electron-accepting(A) moiety, so it represents a typical D-π-A organic framework (Fig. 6.3). The solvatochromic effect of this type of compound can be attributed to the intra-molecular charge transfer process between donor and acceptor units, which promotes dipole-dipole interaction between the dye and the surrounding solvent molecules and also reduces the excited state energy thereby leading the solvent relaxation. In order to execute the solvatochromic effect of CPI, UV-Vis absorption and emission properties of CPI were monitored in the different solvents (hexane, toluene, diethyl ether, tetrahydrofuran, dichloromethane, dimethylformamide and dimethylsulfoxide) of broad range of dielectric constant and the photophysical outcomes were summarized in Fig. 6.4 and Table 6.1.

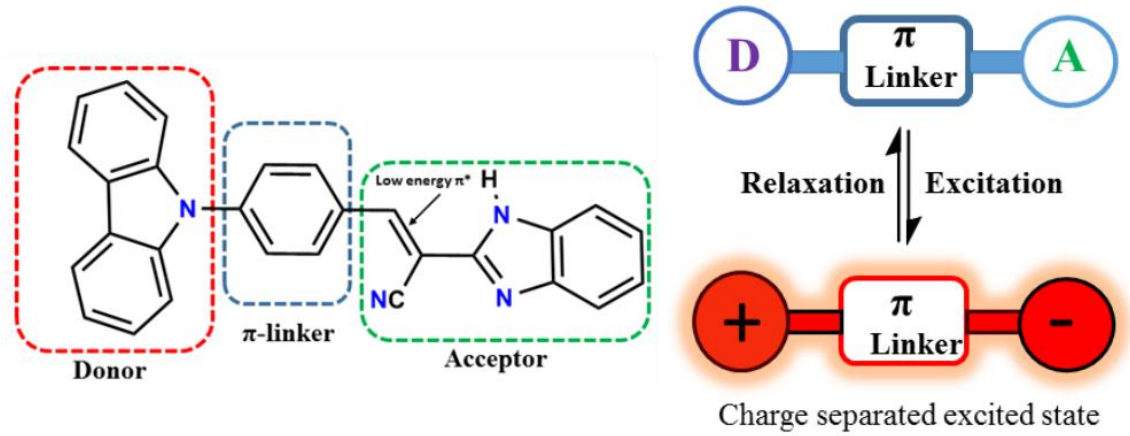

Figure 6.3: Donor-π-Acceptor framework (left side) and intermolecular charge transfer mechanism of the probe CPI (right side).

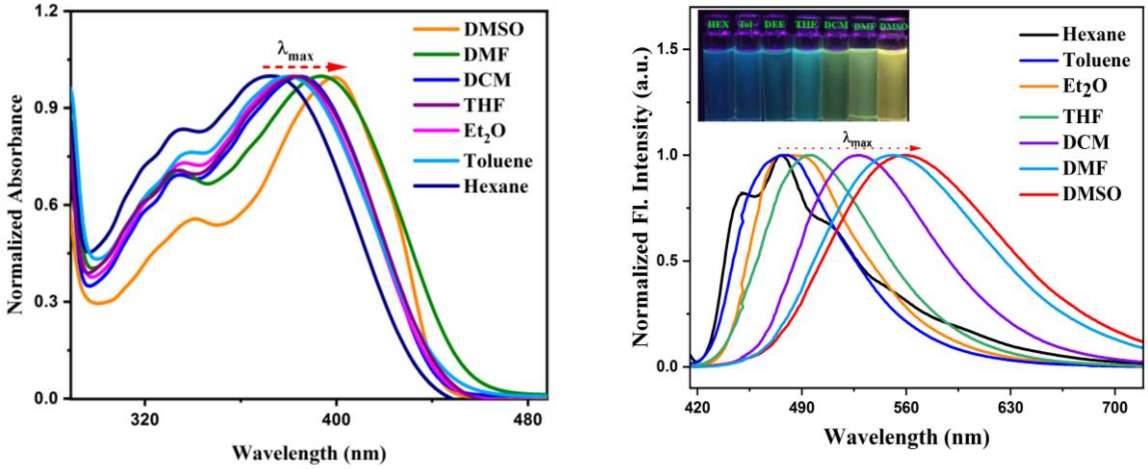

Figure 6.4: Normalized absorbance spectra (a) and emission spectra (b) of CPI (20 μM) in different solvents. Hexane, toluene, diethyl ether(Et_2O), tetrahydrofuran(THF), dichloromethane(DCM), dimethylformamide (DMF), dimethylsulfoxide(DMSO); Inset photographs shows the change in colour of CPI under UV illumination in different solvents.

Absorption spectra of CPI in different solvents display a moderately intense band in the range of 373-393 nm and the absorption maxima gradually red shifted as polarity of surrounding solvents increased from non-polar hexane to more polar DMSO (Fig. 6.4). Mostly, absorption spectra are less dependent to the solvent polarity as the absorption process occurs within very short time period. On the other hand, the investigated probe is highly sensitive to solvent polarity and displayed profound change in emission spectral maximum from 471 nm to 558 nm in varying the solvents from non-polar hexane to highly polar DMSO (Fig. 6.4). This phenomenon can be attributed to the typical ICT process occurring between donor moiety and acceptor unit in the receptor. Such remarkable solvatochromic effect with noticable red shift of about 87 nm in emission spectra led to the distinct and prominent fluorescence color change from blue to yellowish, which could be easily distinguished by naked eyes under UV lamp. At the same time, we have observed that quantum yield of the receptor CPI increase with increase in solvent polarity at the primary region and also showed maximum quantum yield in DMSO solvent with a notable red shift. Thus DMSO was chosen as optimum solvent for selective detection of anions.

To better comprehend the strong solvatochromic effect of the present probe in different solvents, the relationship between stokes shift (Δν) and solvent orientation polarisibility (Δf), which is the

result of both the dipole moment of the solvent and mobility of the electrons in the solvent, was examined using Lippert-Mataga equation[61]:

$$\Delta\nu \equiv \nu_{ab} - \nu_{em} = \frac{2\Delta f}{hca^3}(\mu_e - \mu_g)^2 + \text{constant} \qquad (1)$$

$$\Delta f = \frac{\varepsilon - 1}{2\varepsilon + 1} + \frac{n^2 - 1}{2n^2 + 1} \qquad (2)$$

Where $\Delta\nu$ is the stokes shift between the absorption and emission maximum (cm^{-1}), c is the speed of light, h is Plank's constant and a is the radius of the molecular cavity, μ_e and μ_g are the dipole moments in the excited state and ground state, n and Ɛ are the refractive index and dielectric constant of the solvent respectively. From the Lippert-Mataga equation (Fig. 6.5), the slope of the best-fit line was found to be 7895 cm^{-1}, which is related to the dipole moment change between ground state and excited state. It means when the charge transfers from electron donating carbazole unit to electron accepting cyano vinyl attached benzimidazole moiety in a more polar solvent, the dipole moment in excited state is increased. Consequently, the polarized excited state is considerably stabilized to adapt to the enhanced dipole moment via the relocation of the polar solvent molecules. As a result, the energy gets decreased and emission maxima was red shifted.

Table 6.1: Parameters and spectroscopic properties of sensor CPI in chosen solvents.

Solvent	Orientationalpolarisibility (Δf)	Absorption maxima (λ_{max}, nm)	Emission maxima (λ_{max}, nm)	Stokes shift (cm^{-1})	Quantum yield (Φ)
Hexane	0	373	471	5578.4	0.0536
Toluene	0.013235	377	481	5735.3	0.0547
Et_2O	0.166749	379	495	6183.3	0.0567
THF	0.203848	381	503	6366.1	0.091
DCM	0.22286	385	529	7070.4	0.109
DMF	0.25913	389	544	7324.6	0.131
DMSO	0.263094	393	558	7524.2	0.225

Therefore, the ICT excited state has a greater dipole moment than the ground state because of the substantial charge redistribution process inside the receptor. Hence, CPI is highly sensitive to the solvent polarity with distinct and prominent color changes, which can be visualised by naked-eye, thus has a good chance to utilize as a compatible solvent polarity indicator and roughly qualitatively.

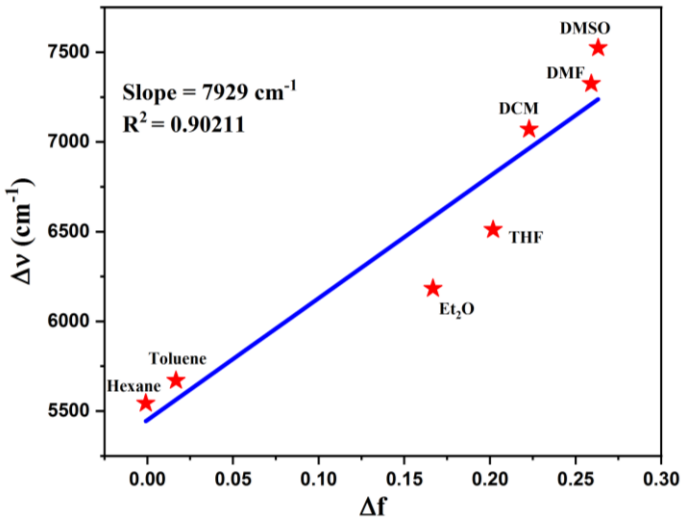

Figure 6.5: Lippert-Mataga plot; The dependence of stokes shift (Δν) as a function of orientation polarisibility(Δf) of the organic solvents with different polarity.

6.4.4 Detection of trace-level water

The solvatochromic study revealed that the emission change is highly responsive to the polarity of surrounding solvents. Based on this, we have established the efficacy of the probe CPI as fluorogenic sensor for detection of trace-level water in three frequently used water miscible organic solvents such as THF, DMF, and DMSO. As demonstrated in Fig. 6.6, the emission intensity of CPI is gradually decreased upon the incremental addition of water into all three probe-treated organic solvents. In THF, the present sensor exhibited strong bathochromic shift with incremental addition of water because of the lower polarity of THF among three used organic solvents, the high sensitivity of CPI toward the more polar solvent, thereby causing more stabilization of excited state in more polar protic water solvent and consequently reduced the excited state energy. Therefore, the emission maxima get more red shifted (Fig. 6.6a).

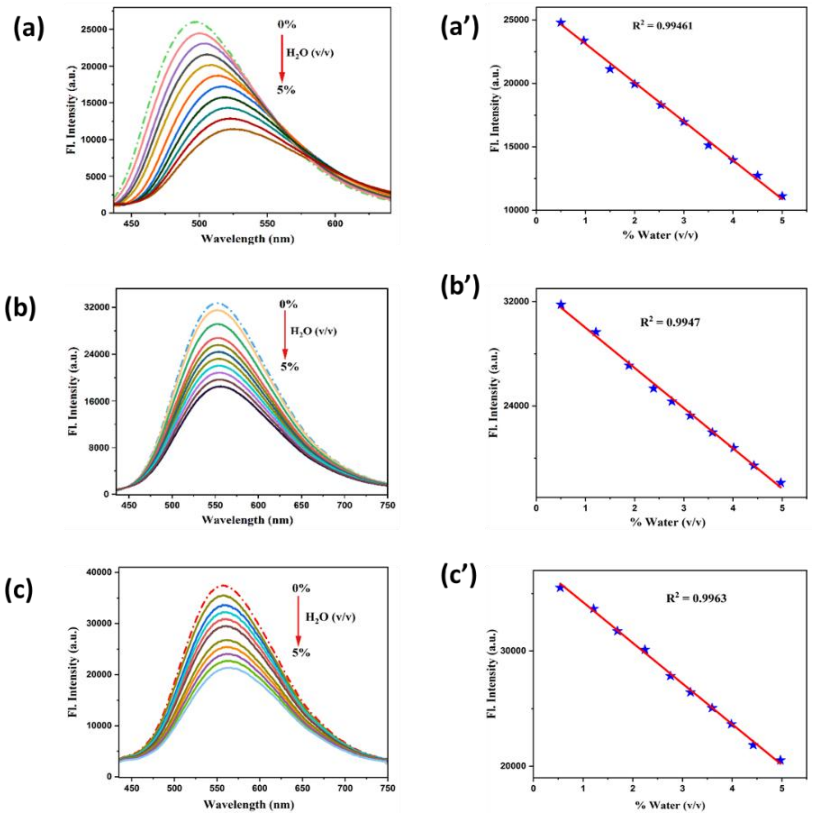

Figure 6.6: Change in emission spectra of CPI (20 µM) upon incremental addition of water (0-5% v/v) in: (a) THF solution (λ_{ex}= 381 nm), (b) DMF solution (λ_{ex}= 389 nm) and (c) DMSO solution (λ_{ex}= 393 nm)); Plot of the fluorescence intensity change of CPI versus varied concentrations of water (0-5%, v/v) in: (a') THF solution at 503 nm (R^2 = 0.9946), (b') DMF solution at 544 nm (R^2 = 0.9947) and (c') DMSO solution at 558 nm (R^2 = 0.9963).

To explain the quenching phenomenon in emission intensity of the probe upon addition of more polar water solvent, we can highlight the aggregation processes induced by hydrogen bonding and low solubility, where molecules are in close proximity, facing extensive π-π intermolecular stacking, which promotes relaxation of the molecules from the excited state to ground state via non-radiative path. This phenomenon is commonly referred as aggregation caused quenching (ACQ). The limit of detection of CPI for water detection in three solvents were determined and compared its efficiency with other reported probes in Table 6.2. Therefore, the sensor CPI can serve as an efficient water indicator to detect trace-level water in the three organic solvents.

Table 6.2: Comparison of LOD's of CPI for water with reported probes

Compounds	Detection limits (% v/v) Fluorescence quenching technique			References
	THF	DMF	DMSO	
Azo dye	------	0.1576	0.2137	[62]
Phenylene-(poly)ethynylene	0.059	0.210	-----	[63]
Nitro-substituted triazaborolopyridinium	0.028	0.048	-----	[64]
Tetraphenylethene derivatives	0.0056, 0.0097	-------	------	[65]
Benzotriazole derivative	0.009	------	------	[66]
Carbazole derivative	0.0082	0.038	0.192	**Present Work**

6.4.5. Detection performance of CPI

In order to investigate the sensing capability of the sensor CPI towards CN^- over various competitive anions like F^-, Cl^-, Br-, I^-, ACO^-, NO_3^-, CO_3^{2-}, SCN^-, HCO_3^-, N_3^-, HSO_4^-, SO_4^{2-}, $H_2PO_4^-$, $HPO_4^{2-}$and PO_4^{3-}, UV-absorption and emission spectroscopy were recorded in DMSO solution at room temperature. In presence of CN^- ion, the yellowish color of CPI instantly changed to reddish in day light. The probe exhibited a maximum absorption band at 392 nm with a shoulder peak at 343 nm. The peak around 343 nm is assigned to pi-pi transition inside the receptor. But the absorption maxima at 392 nm is due to the intramolecular charge transfer (ICT) process from carbazole unit (donor) to cyano vinyl attached benzimidazole moiety (acceptor). Upon incremental addition of cyanide, the peak at 392 nm was gradually disappeared and simultaneously the emergence of a new band with absorption maxima at 447 nm was noticed with an isosbestic point at 410 nm (Fig. 6.7a). No significant spectral change was noticed after addition of above mentioned interfering anions into the probe solution except F^- and ACO^- (Fig. 6.8a). These spectral outcomes are well supported by Fig. 6.9(a) and hence the receptor is highly specific towards CN^- ion. On the other hand, upon excitation at 410 nm, the sensor itself exhibited a strong emission band at 556 nm, which may be attributed to ICT process occurring inside the probe. With incremental addition of cyanide, the emission band at 558 nm gradually vanished along with the appearance of new emission band at 625 nm with red shift of about ~67 nm and an isoemissive point at 561 nm (Fig.

6.7b). The appearance of new emission band at 625 nm in presence of CN^- can be explained by typical ICT process in the deprotonated receptor and the distinct color change from yellowish to orange was noticed under UV irradiation. No such remarkable change in the fluorescence spectrum was noticed while adding various competitive anions such as F^-, Cl^-, Br^-, I^-, ACO^-, NO_3^-, CO_3^{2-}, SCN^-, HCO_3^-, N_3^-, HSO_4^-, SO_4^{2-}, $H_2PO_4^-$, HPO_4^{2-}, PO_4^{3-} into the probe solution except F^- and ACO^- (Fig. 6.8b). These emission spectral changes are well agreed with Fig. 6.9(b).

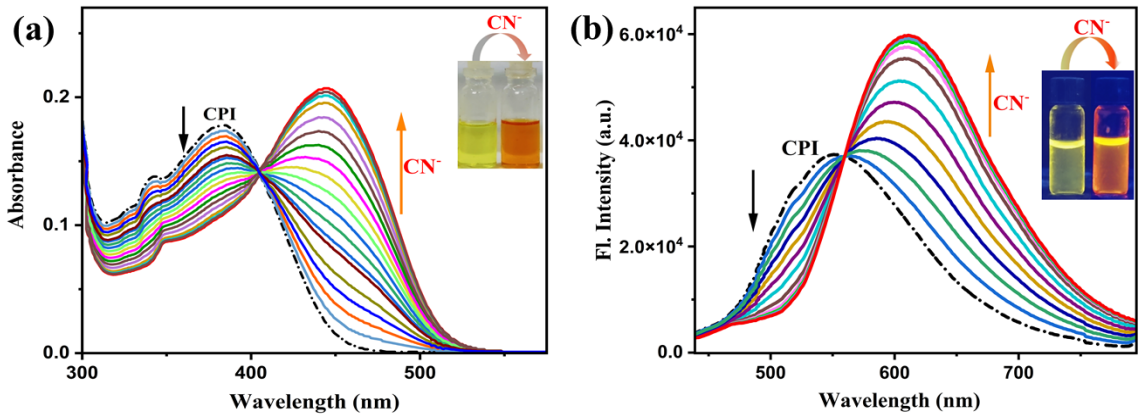

Figure 6.7: (a) Change in UV-Vis spectrum of CPI (20 µM) upon incremental addition of CN^- (0-40 µM) in DMSO. Inset shows the change in colour of the probe solution in the absence and presence of 40 µM CN^- solution in sunlight; (b) Change in emission spectra of CPI (20 µM) upon gradual addition of CN^- (0-40 µM) in DMSO (λ_{ex}= 410 nm); Inset shows the visible emission color change of CPI solution before and after addition of 40 µM CN^- solution under UV-irradiation.

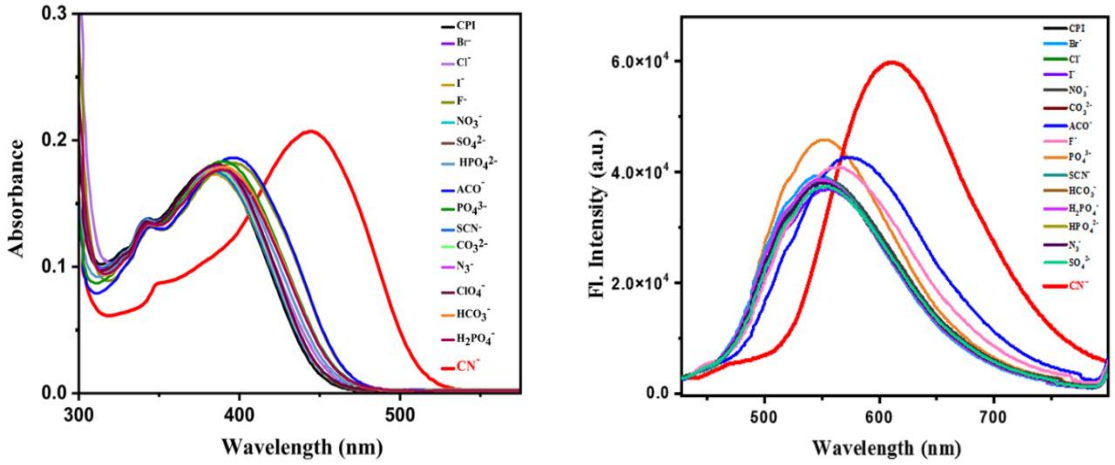

Figure 6.8: UV-Vis spectra of CPI (20 µM) upon addition of different anions (40 µM) in DMSO (left side) and emission spectra of CPI (20 µM) upon addition of various anions (40 µM) in DMSO (right side).

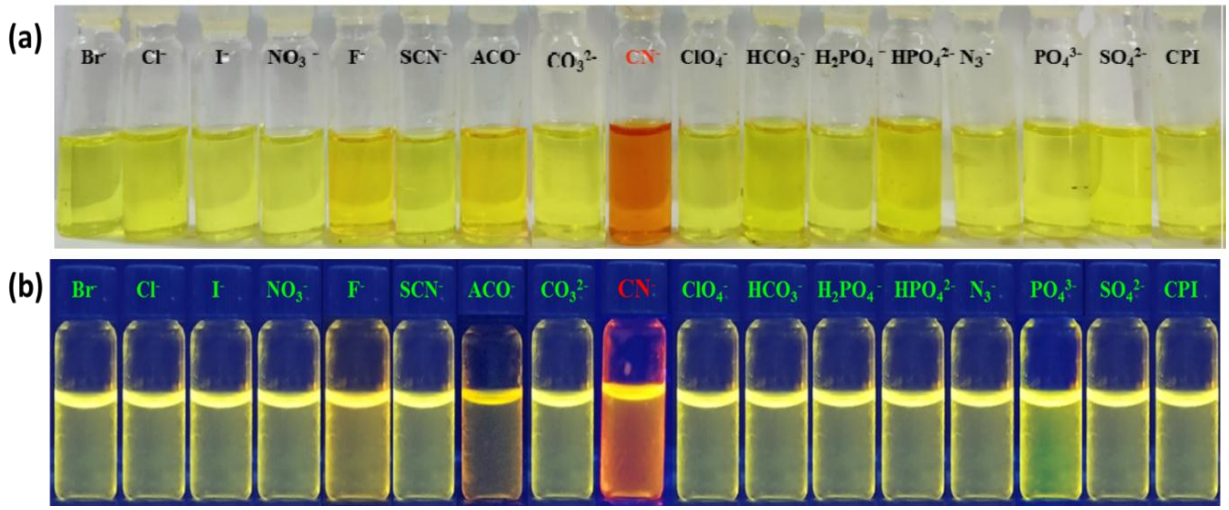

Figure 6.9: Color variations upon addition of different anions such as F^-, Cl^-, Br-, I^-, ACO^-, NO_3^-, CO_3^{2-}, SCN^-, HCO_3^-, N_3^-, HSO_4^-, SO_4^{2-}, CN^-, $H_2PO_4^-$, HPO_4^{2-} and PO_4^{3-} (40 µM) into the probe solution (20 µM) in DMSO in sunlight (a) and under UV light (b).

6.4.6. Sensing performance of sensor CPI towards CN^-

To interpret the sensitivity and selectivity of the present receptor (CPI) towards CN^- ion, the limit of detection of the sensor for CN^- was determined based on fluorescence titration method and found to be 4.48 X 10^{-8} (M) using the well-known equation, LOD = k X (SD/S), where SD and S are the standard deviation and the slope of the linear response curse respectively (Fig. 6.10). This low LOD value eventually signifies effectiveness of CPI in detecting CN^- in a very minute level and well compared with other published receptors in Table S5 (ESI†). In addition, mole-ratio plot revealed that after addition of almost 21 µM of CN^-, no significant change was observed in the emission spectra at 625 nm thereby indicating saturation level has been achieved (Fig. 6.10). Furthermore, time-dependent course was also studied for monitoring reaction time of the probe with CN^-. This experiment disclosed that the absorption intensity at 447 nm and fluorescence intensity at 625 nm gradually increased as the reaction progresses and finally achieved its maximum and stable value within 50 s, suggesting the completion of the reaction (Fig. 6.11). These outcomes indicate that CPI can serve as an efficient candidate in portable device for rapid cyanide detection.

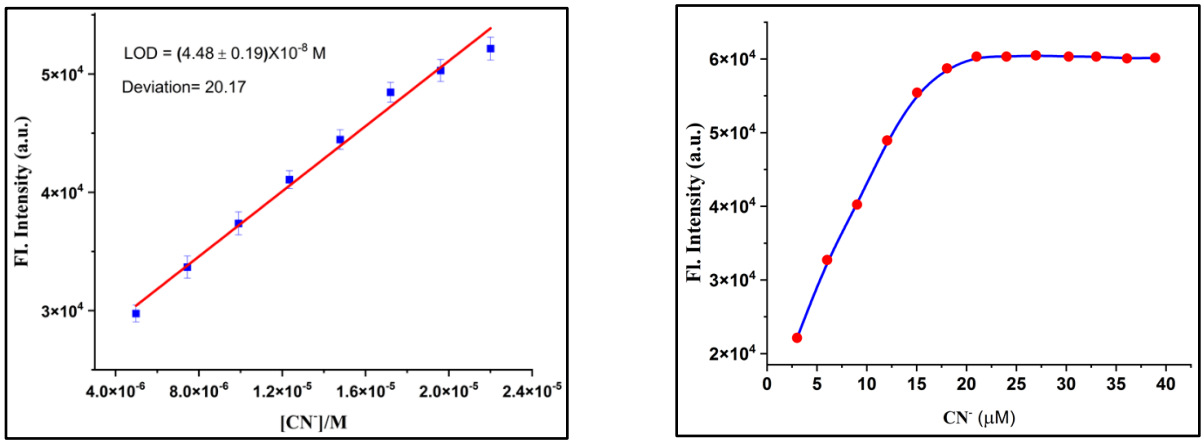

Figure 6.10.: Linear response curve of CPI at 625 nm depending on the CN^- concentration (left side) and mole ratio plot of CPI (20 μM) for CN^- (40 μM) at 625 nm using fluorescence titration method (λ_{ex}= 410 nm) (right side).

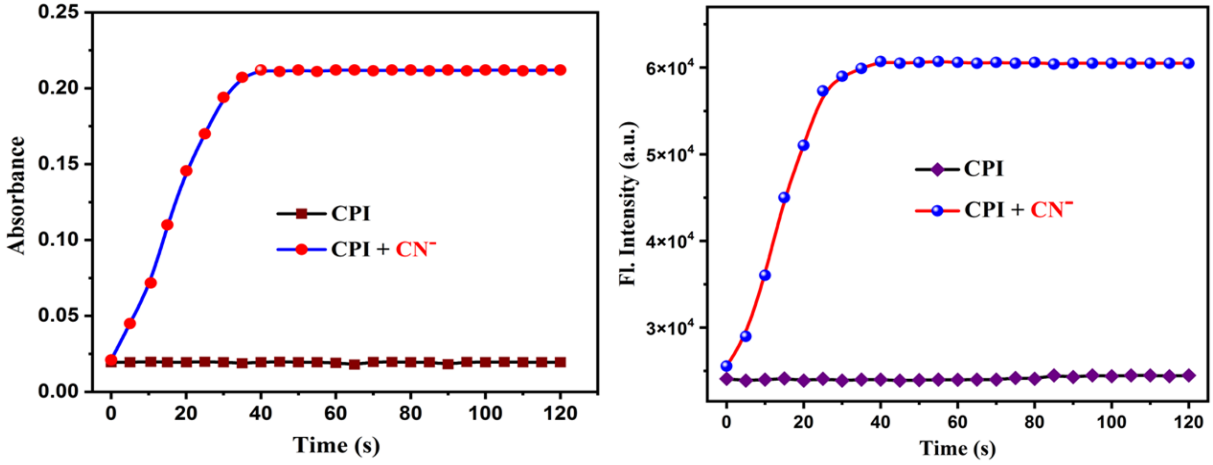

Figure 6.11: Time-dependent absorbance spectra at 447 nm (left side) and emission spectra at 625 nm (right side, λ_{ex}=410 nm) for CPI and CPI-CN^- adduct obtained within 0-2 min time interval in DMSO solution.

In order to explain the real-time application of sensor CPI, as an anionic identification sensor for CN^-, competitive experiments were performed in presence of CN^- ion and other various anions in DMSO. As shown in Fig. 6.12, emission intensity induced by CN^- ion at 625 nm remained almost unaltered in presence of other interfering anions except ACO^- and F^-, which is known as binary competitive system "target + anions" in the same solution phase, thereby indicating high CN^- sensing aptitude of CPI and significant anti-interference sensing capability of CPI-CN^- system.

The pH effect on CPI and CPI-CN^- were studied by fluorescence method and the experiment revealed the fact that the new fluorogenic sensor, CPI did not experience any remarkable change in the emission profile at 625 nm up to pH 8, thereby suggesting that the probe is almost independent of pH upto 8. After that, the emission intensity gradually increased with increase in pH. This change could be accredited to deprotonation of acidic proton in imidazole moiety in basic medium, whereas in case of CPI-CN^-, the emission remained almost unaltered between pH rang of 4 and 8 (Fig. 6.12). But emission intensity gradually decreased below pH 4. This decrease in emission intensity may occur due to protonation of cyanide ions and after pH 8, emission intensity increased and became same as that of probe due to simple deprotonation in basic medium. Consequently, for applicability in real samples, chemosensor performance of the receptor can be evaluated in the pH rang of 4.5 to 7.5 to avoid the interference of acidic and basic substances.

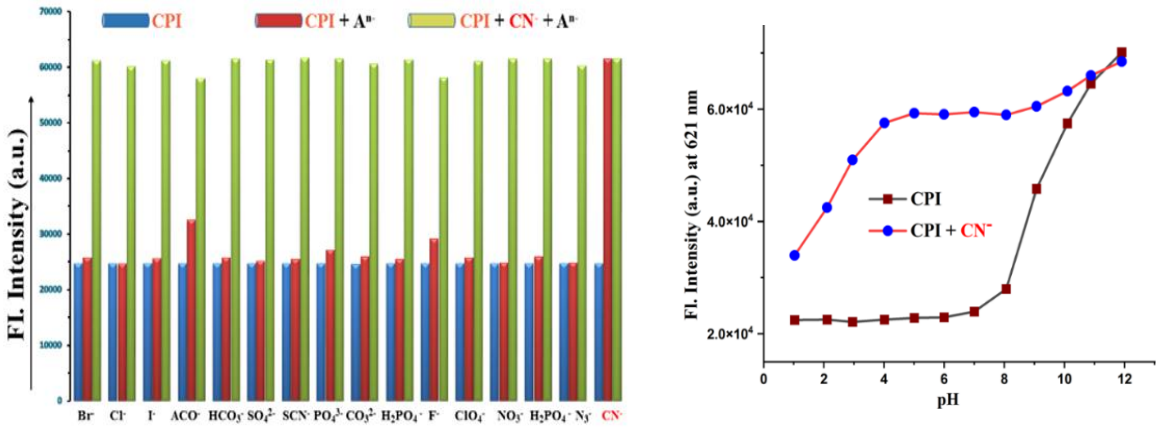

Figure 6.12: Competitive experiments of CPI (20 µM) for CN^- (40 µM) in presence of common anions (40 µM). Fluorescence intensity at 625 nm for CPI itself (20 µM) (blue bar), with various coexisting anions (40 µM, red bar) such as F^-, Cl^-, Br-, I^-, ACO^-, NO_3^-, CO_3^{2-}, SCN^-, HCO_3^-, N_3^-, HSO_4^-, SO_4^{2-}, $H_2PO_4^-$, HPO_4^{2-} and PO_4^{3-} and upon subsequent addition of CN^- (40 µM) (green bar); λ_{ex}= 410 nm.

To interpret the excited state behavior of the ratiometric fluorescence responses of the probe towards CN^-, the TRPL experiment was carried out (Fig. 6.13). CPI has significant fluorescence life time about 2.95 ns whereas in presence of CN^- ion, the longer average fluorescence life-time of 3.51 ns was detected which is due to the deprotonation of imidazole –NH proton followed by new ICT process in CPI-CN^- specie. Radiative rate constant (K_r) and total non-radiative rate constant (K_{nr}) have been calculated and summarized in Table A6.4. The significant change in the value of τ, K_r and K_{nr} confirmed the adduct formation of the receptor with CN^- to form a new

fluorogenic compound CPI-CN^-, which has higher life-time than the free probe itself. Sensor owing to high photostability with steady analytical signals is greatly desired for fluorescence based sensing applications. Therefore, in order to evaluate the photosensitivity, sensor CPI and CPI-CN^- were exposed over 2 min in day light under optimal conditions according to the reported literatures.[67] As seen in Fig. 6.13, probe CPI and CPI-CN^- displayed highly photostable relative fluorescence responses throughout the experimental time (2 min) with negligible signal change. This experimental results revealed to the fact that the receptor CPI and CPI-CN^- have highly photostable fluorescence signal response thereby making it compatible for the analysis of real samples spectrofluorimetrically.

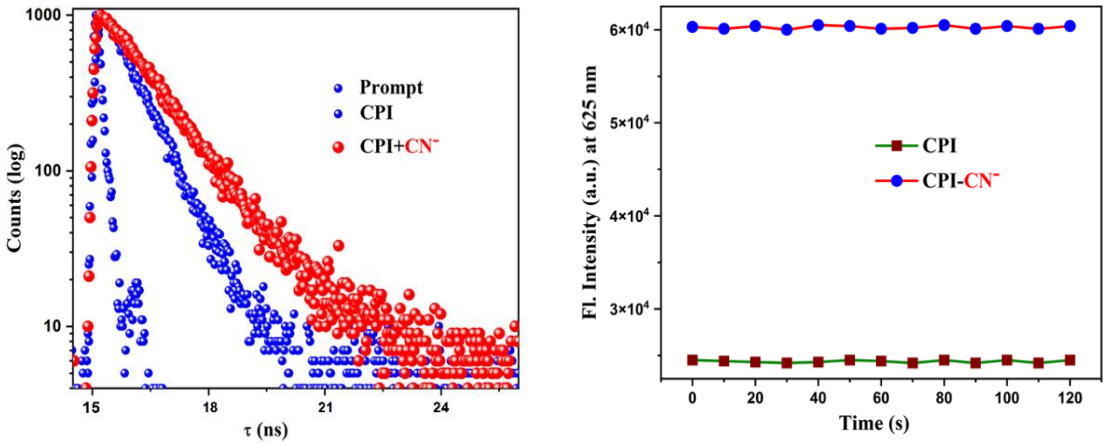

Figure 6.13: Lifetime decay profile of CPI (●●●) and CPI-CN^- adduct (●●●) (left side) and photostability curve of CPI and CPI-CN^- adduct (right side).

6.4.7. Recyclability and reusability

Recyclability is very important for chemosensor. We carefully examined the reusability of CN^- identification properties by adding TFA (Trifluoroacetic acid) into the CN^- treated probe solution alternatingly. Consequently, the fluorescence color of the receptor changed from yellow to orange repeatedly several times with little loss of fluorescence efficiency (Fig. 6.14). This phenomenon can be explained by the deprotonation and protonation mechanism of CPI upon addition of CN^- and TFA respectively. The increase of emission intensity of CPI after addition of CN^- occurs due to the hydrogen bonding followed by subsequent deprotonation of acidic –NH proton. But the decrease in the emission intensity can be accredited due to the addition of TFA in CN^- treated probe solution as the hydrogen bonding gets interrupted which consequently results into the

inhibition of the deprotonation of acidic -NH fragments in the imidazole unit and subsequent protonation of deprotonated CPI. Thus the emission intensity reverts back to the original fluorescence intensity of the free probe thereby proving the fact that the sensor is reversible in nature. Hence, the probe can be considered as recyclable as well as reusable for CN^- sensor.

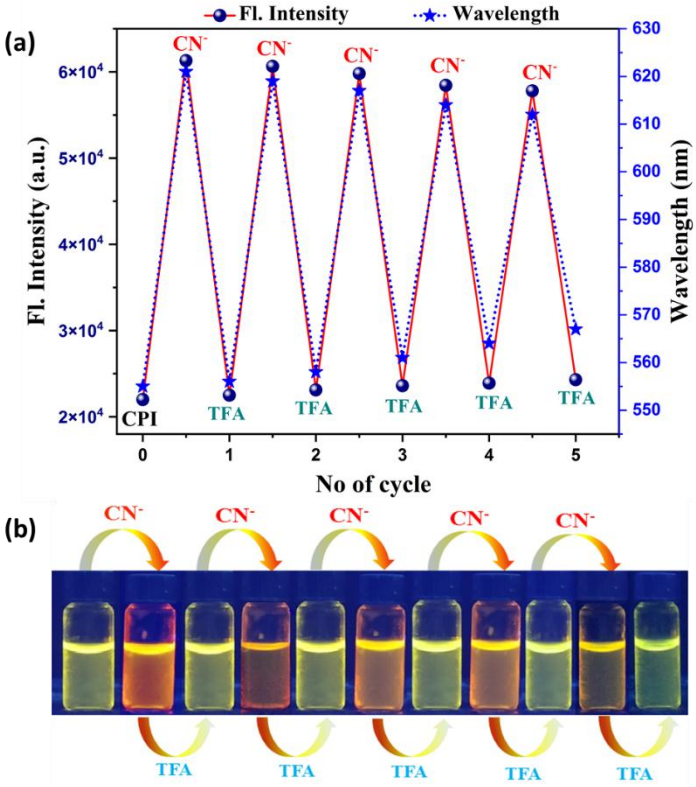

Figure 6.14: (a) Fluorescence switching cycles of sensor CPI controlled by alternating the addition of CN^- (1 eq.) and TFA (1 eq.) several times (λ_{ex} = 410 nm); (b) Photograph shows the fluorescence color change of the probe solution after each sequential addition of CN^- and TFA.

6.4.8. Possible sensing mechanism

In order to confirm the sensing mechanism of the receptor to CN^-, ^{1}H-NMR titrations were carried out in DMSO-d_6 upon addition of different concentration of cyanide. As shown in Fig. 6.15, the –NH peak of the receptor appeared at 12.5 ppm whereas upon incremental addition of CN^- ion into the probe solution, the peak at 12.6 ppm was found to be gradually vanished, suggesting the formation of H-bonding followed by deprotonation of imidazole –NH proton. All aryl protons shifted upfield after addition of CN^- because of the formation of –ve charge on the imidazole unit.

The FT-IR spectroscopy was also investigated to further confirm the interaction between CN^- and receptor. In FT-IR spectroscopy of CPI, the peak at 3260 cm^{-1} appeared due to the vibration of –NH, while in presence of CN^- ion, the -NH vibration peak disappeared (Fig. 6.16), which evidenced to the fact that the deprotonation of -NH has been taken place. When the strong basic CN^- comes closer to the acidic –NH fragment of the probe (CPI), hydrogen bonding interaction takes place which eventually leads to the proton transfer from CPI to CN^- ion. Consequently, an accumulation of electron density on CPI center occurs and hence red shift of the absorption is observed with the change in ratiometric emission. The brilliant selectivity of CPI towards CN^- can be attributed to the suitability in the activity of its NH groups in CPI, thereby making the probe to be able to discriminate the delicate difference in the affinity of CN- to acidic proton compared to other coexisting anions. Furthermore, to estimate the exact stoichiometry ratio of the adduct formation, Job's plot experiment was also carried out and 1:1 adduct formation between CPI and CN^- was found (Fig. 6.16). A possible sensing mechanism for the detection of CN^- ion was depicted in Fig. 6.17.

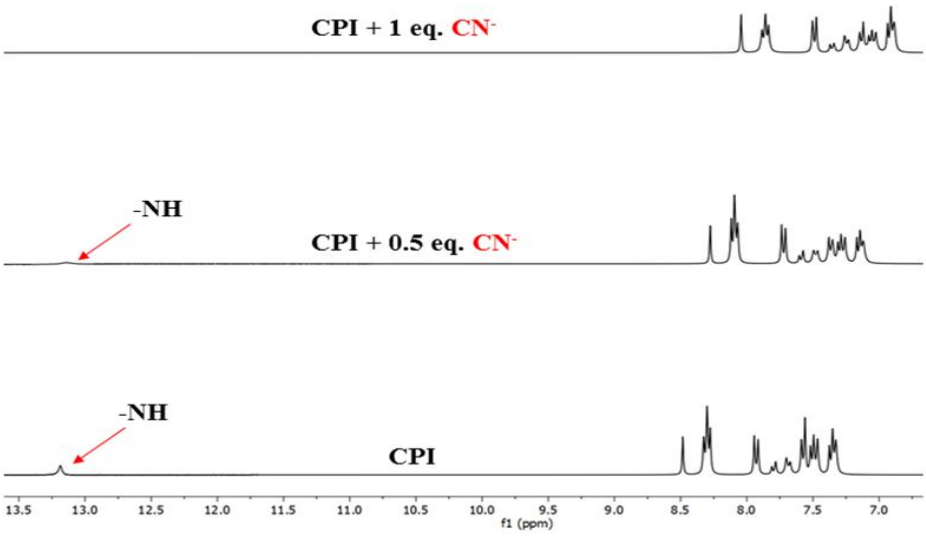

Figure 6.15: ^{1}H-NMR (300 MHz) titration of CPI in DMSO-d_6 upon addition of varying amounts of CN^- (0 eq., 0.5 eq. and 1 eq.).

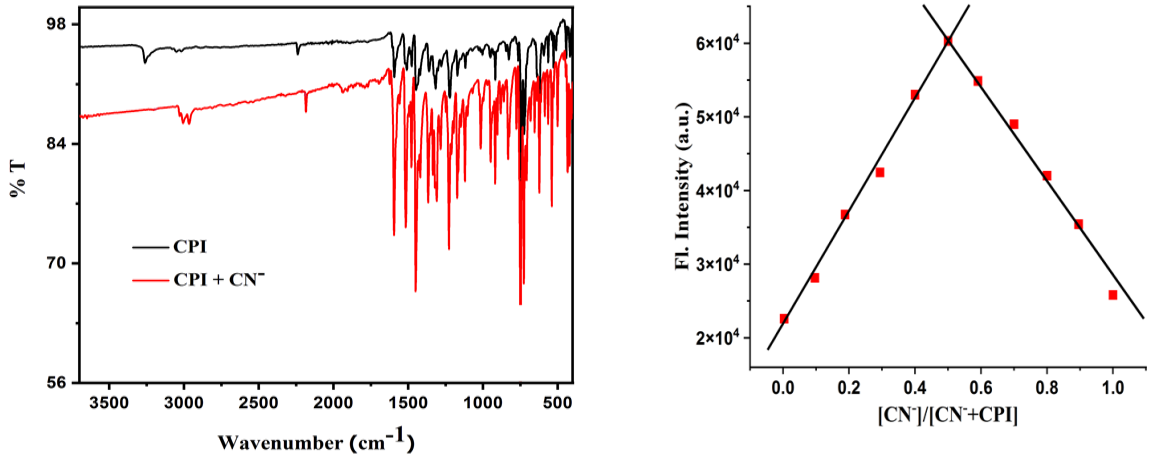

Figure 6.16: IR spectra comparison (left side) and stoichiometry plot for CPI-CN^- adduct formation by recording fluorescence intensity changes at 625 nm (λ_{ex}= 410 nm) (right side).

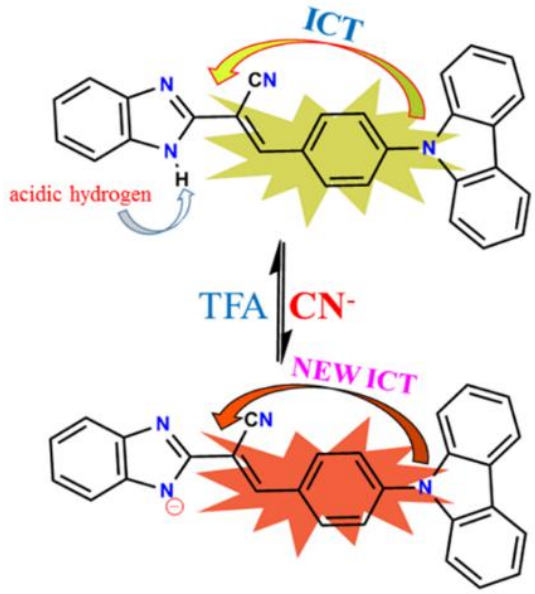

Figure 6.17: Proposed sensing mechanism of CPI towards CN^-.

6.4.9. Sensing response in Solid State

In solid phase, the sensor CPI exhibited yellow color which is turned to reddish color in presence of CN^- (TBACN) in ambient light, whereas the yellowish fluorescence color of free probe changed

to red color (Fig. 6.18) when simply ground with TBACN in the solid state according to the reported procedure,[68,69] which signifies the formation of CPI-CN^- species.

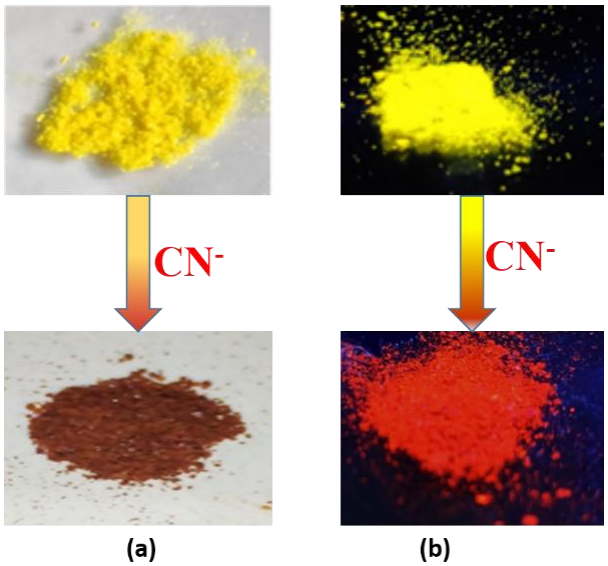

Figure 6.18: The color change of the probe CPI in solid state (right side) without and with addition of CN^- in day light(a) and under UV light(b).

To show the selectivity of CPI towards CN^- in solid state, we have established solid state sensing platform with various relative anions and observed that the color induced by sensor CPI with CN^- was clearly distinguishable compared to any other interfering anions. This observable and prominent color change for CN^- in both ambient light and under UV light confirmed its sensing aptitude in solid state.

6.4.10. Dip-stick experiment: Detection of CN^- using TLC plate

For visual identification of CN^- ion, we have carried out a cheap and proficient portable method known as Dip-stick experiment. To execute this experiment, few thin-layer TLC plats were prepared and immersed into CPI-treated DMSO solution ($2x10^{-4}$ M) and then the test strips were allowed to dry in air for sometimes. Probe-loaded test strips displayed greenish-yellow color in ambient light and yellowish under UV light. When the test strips were dipped into CN^- solution and dried in air, distinct color change was observed (Fig. 6.19). This color change can be easily distinguished by naked eye when exposed the strips in ambient light as well as under UV-light. Additionally, we also demonstrated the colorimetric and fluorometric response of CPI-coated test

strips in different concentration of CN^- (Fig. 6.19). Interestingly, the test strips used for CN^- detection can be made reusable by dipping into TFA solution (Fig. 6.19). This simple, reusable and easy-to-handy protocol disclosed that CPI is highly efficient to detect CN^- ion qualitatively.

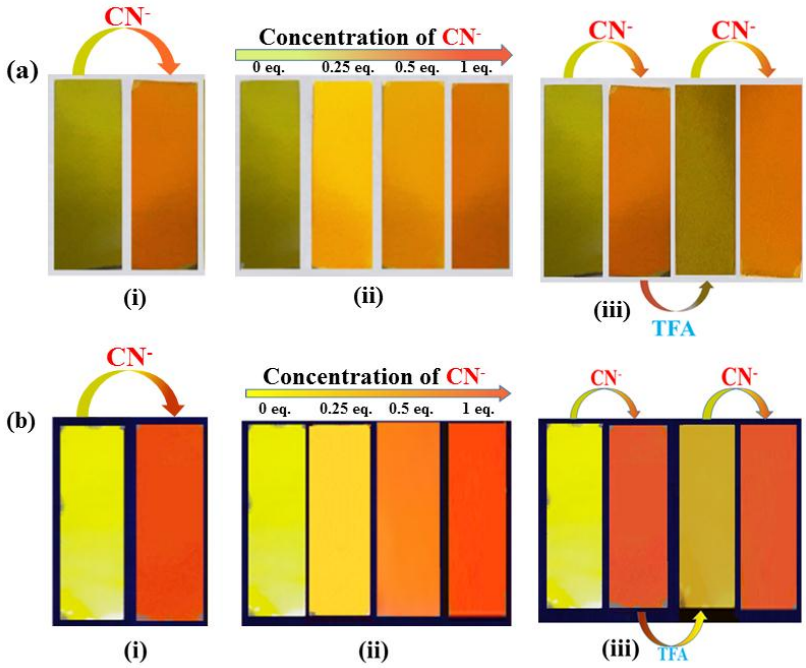

Figure 6.19: (a**)** Pictures of TLC plates after immersion into DMSO solution of CPI and CPI-CN^-(i), after immersion into DMSO solution of CPI in presence of different concentration of CN^- (ii) and after each sequential immersion into CN^- and TFA solution(iii) in sunlight; (b) Pictures of TLC plates after immersion into DMSO solution of CPI and CPI-CN^- (i), after immersion into DMSO solution of CPI in presence of different concentration of CN^- (ii) and after each sequential immersion into CN^- and TFA solution(iii) under UV irradiation. [CPI] = 2×10^{-4} M, [CN^-] = 2×10^{-3} M CPI.

6.4.11. Practical application in real samples

6.4.11.1. Wastewater treatment

Cyanide in different wastes could possibly be dumped into water and pollutes the natural water resources. So it is very much urgent to detect concentration level in these contaminated water resources. To check the practicality of our proposed method, we tested natural water resources (tap, pond and river) for sensing of CN^- by means of fluorescence technique according to the following reported procedure.[70,71]

Table 6.3: Recovery of CN^- concentration from various natural water samples using the proposed method

Source	Sample	CN^- Spiked (μg/lit)	CN^- recovered[b] (μg/lit)	Recovery (%)
Tap water	Tap water 1	0	Not detected	
	Tap water 2	4.00×10^{-4}	$(3.96 \pm 0.04)\times10^{-4}$	99
	Tap water 3	3.00×10^{-3}	$(2.93 \pm 0.05)\times10^{-3}$	97
Lake water	Lake water 1	0	Not detected	
	Lake water 2	4.00×10^{-4}	$(3.94 \pm 0.03)\times10^{-4}$	98.5
	Lake water 3	3.00×10^{-3}	$(2.97 \pm 0.02)\times10^{-3}$	97
River water	River water 1	0	Not detected	
	River water 2	4.00×10^{-4}	$(4.05 \pm 0.03)\times10^{-4}$	101.2
	River water 3	3.00×10^{-3}	$(2.97\pm 0.04)\times10^{-3}$	98

[b]Relative standard deviations were calculated based on three times of measurement.

Cyanide in these natural water sources were not determined. Now different concentrations of CN^- ion were added into these natural water samples and the probe CPI was engaged to detect the concentrations level of cyanide in these contaminated samples. From Table 6.3, it is concluded that the sensor is highly efficient to recover the concentration of cyanide from contaminated water samples with excellent recovery. Therefore, this approach established that the present probe CPI is capable of determining cyanide concentration level quantitatively in the contaminated natural water resources.

6.4.11.2. Food samples analysis

The detection of endogenous biological cyanide in food samples such as sprouting potatoes, apple seeds and bitter almonds is an interesting and important aspect in chemosensor chemistry nowadays. In order to explore the real-time application of the present sensor (CPI), the three different food samples were prepared according to the reported procedures.[72,73] The collected sprouting potatoes and apple seeds were first smashed finely and soaked using double distilled water (200 ml) for 4 days separately until the extract became muddy.

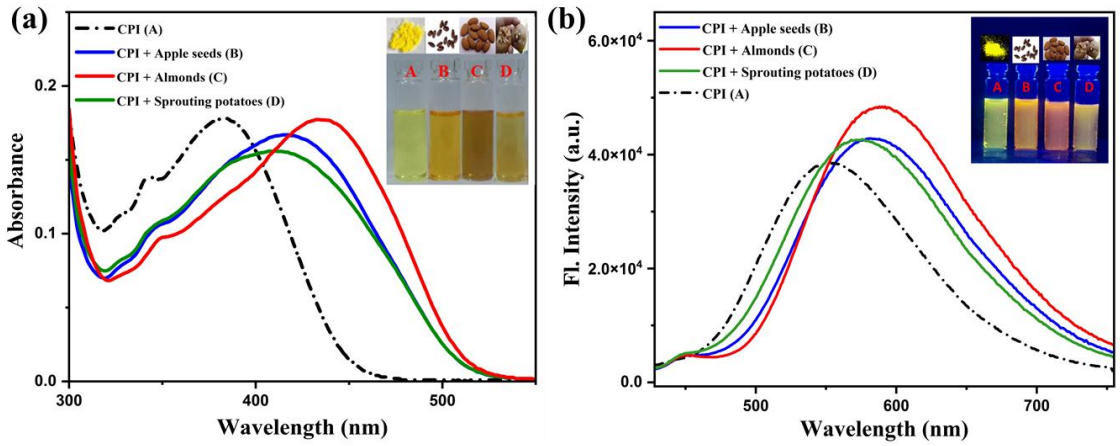

Figure 6.20: (a) UV-Vis spectra of CPI (black line) and upon addition of various food samples extracts: apple seeds (blue line), bitter almonds (red line), sprouting potatoes (green line). (Inset shows the change in colour upon addition of different food sample extract in day light and photographs of food samples with probe). (b) Emission spectra of CPI (black line) and upon addition of various food samples extracts, (λ_{ex}= 410 nm): apple seeds (blue line), bitter almonds (red line), sprouting potatoes (green line). (Inset shows the change in colour upon addition of different food sample extract under UV lamp and photographs of food samples with probe).

Then the turbid solutions were filtered and the extracts were treated with 0.8 (N) NaOH solution to get the cyanoglycoside test samples and the pH was adjusted to 7.1. A mixture of 10 g crushed bitter almonds and 0.2 g NaOH in 30 ml double distilled water was stirred for 40 min to obtain cyanoglycoside test solution. Similarly, the extract was then filtered and the pH was fixed to 7.1. Surprisingly, upon addition of the three different test samples into the probe treated DMSO solution separately, prominent color change was observed which can be easily distinguished by naked eyes in ambient light and under UV lamp along with the significant spectral changes (Fig. 6.20). This experiment revealed that the detection process is easy, handy and provides rapid response. Hence, CPI could possibly be employed for the selective identification of cyanide in cyanogenic glycosides of the food samples.

6.4.12. Theoretical computations

We conducted theoretical investigations to get a comprehensive knowledge of the interplay between CPI and CN^-. Figure 6.21 displayed the optimized structure of CPI and CPI-CN^- respectively. Contour plots of selected molecular orbitals of the CPI and CPI-CN^- adduct are

shown in Fig. A6.5 and Fig. A6.6 respectively. For CPI, the HOMO electron density was located over the carbazole moiety while the LUMO electron density was on the phenyl ring and cyano vinyl group (Fig. 6.22). However, for CPI-CN^-, the prolonged π conjugation caused the HOMO electrons to be primarily localised over the benzimidazole moiety.

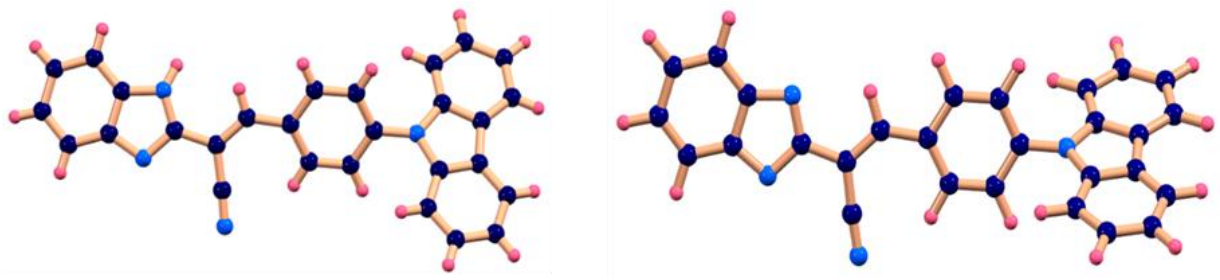

Figure 6.21: Optimized structure of CPI (left side) and optimized structure of CPI^- (right side) calculated by DFT/B3LYP/6-31+G(d) method.

Significant variations in the electron density distribution results from the accelerated donor to acceptor ICT transition in the receptors following CN^- induced deprotonation. The energy gap between HOMO and LUMO of CPI was calculated to be 3.04 eV which decreased upon deprotonation by CN^- ion to 2.66 eV (Fig. 6.22). This narrowing of energy gap was confirmed by the red-shifted ICT mechanism observed in absorption experiment of CPI on interaction with cyanide.

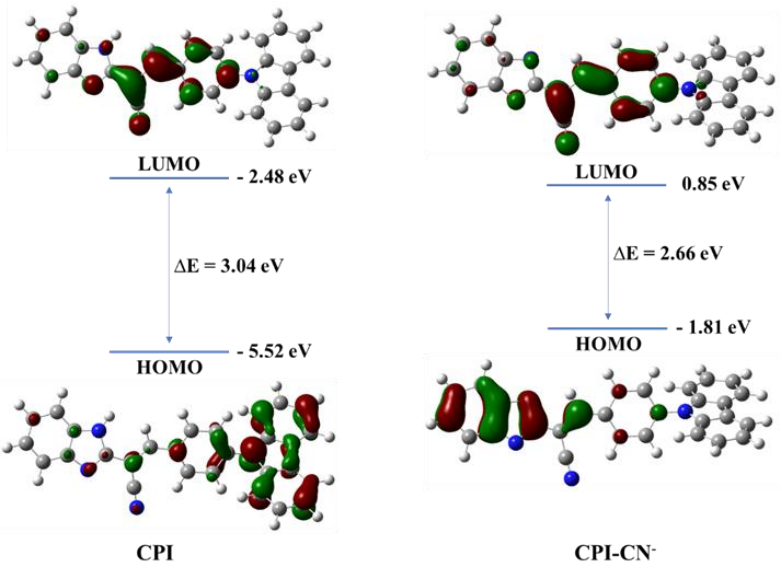

Figure 6.22: The HOMO-LUMO energy gap of CPI and its addition product CPI-CN^- calculated using the DFT/B3LYP/6-31+G(d) method.

6.5. Experimental section

6.5.1. Materials and instrumentations

All the organic chemicals, reagents and solvents used in the synthetic procedure of CPI such as 4-fluorobenzaldehyde, 9H-carbazole, o-phenylenediamine, ethyl cyanoacetate, dioxane, potassium tert-butoxide, dimethyl formamide and ethanol are purchased from Sigma Aldrich and used without further purification. All spectroscopic grade solvents were from other commercial sources and used with no additional refinement. ^{1}H and ^{13}C NMR spectra were recorded on Brucker 300 MHz instrument and DMSO-d_6 was used as solvent using TMS as an internal standard. The chemical shifts are reported as □ in units of parts per million (ppm). HRMS mass spectra were confirmed on Waters (Xevo G2 Q-TOF) mass spectrometer. Elemental analysis was carried out in a 2400 Series-II CHN analyzer, PerkinElmer, USA. A PerkinElmer Lambda 750 spectrophotometer was used to obtain absorbance spectra and emission property was measured using Shimadzu RF-6000 fluorescence spectrophotometer at room temperature (298 K). Lifetimes were measured using a time-resolved spectrofluorometer from IBH, UK.

6.5.2. UV-Vis and fluorescence method

For UV-Vis titrations, stock solution of the probe, CPI (20 μM) was prepared in DMSO (at 25°C). Deionized water was used to prepare all the solutions of guest anions using their sodium salts (1×10^{-5} M). The solution of cyanide ion (1×10^{-5} M) was prepared using tetrabutylammonium cyanide salt at physiological pH. Solutions of different concentrations of the receptor and all the anions were prepared separately and then the spectra of these solutions were recorded with the help of UV-Vis method. Similarly, for fluorescence titrations, stock solutions were prepared following the similar procedures and then the spectra were recorded by means of fluorescence method.

6.5.3. pH solution preparation method

For pH dependent study, stock solution of the sensor, CPI (20 μM) was prepared in 100% DMSO (at 25°C). Aqueous solution of 1M HCl and 1M NaOH were used to adjust the pH.The probe solution and the different concentration of acids and bases were arrangedseparately. The emission spectra of these solutions were monitored by means of fluorescence technique. Similar experiment was carried out while recording the pH titration of receptor (CPI) in presence of cyanide.

6.5.4. Synthesis of (E)-3-(4-(9H-carbazol-9-yl)phenyl)-2-(1H-benzo[d]imidazol-2-yl)acrylonitrile(CPI)

4-(9H-carbazol-9-yl)benzaldehyde[74] and 2-(1H-benzo[d]imidazol-2-yl)acetonitrile[75] were synthesized according to the previously reported procedures. 2-(1H-benzo[d]imidazol-2-yl)acetonitrile (0.09 g, 0.52 mmol) and piperidine (0.52mmol) were added into the ethanolic solution of 4-(9H-carbazol-9-yl)benzaldehyde (0.155 g, 0.52 mmol). Then the whole mixture was stirred under refluxing condition for 7 h in inert atmosphere. After completion of the reaction, the reaction mixture was allowed to cool and the yellow precipitation was collected through filtration and washed with ethanol. The product is purified using column chromatography to get the desired product. Yield was, 0.179 g, 84%.

^{1}H-NMR (300 MHz, DMSO-d_6): δ(ppm)7.35 (t, J=7.37, 3H), 7.46-7.58 (m, 7H), 7.68 (d, J= 8.6 Hz, 1H), 7.8 (d, J= 8.5, 1H), 7.93 (d, J= 8.4 Hz, 2H), 8.31 (t, J=7.1 Hz, 3H), 8.48 (s, 1H), 13.19 (s, 1H)

^{13}C-NMR (75 MHz, DMSO-d_6): δ(ppm)50.2, 102.9, 103.9, 110.4, 112.1, 116.7, 121.0, 121.2, 123.6, 126.8, 127.0, 127.4, 131.8, 131.9, 132.6, 140.0, 144.7, 147.9, 148.8

IR (KBr): ν(cm^{-1}) 3260 (-NH stretching), 2234 (-CN stretching)

HRMS: calculated for $C_{28}H_{19}N_4^+[MH]^+$, (m/z) = 411.1604; found = 411.1570.

6.5.5. Determination of fluorescence Quantum Yields (Φ) of CPI and its adduct with CN^-

The luminescence quantum yield was determined using coumarin-153 as reference dye. The compounds and the reference dye were excited at the similar wavelength and the emission spectra were then studied. The area of the emission spectrum was integrated and the quantum yield is determined according to the following equation:

$$\phi_S/\phi_R = [A_S / A_R] \times [(Abs)_R /(Abs)_S] \times [n_S^2/n_R^2]$$

Here, ϕ_S and ϕ_R are the luminescence quantum yields of the sample and reference dye, respectively. A_S and A_R are the area under the emission spectra of the sample and the reference respectively, $(Abs)_S$ and $(Abs)_R$ are the respective optical densities of the sample and the reference solution at the wavelength of excitation, and n_S and n_R stand for the values of refractive index for the respective solvent used for the sample and reference.

The quantum yields of CPI and CPI-CN^- are determined using the above mentioned equation and the values are found to be 0.225 and 0.305 respectively. Radiative rate constant K_r and total non-radiative rate constant K_{nr} have been calculated using the equation $\tau^{-1} = K_r + K_{nr}$ and $K_r = \Phi_f / \tau$ (Table. S1).

6.5.6. X-ray crystallography

The Bruker AXS D8 Quest CMOS diffractometer was used to acquire diffraction data using graphite monochromatized Mo-Kα radiation (λ = 0.71073) at 293°C and reflection data were recorded using the ω scan technique. All data were polarization and Lorentz adjusted, and the non-hydrogen atoms were anisotropically refined. The refinement procedure considered hydrogen atoms in accordance with the riding model. The structures were resolved by direct method and refined using SHELXL-2016/6 program[76] by full-matrix least-squares techniques. Details of crystal analysis, data collection and structure refinement data for **CPI** is given in Table S2 (ESI†). Some selected bond distance and angles of **CPI** is given in Table S3 (ESI†). The ORTEP view of **CPI** is shown in Fig. 1.

6.5.7. Computational study

Density functional theory (DFT) was used to optimize the full geometry of **CPI** and **CPI-CN**$^-$ using B3LYP[77] hybrid exchange correlation functional and 6-31G(d) basis set. On the optimized geometries, vibrational frequency calculations were done to make sure that each configuration is actually a local minimum on the potential energy surface. The Gaussian09 program[78] and the Gauss-View, Version 5 visualization program were used for all calculations. Electronic transitions were calculated using the time-dependent density functional theory (TDDFT) formalism[79] using conductor-like polarizable continuum model (CPCM)[80] in DMSO to simulate the solvent.

6.6. Conclusions

In this present communication, a novel carbazole-benzimidazole based colorimetric and fluorometric solvatochromic sensor (CPI) has been successfully reported which displayed selective rapid response for cyanide in both liquid and solid phase. The prominent and distinguishable color change in presence of CN^- over other co-existing competitive anions has been observed by naked eyes in day light as well as under UV lamp. The stoichiometry experiment indicates 1:1 binding ratio of CPI with CN^- ion. The observed photophysical changes are based on the formation of H-bonding followed by deprotonation of –NH fragment in imidazole ring in presence of CN^-, which induced a typical ICT process in the deprotonated CPI and is further ascertained by ^{1}H-NMR titration studies. The details of the sensing mechanism are further verified by DFT and TDDFT calculations. The LOD value of (4.48±0.19) x 10^{-8} M for CN^- detection in DMSO is very much lower than WHO recommended value (1.9 x 10^{-6} M). Due to the excellent solvatochromic behaviour, the sensor CPI can act as an environmental sensor, e.g. a solvent sensitive indicator. Additionally, the probe can be employed as a fluorescence based chemosensor for the efficient detection of trace-level water in organic solvents. Surprisingly, real samples analysis (water and foods) and test-strip response provide an extensive range of practical application of the probe for selective detection of CN^- ion in environment.

6.7. Notes and references

1. J. M. Holloway, R. A. Dahlgren, B. Hansen and W. H. Casey, Contribution of bedrock nitrogen to high nitrate concentrations in stream water, *Nature*, 1998, **395**, 785.
2. C. Caltagirone and P. A. Gale, Anion receptor chemistry: highlights from 2007, *Chem. Soc. Rev.*, 2009, **38**, 520.
3. S. V. Krivovichev, O. Mentr´e, O. I. Siidra, M. Colmont and S. K. Filatov, Anion-centered tetrahedral in inorganic compounds, *Chem. Rev.*, 2013, **113**, 6459.
4. N. Busschaert, C. Caltagirone, W. V. Rossom and P. A. Gale, Applications of supramolecular anion recognition, *Chem. Rev.*, 2015, **115**, 8038.
5. K. Yang, Y. Pei, J. Wen and Z. Pei, Recent advances in pillar[n]arenes: synthesis and applications based on host-guest interactions, *Chem. Commun.*, 2016, **52**, 9316.
6. Y. Yao, M. Xue, Z. Zhang, M. Zhang, Y. Wang and F. Huang, Gold nanoparticles stabilized by an amphiphilic pillar[5]arene: preparation, self-assembly into composite microtubes in water and application in green catalysis, *Chem. Sci*., 2013, **4**, 3667.

7. M. T. Wilson, G. Antonini, F. Malatesta, P. Sarti and M. Brunori, Probing the oxygen binding site of cytochrome c oxidase by cyanide, *J. Biol. Chem.*, 1994, **269**, 24114-24119.
8. A. V. Gourine, N. Dale, E. Liaudet, D. M. Poputnikov, K. M. Spyer and V. N. Gourine, Release of ATP in the central nervous system during systemic inflammation: real-time measurement in the hypothalamus of conscious rabbits, *J. Physiol.*, 2007, **585**, 305-316.
9. M. A. Holland and L. M. Kozlowski, Clinical features and management of cyanide poisoning, Clin. Pharmacol., 1986, **5**, 737.
10. F. J. Baud, Cyanide: critical issues in diagnosis and treatment, Hum. Exp. *Toxicol*., 2007, **26**, 191.
11. D. A. Jones, Why are so many food plants cyanogenic?, *Phytochem*., 1998, **47**, 155-162.
12. M. Zagrobelny, S. Bak and B. L. Moller, Cyanogenesis in plants and arthropods, *Phytochem*., 2008, **69**, 1457-1468.
13. D. G. Barceloux, Cyanogenic foods (cassava, kernels, and cycad seeds), *Dis. Mon.*, 2009, **55**, 336-352.
14. L. D. Tivana, J. D. C. Francisco, F. Zelder, B. Bergenstahl and P. Dejmek, Straightforward rapid spectrophotometric quantification of total anogenic glycosides in fresh and processed cassava products, *Food Chem.*, 2014, **158**, 20-27.
15. F. Wang, L. Wang, X. Chen and J. Yoon, Recent progress in the development of fluorometric and colorimetric chemosensors for detection of cyanide ions, *Chem. Soc. Rev*., 2014, **43**, 4312-4324.
16. D. Cheng, H. H. Ngo, W. Guo, S. W. Chang, D. D. Nguyen, Y. Liu, Q. Wei and D. Wei, A critical review on antibiotics and hormones in swine wastewater: water pollution problems and control approaches, *J. Hazard. Mater.*, 2020, **387**, 121682.
17. B. Zuo, Q. Deng, H. Shao, B. Cao, Y. Fan, W. Li and M. Huang, Fe_3O_4@Mesoporous-SiO2@polyaniline core-shell nanoparticles as recyclable adsorbents and reductants for hexavalent chromium, *ACS Appl. Nano Mater*., 2021, **4(2)**, 1831-1840.
18. B. Zuo, W. Li, X. Wu, S. Wang, Q. Deng and M. Huang, Recent advances in the synthesis, surface modifications and applications of core-shell magnetic mesoporous silica nanospheres, *Chem. Aian. J*., 2020, **15(8)**, 1248-1265.
19. S. Wang, H. Xu, Q. Yang, Y. Song and Y. Li, A triphenylamine-based colorimetric and "turn-on" fluorescent probe for detection of cyanide anions in live cells, *RSC Adv*., 2015, **5**, 47990-47996.
20. L. J. Tang and M. J. Cai, A highly selective and sensitive fluorescent sensor for Cu^{2+} and its complex for successive sensing of cyanide via Cu^{2+} displacement approach, *Sens. Actuators, B*, 2012, **173**, 862.
21. I. J. Kim, M. Ramalingam and Y. A. Son, A reaction based colorimetric chemosensors for the detection of cyanide ion in aqueous solution, *Sens. Actuators, B*, 2017, **246**, 319.
22. Y.-Y. Guo, X.-L. Tang, F.-P. Hou, J. Wu, W. Dou, W.-W. Qin, J.-X. Ru, G.-L. Zhang, W.-S. Liu and X.-J. Yao, A reversible fluorescent chemosensor for cyanide in 100% aqueous solution, *Sens. Actuators, B, Chem.*, 2013, **181**, 202.

23. R. Misra, T. Jadhav, B. Dhokale and S. M. Mobin, Colorimetric and fluorimetric detection of fluoride and cyanide ions using tri and tetra coordinated boron containing chromophores, *Dalton Trans*., 2015, **44**, 16052.
24. T. S. Reddy, R. Maragani and R. Misra, Triarylborane substituted naphthalimide as a fluoride and cyanide ion sensor, *Dalton Trans*., 2016, **45**, 2549.
25. R. Maragani, T. S. Reddy and R. Misra, C_s-symmetric triarylborane substituted bisthiazole for selective detection of F^- and CN^- ions, *Tetrahedron Lett*., 2016, **57**, 3853.
26. A. Maji, A. Biswas, A. Das, S. Gharami, K. Aich and T. K. Mondal, A novel carbazole-benzothiazole based chemodosimeter for chromogenic and fluorogenic recognition of CN^-, *New J. Chem*., 2023, **47**, 11557-11564.
27. Q. Zou, J. Du, C. Gu, D. Zhang, F. Tao and Y. Cui, A new dibenzothiophene-based dual-channel chemosensor for cyanide with aggregation induced emission, *J. Photochem. Photobiol. A*, 2021, **405**, 112993.
28. V. Kumar, M. P. Kaushik, A. K. Srivastava, A. Pratap, V. Thiruvenkatam and T. N. Row, Thiourea based novel chromogenic sensor for selective detection of fluoride and cyanide anions in organic and aqueous media, *Anal. Chim. Acta*, 2010, **663**, 77.
29. M. Shahid, S. S. Razi, P. Srivastava, R. Ali, B. Maiti and A. Misra, A useful scaffold based on acenaphthene exhibiting Cu^{2+} induced excimer fluorescence and sensing cyanide via Cu^{2+} displacement approach, *Tetrahedron*, 2012, **68**, 9076.
30. N. Kumari, S. Jha, and S. Bhattacharya, Colorimetric probes based on anthraimidazolediones for selective sensing of fluoride and cyanide ion via intramolecular charge transfer, *J. Org. Chem*., 2011, **76**, 8215–8222.
31. J. You, H. Jeong, H. Seo, and S. Jeon, A new fluoride ion colorimetric sensor based on dipyrrolemethanes, *Sens. Actuators, B*, 2010, **146**, 160–164.
32. P. Piatek, J. Jurczak, A selective colorimetric anion sensor based on an amide group containing macrocycle, *Chem. Commun*., 2002, **20**, 2450–2451.
33. Y. Zhang, and S. Jiang, Fluoride-responsive geletor and colorimetric sensor based on simple and easy-to-prepare cyano-substituted amide, *Org. Biomol. Chem*., 2012, **10**, 6973-6979.
34. X. Bao and Y. Zhou, Synthesis and recognition properties of a class of simple colorimetric anion chemosensors containing OH and CONH groups, *Sens. Actuators, B*, 2010, **147**, 434–441.
35. P. A. Gale, Synthesis indole, carbazole, biindole and indolocarbazole-based receptors: applications in anion complexation and sensing, *Chem. Commun*., 2008, **38**, 4525–4540.
36. S. Wang, J. Chir, Y. Jhong, and A. Wu, A turn-on fluorescent sensor for detection of cyanide in aquesous media, *J. Lumin*., 2015,**167**, 413–417.
37. W. Huang, X. Yu, H. Lin, and H. Lin, A colorimetric sensor for the recognition of biologically important anions, *J. Incl. Phenom. Macrocycl Chem*., 2011, **69**, 69–73.
38. Y. Jiang, L. Sun, G. Ren, X. Niu, and Z. Hu, A novel colorimetric and fluorescent iminocoumarin-based chemosensor for acetate ion and its application to living cell imaging, *Talanta*, 2016, **146**, 732–736.

39. W. I. S. Galpothdeniya, B. P. Regmi, K. S. McCarter, S. L. D. Rooy, N. Siraj and I. M. Warner, Virtual colorimetric sensor array: single ionic liquid for solvent discrimination, *Anal. Chem*., 2015, **87**, 4464; J. C. de Jesus, P. A. R. Pires, R. Mustafa, N. Riaz and O. A. El Seoud, Experimental and theoretical studies on solvation in aqueous solutions of ionic liquids carrying different side chains: the n-butyl-group versus the methoxyethyl group, *RSC Adv*., 2017, **7**, 15952.

40. R. Christian, Solvatochromic dyes as solvent polarity indicators, Chem. Rev., 1994, **94**(8), 2319; Y. Li, T. Tan, S. Wang, Y. Xiao and X. Li, Highly solvatochromic fluorescence of anthraquinone dyes based on triphenylamines, *Dyes Pigm*., 2017, **144**, 262.

41. Z. L. Zhen, Z. Rui, L. Z. Yi, G. J. Zi and Z. G. He, Solvatochromic behavior of a nanotubular metal-organic framework for sensing small molecules, *J. Am. Chem. Soc*., 2011, **133**, 4172; S. Gao, L. Zhao, L. Han, Z. Zhang and H. Zhao, Synthesis, structure and characterization of two solvatochromic metal-organic frameworks for chemical sensing applications, *CrystEngComm*, 2018, **20**, 2237–2240.

42. S. Takagi, S. Tetsuya, M. Dai, T. Hiroshi, I. Yohei and A. T. Donald, Unique solvatochromism of a membrane composed of a cationic porphyrin-clay complex, *Langmuir*, 2010, **26**, 4639; Y. Choi, S. Kim, Y. Choi, J. Song, T.-H. Kwon, O.-H. Kwon and B.-S. Kim, Morphology tunable hybrid carbon nanosheets with solvatochromism, *Adv. Mater*., 2017, **29**, 1701075.

43. D. Racz, M. Nagy, A. Mandi, M. Zsuga and S. Keki, Solvatochromic properties of a new isocyanonaphthalene based fluorophore, *J. Photochem. Photobiol. A,* 2013, **270**, 19; H. Bouvrain, T. Pott, L. A. Bagatolli, J. H. Ipsen and P. Meleard, Impact of membrane-anchored fluorescent probes on the mechanical properties of lipid bilayers, *Biochim. Biophys. Acta*, 2010, **1798**, 1333.

44. G. Feng, Z. Wang, X. Yu, H. Lan, J. Ren, L. Geng and T. Yi, An ultrasound triggered gelation approach to selectivity solvatochromic sensors, *Sens. Actuators, B*, 2017, **243**, 1020.

45. D.-H. Park, B. Kim and J.-M. Kim, A tetrahydrofuran-selective optical solvent sensor based on solvatochromic polydiacetylene, *Bull. Korean Chem. Soc*., 2016, **37**, 793.

46. Y. Zhang, C. Liang and S. Jiang, A solvatochromic cyanostilbene derivative as an intensity and wavelength-based fluorescent sensor for water in organic solvents, *New J. Chem.*, 2017, **41**, 8644-8649.

47. W. Liu, Y. Wang, W. Jin, G. Shen and R. Yu, Solvatochromogenic flavone dyes for the detection of water in acetone, *Anal. Chim. Acta*, 1999, **383**,299-330; H. Mishra, V. Mishra, M. S. Meheta, T. C. Pant and H. B. Tripathi, Fluorescence studies of salicyclic acid doped in polyvinyl alcohol film as a water humidity sensor, *J. Phys. Chem. A*, 2004, **108**, 2346-2352; J. S. Kim, M. G. Choi, Y. Huh, M. H. Kim, S. H. Kim, S. Y. Wang and S. K. Chang, Determination of water content in aprotic organic solvents using 8-hydroxyquinoline based fluorescent probe, *Bull. Korean Chem. Soc*., 2006, **27**, 2058-2060.

48. D. Citterio, K. Minamihashi, Y. Kuniyoshi, H. Hisamoto, S. Sasaki and K. Suzuku, Optical determination of low-level water concentrations in organic solvents using fluorescent acridinyl dyes and dye-immobilized polymer membranes, *Anal. Chem*., 2001, **73**, 5339-5345; C. G. Niu, A. L. Guan, G. M. Zeng, Y. G. Liu and Z. W. Li, Fluorescence water sensor based on covalent immobilization of chalcone derivative, *Anal. Chim. Acta,* 2006, **577**, 264-270; Y. Zhang, D. Li, Y. Li and J. Yu, Solvatochromic AIE iuminogens as

supersensitive water detection in organic solvents and highly efficient cyanide chemosensors in water, *Chem. Sci.*, 2014, **5**, 2710-2716.

49. G. Men, G. R. Zhang, C.S. Liang, H. I. Liu, B. Yang, Y. Y. Pan, Z. Y. Wang and S. M. Jiang, A dual channel optical detector for trace water chemodosimetry and imaging of live cells, *Analyst*, 2013, **138**, 2847-2857*;* G. Men, C. Chen, C. Liang, W. Han and S. Jiang, A novel cascade strategy with supermolecular and chemodosimetric methods for designing a fluorescent ratiometric detector hypersensitive to trace water, *Analyst*, 2015, **140**, 5454-5458;W. Y. Kim, H. Shi, H. S. Jung, D. Cho, P. Verwilst, J. Y. Lee and J. S. Kim, Coumarin- decorated Schiff base hydrolysis as an efficient driving force for the fluorescence detection of water in organic solvents, *Chem. Commun.*, 2016, **52**, 8675-8678.
50. Y. Ooyama, A. Matsugasako, K. Oka, T. Nagano, M. Sumomogi, K. Komaguchi, I. Imae and Y. Harima, Fluorescence PET (photo-induced electron transfer) sensors for water based on antracene-boronic acid ester, *Chem. Commun.*, 2011, **47**, 4448-4450;Y. Ooyama, H. Egawa and K. Yoshida, The design of a novel fluorescent PET sensor for proton and water: A phenylaminonaphtho[1,2-d]oxazol-2yl-type fluorophore containing proton donor and acceptor groups, *Dyes Pigm.*, 2009, **82**, 58-64;Y. Ooyama, M. Hota, T. Enoki, S. Aoyama, K. Furue, N. Tsunoji and J. Ohshita, A BODIPY sensor for water based on a photo-induced electron transfer method with fluorescence enhancement and attenuation systems, *New J. Chem.*, 2016, **40**, 7278-7281.
51. D. L. Deng, Y. L. Li, J. H. Wu, Y. Liu, G. Z. Fang, S. O. Wang and Y. K. Zhang, *Chem. Commun.*, 2012, **48**, 3009-3011*;* D. Wang, H. Zhao, H. Li, S. Sun and Y. Xu, A fluorescent "glue" of water triggered hydrogen-bonding cross-linking, *J. Mater.* Chem. C, 2016, **4**, 11050-11054.
52. M. Shimizu and T. Hiyama, Organic fluorophores exhibiting highly efficient photoluminescence in the solid state, *Chem. Asian J*., 2010, **5**, 1516-1531.
53. Z. Zhang, B. Xu, J. Su, L. Shen, Y. Xie and H. Tian, Color-tunable soli-state emission of 2,2'-biindenyl-based fluorophores, *Angew. Chem., Int. Ed*., 2011, **50**, 11654-11657.
54. H.-L. Liu, X.-L. Hou and L. Pu, Enantioselective precipitation and solid state fluorescence enhancement in the recognition of α-hydroxycarboxylic acids, *Angew. Chem., Int. Ed.*, 2009, **48**, 382-385.
55. I. D. W. Samuel and G. A. Turnbull, Organic semiconductors lasers, *Chem. Rev*., 2007, **107**, 1272-1295
56. A. P. Kulkarni, C. J. Tonzola, A. Babel and S. A. Jenekhe, Electron transport materials for organic light-emitting diodes, *Chem. Mater*., 2004, **16**, 4556-4573.
57. Introduction to Organic Electronics and Optoelectronic Materials and Devices Vol.**2** (Eds:). TAYLOR & FRANCIS, New York, 2008, 130-167)
58. S.-W. Zhang and T. M. Swager, Fluorescent detection of chemical warfare agents: functional group specific ratiometric chemosensors, *J. Am. Chem. Soc*., 2003, **125**, 3420-3421.
59. J.-S. Yang and T. M. Swager, Porous shape persistent fluorescent polymer films: an approach to TNT sensory materials, *J. Am. Chem. Soc*., 1998, **120**, 5321-5322.
60. A. C. Arias, J. D. MacKenzie, I. McCulloch, J. Rivnay and A. Salleo, Materials and applications for large area electronics: solution-based approaches, *Chem. Rev*., 2010, **110**, 3-24.

61. (a) E. Lippert, Dipolmoment und elektronenstruktur von angeregten molekülen, Z. Naturforsch A, 1955, **10a**, 541-545; (b) N. Mataga, Y. Kaifu and M. Koizumi, Solvent effects upon fluorescence spectra and the dipole moments of excited molecules, *Bull. Chem. Soc. Jpn*., 1956, **29**, 465-470.
62. S. Uzan, Determination of water content in dimethyl sulfoxide/N, N-dimethyl formamide and methanol content in ethanol by solvatochromism azo dye, 2-(tert-butyl)-4-methoxy-6-(naphthalene-1-yldiazenyl) phenol, *Anal. Chim. Acta*, 2023, **1239**, 340747.
63. X. L. Guan, T. M. Jia, D. H. Zhang, Y. Zhang, H. C. Ma, D. D. Lu, S. J. Lai and Z. Q. Lei, A new solvatochromic linear π-conjugated dye based on phenylene-(poly)ethynylene as supersensitive low-level water detector in organic solvents, *Dyes Pigm*., 2017, **136**, 873-880
64. J. Nootem, C. Sattayanoon, S. Namuangruk, P. Rashatasakhon, W. Wattanathana, G. Tumcharern and K. Chansaenpak, Solvatochromic triazaborolopyridinium probes toward ultra-sensitive trace water detection in organic solvents, *Dye Pigm*., 2020, **181,** 108554
65. Y. Zhang, D. Li and Y. Li and J. Yu, Solvatochromic AIE luminogens as supersensitive water detectors in organic solvents and highly efficient cyanide chemosensors in waters, *Chem. Sci*., 2014, **5**, 2710
66. F. Hou, X. Liu, X. Hao, G. Li, F. Lu and Q. Deng, New benzotriazole-based D-A-D type solvatochromic dyes for water content detection in organic solvents, *Dye Pigm*., 2021, **195**, 109667
67. S. OğuzTümay, A. Şenocak and A. Mermer, A "turn-on" small molecule fluorescent sensor for the determination of Al^{3+} ion in real samples: theoretical calculations, and photophysical and electrochemical properties, *New J. Chem*., 2021, **45**, 18400-18411.
68. M. J. Kim, R. Manivannan, I. J. Kim and Y. Son, A colorimetric and fluorometric chemosensor for the selective detection of cyanide ion in both the aqueous and solid phase, *Sens. Actuators, B*, 2017, **253**, 942-948.
69. C. Nandhini, P.S. Kumar, K. Poongodi, R. Shanmugapriya and K. P. Elango, A multi-site probe for selective detection of cyanide and sulphite ions via different mechanisms with concomitant different fluorescent behaviors, *J. Mol. Liq.*, 2021, **327**, 114833.
70. C.-B Bai, J. Zhang, R. Qiao, Q.-Y. Zhang, M.-Y. Mei, M.-Y. Chen, B. Wei, C. Wang and C.-Q. Qu, Reversible and selective turn-on fluorescent and naked-eye colorimetric sensor to detect cyanide in tap water, food samples, and living systems, *Ind. Eng. Chem. Res*., 2020, **59**, 8125-8135.
71. R. Bhaskar, V. Vijayakumar, V. Srinivasadesikan, S. Lee and S. Sarveswari, Rationally designed imidazole derivative as colorimetric and fluorometric sensor for selective, qualitative and quantitative cyanide ion detection in real time samples, *Spectrochim. Acta A*, 2020, **234**, 118212.
72. P. S. Kumar, P. R. Lakshmi and K. P. Elango, An easy to make chemoreceptor for the selective ratiometric fluorescent detection of cyanide in aqueous solutiond in food materials, *New J. Chem*., 2019, **43**, 675.
73. Z. Guo, T. Hu, T. Sun, T. Li, H. Chi and Q. Niu, A colorimetric and fluorometric oligothiophene-indenedione-based sensor for rapid and highly sensitive detection of cyanide in real samples and bioimaging in living cells, *Dyes Pigm*, 2019, **163**, 667-674.

74. B. Patil, J. Lade, S. Chiou, Y. Cheng, Y. Lin, Y. Jadhav, P. Chetti, C. Chang and A. Chaskar, Carbazole/triphenylamine-cyanobenzimidazole hybrid bipolar host materials for green phosphorescent organic light-emitting diodes, *Org. Electron.*, 2021, **92**, 106090.
75. L. Patra, K. Aich, S. Gharami and T. K. Mondal, Fabrication of a new fluorogenic probe for detection of phosgene in solution and vapour phase, *Sens. Actuators, B*, 2021, **326**, 128837.
76. G. M. Sheldrick, A short history of SHELX, *Acta Cryst.*, 2008, **A64**, 112; G. M. Sheldrick, SHELXT-Integrated space-group and crystal-structure determination, *Acta Cryst.*, 2015, **C71**, 3.
77. A. D. Becke, Density-functional thermochemistry III. The role of exact exchange, *J. Chem. Phys.*, 1993, **98**, 5648.
78. Gaussian 09, Revision D.01, M. J. Frisch, G. W. Trucks, H. B. Schlegel, G. E. Scuseria, M. A. Robb, J. R. Cheeseman, G. Scalmani, V. Barone, B. Mennucci, G. A. Petersson, H. Nakatsuji, M. Caricato, X. Li, H. P. Hratchian, A. F. Izmaylov, J. Bloino, G. Zheng, J. L. Sonnenberg, M. Hada, M. Ehara, K. Toyota, R. Fukuda, J. Hasegawa, M. Ishida, T. Nakajima, Y. Honda, O. Kitao, H. Nakai, T. Vreven, J. A. Montgomery, Jr., J. E. Peralta, F. Ogliaro, M. Bearpark, J. J. Heyd, E. Brothers, K. N. Kudin, V. N. Staroverov, R. Kobayashi, J. Normand, K. Raghavachari, A. Rendell, J. C. Burant, S. S. Iyengar, J. Tomasi, M. Cossi, N. Rega, J. M. Millam, M. Klene, J. E. Knox, J. B. Cross, V. Bakken, C. Adamo, J. Jaramillo, R. Gomperts, R. E. Stratmann, O. Yazyev, A. J. Austin, R. Cammi, C. Pomelli, J. W. Ochterski, R. L. Martin, K. Morokuma, V. G. Zakrzewski, G. A. Voth, P. Salvador, J. J. Dannenberg, S. Dapprich, A. D. Daniels, Ö. Farkas, J. B. Foresman, J. V. Ortiz, J. Cioslowski and D. J. Fox, Gaussian, Inc., Wallingford CT, 2009.
79. R. E. Stratmann, G. E. Scuseria and M. J. Frisch, An efficient implementation of time-dependent density-functional theory for the calculation of excitation energies of large molecules, *J. Chem. Phys.*,1998, **109**, 8218.
80. M. Cossi, N. Rega, G. Scalmani and V. Barone, Energies, structures, and electronic properties of molecules in solution with the C-PCM solvation model, *J. Comput. Chem.*, 2003, **24**, 669.

APPENDIX

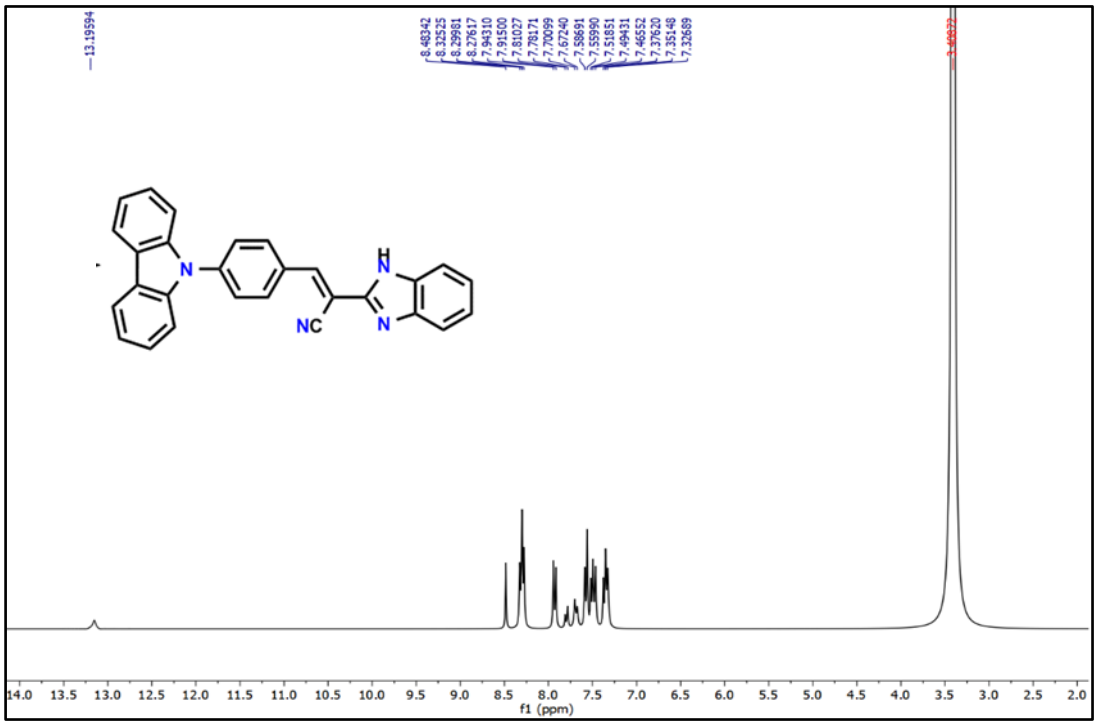

Fig. A6.1: ^{1}H NMR (300 MHz) spectra of the probe CPI in DMSO-d_6

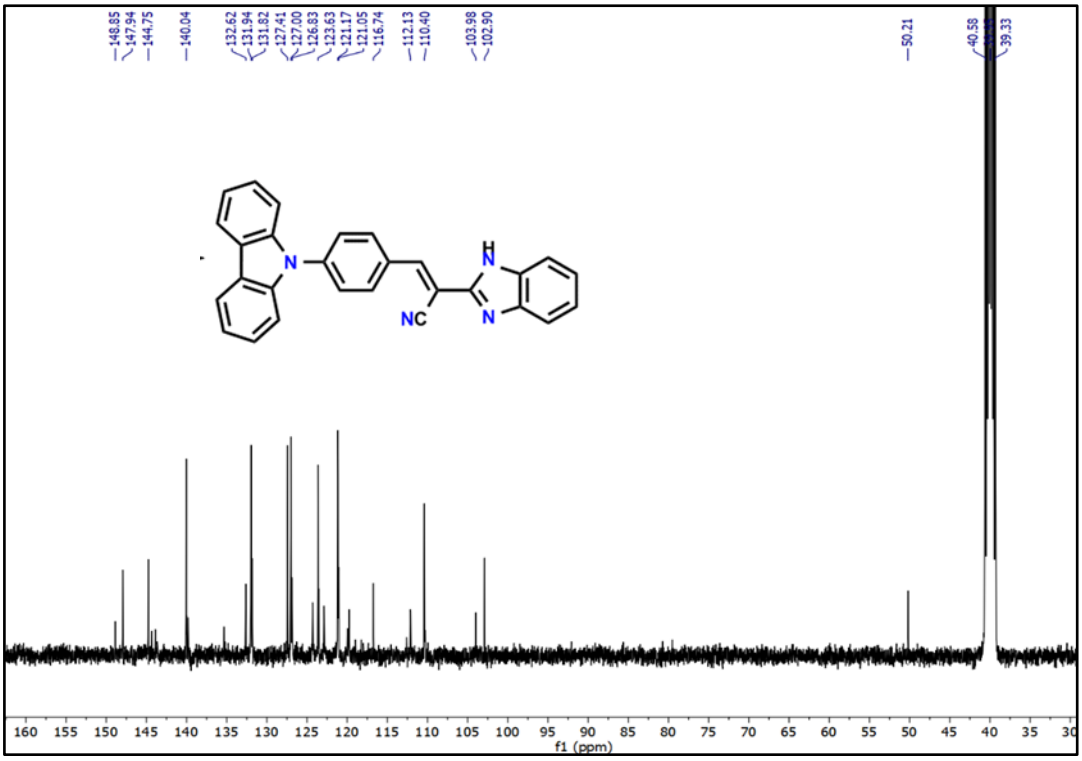

Fig. A6.2: ^{13}C NMR (75 MHz) spectra of the receptor (CPI) in DMSO-d_6.

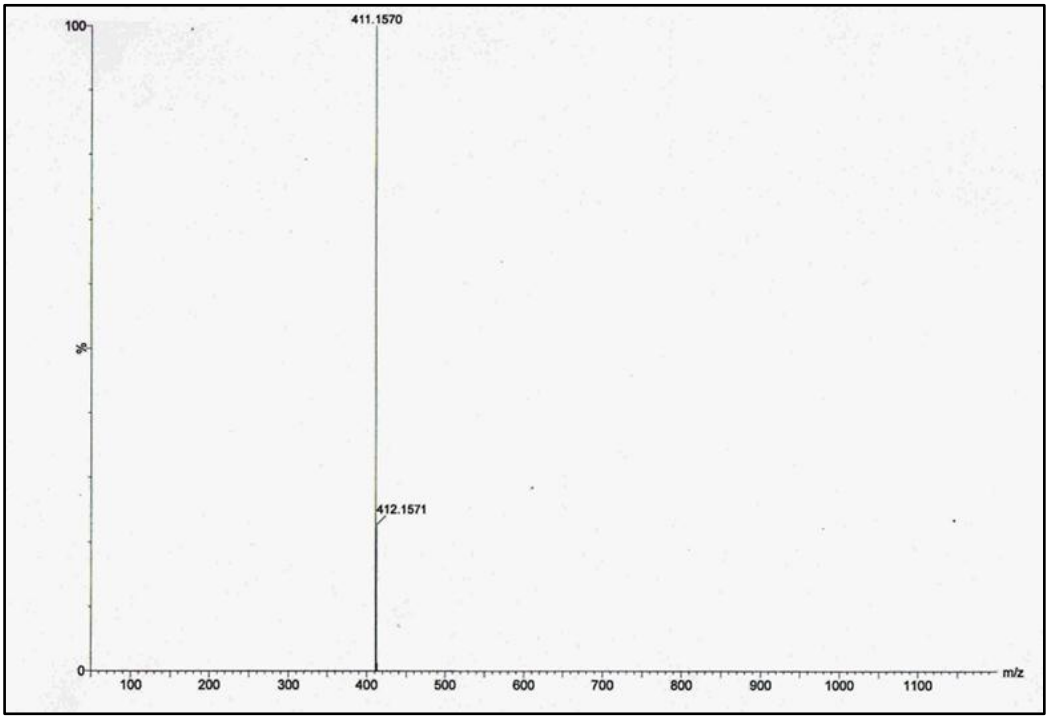

Fig. A6.3: HRMS of the receptor (CPI)

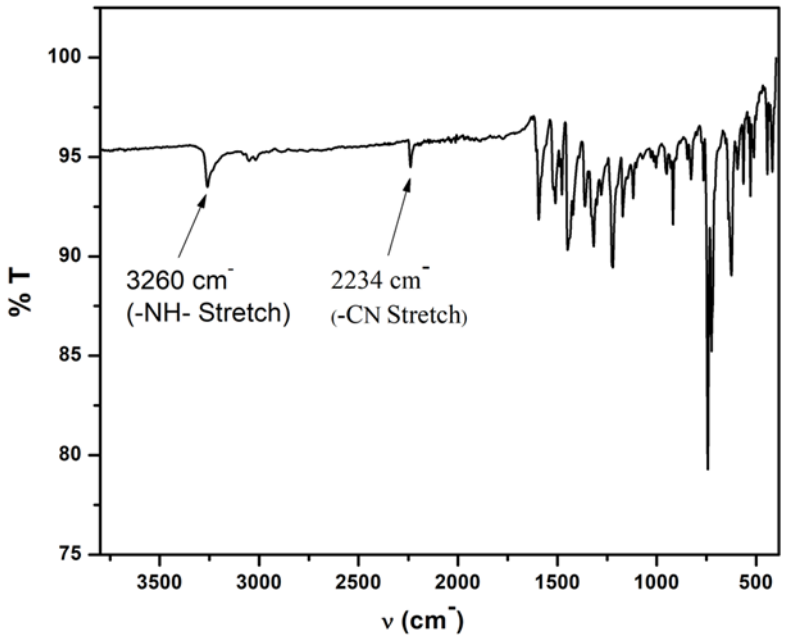

Fig. A6.4: IR Spectrum of CPI

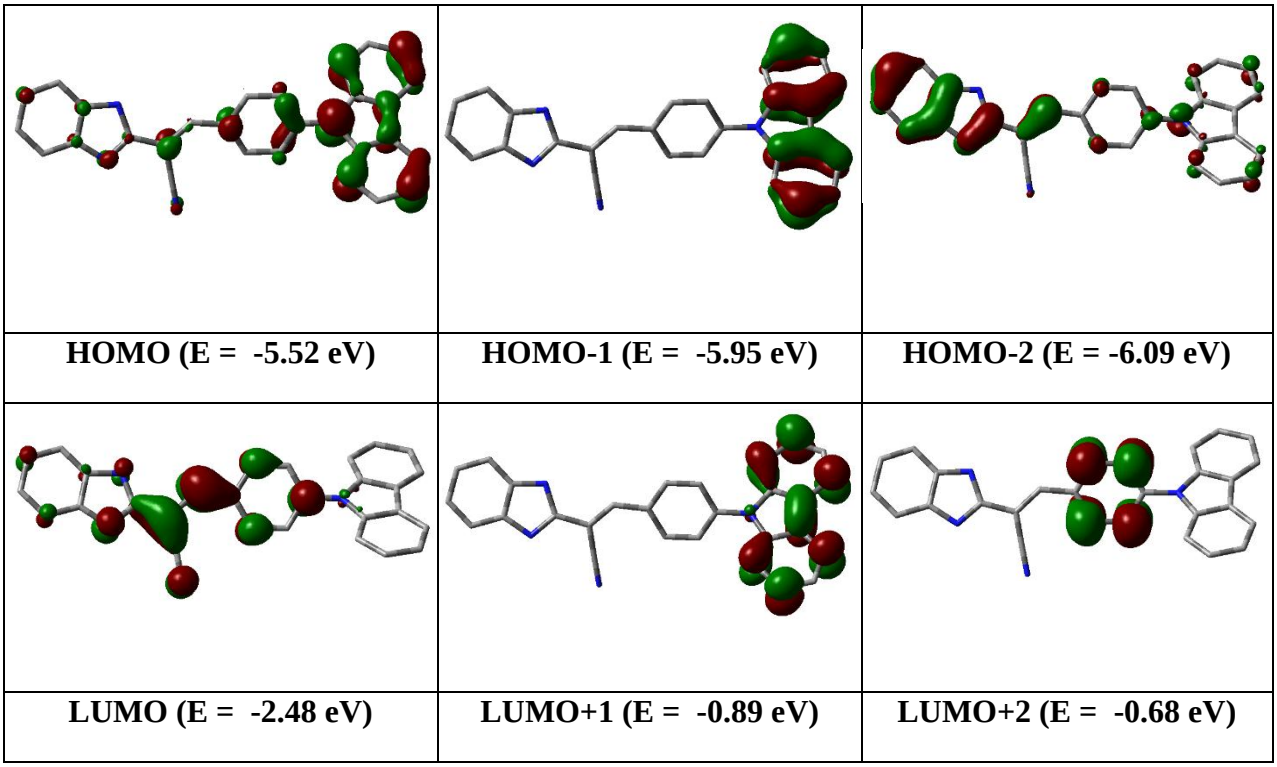

Fig. A6.5: Contour plots of some selected molecular orbitals of CPI.

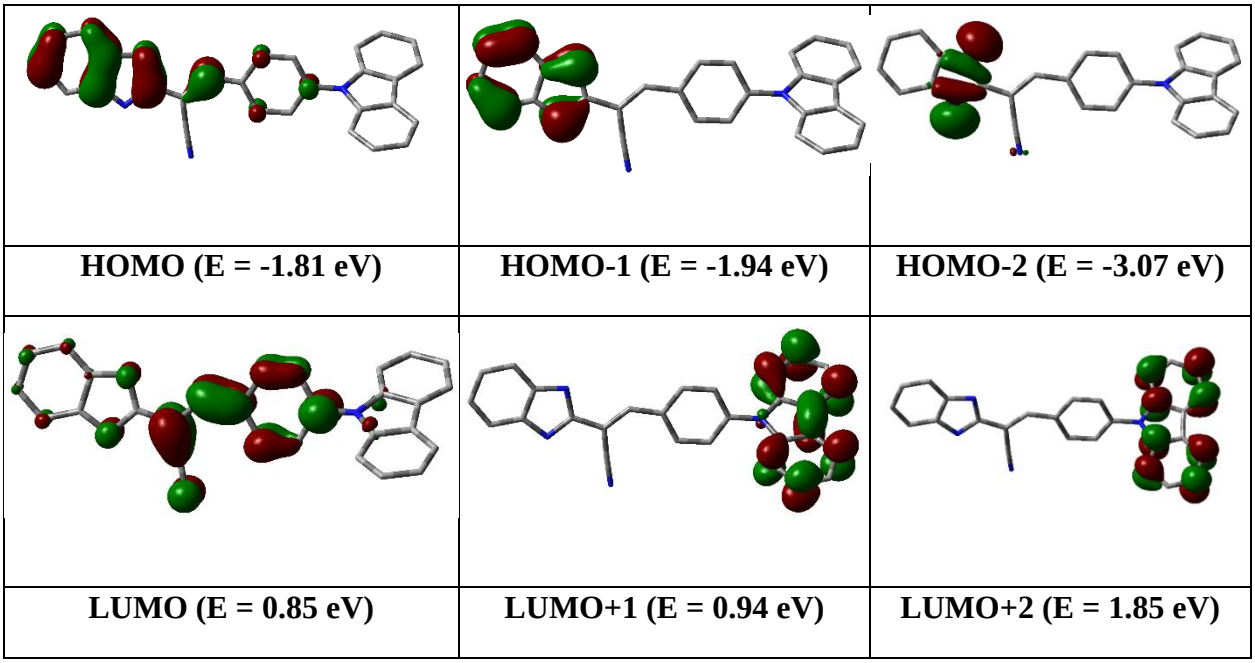

Fig. A6.6: Contour plots of some selected molecular orbitals of CPI^{-}.

Table A6.1. Crystallographic data and refinement parameters of the sensor (**CPI**)

Chemical formula	C28 H18 N4
Formula weight	410.46
Temperature of study	293(2)
Crystal system	*orthorhombic*
Space group	*Pbca*
a, b, c [Å]	9.1730(7), 19.8496(16), 25.741(2)
α/ β/ γ [°]	90
V [$Å^3$]	4686.9(7)
Z	8
D(calc) [g/cm^3]	1.163
Mu(MoKa) [/mm]	0.070
Radiation [Å]	0.71073
F(000)	1712
θ(Min-Max) [°]	2.052-25.048
Dataset (h; k; l)	-10 to 10, -21 to 23, -25 to 30
Total collected data	32712
Unique data [R_{int}]	4130 [0.0674]
Refined parameters	325
R, wR_2	0.0813, 0.2197
Goodness of fit	1.034
Residual density	-0.346/0.403
CCDC Number	2287312

Table A6.2. Selected X-ray and calculated bond distances and angles of the sensor (**CPI**)

Bonds(Å)	X-ray	Calc.
N1 – C1	1.364(4)	1.31654
N1 – C7	1.383(4)	1.38191
N2 – C1	1.312(4)	1.38581
N2 – C2	1.386(4)	1.38391
N3 – C9	1.140(5)	1.16337
C1 – C8	1.463(4)	1.46462
C8 – C9	1.434(5)	1.43369
C8 – C10	1.339(5)	1.36552
C10 – C11	1.452(4)	1.45505
Angles(°)	X-ray	Calc.
C1–N1–C7	106.5(3)	105.36614
C1–N2–C2	105.5(3)	106.99332
N2–C1–N1	112.8(3)	112.61983
N2–C1–C8	124.8(3)	123.45340
N1–C1–C8	122.4(3)	123.92247
C10–C8–C9	122.7(3)	123.09967
C10–C8–C1	122.2(3)	122.51273
C9–C8–C1	115.2(3)	114.38222
N3–C9–C8	176.9(4)	178.70198

Table A6.3. Vertical electronic transitions of CPI and CPI^- calculated by TDDFT/CPCM method

Compd.	λ (nm)	E (eV)	Osc. Strength (f)	Key excitations	Character
CPI	468.32	2.6474	0.7727	(99%) HOMO→LUMO	$\pi \rightarrow \pi^*$
	377.16	3.2873	0.5368	(97%) HOMO-2→LUMO	$\pi \rightarrow \pi^*$
CPI^-	473.41	2.6189	0.7941	(85%) HOMO→LUMO	$\pi \rightarrow \pi^*$
	448.02	2.7674	0.3516	(86%) HOMO-1→LUMO	$\pi \rightarrow \pi^*$

Table A6.4: Determination of Fluorescence life-time data, quantum yield, radiative and non-radiative rate constants

Compd.	Quantum yield(φ)	τ(ns)	$K_r(10^8 \times S^{-1})$	$K_{nr}(10^8 \times S^{-1}$
CPI	0.225	2.95	0.7627	2.6271
CPI-CN^-	0.305	3.51	0.8689	1.9801

Table A6.5: Sensing performance of CPI towards CN^- compared to other previously reported receptors.

Probe	Solvent System	Detection limit	Reaction time	Reference
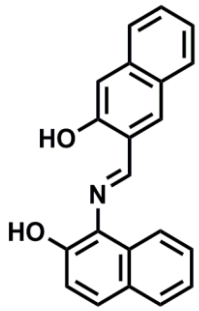	DMF:H_2O (1:1, v/v	0.21 µM		**[1]**
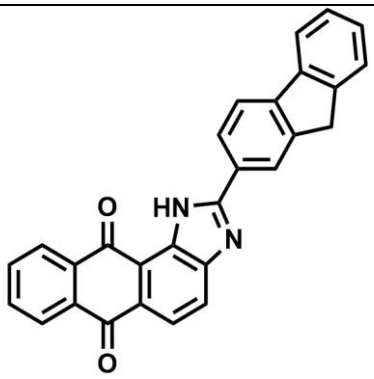	CH_3CN-H_2O(8:2, pH=3-10	4.11×10^{-8} M		**[2]**
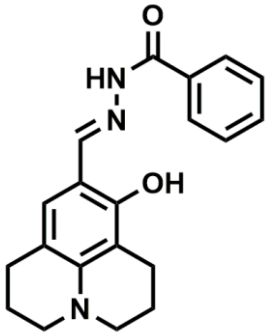	CH_3CN-H_2O (v/v, 19:1)	9.4×10^{-10} M		**[3]**
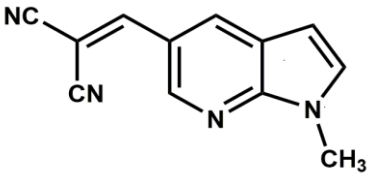	THF-H_2O (9:1)	2×10^{-6} M		**[4]**

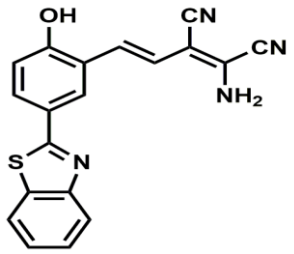	DMSO/H_2O(7:3)	1.4×10^{-7} M		**[5]**
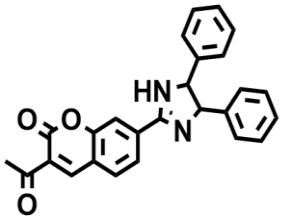	Dioxane	1.0 µM	Within 60 s	**[6]**
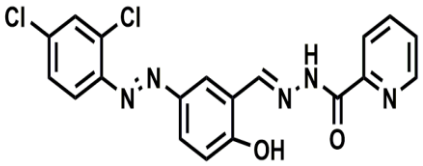	DMSO-H2O (6:4,v/v), pH=7.1	6.4 µM		**[7]**
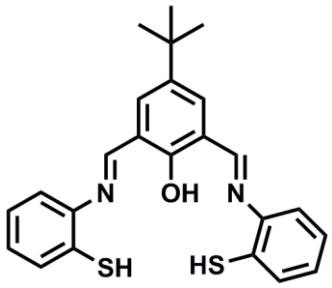	DMSO-H_2O (20-80% v/v)	0.96 µM		**[8]**
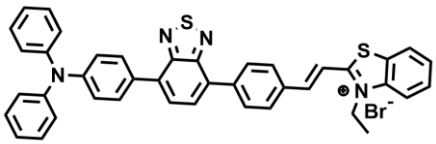	H_2O/THF(8:2)	$1.3x10^{-7}$ M		**[9]**
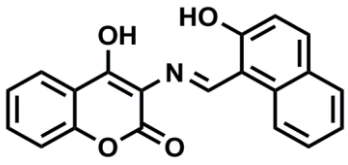	DMSO	0.11 µM		**[10]**

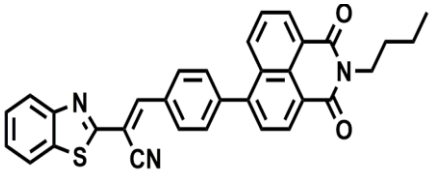	THF	0.034 µM		**[11]**
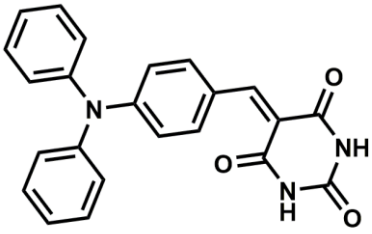	DMSO/H_2O (1:99**)**	2.95×10^{-8} M		**[12]**
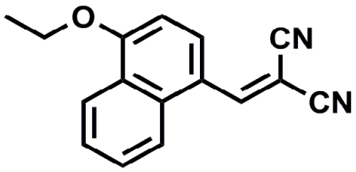	THF-H2O (9:1, V/V), HEPES Buffer, pH=7.3	1.1×10^{-6} M		**[13]**
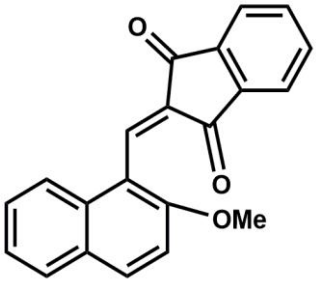	H_2O-DMF(9:1,v/v)	1.15-1.2 nM	10-30 sec	**[14]**
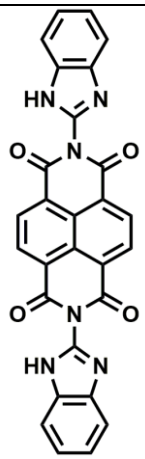	DMSO-H2O (9:1, V/V), HEPES Buffer, pH=6-9	8.32×10^{-7} M	Less than 1 min	**[15]**

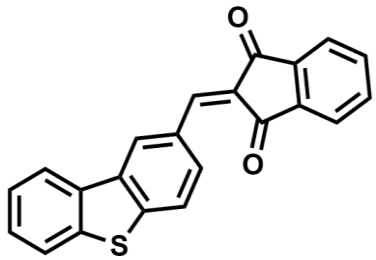	DMSO/H_2O (1:99,v/v)	2.26×10^{-7} M	15 sec	**[16]**
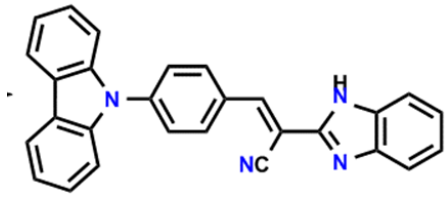	DMSO	4.48×10^{-8} M	50 sec	**Present work**

References

1. B. Yilmaz, M. Keskinates, Z. Aydin and M. Bayrakci, A highly selective optical sensor for the detection of cyanide ions in aqueous solution and living cells, *J. Photochem. Photobiol. A*, 2022, **424**, 113651.
2. R. Bhaskar, V. Vijayakumar, V. Srinivasadesikan, S. Lee and S. Sarveswari, Rationally designed imidazole derivative as colorimetric and fluorometric sensor for selective, qualitative and quantitative cyanide ion detection in real time samples, *Spectrochim. Acta A*, 2020, **234**, 118212.
3. C.-B. Bai, J. Zhang, R. Qiao, Q.-Y. Zhang, M.-Y. Mei, M.-Y. Chen, B. Wei, C.-Q. Wang and C. Qu, Reversible and selective turn on fluorescent and naked-eye colorimetric sensor to detect cyanide in tap water, food samples, and living systems, *Ind. Eng. Chem. Res*., 2020, **59**, 8125-8135.
4. K.-Y. Chen and W.-C. Lin, A simple 7-azaindole-based ratiometric fluorescent sensor for detection of cyanide in aqueous media, *Dyes Pigm.*, 2015, **123**, 1-7.
5. S. Malkondu, S. Erdemir and S. Karakurt, Red and blue emitting fluorescent probe for cyanide and hypochlorite ions: Biological sensing and environmental analysis, *Dyes Pigm*., 2020,**174**,108019.
6. R. Ali, S. K. Dwivedi, H. Mishra and A. Misra, Imidazole-Coumarin containing D-A type fluorescent probe: synthesis photophysical properties and sensing behaviour for F^- and CN^- anions, *Dyes Pigm*., 2020, **175**, 108163.
7. Z. Li, C. Liu, S. Wang, L. Xiao and X. Jing, Visual detection of cyanide ion in aqueous medium by a new chromogenic azo-azomethine chemosensor, *Spectrochim. Acta A*, 2018, **210**, 321-328.
8. P. S. Kumar, P. R. Lakshmi and K. P. Elango, An easy to make chemoreceptor for the selective ratiometric fluorescent detection of cyanide in aqueous solution and in food materials, *New J. Chem*., 2019, **43**, 675.

9. B. Zhai, Z. Hu, C. Peng, B. Liu, W. Li and C. Gao, Rational design of a colorimetric and fluorescence turn-on chemosensor with benzothiazolium moiety for cyanide detection in aqueous solution, *Spectrochim. Acta A*, 2020, **224**, 117409.
10. Z. Aydin, M. Keskinates, B. Yilmaz, M. Durmaz and M. Bayrakci, A rapid responsive coumarin-naphthalene derivative for the detection of cyanide ions in cell culture, *Anal. Biochem*., 2022, **654**, 114798.
11. T. S. Reddy, H. Moon and M. S. Choi, Turn-on fluorescent naphthalimide-benzothiazole probe for cyanide detection and its two-mode aggregation-induced emission behavior, *Spectrochim. Acta A*, 2021, **252**, 119535.
12. B. Zuo, L. Liu, X. Feng, D. Li, W. Li, M. Li, M. Huang and Q. Deng, A novel fluorescent sensor based on triphenylamine with AIE properties for the highly sensitive detection of CN^-, *Dyes Pigm*., 2021, **193**, 109534.
13. S. D. Padghan, C. Wang, W. Liu, S. Sun, K. Liu and K. Chen, A naphthalene-based colorimetric and fluorometric dual-channel chemodosimeter for sensing cyanide in a wide pH rang, *Dyes Pigm*., 2020, **183**, 108724.
14. N. Maurya and A. K. Singh, Selective naked eye and "turn-on" fluorescence chemodosimeter for CN- by activated Michael acceptor possessing different polar substituents: reduced ICT-based signal transduction, *Sens. Actuators, B*, 2017, **245**, 74–80.
15. Q. Lin, L. Liu, F. Zheng, P. Mao, J. Liu, Y. Zhang, H. Yao and T. Wei, A benzimidazole functionalized NDI derivative for recyclable fluorescent detection of cyanide in water, *RSC Adv*., 2017, **7**, 38458.
16. Q. Zou, J. Du, C. Gu, D. Zhang, F. Tao and Y. Cui, A new dibenzothiophene–based dual channel chemosensor for cyanide with aggregation induced emission, *J. Photochem. Photobiol. A*, 2021, **405**, 112993.

A chemodosimetric approach for visual detection of nerve agent simulant diethyl chlorophosphate (DCP) in liquid and vapour phase

A chemodosimetric approach for visual detection of nerve agent simulant diethyl chlorophosphate (DCP) in liquid and vapour phase

Abstract

In this work, a novel fluorescent ratiometric switch, 8-((6-(1H-benzo[d]imidazol-2-yl) pyridin-2-yl) methoxy)quinoline (BIPQ) has been introduced for sensing of organophosphorus (OP) chemical vapor threat, diethyl chlorophosphate (DCP), the low toxic mimic of real nerve agent sarin (GB). BIPQ is efficient to detect DCP in both solution as well as in gaseous phase and has potential practical application with high sensitivity and selectivity. The probe shows significant ratiometric emission in presence of DCP along with the distinct color change from blue to cyan under UV light. Sensing mechanism of the chemodosimeter is based on the generation of new adduct, BIPQ-DCP through nucleophilic substitution reaction with DCP followed by a ring closure process to form the final product. The detection limit of BIPQ for DCP was determined to be in the order of 10^{-8} (M) in liquid state. DFT and TDDFT computational techniques were carried out in order to interpret the electronic properties theoretically.

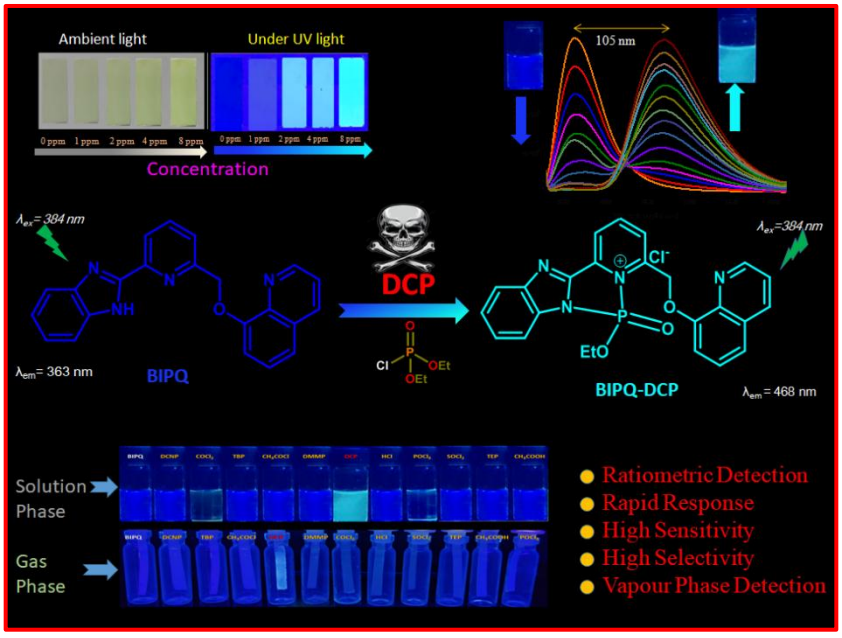

7.1. Introduction

Nowadays organophosphorus compounds are used in preparing many pesticides and herbicides in modern agriculture. Organophosphorus compounds are conceived as one of the most exceptional hazardous nerve agent and extremely harmful towards the nervous system of every living beings if inhaled through breathing or any kind of contamination to food or drinks.[1-4] Some of the known nerve agents including tabun (GA), soman (GD) and sarin (GB) are extremely dangerous organophosphates (Scheme 7.1), which bears excellent leaving groups owing to which they are known as essential phosphonylating and phosphorylating agents.[5-9] These poisonous chemicals along with the advantages of their cheap, simplicity in manufacturing and demolishing effects on civilians encourages terrorism. The phosphate group present in these chemicals binds irreversibly with the hydroxyl group present in the acetylcholinesterase (AChE), blocks the hydrolysis of acetylcholine neurotransmitters and detained the decomposition of acetylcholine.[10-13] This excessive storage of acetylcholine causes the neuromuscular paralysis, neurological imbalance in the cholinergic synapse, resistance of muscle relaxation, organ failure, finally leading to sudden death.[14-20] So it becomes a massive threats to the all man-kind. As most of these compounds are odorless, colorless and tasteless, making them very difficult to detect,[21] it is very urgent to develop a very sensitive, reliable and rapid method for easy and quick detection of these substances in both the solution and vapour phase. Our present work is based on the recognition of highly volatile sarin (GB) as it is one of the forbidden CWAs used by terrorists. But due to its too much toxic nature and hard availability, an associated substance, diethyl chlorophosphate (DCP) has used as a nerve gas-mimic agent for experiments which has similar chemical structure, comparable reactivity and very low toxicity.

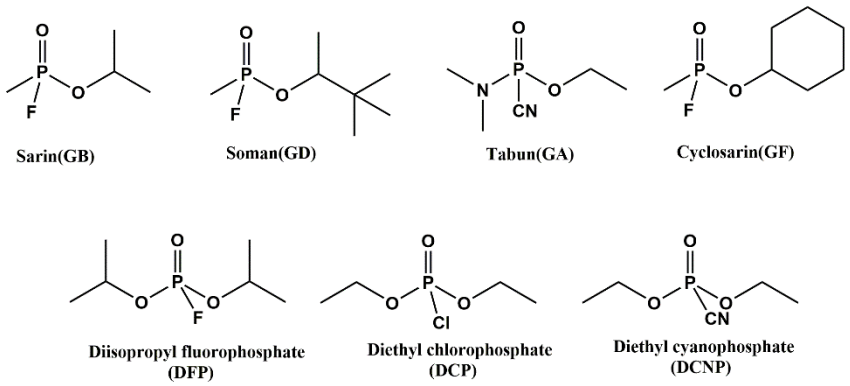

Scheme 7.1: The structures of chemical warfare agents (CWAs) and their less toxic simulants.

7.2. Prior works

In recent years, many research groups already has been introduced a variety of noteworthy tools for detecting the nerve agent mimics substances which includes colorimetry,[22-24] fluorometry,[25-27] electro-chemistry,[28-30] mass spectrometry,[31-33] interferometry,[34] enzyme-based biosensors,[35-38] surface acoustic wave (SAW) devices,[39,40] enzymatic assays,[41] photoacoustic spectroscopy,[42] PET based probes,[43] ion mobility spectroscopy,[44] cyclization reactions,[45] photonic crystals,[46] nucleophilic substitution reactions,[47,48] lanthanide luminescence,[49] complex formation-based probes,[50] optical fibre arrays,[51] nanomaterials (nanowires or nanotubes)[52-54] etc. Among these methods, fluorometric methods is considered to be the best methods to discriminate these hazardous poisonous nerve agents due to its low-cost, strong sensitivity and stability, easy portability, easiness in real-time monitoring and operational simplicity.[55,56] Recently, Cheng et el. published a fluorescent sensor which detects DCP vapour based on reactive activation in aggregation state followed by intramolecular charge transfer (ICT) process.[57] Swager et al. explored a conjugated polymer sensor to detect DCP based on phosphorylation and ionization.[58] Zhang et el. reported small organic fluorescent probes based on terpyridine as fluorometric /colorimetric as dual channel sensors towards diethyl chlorophosphate in solution phase as well as in vapour state.[59] Wasterby et el. introduced a compound to distinguish tabun, sarin, VX, soman and their mimics in organic solvents and water.[60] Although there are some great progress made in the field of sole recognition of DCP via a fluorescent sensor, it still remains an interesting and challenging among researchers to develop cheap, simple manufacture, visual fluorescent sensors with quick response, selectivity and sensitivity in detection of DCP to drive their potential practical application.

7.3. Present work

In this contribution, we have designed and synthesized the ratiometric fluorescent probe, BIPQ which consists of a pyridine and benzimidazole groups. Our probe can selectively and sensitively detect diethyl chlorophosphate (DCP), a mimic of a very dangerous and highly toxic real nerve agents, sarin in both liquid and vapour state. The chemical reaction behinds the detection of DCP by the probe involves the nucleophilic attack of nitrogen atom of the benzimidazole units to the phosphonyl group of diethyl chlorophosphate followed by ring closure process to form the final

product. The ratiometric emission profile of BIPQ upon addition of DCP can be attributed to intramolecular charge transfer (ICT) process occurring in the adduct.

7.4. Results and discussions

7.4.1. Synthesis of the probe, BIPQ

The synthesis of the receptor is outlined in Scheme 7.2. 6-((quinolin-8-yloxy) methyl)picolinaldehyde was synthesised by the simple nucleophilic substitution reaction between 6-(chloromethyl)picolinaldehyde and 8-hydroxy quinoline. Then 6-((quinolin-8-yloxy)methyl)picolinaldehyde was treated with o-phenylenediamine to get the desire receptor (BIPQ). The chemical structure of the sensor was characterised by ^{1}H NMR, ^{13}C NMR and HRMS spectroscopy (Fig. A1–A3, Appendix).

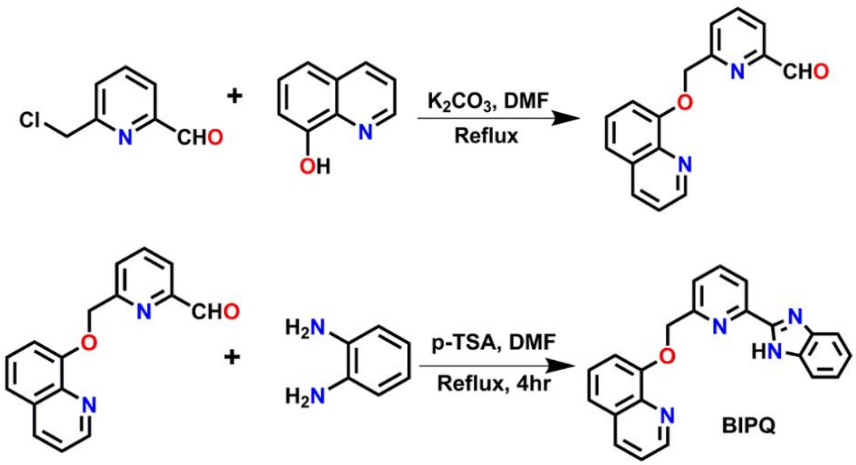

Scheme 7.2: Synthesis of the probe (BIPQ)

7.4.2. Spectral characterization and analysis of BIPQ & BIPQ-DCP

^{1}H-NMR spectrum of BIPQ is recorded in DMSO-d_6 which displays a singlet at δ ~13 ppm which is due to the presence of -NH proton in the probe. The aromatic ring protons appeared as expected in the region δ 7.24-8.92 ppm. The singlet for the methyl protons appeared at 5.54 ppm. In case of BIPQ-DCP complex, the singlet proton for -NH group is disappeared due to binding to DCP while all aromatic protons signals shifted to downfield in ^{1}H-NMR spectrum of BIPQ-DCP product. HRMS of the probe (BIPQ) exhibits a peak at m/z 353.175, while for BIPQ-DCP, a new peak at m/z 524.0658 is noticed, which may be due to the formation of $[BIPQ\text{-}DCP + 2Na^{+} + Cl^{-}]^{+}$.

7.4.3. Sensing studies of the probe (BIPQ) using UV-Vis spectroscopy

To conveniently observe the sensing characteristics of the probe BIPQ, the UV-visible spectral studies of BIPQ were recorded in a chloroform solution upon addition of various chosen guest analytes. The probe shows a peaks at 315 nm along with a hump at 329 nm. Upon gradual addition of DCP in the probe solution, the peaks at 315 nm decreased along with the disappearance of the hump at 329 nm. In contrast, a new band at 387 nm was noticed with the formation of two distinct isosbestic points at 278 nm and 335 nm respectively (Fig.7.1). To establish the selectivity of the probe solely for DCP, absorption spectral studies of BIPQ were accomplished in the presence of other relevant guest analytes. No other analytes displayed any remarkable change in the absorption spectral profile of BIPQ except for phosgene and $POCl_3$ (Fig. 7.1). The appearance of a new peak at 387 nm after addition of DCP to the probe solution may be attributed to the internal charge transfer (ICT) process occurring in the BIPQ-DCP adduct.

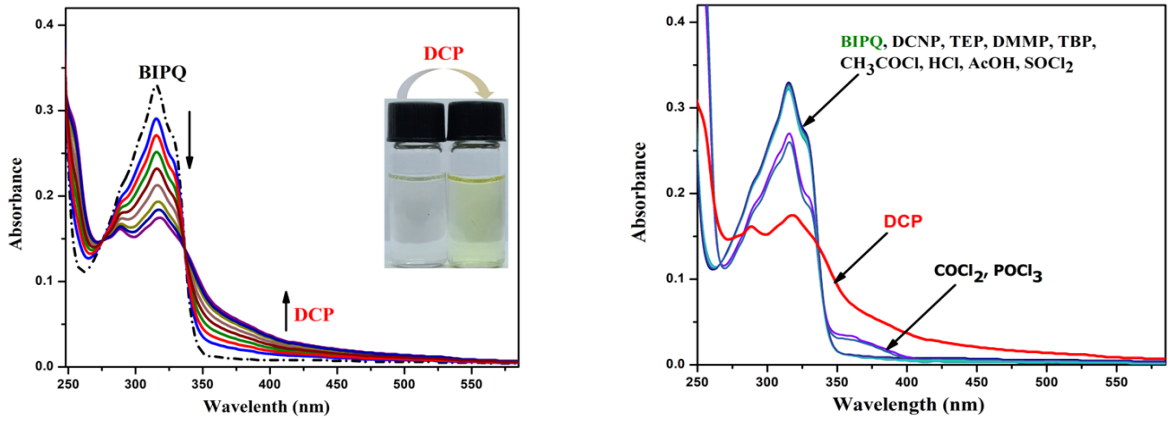

Figure 7.1: Change in absorption spectra of BIPQ (10 µM) upon gradual addition of DCP (0-20 µM) in $CHCl_3$ solution (left side) and change in absorption spectra of BIPQ upon addition of different guest analytes (20 µM) in $CHCl_3$ solution (right side).

7.4.4. DCP sensing studies of BIPQ using fluorescence spectroscopy

Under the excitation wavelength of 384 nm, the emission spectrum of BIPQ (10 µM) displays a moderately strong emission band at 363 nm in $CHCl_3$ solution. However, upon the incremental addition of DCP to the probe solution, the peak at 363 nm gradually decreased along with the appearance of a new peak at 468 nm, a sharp red shift of about 105 nm was observed, fairly accounting for the ratiometric emission enhancement of BIPQ with a distinguishable isoemissive

point at 417 nm (Fig.7.2). Additionally, this spectral changes caused a distinct colour change from blue to cyan under the UV lamp. The sensing aptitude of the probe BIPQ was also studied in the presence of other similar toxic guest analytes such as DCNP, $COCl_2$, HCl, CH_3COOH, TBP, DMMP, TEP, $SOCl_2$, $POCl_3$ and CH_3COCl only to disclose that they do not show any notable change in fluorescence emission spectral pattern of BIPQ except $POCl_3$ and phosgene (Fig.7.2). These spectral outcomes are in well agreement with the color observed under UV light in Fig. 7.7a. Thus BIPQ can be served as an efficient ratiometric switch for the exclusive recognition of DCP in chloroform solution.

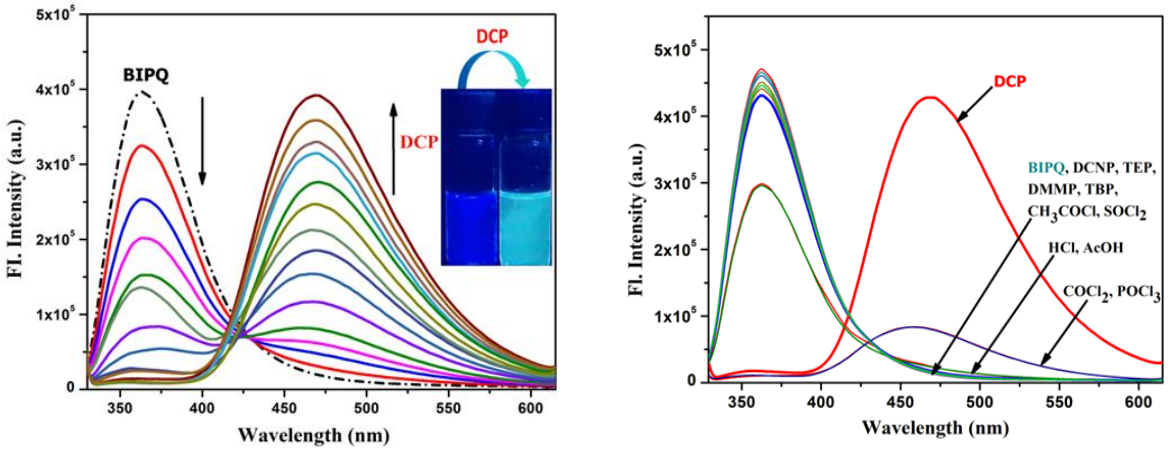

Figure 7.2: Change in emission spectra of BIPQ (10 µM) upon the incremental addition of DCP (0-20 µM) in $CHCl_3$ solution. Inset: visible emission color change of BIPQ in the absence and presence of 20 µM of DCP under UV light (left side) and change of emission spectra of BIPQ (10 µM) after addition of different guest analytes (20 µM) in $CHCl_3$ solution. λ_{ex} = 384 nm (right side).

7.4.5. The binding studies of BIPQ with DCP

Importantly, when the concentration of DCP added in the solution of BIPQ overcomes 10 µM, these fluorescence emission changes ceased abruptly. From the mole ratio plot of BIPQ, it can be established that after addition of almost 9 µM of DCP, no significant changes in emission intensity at 468 nm is exhibited thereby indicating to the fact that the saturation has taken place (Fig. 7.3). The fluorescence emission intensity of the receptor (BIPQ) at 468 nm increases linearly within the range of 0 to 9.5 µM with the gradual addition of DCP and followed the linear relationship with a good R^2 value of 0.9921 (Fig. 7.3). The fluorescence spectral data acquired from the fluorescence titration experiment using the equation DL = K × Sb_1/S, where K = 3, S is the slope of the

calibration curve[65] and Sb_1 is the standard deviation of the blank solution. The limit of detection of the probe was determined to be (1.21 ± 0.052) × 10^{-8} M (Fig. 7.3) and compared with the previous reported receptors in Table A3 (Appendix).

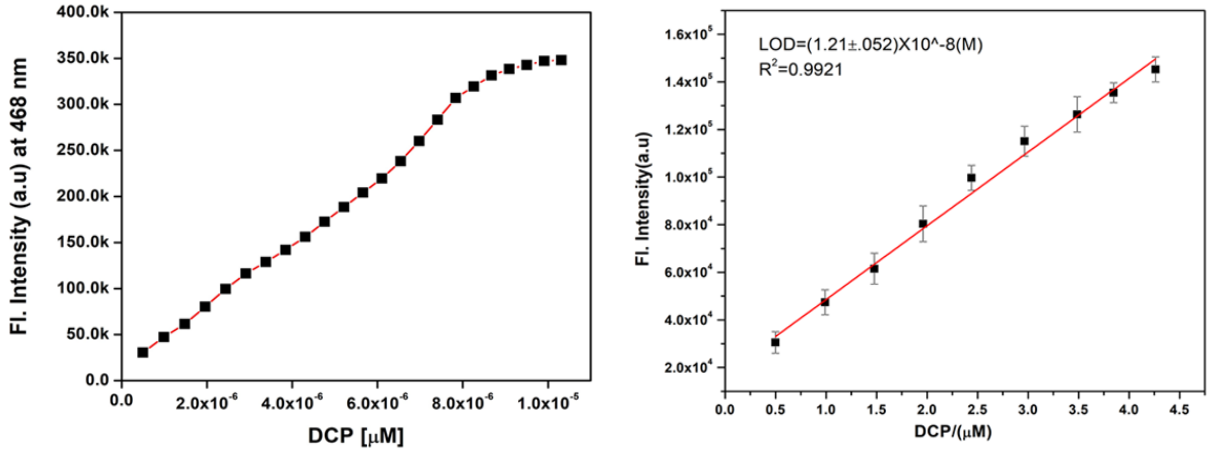

Figure 7.3: Mole ratio plot of BIPQ for DCP (left side) and the linear response curve of BIPQ at 468 nm depending on the DCP concentration (right side).

Moreover, a good chemosensor should detect guest analytes quickly and selectively in minute level in presence of various relative interfering species for useful in practical application. So in order to interpret the fast fluorescence response of every chemodosimetric receptor, the time dependent study has been found to be a very important factor. The fluorescence response profile of BIPQ (10 μM) was recorded over a 0-2 minute time period with addition of three different concentration of DCP (5 μM, 10 μM, 15 μM) into the probe solution (Fig. 7.4). From the time dependent emission response of BIPQ at three different concentrations of DCP, it was observed that the fluorescence emission intensity enhancement of the probe observed at 468 nm reached its saturation level after almost 40 seconds which basically implies the completion of the reaction. Thus it can be revealed that this novel probe, BIPQ is highly proficient for the identification of DCP within a very short time-period (almost 40 seconds) thereby making itself a very efficient switch in detecting DCP. Further the sensing aptitude of the probe towards DCP in absence and presence of various relative interfering guest analytes were also examined (Fig. 7.4). For this experiment, a set of the solutions containing the probe and different guest analytes were prepared first separately. Then DCP was added into these solutions and emission were also recorded one by one. No significant interference

in the sensing aptitude for DCP was observed in presence of other guest analytes except for $POCl_3$ and phosgene.

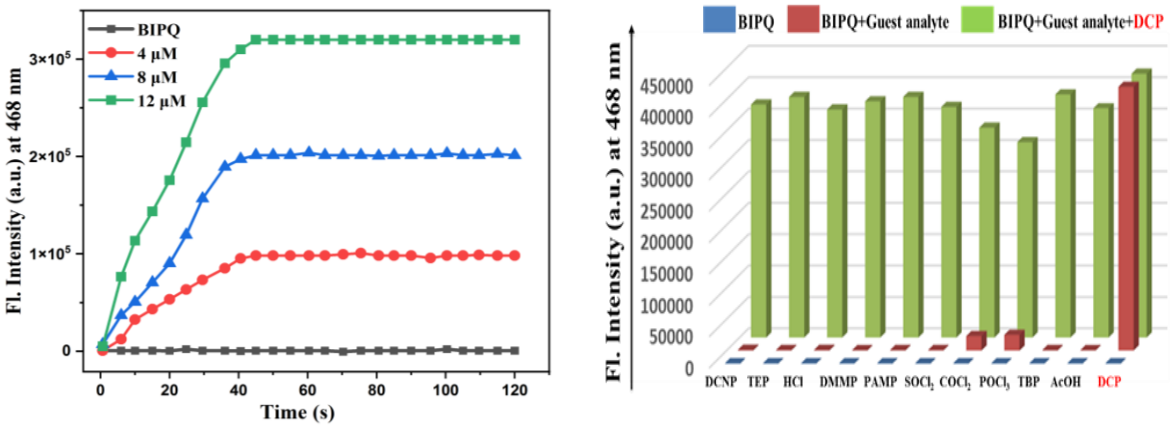

Figure 7.4: Time dependent emission spectra of BIPQ (10 μM) after addition of DCP (5 μM, 10 μM, 15 μM), noted within 0-2 min time interval in $CHCl_3$ solution (left side) and competitive experiments of BIPQ (10 μM) for DCP (20 μM) in presence of common interfering guest analytes (right side).

To better understand the excited state behavior, fluorescence lifetime measurements were also carried out for the probe (BIPQ) and BIPQ-DCP adduct (Fig. 7.5). The lifetime decay profile of both BIPQ and BIPQ-DCP moiety shows mono-exponential decay and the lifetime is found to be 1.71 ns and 2.31 ns respectively at room temperature. The high life time value of BIPQ-DCP adduct is due to the low non-radiative decay process in comparison to the free receptor (Table S1). Further, the change in life-time value may be attributed to the internal conversation between excited singlet states.

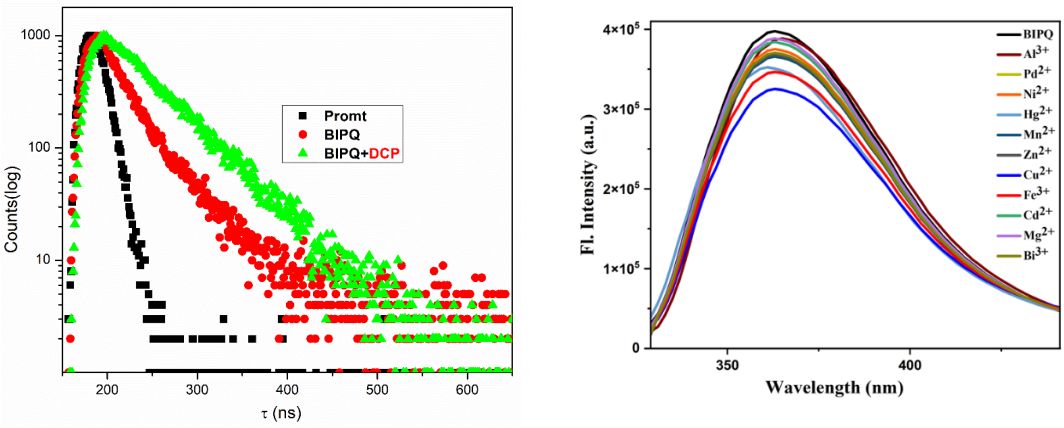

Figure 7.5: Lifetime decay profile of BIPQ and BIPQ-DCP (left side) and the change in emission spectra of BIPQ (10 μM) in presence of various metal ions (20 μM) in $CHCl_3$ (right side).

7.4.6. Molecular design strategy and reaction mechanism

For molecular design of the probe (BIPQ), 8-hydroxyquinoline unit was used to replace Cl in 6-((quinolin-8-yloxy)piconaldehyde. Especially, 8-hydroxyquinoline was chosen here to develop the sensor (BIPQ) and the sensor was employed to detect metal ions similar to some previously reported probes.[66,67] But no significant change in the emission spectra of BIPQ was observed for any metal ions (Fig. 7.5). In addition, to design the probe (BIPQ), we have also selected o-phenylenediamine to introduce a benzimidazole ring adjoined to nitrogen atom of the pyridine moiety that initiated the suitable binding sites for DCP. The sensing mechanism of the chemodosimeter (BIPQ) with DCP is discussed and depicted in scheme 7.3. On addition of DCP, the substituted product, BIPQ-DCP is formed which is actually responsible for all the spectral changes of BIPQ. The formation of BIPQ-DCP adduct moiety involves the nucleophilic attack from N-atom of benzimidazole group towards the electrophilic phosphonyl group of diethyl chlorophosphate followed by further ring closure from pyridine nitrogen. The visible colour change through naked eye as well as ratiometric emission change of BIPQ upon addition of DCP may be ascribed to the internal charge transfer (ICT) process occurring in the BIPQ-DCP adduct moiety. The probable sensing mechanism was well supported by ^{1}H, ^{13}C, ^{31}P NMR spectroscopy and mass spectrometric measurements of the isolated BIPQ-DCP adduct (Fig. A7.4-A7.7, Appendix).

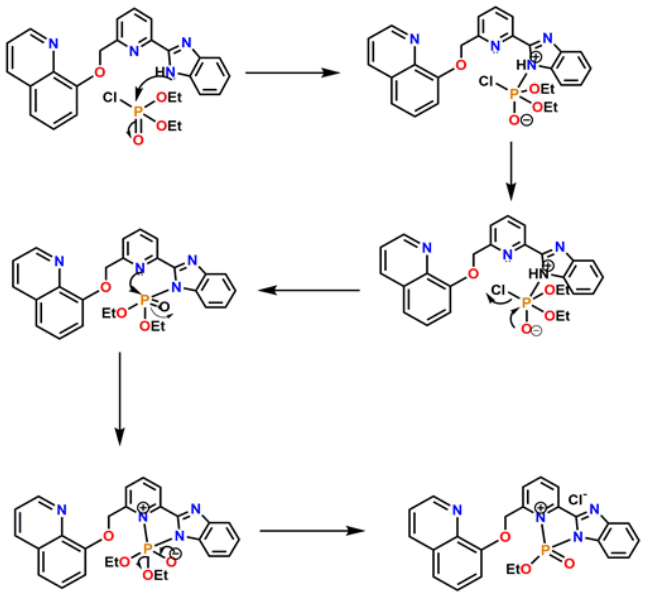

Scheme 7.3: Probable sensing mechanism of BIPQ with DCP.

In ^{1}H-NMR, the singlet peak at 13 ppm for –NH proton in BIPQ is disappeared after titration with DCP. All aromatic protons signals shifted to downfield in ^{1}H-NMR spectrum of BIPQ-DCP product (Fig. A7.4). In the ^{31}P NMR, the singlet peak at 4.94 ppm appeared for DCP itself,[68] whereas BIPQ-DCP showed a new upfield signal at -1.525 ppm, thereby supporting the formation of the BIPQ-DCP adduct (Fig. A7.6). In order to further support the formation of BIPQ-DCP product, HRMS was also carried out. The HRMS of the receptor (BIPQ) itself displayed a peak at 353.175 (m/z) while for BIPQ-DCP, the appearance of a new peak at 524.0658 (m/z) may be due to the formation of [BIPQ-DCP+2Na^{+}+Cl^{-}]$^{+}$ (Fig. A7.7). Therefore, from the spectroscopic results of BIPQ-DCP adduct, it is evidently confirmed the formation of the aforementioned adduct (BIPQ-DCP).

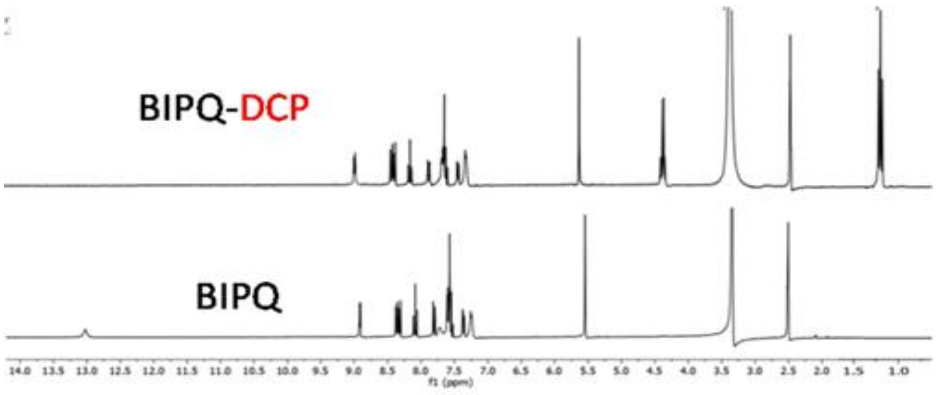

Figure 7.6: ^{1}H-NMR spectrum of BIPQ and BIPQ-DCP in DMSO-d_6

7.4.7. Dip-stick experiment for vapour phase detection of DCP by BIPQ

The detection of DCP in liquid and solid phase has its own notable effects but its identification in gas phase is of great interest which could be accomplished by so called dip-stick method in the presence of DCP and other relative interfering organophosphorus nerve agents. The probe, BIPQ has shown an instant response in presence of DCP thereby proving its potential in order to use it as an efficient portable kit for detecting the nerve agent mimic. The detection of DCP in solid and liquid state has its own notable effects but its identification in vapour phase is of outmost interest and a significantly demanding application which could be achieved via introducing an important experiment known as “dip-stick method”. This trouble-free procedure provides instantaneous qualitative information by quick visual response without even the aid of any sophisticated instrument. So to facilitate the execution of this experiment, Whatman filter papers were used to

prepare test strips which were dipped into the solution of BIPQ (2×10^{-4} M) in $CHCl_3$ and then drying them by evaporating the solvent in air. After drying these BIPQ-coated filter papers, they were placed in a sealed vial container in order to come into contact with the vapour of nerve agent mimic, DCP and others possible interfering toxic analytes as displayed in Figure 7.7. From Fig.7.7, it is clear that probe-loaded strips turned to cyan color in presence of DCP vapour and no notable change of BIPQ is detected in presence of other toxic guest analytes except a slight change in case of $COCl_2$ and $POCl_3$ vapour. Hence BIPQ can be used as a proficient fluorescence portable kit for detecting the nerve agent mimic DCP in vapour phase.

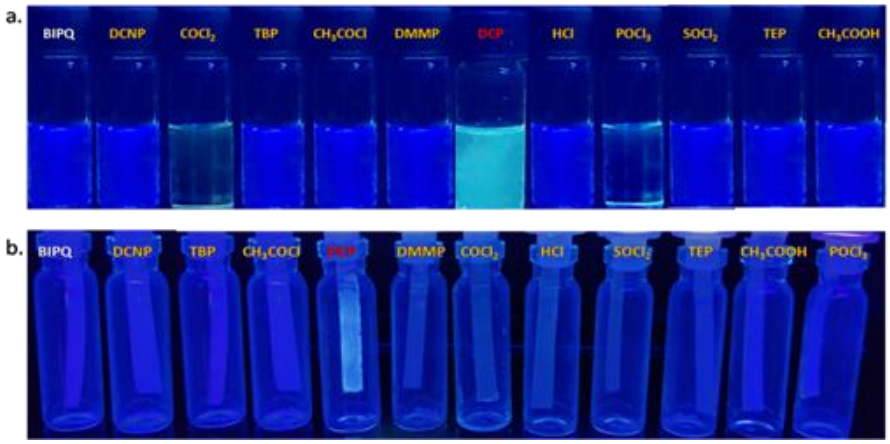

Figure 7.7: Fluorescence response of BIPQ towards various toxic guest analytes in solution phase(a); in vapour phase (b) after 60 s exposure to other toxic guest analytes (experimented using Whatman filter papers). Photos are taken in UV-chamber (λ_{ex} = 384 nm).

In addition, we have also demonstrated Dip-Stick experiment with different concentration of DCP via BIPQ-loaded TLC plates (Fig. 7.8). The probe-loaded TLC plates were blue color at first but turned to a cyan color change when immersed into different concentrations of 1.0, 2.0, 4.0 and 8.0 ppm of DCP under UV-light (Fig. 7.8). From this observation, we have concluded that the receptor (BIPQ) can identify DCP with a concentration of as low as 2 ppm thereby confirming our present probe to be an exceptionally reliable and facile contender to recognise nerve agent mimic Diethyl chlorophosphate (DCP).

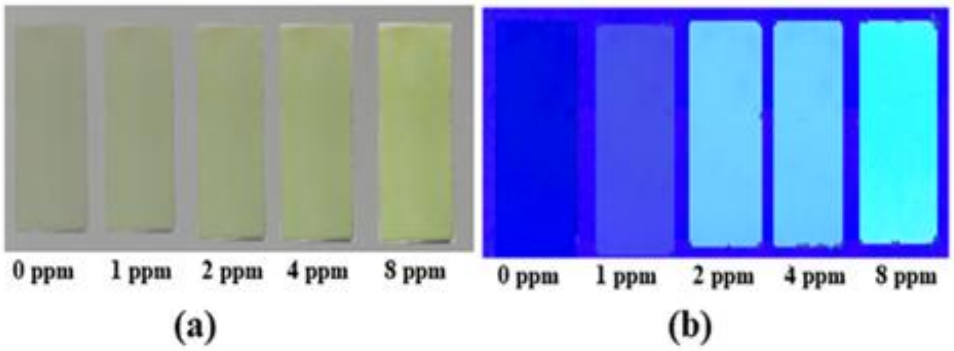

Figure 7.8: Pictures of BIPQ-coated TLC plates and after dipped into various concentration of DCP for 60 sec taken in ambient light (a) and under UV-light (b)**.**

7.4.8. Computational study

To comprehend the structural changes of BIMQ during interaction with DCP, density functional theory (DFT) calculations were performed by B3LYP/6-31+G(d) method using Gaussian 09 program. The optimized structures of BIPQ and BIPQ-DCP adduct are displayed in figure 10. The Fig. A7.11 and Fig. A7.12) shows the contour plots of selected higher energy occupied molecular orbitals (HOMOs) and lower energy unoccupied molecular orbital (LUMOs) of BIPQ and BIPQ-DCP product respectively. The HOMO-LUMO energy gap of BIPQ and BIPQ-DCP complex is found to be 4.2 eV and 2.21 eV respectively. This significant change in HOMO-LUMO energy gap is well substantiated with the bathochromic shift in low energy band in UV-Visible spectrum of BIPQ-DCP. To illustrate the electronic spectra, vertical electronic transitions were calculated by time dependent density functional theory (TDDFT) calculation (solvent correction is incorporated by CPCM model and $CHCl_3$ is chosen as solvent) and summarized in Table A2, (Appendix). The calculated vertical excitations of BIPQ exhibits strong transitions at 327 nm (f=0.2264) due to HOMO→LUMO. However for BIPQ-DCP, HOMO-2→LUMO and HOMO-1→LUMO transitions are shifted to 418 nm (f=0.1445) (Table A2, Appendix). Moreover, the calculated absorption peaks of BIPQ and BIPQ-DCP have agreed well with the experimental outcomes.

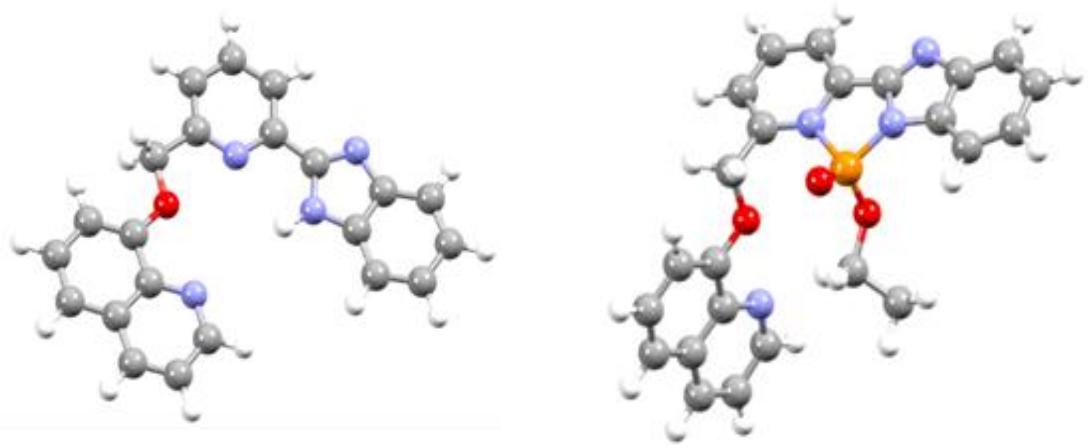

Figure 7.9: Optimized structure of BIPQ (left side) and BIPQ-DCP (right side) calculated by DFT/B3LYP/6-31+G(d) method

7.5. Experimental Section

7.5.1. Materials and methods

All the organic reagents used in the synthetic procedure of BIPQ, including 8-Hydroxy quinoline and o-phenylenediamine were purchased from commercial sources and all spectroscopic grade solvents were from other commercial sources and used without further refinement. $CDCl_3$ and DMSO-d_6 were used as solvent in order to achieve NMR spectra and chemical shifts were recorded in □ units in ppm using tetramethylsilane (TMS) as an internal standard. ^1H and ^{13}C Elemental analysis was carried out in a 2400 Series-II CHN analyzer, Perkin Elmer, USA.NMR spectra were recorded on Brucker 300 MHz instrument. HRMS mass spectra were recorded on Waters (Xevo G2 Q-TOF) mass spectrometer. UV-Vis spectra were taken on a PerkinElmer Lambda 750 spectrophotometer. The luminescence properties were studied using Shimadzu RF-6000 fluorescence spectrophotometer at room temperature (298 K). Thin layer chromatography (TLC) was done using Merck 60 F_{254} plates having thickness of 0.25 mm. The lifetimes were measured using a time-resolved spectrofluorometer from IBH, UK.

7.5.2. Synthesis of 6-((quinolin-8-yloxy)methyl)picolinaldehyde

6-(chloromethyl)picolinaldehyde (0.14 g, 0.9 mmol) was taken in a round bottom flux and dissolved in DMF (5 ml) solvent. 8-Hydroxy quinoline (0.13 g, 0.9 mmol) and K_2CO_3 (0.124 g,

0.9 mmol) were added to it and refluxed for 5 h. After completion of the reaction, the whole reaction mixture was poured into cold water. The precipitate appeared which was collected by filtration and dried. Column chromatography was performed for purifying the crude product. Yield, 0.195 g (82%).

Anal. Calc. for $C_{16}H_{12}N_2O_2$: calc. (%) C 72.72, H 4.58, N 10.6, O 12.11. Found (%), C 73.32, H 4.46, N 11.10, O 11.12.

^{1}H NMR (300 MHz, DMSO-d_6): δ(ppm): 10.0384 (s, 1H), 5.5298 (s, 2H), 7.7144 (d, J = 7.77 Hz, 1H), 7.9514 (d, J= 7.8, 1H), 8.0167 (d, J= 7.65, 1H), 8.1634 (t, J = 7.68 Hz, 1H), 8.3498 (t, J = 7.8 Hz, 1H), 8.9098 (d, J = 8.1 Hz, 1H), 7.5936-7.4527 (m, 3H).

^{13}C NMR (75 MHz, DMSO-d_6): δ(ppm): 84.5, 103.04, 110.7, 120.8,121.4, 122.5, 123.08, 127.2, 129.6, 136.3, 137.8, 139.2, 140.2, 149.7, 152.3, 154.1, 155.8, 156.5, 158.3, 193.9

HRMS: Calculated for $C_{16}H_{13}N_2O_2^+$ $[M + H]^+$(m/z) = 265.0972; found = 265.1005

7.5.3. Synthesis of 8-((6-(1H-benzo[d]imidazol-2-yl)pyridin-2-yl) methoxy) quinoline (BIPQ)

The mixture of 6-((quinolin-8-yloxy)methyl)picolinaldehyde (0.237 g, 0.9 mmol) and o-phenylenediamine (0.097 g, 0.9 mmol) in $CHCl_3$ (5 ml) solution were refluxed for 4 hours in presence of a catalytic amount of p-TSA (~15 mg) under inert atmosphere. After completion of the reaction, the reaction mixture was cooled at room temperature and then the whole of it was poured into ice-cooled water. The formation of a grey colored precipitate was observed as soon as the reaction mixture came in contact with the ice-cold water. The precipitate was filtered using suction and the product was purified by column chromatography to get our desired final product. yield was 0.256 g (81%).

Anal. Calc. for $C_{19}H_{17}ClN_3O_3P$ (BIMQ-DCP): calc. (%) C 74.98, H 4.58, N 15.9, O 4.54. Found (%), C 75.22, H 4.64, N 16.11, O 4.03.

^{1}H NMR (300 MHz, DMSO-d_6): δ(ppm): 13.0043 (s, 1H), 8.9239-8.9043 (d, J= 6 Hz, 2H), 8.3802-8.3066 (m, 3H), 8.0867 (t, J= 9 Hz, 1H), 7.8056 (d, J = 7.68 Hz, 1H), 7.6110-7.5480 (m, 3H), 7.3795-7.3565 (m, 2H), 7.25 (d, J=6 Hz, 1H), 5.5450 (s, 2H).

^{13}C NMR (100 MHz, $CDCl_3$): δ(ppm): 71.5, 110.7, 112.7, 119.7, 120.8, 121.1, 122.5, 123.5, 127.3, 129.6, 135.4, 136.4, 138.9, 140.3, 144.3, 148.6, 149.7, 150.9, 154.3, 157.3.

HRMS: calculated for $C_{22}H_{17}N_4O^+$ $[M + H]^+$ (m/z) = 353.1397; found = 353.1750.

7.5.4. Synthesis of BIPQ-DCP

8-((6-(1H-benzo[d]imidazol-2-yl)pyridine-2-yl)methoxy) quinoline (BIPQ) (0.053 g, 0.15 mmol) and DCP (0.026 g, 0.15 mmol) were added in a round-bottomed flask and $CHCl_3$ (5 ml) was added into the mixture and was stirred for 2 h at room temperature. After completion of the reaction, a white precipitate was formed which was then filtered and collected.

Anal. Calc. for $C_{24}H_{20}N_4O_3P$ (BIPQ-DCP): Calc. (%) C: 65.01, H: 4.55, N: 12.64, O: 10.82, P: 6.99. Found (%), C: 64.92, H: 4.48, N: 12.75, O: 11.03, P: 6.82.

^{1}H NMR (300 MHz, DMSO-d_6): δ(ppm): 1.1758 (t, J = 6.99 Hz, 3H), 4.3375 (q, 2H), 5.6602 (s, 2H), 7.3691 (d, J = 7.86 Hz, 1H), 7.4648-7.4877 (m, 2H), 7.6632-7.7262 (m, 3H), 7.9208 (d, J=7.68 Hz, 1H), 8.2019 (t, J = 7.78, 1H), 8.4218-8.4954 (m, 3H), 9.0195-9.0391 (m, 2H).

^{13}C NMR (75 MHz, DMSO-d_6): δ(ppm): 16.2, 64.4, 76.29, 115.5, 117.5, 124.6, 125.8, 127.3, 128.3, 132.1, 134.4, 140.2, 141.2, 143.7, 145.06, 149.1, 153.4, 154.5, 155.7, 159.1, 162.1

^{31}P NMR (100 MHz, $CDCl_3$): δ(ppm): -1.525

HRMS: calculated for $C_{24}H_{20}ClN_4Na_2O_3P$[BIPQ-DCP+2$Na^+$+$Cl^-$]$^+$ (m/z) = 524.0757; found = 524.0658.

7.5.5. General Method for UV-Vis and Fluorescence Titration

7.5.5.1. UV-Vis Method

For UV-vis titration, the host solution was prepared in $CHCl_3$ solution in the order of 10 μM. The solutions of all the guest analytes in the order of 1×10^{-5} M, were prepared in chloroform. solvent of a variety of concentrations of the probe and all other analytes were prepared separately. The spectra of these solutions were recorded with the help of UV-vis method.

7.5.5.2. Fluorescence Method

For fluorescence titrations, the stock solution of the probe (10 μM) used was the same as that used for UV-vis titration. The solutions of all the analytes were prepared in chloroform in the order of 10^{-5} M. The host solution and the solution of all the analytes were prepared separately in different concentrations. The spectra of these solutions were recorded by means of fluorescence method.

7.5.6. Determination of Quantum yield

For measurement of the quantum yields of BIPQ and the adduct BIPQ-DCP, we recorded the absorbance of the compounds in $CHCl_3$ solution. The emission spectra were recorded using the

maximal excitation wavelengths and the integrated areas of the fluorescence-corrected spectra were measured. The quantum yields were then calculated by comparison with coumarin 153 (Φs= 0.544 in $CHCl_3$) as reference using the following equation:

$$\Phi_x = \Phi_s \times \left(\frac{I_x}{I_s}\right) \times \left(\frac{A_s}{A_x}\right) \times \left(\frac{n_x}{n_s}\right)^2$$

Where, x & s indicate the unknown and standard solution respectively, Φ is the quantum yield, I is the integrated area under the fluorescence spectra, A is the absorbance and n is the refractive index of the solvent. We calculated the quantum yields of BIPQ and BIPQ-DCP using the above equation and the values are 0.21 and 0.35, respectively.

7.5.7. Theoretical study

All calculations were performed with Gaussian 09 program package[61]. Full geometry optimizations were carried out using the density functional theory (DFT) method at the B3LYP[62] level for the compounds. The vibrational frequency calculations were performed to certain that the optimized geometries represent the local minima having only positive eigen values. All elements were assigned 6-31+G(d) basis set. Vertical electronic excitations based on B3LYP optimized geometries were computed using the time-dependent density functional theory (TDDFT) formalism[63] in chloroform using conductor-like polarizable continuum model (CPCM).[64]

7.6. Conclusions

In summary, a very simple fluorescent ratiometric switch (BIPQ) is introduced for efficient and selective detection of DCP, a harmful nerve-agent mimic, in both solution and gas phase. The limit of detection in solution phase was calculated to be in the order of 10^{-8} (M). Fascinatingly, this probe exhibited a noticeable ratiometric fluorescence change with a red shift upon incremental addition of DCP. The fluorescence change is mainly based on the ICT process occurring in BIPQ-DCP adduct showed this ratiometric change towards DCP solely in presence of other toxic guest analytes. These outcomes conclude that our probe can be considered as a potential chemodosimeter with an instantaneous detection capability upon exposure to the nerve agent mimics. More importantly, we expect our synthesized probe can be employed in real time monitoring of real nerve agent sarin in terrorists attacked areas.

7.7. Notes and references

1. Y. J. Jang, K. Kim, O. G. Tsay, D. A. Atwood and D.G. Churchill, *Chem. Rev*., 2015, **115**, PR1-PR76.
2. V. V. Singh, K. Kaufmann, B. E. de Ávila, M. Uygun and J. Wang, *Chem. Commun.*, 2016, **52**, 3360.
3. A. Balamurugan and H. Lee, *Macromolecules*, 2016, **49**, 2568.
4. Y. J. Jang, S.V. Mulay, Y. Kim, P. Jorayeva and D.G. Churchill, *New. J. Chem*., 2017, **41**, 1653-1658.
5. A. J. Russell, J. A. Berberich, G. F. Drevon and R. R. Koepsel, *Annu. Rev. Biomed. Eng.*, 2003, **5**, 1.
6. H. S. So, S. Angupillai and Y. A. Son, *Sens. Actuators B Chem.*, 2016, **235**, 447.
7. T. Alizadeh and L. H. Soltani, *Sens. Actuators B Chem.*, 2016, **234**, 361.
8. H. Mao, Y. Yan, N. Hao, Q. Liu, J. Qian, S. Chen and K. Wang, *Sens. Actuators, B Chem.*, 2017, **238**, 239.
9. K. Kim, O. G. Tsay, D. A. Atwood and D. G. Churchill, *Chem. Rev.*, 2011, **111**, 5345.
10. F. R. Sidell and J. Borak, *Ann. Emerg. Med.*, 1992, **21**, 865.
11. T. C. Marrs, *Pharmacol. Ther.*, 1993, **58**, 51.
12. K. Tuovinen, *Toxicology*, 2004, **196**, 31.
13. S. Huang, Y. Wu, F. Zeng, L. Sun and S. Wu, *J. Mater. Chem. C*, 2016, **4**, 10105.
14. M. Ehrich, in Encyclopedia of Toxicology, ed. P. Wexler, Academic Press, San Diego, CA, 1998, p. 467.
15. F. R. Sidell and J. Borak, *Ann. Emerg. Med.*, 1992, **21**, 865.
16. T. C. Marrs, *Pharmacol. Ther.*, 1993, **58**, 51.
17. L. Szinicz, *Toxicology*, 2005, **214**, 167.
18. S. M. Somani, Chemical Warfare Agents, Academic, San Diego, 1992.
19. T. I. Kim, S. B. Maity, J. Bouffard and Y. Kim, Anal. Chem., 2016, **88**, 9259-9263.
20. K. Kim, O.G. Tsay, D. A. Atwood and D. G. Churchill, *Chem. Rev.*, 2011, **11**1, 5345-5403.
21. Y. C. Yang, *Acc. Chem. Res*., 1999, 32, 109-115.
22. M. P. N. Bui and A. Abbas, *Sens. Actuators B Chem.*, 2015, **207**, 370-374.
23. K. J. Wallace, J. Morey, V. M. Lynch and E. V. Anslyn, *New J. Chem.*, 2005, **29**, 1469-1474.
24. R. Gotor, *Tetrahedron*, 2012, **68,** 8612-8616.
25. A. K. Mahapatra, K. Maiti, S. K. Manna, R. Maji, S. Mondal, C. D. Mukhopadhay, P. Sahoo and D. Mandal, *Chem. Commun.*, 2015, **51**, 9729-8732.
26. H. S. So, S. Angupillai and Y. A. Son, *Sens. Actuators B Chem.*, 2016, **235,** 447-456.
27. X. Wu, Z. Wu and S. Han, *Chem. Commun*., 2011, 47, 11468-11470.
28. Y. Zhou, B. Yu, E. Shiu, K. Levon, *Anal. Chem*., 2004, **76**, 2689-2693.
29. D. Yu, J. Volponi, S. Chhabra, C. J. Brinker, A. Mulchandani and A. K. Singh, *Biosens. Bioelectron*., 2005, **20**, 1433-1437.
30. M. H. Hammond, K. J. Johnson, S. L. Rose-Pehrsson, J. Ziegler, H. Walker, K. Caudy, D. Gary and D. Tillett, *Sens. Actuators B Chem.*, 2006, **116**, 135-144.
31. W. E. Steiner, S. J. Klopsch, W. A. English, B. H. Clowers and H. H. Hill, *Anal. Chem.*, 2005, **77**, 4792.
32. Y. Bao, Q. Liu, J. Chen, Y. Lin, B. D. Wu and J. W. Xie, *J. Chromatogr. A*, 2012, **1229**, 164.

33. F. Zydel, J. R. Smith, V. S. Pagnotti, R. J. Lawrence, C. N. McEwen and B. R. Capacio, *Drug Test. Anal.*, 2012, **4**, 308.
34. H. Sohn, S. Letant, M. J. Sailor and W. C. Trogler, *J. Am. Chem. Soc.*, 2000, **122**, 5399-5400
35. M. H. Hammond, K. J. Johnson, S. L. Rose-Pehrsson, J. Ziegler, H. Walker, K. Coudy, D. Gary and D. Tillett, *Sens. Actuators B Chem.*, 2006, **116**, 135.
36. P. Kuban, A. Seiman, N. Makarotseva, M. Vaher and M. Kaljurand, *J. Chromatogr A*, 2011, **1218**, 2618.
37. J. Orbulescu, C. A. Constantine, V. K. Rastogi, S. S. Shah, J. J. De-Frank and R. M. Leblanc, *Anal. Chem.*, 2006, **78**, 7016.
38. L. Viveros, S. Paliwal, D. McCrae, J. Wild and A. Simonia, *Sens. Actuators B Chem.*, 2006, **115**, 150.
39. Y. Yang, H. F. Ji and T. Thundat, *J. Am. Chem. Soc.*, 2003, **125**, 1124-1125.
40. C. H. Thompson, J. Hu, S. N. Kaganove, S. E. Keinath, D. L. Keeley and P. R. Dvornic, *Chem. Mater.*, 2004, **16**, 5357-5364.
41. S. Jin, Z. Xu, J. Chen, X. Liang, Y. Wu and X. Qian, *Anal. Chim. Acta.*, 2004, **523**, 117.
42. M. Wheelis, *Pure Appl. Chem.*, 2002, **74**, 2247
43. T. J. Dale and J. Rebek Jr., *J. Am. Chem. Soc.*, 2006, **128**, 4500;
44. G. Liu and Y. Lin, *Anal. Chem.*, 2006, **78**, 83.
45. A. M. Costero, S. Gil, M. Parra, P. M. E. Mancini, R. Martínez-Máñez, F. Sancenón and S. Royo, *Chem. Commun.*, 2008, 6002.
46. A. F. Matthews, S. F. Mingaleev and Y. S. Kivshar, *Laser Phys.*, 2004, **14**, 631.
47. A. D. Rusu, I. A. Moleavin, N. Hurduc, M. Hamela and L. Rochaa, *Chem. Commun.*, 2014, **50**, 9965.
48. Q. Chen, J. Liu, S. Liu, J. Zhang, L. He, R. Liu, H. Jiang, X. Han and K. Zhang, *Anal. Chem*., 2023, **95**, 4390-4394.
49. G. Mathis and H. Bazin, *Springer Ser. Fluoresc.*, 2010, **7**, 47.
50. A. Barba-Bon, A. M. Costero, S. Gil, F. Sancenón and R. Martínez-Máñez, *Chem. Commun.*, 2014, **50**, 13289.
51. W. H. Wu, J. J. Dong, X. Wang, J. Li, S. H. Sui, G. Y. Chen, J. J. Liu and M. Zhang, *Analyst*, 2012, **137**, 3224.
52. A. K. Mahapatra, K. Maiti, S. K. Manna, R. Maji, S. Mondal, C. D. Mukhopadhyay, P. Sahoo and D. Mandal, *Chem. Commun.*, 2015, **51**, 9729.
53. F. Wang, H. Gu and T. M. Swager, *J. Am. Chem. Soc.*, 2008, **130**, 5392.
54. Q. Chen, Y. Sun, S. Liu, J. Zhang, C. Zhang, H. Jiang, X. Han, L. He, S. Wang and K. Zhang, *Sens. Actuators B Chem*., 2021, **344**, 130278
55. (a) A. Wild, A. Winter, M. D. Hagerab and U. S. Schubert, *Chem. Commun.*, 2012, **48**, 964; (b) W. h. Wu, J. J. Dong, X. Wang, J. Li, S. h. Sui, G. Y. Chen, J. W. Liu and M. Zhang, *Analyst*, 2012, **137**, 3224; (c) W. Xuan, Y. Cao, J. Zhou and W. Wang, *Chem. Commun.*, 2013, **49**, 10474.

56. (a) M. R. Sambrook, S. Notman, M. R. Sambrook and S. Notman, *Chem. Soc. Rev.*, 2013, **42**, 9251; (b) A. K. Mahapatra, S. S. Ali, K. Maiti, S. Mondal, R. Maji, S. Manna, S. K. Manna, M. R. Uddin and S. Mandal, *RSC Adv.*, 2016, **6**, 113219; (c) I. Bhowmick and Neelam, *Analyst*, 2014, **139**, 4154.

57. W. Xu, Y. Fu, J. Yao, T. Fan, Y. Gao, Q. He, D. Zhu, H. Cao and J. Cheng, *ACS Sens.*, 2016, **1**, 1054-1059.

58. S. W. Thomas III, G. D. Joly and T. M. Swagar, *Chem. Rev.*, 2007, **107**, 1339-1386.

59. P. Zheng, Z. Cui, H. Liu, W. Cao, F. Li and M. Zhang, *J. Hazard. Mater.*, 2021, **415**, 125619.

60. B. D. Grenu, D. Moreno, T. Torroba, A. Berg, J. Gunnars, T. Nilsson, R. Nyman, M. Persson, J. Pettersson, I. Eklind and P. Wasterby, *J. Am. Chem. Soc.*, 2014, **136**, 4125-4128.

61. Gaussian 09, Revision D.01, M. J. Frisch, G. W. Trucks, H. B. Schlegel, G. E. Scuseria, M. A. Robb, J. R. Cheeseman, G. Scalmani, V. Barone, B. Mennucci, G. A. Petersson, H. Nakatsuji, M. Caricato, X. Li, H. P. Hratchian, A. F. Izmaylov, J. Bloino, G. Zheng, J. L. Sonnenberg, M. Hada, M. Ehara, K. Toyota, R. Fukuda, J. Hasegawa, M. Ishida, T. Nakajima, Y. Honda, O. Kitao, H. Nakai, T. Vreven, J. A. Montgomery, Jr., J. E. Peralta, F. Ogliaro, M. Bearpark, J. J. Heyd, E. Brothers, K. N. Kudin, V. N. Staroverov, R. Kobayashi, J. Normand, K. Raghavachari, A. Rendell, J. C. Burant, S. S. Iyengar, J. Tomasi, M. Cossi, N. Rega, J. M. Millam, M. Klene, J. E. Knox, J. B. Cross, V. Bakken, C. Adamo, J. Jaramillo, R. Gomperts, R. E. Stratmann, O. Yazyev, A. J. Austin, R. Cammi, C. Pomelli, J. W. Ochterski, R. L. Martin, K. Morokuma, V. G. Zakrzewski, G. A. Voth, P. Salvador, J. J. Dannenberg, S. Dapprich, A. D. Daniels, Ö. Farkas, J. B. Foresman, J. V. Ortiz, J. Cioslowski and D. J. Fox, *Gaussian*, Inc., Wallingford CT, 2009.

62. (a) A. D. Becke, *J. Chem. Phys.*, 1993, **98**, 5648; (b) C. Lee, W. Yang and R. G. Parr, *Phys. Rev. B*, 1988, **37**, 785; (c) D. Andrae, U. Haeussermann, M. Dolg, H. Stoll and H. Preuss, *Theor. Chim. Acta*, 1990, **77**, 123

63. a) R. Bauernschmitt and R. Ahlrichs, *Chem. Phys. Lett.*, 1996, **256**, 454. (b) R. E. Stratmann, G. E. Scuseria and M. J. Frisch, *J. Chem. Phys.*, 1998, **109**, 8218. (c) M. E. Casida, C. Jamorski, K. C. Casida and D. R. Salahub, *J. Chem. Phys.*, 1998, **108**, 4439

64. V. Barone and M. Cossi, *J. Phys. Chem., A* 1998, **102**, 1995. (b) M. Cossi and V. Barone, *J. Chem. Phys.*, 2001, **115,** 4708. (c) M. Cossi, N. Rega, G. Scalmani and V. Barone, *J. Comput. Chem.*, 2003, **24**, 669.

65. (a) W. Lin, L. Yuan, Z. Cao, Y. Feng and L. Long, *Chem. -Eur. J.*, 2009, **15**, 5096; (b) S. Goswami, K. Aich, S. Das, A. K. Das, D. Sarkar, S. Panja, T. K. Mondal and S. K. Mukhopadhyay, *Chem. Commun.*, 2013, **49**, 10739; (c) S. Goswami, S. Das, K. Aich, B. Pakhira, S. Panja, S. K. Mukherjee and S. Sarkar, *Org. Lett.*, 2013, **15**, 5412; (d) S. Goswami, K. Aich, A. K. Das, A. Manna and S. Das, *RSC Adv.*, 2013, **3**, 2412; (e) K. Aich, S. Das, S. Goswami, C. K. Quah, D. Sarkar, T. K. Mondal and H.-K. Fun, *New J. Chem.*, 2016, **40**, 6907

66. Y. Wang, F. Duan, G. Liu, P. Liu, and C. Fan and S. Pu, Tetrahedron, 2019, 75, 2284-2290.

67. J. H. Wang, Y. M. Liu, Z. M. Dong, J. B. Chao, H. Wang, Y. Wang and *S.* Shuang, *J. Hazard. Mater.*, 2020, **382**, 121056.

68. Y. J. Jang, S. V. Mulay, Y. Kim, P. Jorayev and D. G. Churchill, *New J. Chem.*, 2017, **41**, 1653.

APPENDIX

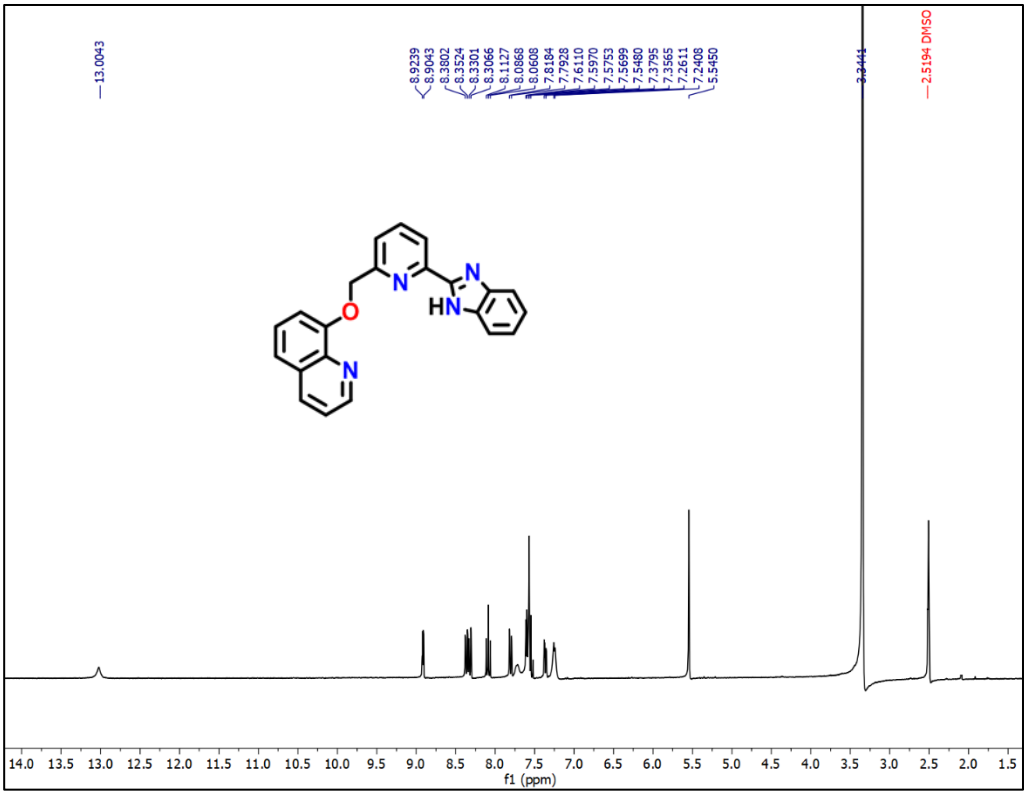

Fig. A7.1: ^{1}H NMR (300 MHz) spectrum of the probe (BIPQ) in DMSO-d_6

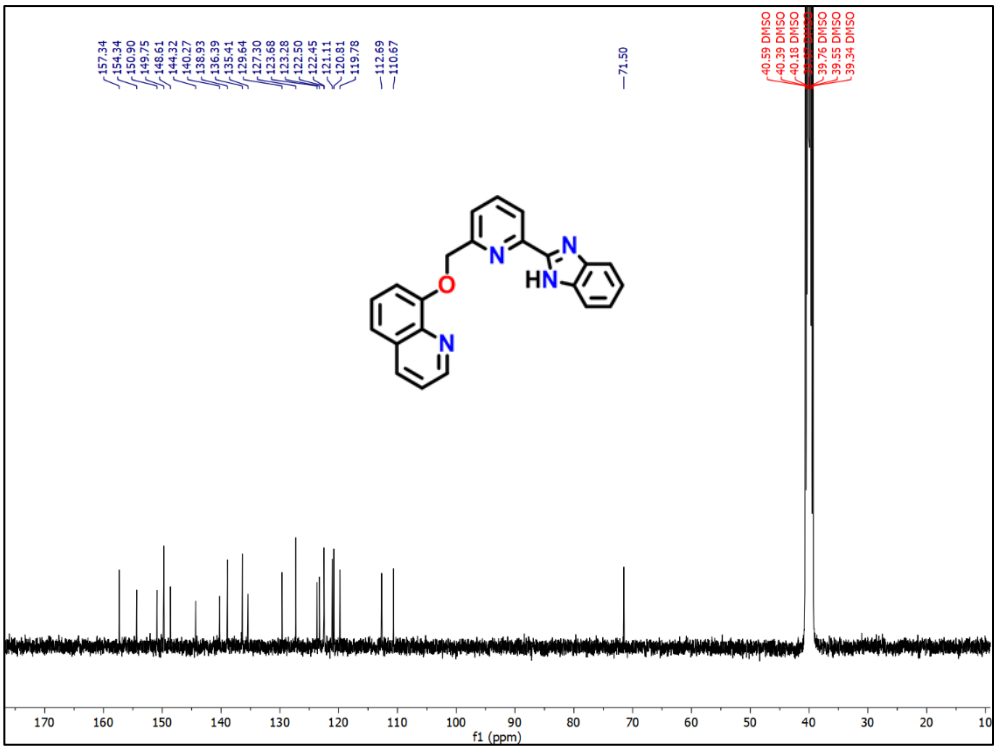

Fig. A7.2: ^{13}C NMR (75 MHz) spectrum of the probe (BIPQ) in DMSO-d_6

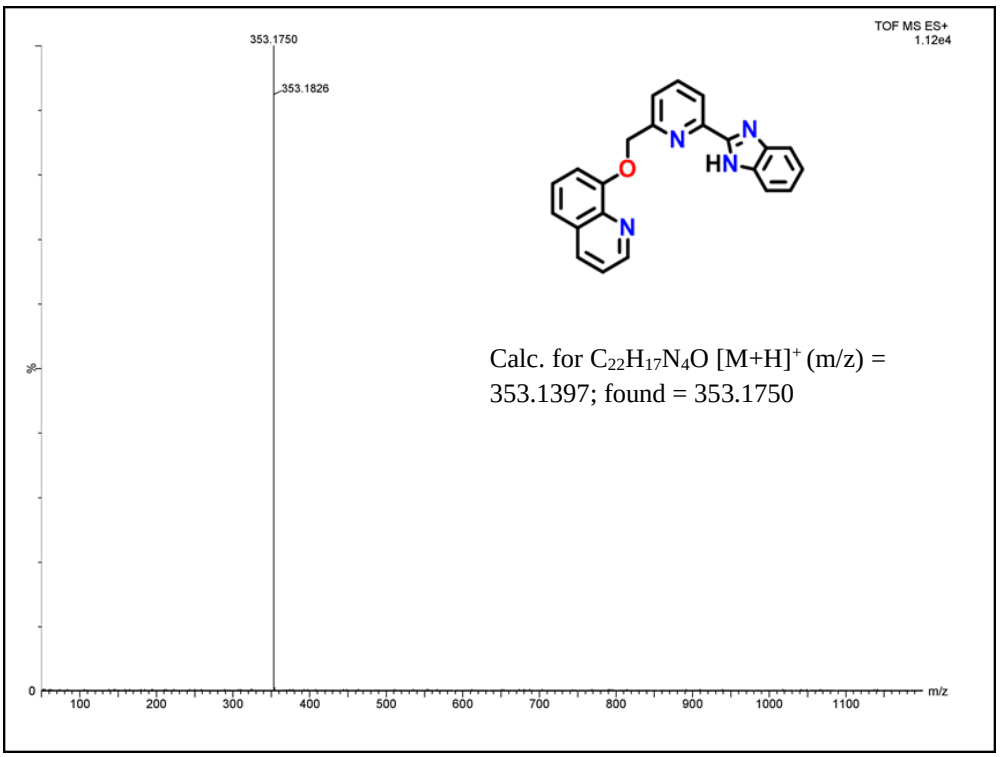

Fig. A7.3: HRMS of the probe (BIPQ)

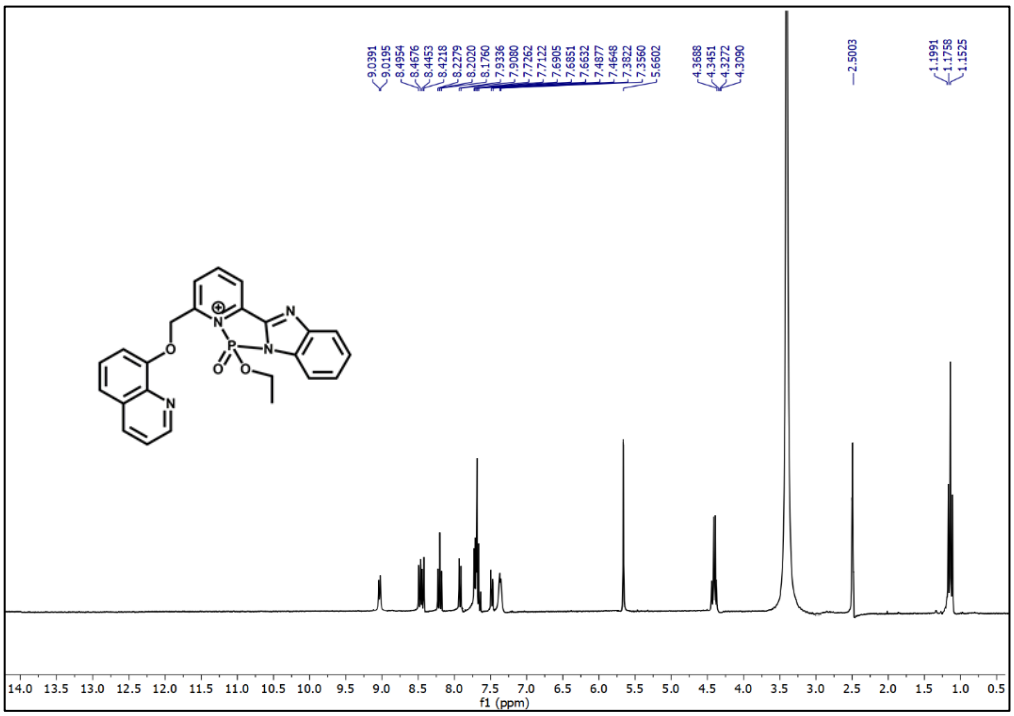

Fig. A7.4: ^{1}H NMR (300 MHz) spectrum of the BIPQ-DCP in DMSO-d_6

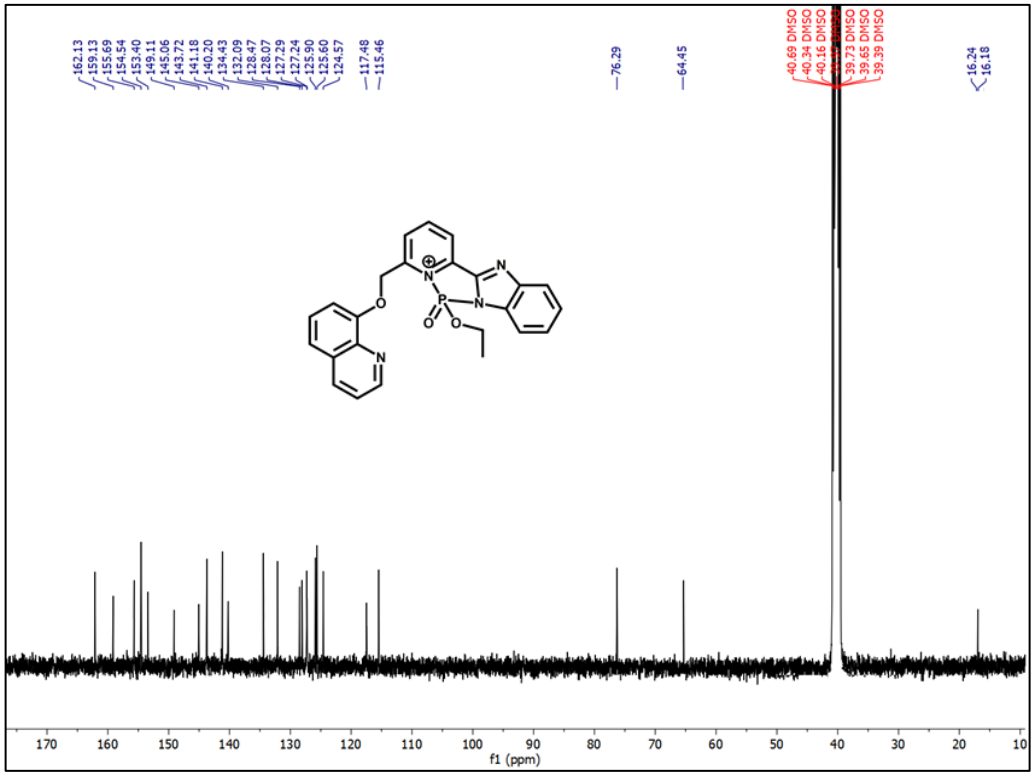

Fig. A7.5: ^{13}C NMR (75 MHz) spectrum of the BIPQ-DCP in DMSO-d6

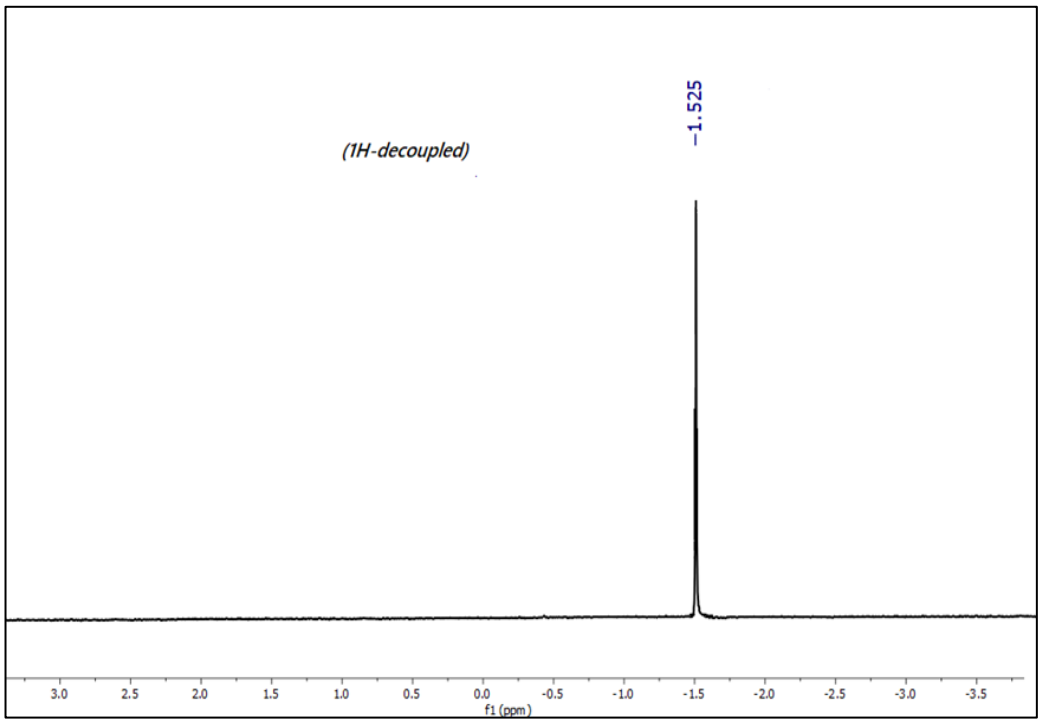

Fig. A7.6: ^{31}P NMR (100 MHz) spectrum of the BIPQ-DCP in $CDCl_3$

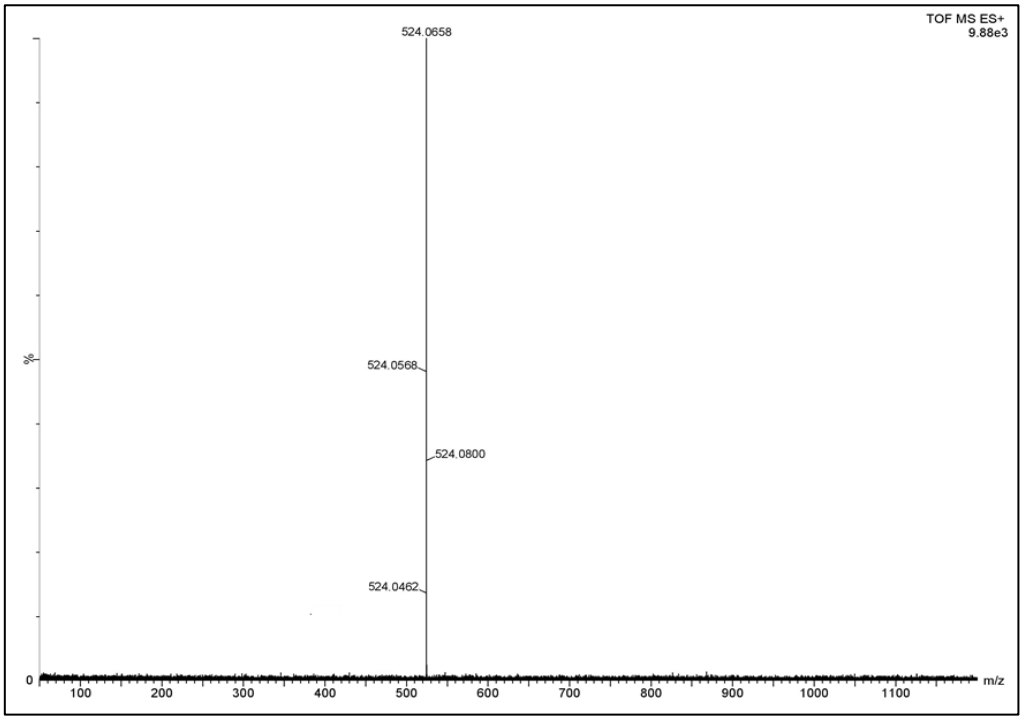

Fig. A7.7: HRMS of BIPQ-DCP

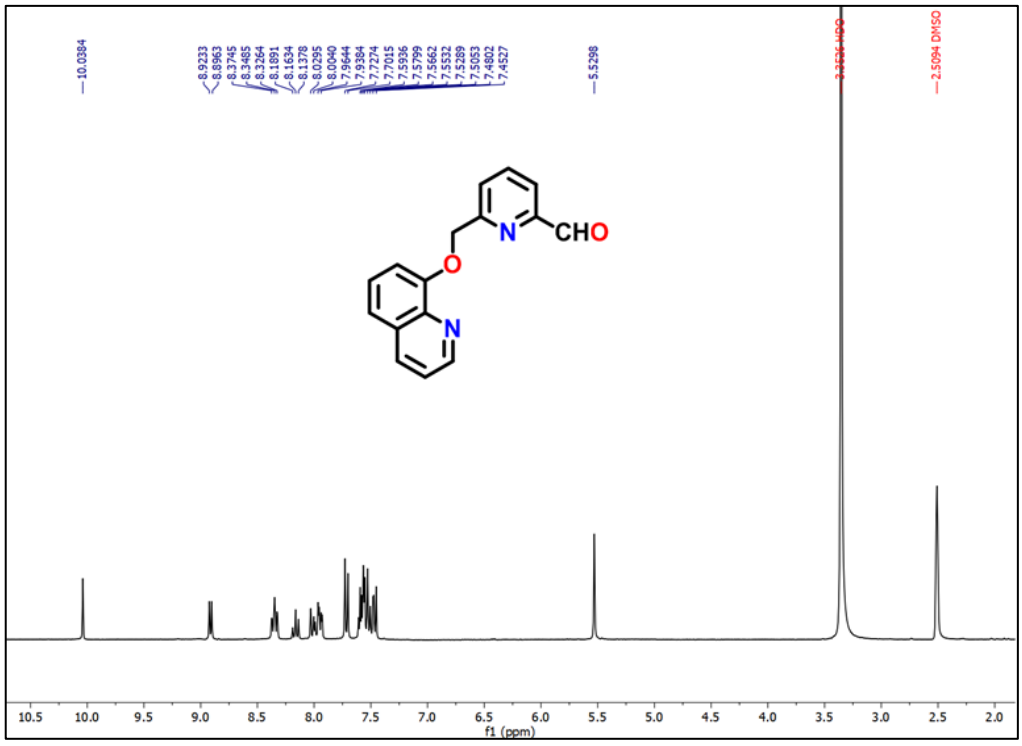

Fig. A7.8: ^{1}H NMR (300 MHz) spectrum of 6-((quinolin-8-yloxy)methyl)picolinaldehyde in DMSO-d_6

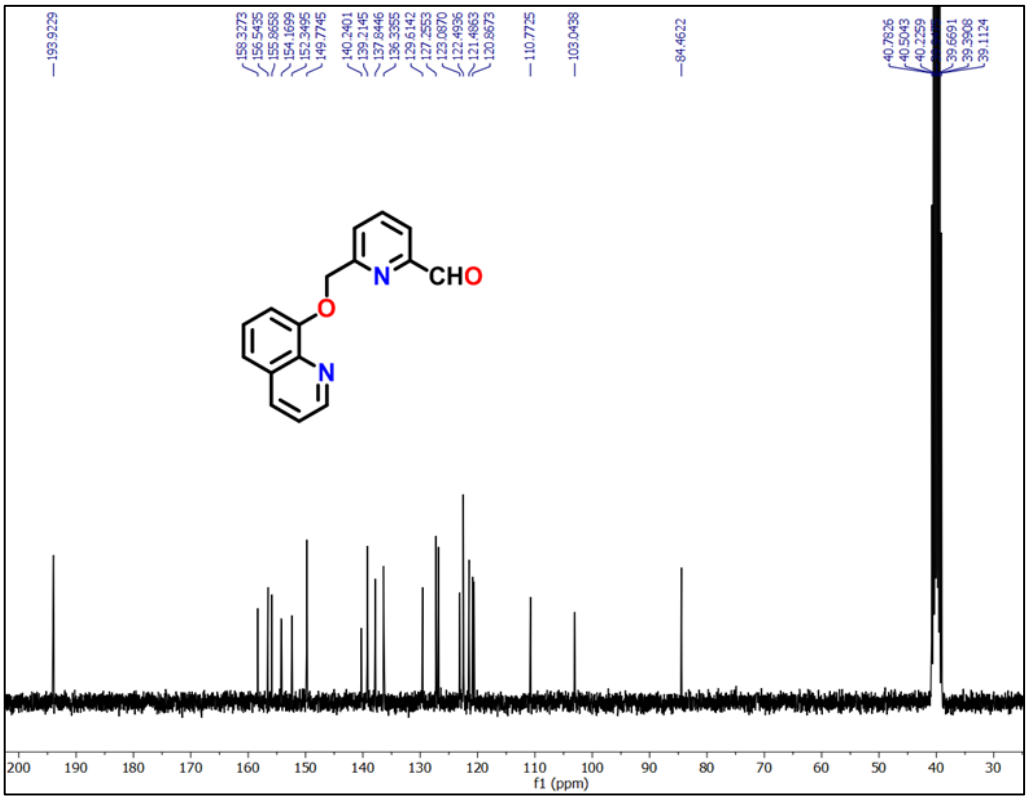

Fig. A7.9: ^{13}C NMR (75 MHz) spectrum of 6-((quinolin-8-yloxy)methyl)picolinaldehyde in DMSO-d6

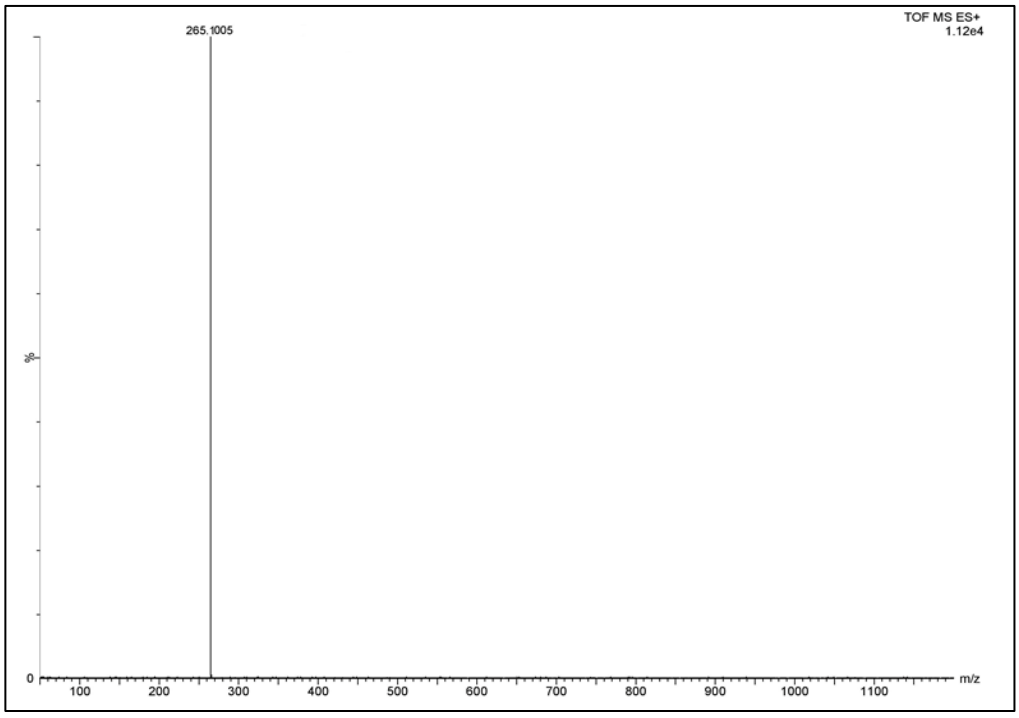

Fig. A7.10: HRMS of 6-((quinolin-8-yloxy)methyl)picolinaldehyde

Table A7.1: Fluorescence lifetimes, quantum yields and radiative and non-radiative rate constants

$CHCl_3$ (solvent)	Quantum yield *(φ)*	τ (ns)	k_r ($10^8 \times s^{-1}$)	k_{nr} ($10^8 \times s^{-1}$)
BIPQ	0.21	1.71	1.228	4.619
BIPQ-DCP	0.35	2.31	1.515	2.814

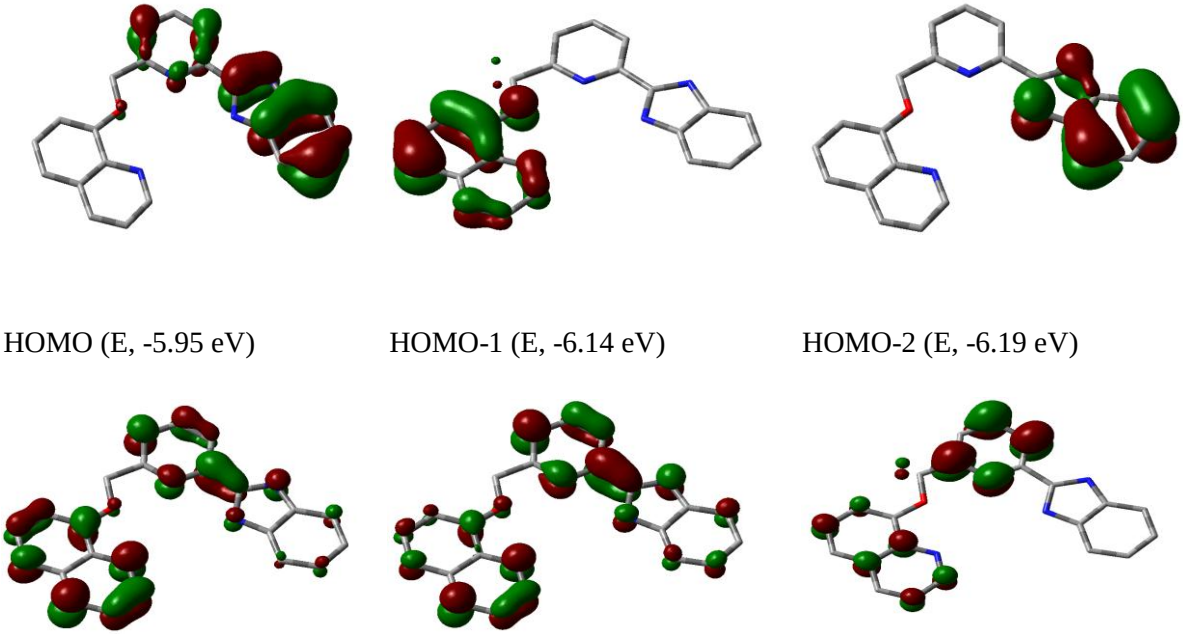

HOMO (E, -5.95 eV) HOMO-1 (E, -6.14 eV) HOMO-2 (E, -6.19 eV)

LUMO (E, -1.75 eV) LUMO+1 (E, -1.65 eV) LUMO+2 (E, -1.02 eV)

Fig. A7.11: Contour plots of selected molecular orbitals of receptor BIPQ

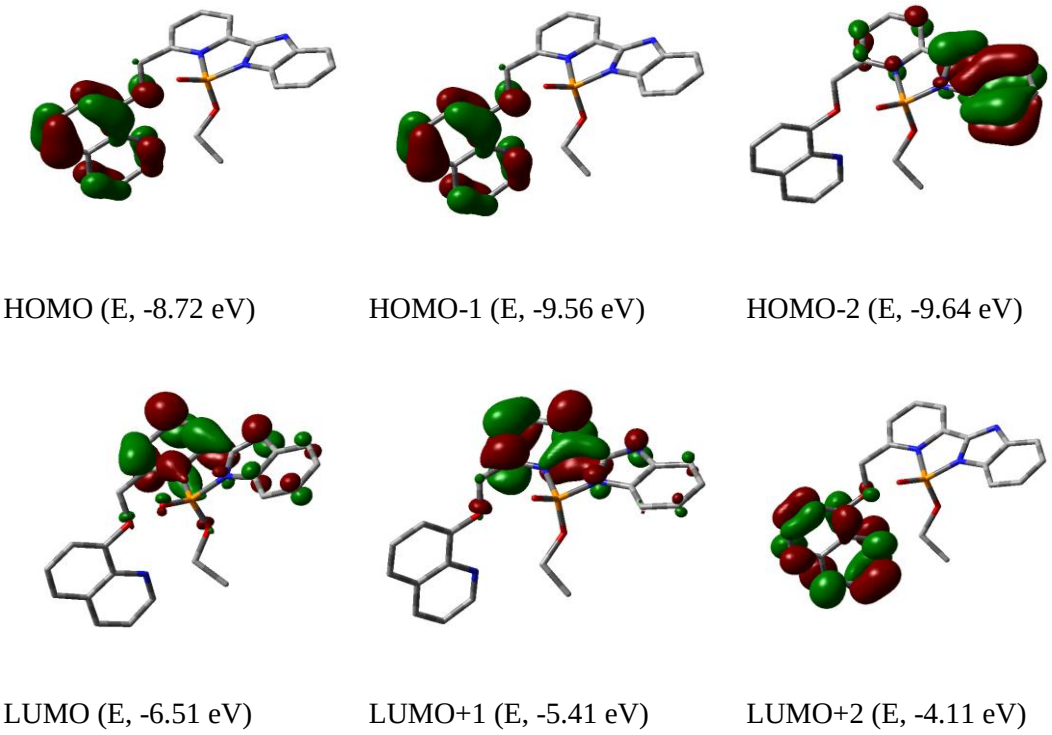

Fig. A7.12: Contour plots of selected molecular orbitals of BIPQ-DCP adduct

Table A7.2: Vertical electronic transitions of BIPQ and BIPQ-DCP adduct calculated by TDDFT/CPCM method

Compds.	λ (nm)	E (eV)	Osc. Strength (f)	Key excitations
BIPQ	327.07	3.7907	0.2264	(86%)HOMO→LUMO
	317.76	3.9018	0.1604	(73%)HOMO→LUMO+1
	316.42	3.9184	0.4604	(92%)HOMO-1→LUMO
	236.65	5.2391	0.1650	(65%)HOMO-2→LUMO+3
	236.58	5.2406	0.3821	(30%)HOMO-3→LUMO+1

				(29%)HOMO-2→LUMO+3
	234.94	5.2772	0.3931	(35%)HOMO-6→LUMO
	208.88	5.9357	0.1484	(45%)HOMO-8→LUMO+1
BIPQ-DCP	568.57	2.1806	0.0184	(99%)HOMO→LUMO
	425.72	2.9123	0.3260	(33%)HOMO-2→LUMO
				(66%)HOMO-1→LUMO
	417.74	2.9680	0.1445	(65%)HOMO-2→LUMO
				(33%)HOMO-1→LUMO
	310.00	3.9995	0.1738	(97%)HOMO-1→LUMO+1
	309.11	4.0110	0.1178	(95%)HOMO→LUMO+2
	259.50	4.7777	0.1252	(91%)HOMO-7→LUMO
	232.98	5.3217	0.1931	(75%)HOMO-4→LUMO+3
	232.14	5.3409	0.6233	(32%)HOMO-3→LUMO+2
				(29%)HOMO→LUMO+3

Table A7.3: Comparison of the present receptor (BIPQ) with some reported receptors for the selective detection of DCP

Receptor	Solvent system	Detection limit	Reference
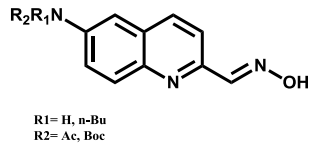	CH_3CN	21×10^{-9} M	[1]
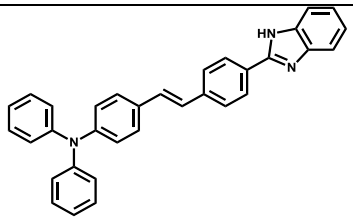	THF/H_2O (4/1, v/v)	8.45×10^{-8} M	[2]
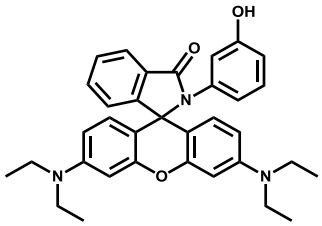	H_2O-CH_3CN (10:1, v/v)	5.6×10^{-9} M	[3]
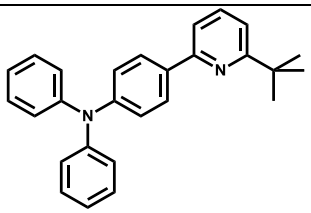	THF	1.5×10^{-8} M	[4]
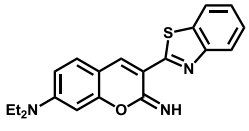	DMF (Fluorescence turn off chemosensor)	0.065 μM	[5]

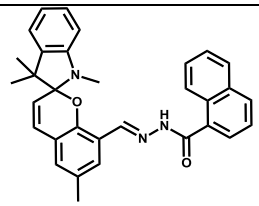	CH_3CN/H_2O (1/1, v/v)	2.1×10^{-8} M	[6]
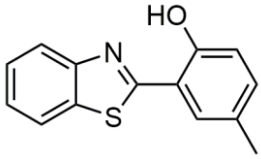	CH_3CN	0.186 µM	. [7]
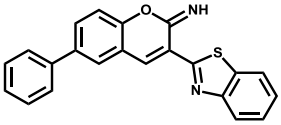	CH_3CN/H_2O (1/1, v/v)	15.8×10^{-9} M	[8]
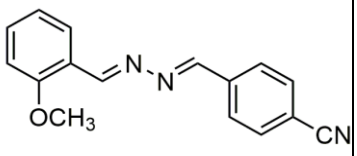	CH_3CN	9.86 nM	[9]
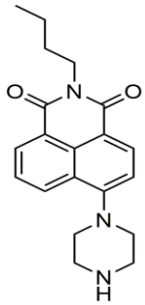	DMF	5.5 nM	[10]
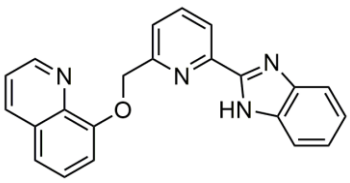	$CHCl_3$	$1.21\text{x}10^{-8}$ M	**This work**

References

1. Y. Cai, C. Li and Q. Song, *J. Mater. Chem. C*, 2017, **5**, 7337-7343
2. K. Aich, S. Das, S. Gharami, L. Patra and T. K. Mondal, *New J. Chem.*, 2017, **41**, 12562-12568
3. H. S. Sarkar, A. Ghosh, S. Das, P. K. Maiti, S. Maitra, S. Mandal and P. Sahoo, *Sci Rep.*, 2018, **8**, 3402
4. J. Yao, Y. Fu, W. Xu, T. Fan, Y. Gao, Q. He, D. Zhu, H. Cao and J. Cheng, *Anal. Chem.*, 2016, **88**, 2497-2501
5. M. S. J. Khan, Y. W. Wang, M. O. Senge and Y. Peng, *J. Hazard. Mater.*, 2018, **342**, 10-19.
6. S. Goswami, S. Das, and K. Aich, *RSC Adv.*, 2015**, 5**, 28996-29001
7. X. Hu, H. Zeng, T. Chen. H. Yuan and L. Zeng, Sens. Actuators B Chem., 2020, **319**, 128282.
8. L. Patra, P. Ghosh, S. Das, S. Gharami, N. Murmu and T. K. Mondal, *J. Photo. Photobiol. A. Chem.*, 2020, **388**, 112188.
9. R. Suhasini, R. Karpagam, K. Thirumoorthy and V. Thiagaranjan, *Spectro. Acta, Mol. Bio. Spec.*, 2021, **263**, 120206.
10. H. Xu, H. Zhang, L. Zhao, C. Peng, G. Liu and T. Cheng, *New J. Chem.*, 2020, **44**, 10713.

List of publications

Thesis works:

1. Fabrication of a new coumarin based fluorescent "turn-on" probe for distinct and sequential recognition of Al^{3+} and F^- along with its application in live cell imaging. **Atanu Maji**, Rahul Naskar, Debarpan Mitra, Saswati Gharami, Nabendu Murmu and Tapan Kumar Mondal, ***Journal of Fluorescence,*** 33, 2403–2414, 2023,
2. A novel carbazole-benzothiazole based chemodosimeter for chromogenic and fluorogenic recognition of CN^-, **Atanu Maji**, Amitav Biswas, Akash Das, Saswati Gharami and Tapan Kumar Mondal, ***New Journal of Chemistry,*** 47, 11557-11564, 2023
3. A chemodosimetric Approach for the visual detection of nerve agent simulant Diethyl chlorophosphate (DCP) in liquid and vapour phase. **Atanu Maji**, Amitav Biswas, Biswajit Bera and Tapan Kumar Mondal, ***Analytical Methods***, 15, 6417-6424, 2023
4. Efficient solid and solution state emissive resuable solvatochromic fluorophore for colorimetric and fluorometric detection of CN^-. **Atanu Maji**, Amitav Biswas, Krishnendu Aich, Saswati Gharami, Biswajit Bera and Tapan Kumar Mondal, ***Analyst***, https://doi.org/10.1039/D3AN01697H, 2024

Other works:

1. An ICT based organic framework for fluorogenic detection of lethal pulmonary agent phosgene, Amitav Biswas, **Atanu Maji**, Saswati Gharami and Tapan Kumar Mondal, ***New Journal of Chemistry***, 47, 17154-17162, 2023
2. A biphenyl thiosemicarbazide based fluorogenic chemosensor for Cd^{2+}: Application in cell bioimaging, Amitav Biswas, Debarpan Mitra, Rahul Naskar, **Atanu Maji**, Akash Das, Nabendu Murmu and Tapan Kumar Mondal, ***Analytical Methods***, 15, 2745-2754, 2023.

Journal of Fluorescence (2023) 33:2403–2414
https://doi.org/10.1007/s10895-023-03208-0

RESEARCH

Fabrication of a New Coumarin Based Fluorescent "turn-on" Probe for Distinct and Sequential Recognition of Al^{3+} and F^- Along With Its Application in Live Cell Imaging

Atanu Maji[1] · Rahul Naskar[1] · Debarpan Mitra[2] · Saswati Gharami[1] · Nabendu Murmu[2] · Tapan Kumar Mondal[1]

Received: 8 February 2023 / Accepted: 9 March 2023 / Published online: 21 April 2023

Abstract

A new coumarin based fluorescent switch PCEH is fabricated which displays high selective sensing towards Al^{3+} among other metal cations at physiological pH. On gradual addition of Al^{3+}, PCEH shows a brilliant "turn-on" emission enhancement in MeOH/H_2O (4/1, v/v) solution. This new fluorescent switch is proven to be a reversible probe by gradual addition of F^- into the PCEH-Al^{3+} solution. Detection limit as well as binding constant values are calculated to be in the order of 10^{-9} M and 10^4 M^{-1} respectively. We have also explored its potential as a biomarker in the application of live cell imaging using breast cancer cells (MDA-MB-231 cell).

Keywords Fluorescence "OFF–ON-OFF" sensor · Coumarin · Chemosensor · Recognition of Al^{3+} · Dip-stick experiment · Live cell imaging

Introduction

Fluorescent molecular switches which can distinctly detect specific metal cations just by turning on their photophysical properties have been a tremendous source of attraction of the budding researchers over the last few years [1–3]. The interest in the fabrication of these fluorescent molecules is at peak owing to their huge need for the recognition and identification of lethal heavy metal ions present in the environment and also in living organisms [4, 5]. This interest has stimulated the fabrication of a significant number of fluorescent sensors for cations which consists of a variety of organic fluorophores, for instance coumarin [6, 7], fluorescein [8, 9] pyrene [10, 11] and boron-dipyrromethene [12, 13]. Recently the fluorescent switches procured from Schiff bases have drawn a huge deal of attention for the recognition of metal ions due to their inexpensive and easy synthetic route, compelling complexation capability, fast and immediate response and elevated sensitivity [14–17]. Due to the C = N isomerization, Schiff base fluorescent probes exhibit a weak fluorescence whereas after binding with the metal ions, the probes show a noteworthy emission enhancement along with a noticeable color alteration owing to the inhibition of C = N isomerization. Aluminium is the third most plentiful metallic element of all elements present in the earth's crust and being the most plentiful metallic elements, aluminum ions have been widely utilized in water purification systems, cosmetics, food packaging, food additives and electronic devices [18–22]. Aluminium is widely used in our daily life such as pharmaceutical manufacturing, food processing and purifying and industrial fabrication [23, 24]. It has extensive applications in the textile, food, dye production and paper industries along with the production of household tools. Nevertheless, the extensive use of Al^{3+} ions in our daily life in diverse forms has created a threat to damage the ecological atmosphere. Unnecessarily excessive amount of Al^{3+} can result in acute inhibition in bone development that sometimes leads to diseases like osteoporosis, osteomalacia etc. Advance research leads to the fact that too much Al^{3+} will cause memory loss thereby leading to life-menacing diseases like Alzheimer's, Parkinson's, dementia [25–27]. Excessive presence of aluminium can cause severe damage in our nervous system which eventually results into

✉ Tapan Kumar Mondal
tapank.mondal@jadavpuruniversity.in

[1] Department of Chemistry, Jadavpur University, Kolkata 700032, India

[2] Department of Signal Transduction and Biogenic Amines (STBA), Chittaranjan National Cancer Institute, Kolkata 700026, India

NJC

ROYAL SOCIETY OF CHEMISTRY

PAPER

View Article Online
View Journal | View Issue

Cite this: *New J. Chem.*, 2023, **47**, 11557

A novel carbazole-benzothiazole-based chemodosimeter for the chromogenic and fluorogenic recognition of CN^-†

Atanu Maji, Amitav Biswas, Akash Das, Saswati Gharami, Krishnendu Aich and Tapan K. Mondal *

Received 11th March 2023,
Accepted 17th May 2023

DOI: 10.1039/d3nj01157g

rsc.li/njc

A novel colorimetric and fluorescent sensing probe, (*E*)-3-(4-(9H-carbazol-9-yl)phenyl)-2-(benzo[*d*]thiazol-2-yl)acrylonitrile (CBTA), was synthesized and characterized by spectroscopic techniques. CBTA displayed "turn off" fluorescence in the presence of cyanide with a higher selectivity than that of others anions such as Br^-, Cl^-, I^-, NO_3^-, SO_4^{2-}, SCN^-, CO_3^{2-}, N_3^-, OH^-, HCO_3^-, $H_2PO_4^-$, HPO_4^{2-}, F^-, ACO^-, and PO_4^{3-} in a DMSO : H_2O medium (40 : 60, v/v, HEPES buffer, pH = 7.2). The "turn off" fluorescence response mechanism can be attributed to the intra-molecular charge transfer (ICT) process, which is blocked by the nucleophilic attack of cyanide ions at the cyano vinyl group of the probe. The LOD was found to be 3.57×10^{-8} M. The interaction involved behind the sensing of cyanide was investigated by Job's plot analysis, ^{1}H-NMR, and mass spectroscopic studies. DFT and TDDFT were also employed to verify the experimental outcomes. Moreover, the test strip experiment provides a wide application prospect of the receptor for detecting poisonous cyanide in the environment and biological system.

Introduction

The development of a new molecular probe for the detection of anions is of great interest because of their vital roles in a wide range of medicines, catalysis, life science, and environment.[1] Additionally, food safety issues and water pollution by poisonous anions have drawn attention with the development of science and technology nowadays.[2–6] Cyanide is one of the most well-known toxic anions, even at a lower concentration, which can be lethal to human beings, animals, and environment. Cyanide is currently extensively used in many industrial processes such as electroplating, petrochemicals, photography, steel production, gold mining, metallurgy, and the synthesis of resign and fibre due to its critical role in multi-functional reactions.[7] World Health Organization (WHO) stipulates that the permissible acceptable concentration of cyanide in drinking water is 1.9×10^{-6} mol L^{-1}.[8] By the way, cyanide is present in some insects, fruits, seeds, and roots where it is released through the hydrolysis process of cyanogenic glycosides.[9–14] Cyanide binds to the iron ion in cytochrome *c* oxidase, blocks the electron transport in metabolism, and inhibits the production of ATP in cells, making the biological system inefficient to provide sufficient energy to the heart, central nervous system and other vital organs ultimately.[15,16] Considering the above-mentioned fact, the development of simple, efficient and rapid detection tools with high selectivity and sensitivity towards cyanide is an ongoing hot topic to prevent the harmful effect in the human body from contaminated food and environment.

To date, fluorescent molecular probes capable of detecting CN^- have been reported based on fluorescence resonance energy transfer (FRET),[17–19] intra-molecular charge transfer (ICT),[20,21] twisted intra-molecular charge transfer (TICT),[22] excited state intra-molecular proton transfer (ESIPT),[23,24] and photo-induced electron transfer (PET).[25,26] Recently, several groups have reported detection methods by utilizing the nucleophilic addition reaction of cyanide directly involved in the development of covalent bond formation and showed anti-interference ability and high selectivity.[27–38] Compared with the traditional sophisticated analytical tools such as spectrophotometry, voltammetry, chromatography, and potentiometric methods, optical molecular probes based on colorimetric and fluorometric responses towards CN^- are of great preference in virtue of their convenience, simplicity, tenability, low cost, high selectivity and rapid response.[39] Particularly, a naked-eye optical sensor is very much impressive. Since the Tang *et al.* discovery of the AIE phenomenon in 2001, several research groups have been published a growing number of AIE active

Department of Chemistry, Jadavpur University, Kolkata-700032, India.
E-mail: tapank.mondal@jadavpuruniversity.in

† Electronic supplementary information (ESI) available: NMR and MS of all new compounds, limit of detection determination, quantum yield calculation. See DOI: https://doi.org/10.1039/d3nj01157g

Analytical Methods

ROYAL SOCIETY OF CHEMISTRY

PAPER

Check for updates

Cite this: *Anal. Methods*, 2023, **15**, 6417

A chemodosimetric approach for the visual detection of nerve agent simulant diethyl chlorophosphate (DCP) in liquid and vapour phase†

Atanu Maji, Amitav Biswas, Biswajit Bera and Tapan Kumar Mondal *

Received 27th July 2023
Accepted 31st October 2023

DOI: 10.1039/d3ay01296d

rsc.li/methods

In this work, a novel fluorescent ratiometric switch, 8-((6-(1*H*-benzo[*d*]imidazol-2-yl)pyridin-2-yl)methoxy) quinoline (**BIPQ**), has been introduced for sensing an organophosphorus (OP) chemical vapor threat, diethyl chlorophosphate (**DCP**), the low-toxic mimic of the real nerve agent sarin (**GB**). **BIPQ** is efficient at detecting **DCP** in both solution and gaseous phase and has potential practical application with high sensitivity and selectivity. The probe shows significant ratiometric emission in the presence of **DCP** along with a distinct color change from blue to cyan under UV light. The sensing mechanism of the chemodosimeter is based on the generation of a new adduct, **BIPQ–DCP**, through a nucleophilic substitution reaction with **DCP** followed by a ring-closure process to form the final product. The detection limit of **BIPQ** for **DCP** was determined to be in the order of 10^{-8} (M) in the liquid state. DFT and TDDFT computational techniques were carried out in order to interpret the electronic properties theoretically.

Introduction

Nowadays organophosphorus compounds are used in preparing many pesticides and herbicides in modern agriculture. Organophosphorus compounds are conceived as one of the most exceptionally hazardous nerve agents and are extremely harmful to the nervous system of every living being if inhaled or ingested through any kind of contamination of food or drink.[1–4] Some known nerve agents including tabun (**GA**), soman (**GD**) and sarin (**GB**) are extremely dangerous organophosphates (Scheme 1), which bear excellent leaving groups owing to which they are known as essential phosphonylating and phosphorylating agents.[5–9] These poisonous chemicals along with their advantages of cheapness, simplicity in manufacture and destructive effects on civilians encourage terrorism. The phosphate group present in these chemicals binds irreversibly with the hydroxyl group present in acetylcholinesterase (AChE), blocks the hydrolysis of acetylcholine neurotransmitters and restrains the decomposition of acetylcholine.[10–13] The excessive storage of acetylcholine causes neuromuscular paralysis, neurological imbalance in the cholinergic synapse, resistance to muscle relaxation, and organ failure, leading to sudden death.[14–20] So they have became a massive threat to all mankind. As most of these compounds are odorless, colorless and tasteless, making them very difficult to detect,[21] it is very urgent to develop a very sensitive, reliable and rapid method for easy and quick detection of these substances in both solution and vapour phase. Our present work is based on the recognition of highly volatile sarin (**GB**) as it is one of the forbidden CWAs used by terrorists. But due to its too toxic nature and difficult availability, an associated substance, diethyl chlorophosphate (**DCP**), has been used as a nerve-gas-mimicking agent for experiments because it has a similar chemical structure and comparable reactivity but very low toxicity.

In recent years, many research groups have already introduced a variety of noteworthy tools for detecting nerve-agent-mimicking substances, including colorimetry,[22–24] fluorometry,[25–27] electro-chemistry,[28–30] mass spectrometry,[31–33] interferometry,[34] enzyme-based biosensors,[35–38] surface acoustic wave (SAW) devices,[39,40] enzymatic assays,[41] photoacoustic spectroscopy,[42] PET based probes,[43] ion mobility spectroscopy,[44] cyclization reactions,[45] photonic crystals,[46] nucleophilic substitution reactions,[47,48] lanthanide luminescence,[49] complex

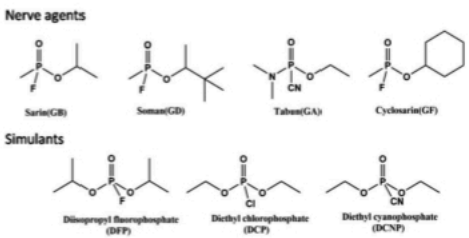

Scheme 1 The structures of chemical warfare agents (CWAs) and their less toxic simulants.

Department of Chemistry, Jadavpur University, Kolkata-700 032, India. E-mail: tapank.mondal@jadavpuruniversity.in

† Electronic supplementary information (ESI) available. See DOI: https://doi.org/10.1039/d3ay01296d

Analyst

ROYAL SOCIETY OF CHEMISTRY

PAPER

View Article Online
View Journal

Cite this: DOI: 10.1039/d3an01697h

Efficient solid- and solution-state emissive reusable solvatochromic fluorophores for colorimetric and fluorometric detection of CN^-†

Atanu Maji, Krishnendu Aich, Amitav Biswas, Saswati Gharami, Biswajit Bera and Tapan K. Mondal *

In this work, a novel organic receptor, CPI [(*E*)-3-(4-(9*H*-carbazol-9-yl)phenyl)-2-(1*H*-benzo[*d*]imidazol-2-yl)acrylonitrile], was rationally designed and successfully fabricated for selective and sole recognition of CN^- ions over other competitive anions through an obvious chromogenic and ratiometric emission change in DMSO. The distinct and prominent color change upon the addition of CN^- can be attributed to the typical ICT process, which is induced by the deprotonation of acidic NH protons in the imidazole moiety. The sensor displayed strong solvatochromic effects in commonly used organic solvents such as *n*-hexane, toluene, diethyl ether, DCM, THF, DMF and DMSO. The chemical structure of the sensor was characterized by single-crystal X-ray diffraction, ^{1}HNMR, ^{13}CNMR, IR and mass spectroscopy. Significantly, the probe can function as a fluorescence-based sensor for the efficient detection of low-level water in organic solvents. The solid-state emission properties of CPI were successfully applied to recognise cyanide in a solid-state platform with naked eye-visualized distinct color change. The probe can be made reusable by adding TFA into the CN^- treated probe solution. The detection limit of CPI towards CN^- was determined to be 4.48×10^{-8} M. More importantly, the sensor is capable of detecting CN^- in food samples and has been employed for wastewater treatment. Besides, easy-to-prepare CPI-coated test strips provide a simple, reusable and easy-to-handle protocol for the qualitative identification of CN^- conveniently. Finally, density functional theory and time-dependent density functional theory were performed to verify the experimental outcomes theoretically.

Received 5th October 2023,
Accepted 13th January 2024

DOI: 10.1039/d3an01697h

rsc.li/analyst

Introduction

Many researchers have recently paid attention to the development of anionic chemosensors due to their broad application in many fields including chemical, biological, medical and technological processes.[1–6] Among various anions, cyanide ion is one of the deadliest poisonous anions towards human beings. Even trace amounts of CN^- ions can affect human health in many ways, and it may lead to several health risks because of their excellent binding affinity towards Fe^{3+} ions in cytochrome c oxidase, eventually leading to the incapability to produce ATP in cells, which subsequently results in respiratory arrest and ultimately death.[7–10] Some insects and food samples such as sprouting potatoes, bitter almonds, apple seeds as well as cassava contain cyanide, and it reaches to the environment through the hydrolysis process of cyanogenic glycosides.[11–14] Despite its toxicity, cyanide has been extensively used in many industrial production such as petrochemicals, electroplating, steel production, photography, metallurgy, gold mining, and synthesis of resins and fibres due to its critical role in multi-functional reactions.[15] Therefore, water pollution and food safety issues by toxic cyanide pose a serious threat to human health and environment nowadays.[16–18] The maximum intake of CN^- ions as per the guidelines approved by WHO and USEPA is 1.9 μM (200 μg L^{-1}).[19] In view of its vital role in industries and toxicity, the development of a new method to monitor trace amounts of CN^- ions in biological and environmental samples is one of the most sensitive hotspots among researchers. In the past few decades, numerous types of chemosensors based on coordination,[20–22] the Sonogashira cross-coupling,[23–25] nucleophilic addition reaction,[26,27] hydrogen-bonding interactions[28,29] and many other mechanisms have been reported for the sole detection of poisonous cyanide. However, these methods have many limitations such as complicated synthetic steps, poor sensitivity and selectivity, use of sophisti-

Department of Chemistry, Jadavpur University, Kolkata- 700032, India.
E-mail: tapank.mondal@jadavpuruniversity.in

†Electronic supplementary information (ESI) available: NMR and MS of all new compounds, limit of detection determination, quantum yield calculation. See DOI: https://doi.org/10.1039/d3an01697h

NJC

ROYAL SOCIETY OF CHEMISTRY

PAPER

View Article Online
View Journal | View Issue

Cite this: *New J. Chem.*, 2023, 47, 17154

An ICT-based organic framework for the fluorogenic detection of lethal pulmonary agent phosgene†

Amitav Biswas, Atanu Maji, Saswati Gharami and Tapan Kumar Mondal *

Received 3rd June 2023,
Accepted 12th August 2023

DOI: 10.1039/d3nj02580b

rsc.li/njc

Fluorescent chemosensor detecting a widely used but highly toxic chemical warfare agent (CWA) such as phosgene is of great importance due to its high sensitivity along with low cost and simple method of preparation. In this study a biphenyl-benzoimidazole based (**BPCl**) chemodosimeter, which displayed a rapid, sensitive and ratiometric detection of the lethal pulmonary agent phosgene, has been developed. Upon the addition of phosgene to the **BPCl** solution in THF, we observed a fluorescence color change from blue to cyan-green. The chemodosimeter (**BPCl**) undergoes nucleophilic substitution reaction with phosgene followed by ring closure to yield the carbamylated final product and shows an explicit ratiometric fluorescence response towards phosgene. The carbamylation was accelerated due to the formation of a six-member ring, which restricts the C–C bond rotation. The probe (**BPCl**) selectively detected phosgene over other toxic relevant analytes. The detection limit (LOD) of **BPCl** for phosgene was established to be in the order of 10^{-7} M in the solution phase, which implied that **BPCl** can detect phosgene at a very minuscule level. This ratiometric switch, which we developed, can be used as a potential portable kit for detecting phosgene in the vapour phase, as well as in the solid phase when supported upon TLC plates. Theoretical calculations using the DFT/B3LYP/6-31+G(d) method were performed to unveil the electronic properties theoretically and to interpret the probable sensing mechanism.

Introduction

In the history of human existence, certain weapons were made for mass destruction (WMD); among them chemical warfare agents are known to be the most ferocious ones created by mankind.[1] These chemical warfare agents (CWAs) can be categorized as nerve agents, blistering agents, pulmonary agents, blood agents, tear gases, psychomimetic agents, incapacitating agents, toxins, *etc.*[2] Among these CWAs, phosgene is included in the list of pulmonary agents as the most threatening to humanity.[3] Due to its catastrophic nature phosgene ($COCl_2$) was employed as a chemical warfare agent (CWC) in World War I and World War II and poisonous gas bombs made from it, caused mammoth causalities to humankind.[4–6] Even with a low exposure limit of this colourless phosgene gas up to 0.1 ppm, it can cause serious irritation to the eyes, skin, nose, lungs, and respiratory system.[7] Outrageous exposure to about 90 ppm of phosgene for 30 minutes can cause dangerous repercussions, such as inducing pulmonary edema, pulmonary emphysema, and finally death.[8–12] The production of nerve agents such as sarin, soman, and tabun is strictly controlled and prohibited by international laws.[13] However, in contrast, due to the dynamic nature of phosgene such as cost effectiveness, high reactivity, and easy availability, it has wide applications in several industries.[14] For instance, it is used as a precursor for the industrial production of chemicals, isocyanate-based polymer materials, pharmaceuticals, aniline dyes, and different types of pesticides such as chloroformates and sulfonylureas.[15–18] Hence due to its in-hand accessibility, it can be potentially exploited by terrorists as chemical weapons. As well as unexpected industrial leakages can also cause havoc and destruction to mankind. Thus, it is indispensable to construct a reliable, cost-effective, selective, and sensitive approach for detecting phosgene, the alerting threat to humanity.

There are various traditional techniques for the detection of phosgene, such as the gas chromatography method, HPLC technique, electrochemical methods, and Raman techniques.[19–26] However these techniques have problems due to the complexity of sample preparation, poor portability, expensive precious instrumentation, and sophisticated procedures. In contrast, fluorescent-based detection of phosgene has gained progressive interest. This could be attributed to several advantages such as a simple preparation procedure, quick response time, suitable field detection, high selectivity with sensitivity, and simple operation

Department of Chemistry, Jadavpur University, Kolkata-700 032, India. E-mail: tapank.mondal@jadavpuruniversity.in

† Electronic supplementary information (ESI) available. See DOI: https://doi.org/10.1039/d3nj02580b

Analytical Methods

ROYAL SOCIETY OF CHEMISTRY

PAPER

View Article Online
View Journal | View Issue

Cite this: *Anal. Methods*, 2023, 15, 2745

A biphenyl thiosemicarbazide based fluorogenic chemosensor for selective recognition of Cd^{2+}: application in cell bioimaging†

Amitav Biswas,[a] Debarpan Mitra,[b] Rahul Naskar,[a] Atanu Maji,[a] Akash Das,[a] Nabendu Murmu[b] and Tapan Kumar Mondal *[a]

A diversified biphenyl thiosemicarbazide based chemosensor (HBMC) has been fabricated and reported for the specific detection of Cd^{2+} in a MeOH : H_2O (4 : 1) solution. We observed a chromogenic change from colorless to light yellow colour, and it showed a "turn-on" fluorogenic change from non fluorescent to blooming cyan colour. In fluorometric titration a sharp "turn-on" emission for Cd^{2+} was observed with a ~16 fold increase in fluorescence intensity value at 496 nm by incremental addition of Cd^{2+} ions in the MeOH : H_2O (4 : 1) solution. The reversibility of the chemosensor (HBMC) was confirmed by a sequential addition of the EDTA solution. Again the binding stoichiometry of HBMC with Cd^{2+} was found to be 2 : 1, as confirmed by Job's plot analysis and HRMS spectra of the HBMC–Cd^{2+} complex. The mechanism for Cd^{2+} sensing in MeOH : H_2O (4 : 1) is based upon the inhibition of C=N isomerization and ESIPT process and simultaneously turning on the CHEF (chelation enhanced fluorescence) process. The limit of detection for Cd^{2+} was found to be in the order of 10^{-8} (M), which implies that HBMC is an efficient probe to detect Cd^{2+} at the microscopic level. A reusability study was performed and on-sight detection of cadmium ions by the chemosensor (HBMC) was established by dip-stick experiment. *In vitro* detection of Cd^{2+} in human breast cancer cells (MDA-MB-231) by HBMC discloses its cell permeability and biocompatible nature. Computational studies (DFT and TDDFT) with the probe HBMC and HBMC–Cd^{2+} complex were also performed.

Received 16th March 2023
Accepted 10th May 2023

DOI: 10.1039/d3ay00403a

rsc.li/methods

Introduction

With reference to human health and the environmental system, discriminative detection of heavy and toxic metal ions is one of the most noteworthy aspects in the field of chemosensors. Among those heavy metal ions Cd^{2+} tops the list in relation to its hazardous nature and detrimental effects.[1] Due to the irreversible damage caused by its use in the fields of batteries, smelting, mining, pigments, metallurgy, and fertilizers it has become a hazardous global pollutant.[2–5] Hence due to its outrageous use, it has triggered an inescapable contamination of our soil, water, food, and air.[6–8] Simultaneously living organisms and human health are also being threatened by the excessive use of cadmium.[9] Mainly through water or air, food and inhalation of cigarette smoke, humans are exposed to cadmium.[10] The toxicity level of cadmium is so soaring that the US Environmental Protection Agency (EPA) and Agency for Toxic Substances and Disease Registry have listed this toxic heavy metal as the seventh on the Top 20 Hazardous Substances Priority List,[11] while the WHO (World Health Organization) has given an enforceable drinking water standard for cadmium of 3 ppb to prevent kidney related diseases.[12] This continuous short and long term cadmium exposure of humans causes different disorders, resulting in lung, breast and prostate cancer.[13–15] Therefore the International Agency for Research on Cancer (IARC) has categorized cadmium compounds as carcinogens of category I.[16] The abnormal concentration of cadmium also causes damage to several organs such as the brain, kidneys, bones, and gastrointestinal tract and has increased the risk of cardiovascular disease.[17–20] Renal and adipose tissue dysfunctions and calcium metabolism are also factors caused by excessive cadmium intake.[21–24] However, the mechanism involved in the uptake of Cd^{2+} by cellular and environmental systems and Cd^{2+} carcinogenesis remains obscured.[25–27] Therefore developing a reliable technique to detect Cd^{2+} in environmental systems is an absolute necessity. However there are several techniques such as atomic absorption/emission spectroscopy (AAS/AES), inductively coupled plasma mass spectrometry (ICP-MS), inductively coupled plasma atomic emission spectroscopy (ICP-AES), and anodic stripping voltammetric analysis, but these techniques

[a]*Department: Chemistry, Jadavpur University, Kolkata-700032, India. E-mail: tapank.mondal@jadavpuruniversity.in*

[b]*Department of Signal Transduction and Biogenic Amines (STBA), Chittaranjan National Cancer Institute, Kolkata-700026, India*

† Electronic supplementary information (ESI) available. See DOI: https://doi.org/10.1039/d3ay00403a